January 2015

# IMPROVED AMORPHOUS SOLID DISPERSION PERFORMANCE USING BINARY POLYMER COMBINATIONS

Tian Xie
*Purdue University*

Follow this and additional works at: https://docs.lib.purdue.edu/open_access_dissertations

**PURDUE UNIVERSITY**
**GRADUATE SCHOOL**
**Thesis/Dissertation Acceptance**

This is to certify that the thesis/dissertation prepared

By Tian Xie

Entitled
IMPROVED AMORPHOUS SOLID DISPERSION PERFORMANCE USING BINARY POLYMER COMBINATIONS

For the degree of  Doctor of Philosophy

Is approved by the final examining committee:

Lynne S. Taylor
Chair

Elizabeth M. Topp

Keith Chadwick

Stephen R. Byrn

To the best of my knowledge and as understood by the student in the Thesis/Dissertation Agreement, Publication Delay, and Certification Disclaimer (Graduate School Form 32), this thesis/dissertation adheres to the provisions of Purdue University's "Policy of Integrity in Research" and the use of copyright material.

Approved by Major Professor(s): Lynne S. Taylor

Approved by: Lynne S. Taylor                                      1/27/2016
　　　　　　　Head of the Departmental Graduate Program                Date

IMPROVED AMORPHOUS SOLID DISPERSION PERFORMANCE USING

BINARY POLYMER COMBINATIONS


A Dissertation

Submitted to the Faculty

of

Purdue University

by

Tian Xie


In Partial Fulfillment of the

Requirements for the Degree

of

Doctor of Philosophy


May 2016

Purdue University

West Lafayette, Indiana

For my parents

## ACKNOWLEDGEMENTS

TABLE OF CONTENTS

LIST OF TABLES

LIST OF FIGURES

ABSTRACT

Tian Xie. Ph.D., Purdue University, May 2016. Improved Amorphous Solid Dispersion Performance Using Binary Polymer Combinations. Major Professor: Lynne S. Taylor.

With increasing attrition rate of new molecular entities due to sub-optimum aqueous solubility, formulation strategies that could improve the dissolution rate and apparent solution concentration are of current interest. Amorphous solid dispersions are attractive over other enabling technologies since they are supersaturating solid dosage forms. However, crystallization may occur during storage as well as during dissolution of ASDs, negating the solubility advantage. Unfortunately, choosing the optimum pharmaceutically acceptable polymeric inhibitor for each of these crystallization pathways is largely empirical. The best polymer for inhibiting solid state crystallization may be ineffective in preventing crystallization during dissolution. Moreover, the release rate of the drug from the ASDs depend on both the type and the amount of the polymer in the formulation. Therefore, an important advance in solid dispersion formulation could be to incorporate combinations of polymers to tailor release profiles, while providing optimized crystallization inhibition. This will expand the application of solid dispersions based on a rational formulation approach that includes both solid state and solution performance characteristics, and provide greater confidence in the use of solid dispersion strategies.

CHAPTER 1. INTRODUCTION

## 1.1 Biopharmaceutics Classification System (BCS)

Bioavailability, by definition, is the fraction of an administered dose of unchanged drug that reaches the systemic circulation. For orally administered drugs, adsorption in the gastrointestinal (GI) lumen is a prerequisite for this purpose. According to the Fick's first law, the flux of drug (J) across the GI wall is given by:

$$J = PC \hspace{4cm} 1\text{-}1$$

Where P is the permeability coefficient of the gastrointestinal barrier to the drug and C is the free drug concentration. Based upon such considerations, Amidon et al[1] developed a Biopharmaceutics Classification System (BCS) to predict the in vivo pharmacokinetic performance of drugs from their permeability and solubility (Table 1-1). High/low permeability is determined by the logP and ClogP parameters. These parameters are measured by the partitioning of neutral/unchanged state of drug molecules between n-octonal and water. Drugs with a logP value greater than that of metoprolol (LogP=1.72) are classified as highly permeable and vice versa. Metoprolol is used as a reference standard because it is known to be 95% absorbed from the GI. In terms of solubility, the criterion for classification is the Dose number (Do), defined as the ratio of the required dose in a glass of water (250ml) to saturation solubility in an aqueous environment. Drugs with Do>1 are classified as low solubility drugs while for high solubility drugs, Do is <1.

It should be acknowledged that other factors important in determining drug absorption and bioavailability such as food effects, absorptive transporters, efflux transporters, and routes of elimination (renal/biliary) were not taken into account in the development of the BCS, but were later addressed by Benet et al[2]. With the introduction of high throughput medicinal chemistry, serious drug solubility problems have emerged. Thousands of new chemical entities are screened for biological activity in the discovery stage using dimethyl sulfoxide (DMSO) or polyethylene glycol (PEG) as the solvent to introduce the compound into the aqueous assay medium. As a result, many candidate molecules with extremely low aqueous solubility (BCS II or BCS IV) give positive results and are moved onto the development stage. They are the so-called "brick dust" or "grease ball" compounds. The poor solubility is usually a consequence of their high crystal lattice energy and/or hydrophobicity. It has been estimated that over 40% of the drugs currently in the market have low solubility. Around 80% to 90% of the drug candidates in the R&D pipeline fall into these categories (Table 1-1)[3]. The unfavorable dissolution property leads to low bioavailability and high drug attrition in late stage development.

## 1.2    Fundamentals of Dissolution

During the preformulation stage, an understanding of the dissolution of a drug candidate is essential as it is considered a major factor influencing bioavailability. The dissolution of crystalline solids can be considered in three stages[4] (Figure 1-1): (1) Removal of a solute molecule from its crystal lattice: energy is required to overcome the solute-solute attractive forces in the solid state. (2) Creation of a cavity in the solvent: the energy required in this step is considerably less than in step 1 and is often negligible. (3) Insertion of the solute

molecule into the cavity by convection and/or diffusion, forming solute-solvent interactions

The mixing of molecules begins at the surface when the solids are placed in the solvent. The thermodynamic driving force for this process is the free energy of mixing:

$$\Delta G_{mix} = \Delta H_{mix} - T\Delta S_{mix} \qquad 1\text{-}2$$

Where, $\Delta H_{mix}$ is the enthalpy of mixing, T is the absolute temperature, and $\Delta S_{mix}$ is the entropy of mixing. $\Delta H_{mix}$ is a factor dependent on intermolecular interactions. Dissolution is favorable when the solute-solvent interaction is stronger than the total of solute-solute and solvent-solvent interactions. The intermolecular forces (e.g. hydrogen bonds, Van der Waals) vary with the molecular conformation in the solids. Hence, for the same compound, the enthalpy term is different among different polymorphs or for the amorphous solid. The entropy of mixing represents the driving force for an increase in the randomness or chaos of the system, and always favors mixing. Spontaneous mixing occurs when the free energy of mixing is negative.

The solution phase will be in equilibrium with the solid phase when the solution contains the amount of solute as limited by its solubility (s), which is temperature dependent. This parameter is usually measured at infinite time (e.g. 24hrs) when the equilibrium is reached. Under certain circumstances, the concentration of drug monomers in the solvent could exceed this limit. The system is said to be supersaturated. The degree of supersaturation, σ, is defined as:

$$\sigma = \ln\left(\frac{c}{s}\right) = \ln S \qquad 1\text{-}3$$

Where, c is the concentration of solute in the supersaturated solution, often referred to as apparent solubility, s is the equilibrium solubility, and S is the supersaturation ratio, respectively. The apparent solubility is often not directly measured due to the possibility of rapid phase conversion in solution. Instead, it is calculated from the following equation:

$$c = s \times \left(\frac{J_m}{J_s}\right) \qquad \text{1-4}$$

Where $J_m$ is the intrinsic dissolution rate of the metastable form, and $J_s$ is the intrinsic dissolution rate of the stable form.

The rate at which the drug dissolves from the solid state is referred to as the dissolution rate. It can be described by the Noyes–Whitney equation:

$$\frac{dC}{dt} = \frac{AD(C_s - C_t)}{h} \qquad \text{1-5}$$

Where dC/dt is the dissolution rate, A is the specific surface area of the drug particle, D is the diffusion coefficient of the compound, $C_s$ is the solubility of the compound in the dissolution medium, $C_t$ is the drug concentration in bulk solution, and h is the diffusion layer thickness. As can be inferred from this equation, the rate of dissolution of a low solubility compound can be increased by manipulating the parameters in this equation. The diffusion coefficient is dependent on the molecular weight of the compound and the viscosity of the luminal contents[6]. The diffusion layer thickness is dependent on the hydrodynamics in the GI tract. The physiological parameters are difficult to change from a formulation perspective. However, the surface area may be increased by particle size reduction (e.g. micronization). However, micronized particles have propensity to aggregate or agglomerate due to the high surface free energy, thereby negating the gains

achieved by the milling procedure. Surface tension is reduced in the presence of surfactants; solvent accessible particle surface area could be increased by improved wetting characteristics. In addition, improved wetting might also decrease the boundary layer thickness. Saturation solubility is dependent on both physiological parameters (e.g. pH, buffer capacity, bile, and food components) and physicochemical parameters (e.g. hydrophilicity, crystal structure and solubilisation). It could be increased by chemical modification of the drug molecule such as prodrug, salt or cocrystal formation. Alternatively, a high energy form (e.g. metastable polymorph, amorphous solid) may be employed to obtain a high apparent solubility. Nano particles may enhance the dissolution by both mechanisms: (1) increased surface area and (2) enhanced apparent solubility as a function of the high curvature for particles below 200um in size[7].

Evaluation of dissolution rate is extremely important for drug development, formulation, and quality control. There are two widely used methods in the pharmaceutical industry to compare the dissolution behavior of solids: powder dissolution and intrinsic dissolution. They are inherently different in several aspects: geometry, solution conditions, and hydrodynamics[8]. Dissolution data obtained from the two methods are analyzed in a different manner, yet are often complementary for interpretation.

In powder dissolution, solid particles are dispersed in dissolution medium which is agitated by a rotating paddle (USP II). In the absence of phase transformation, the dissolution profile will exhibit a continuous increase in solution concentration of the drug until a plateau is reached. The rate of dissolution is given by the Noyes-Whitney equation. When excess solids are added to the dissolution medium, solution concentration increases with time until the plateau concentration is observed which equals drug solubility. Such a

dissolution condition is known as a non-sink condition. In this case, dissolution is retarded by a concentration gradient. On the other hand, sink conditions are generated when the drug that can be dissolved in a given volume of the dissolution medium (as determined by its solubility) is at least 5-10 times greater than the amount of drug to be dissolved. The concentration of drug in bulk solution is thus always maintained at low level ($C_b \ll C_s$), so that the solution concentration does not affect the dissolution rate of the dissolving solids. To achieve this, a large volume of dissolution medium is required, or there must be a certain mechanism to replenish the medium. In vivo, whether sink condition is met is contingent on the composition and volume of luminal fluids as well as the permeability of the mucosa to the drug molecule.

In the presence of a solution mediated phase transformation during powder dissolution testing, the dissolution profile typically exhibits an initial peak concentration (supersaturation) followed by a decrease until a plateau concentration is reached, which equals the solubility of precipitated form. While powder dissolution testing maybe easy to set up and operate, it suffers from several disadvantages[8]. First, the hydrodynamics in the vessel are poorly characterized, varying throughout the vessel and being dependent on paddle speed. Such a variability in hydrodynamics may change the boundary layer thickness of the particles, and hence dissolution rate. Moreover, the surface area of particles also changes with time during a powder dissolution test. Many drug compounds are highly hydrophobic and particles tend to float and/or aggregate in the medium so that the solvent accessible surface area is variable. Finally, solution concentration maybe not uniform throughout the vessel.

The dissolution rate per unit area is the mass flux J, which is referred to as "intrinsic dissolution rate" in pharmaceutics. The quantity is given by:

$$J = \frac{d_m}{d_t}\left(\frac{1}{A}\right) = V\frac{d_c}{d_t}(\frac{1}{A})$$

1-6

Where, j is the mass flux (mg cm$^{-2}$ S$^{-1}$), m is the mass (mg), V is the volume of the dissolution medium, c is the concentration of dissolved drug in the medium (mg/ml), A is the surface area of the sample (cm$^2$), and t is time (s).

The rotating disk method (Wood's Die) is used to measure the IDR, where the drug is placed in a cavity and compressed. The geometry and exposed surface area of the drug are known. In addition, the intrinsic tendency for the material to dissolve can be assessed without formulation excipients. This apparatus also enables the drug to be exposed to lower hydrodynamic variability. The velocity components of fluid flow in a rotating disk apparatus are well defined and can be solved analytically[8]. Under normal operating rotation speed, the fluid flow is considered in laminar flow regime. The intrinsic dissolution rate from the compact is related to the solubility of the drug by:

$$J = 0.62D^{\frac{2}{3}}v^{-\frac{1}{6}}\omega^{\frac{1}{2}}C_s$$

1-7

Where D is the diffusion coefficient, $v$ is the kinematic viscosity, and $\omega$ is the angular viscosity of the die. In the absence of solution-mediated transformation, plotting the cumulative amount dissolved versus time yields a straight line passing through origin. The derivative (i.e. slope) of this line is the intrinsic dissolution rate. If the intrinsic dissolution rate is plotted versus time, the data points will vary randomly about the mean. When solution phase transformation occurs, the solubility of the drug at the surface of the

compact will decrease with time due to the precipitation of a more stable form. A curvature will be observed in the cumulative amount dissolved versus time plot. The intrinsic dissolution rate will decrease with time until a plateau is reached, which indicates that the phase transformation is complete.

### 1.3    Characteristics and Thermodynamics of Amorphous State

Solids can exist in either a crystalline or an amorphous state. The crystalline state is characterized by an ordered lattice structure. The interactions (e.g. hydrogen bonds and electrostatic repulsion) are repeated with regularity. On the other hand, amorphous materials show no long-range three-dimensional molecular order. However, they are not random at a molecular level. They possess local or short-range order over a few molecular dimensions[9]. They may exhibit regions of residual crystallinity and different density (Figure 1-2). Studies of indomethacin[10, 11] revealed that "structural elements" might exist in amorphous solids. Amorphous materials frequently share the same intermolecular bonds as their crystalline counterpart, but differ in range of disorder. The amorphous state can be treated as a precursor to the crystalline state[12].  In fact, the amorphous material has been employed as a starting point for designing crystallization screening procedures for new polymorphs of drug compounds.

Normally, when cooling a melt, there will be a transition from the liquid state to the crystalline state below the melting temperature. A discontinuity in enthalpy and volume exists and is indicative of a first order phase transition (Figure 1-3). Amorphous materials can be prepared by cooling of a melt at a rate faster than the molecules are able to organize

into the crystalline lattice below the melting point. This amorphous state is considered to be equilibrium "supercooled liquid" because it is energetically and structurally similar to a liquid. It is also commonly referred to as rubbery state due to its macroscopic properties, in particular in the polymer literature. In this region, the average timescale of molecular motion is typically less than 100s and the viscosity ranges from $10^{-3}$ to $10^{12}$ Pa s. Upon further supercooling, there is a change from the equilibrium supercooled liquid to a "kinetically frozen" nonequilibrium state with a higher enthalpy and volume than would have been expected for the supercooled liquid. The amorphous material becomes a brittle glass with very high viscosity ($>10^{12}$Pa s). This process is called vitrification. The temperature at the transition is the glass transition temperature ($T_g$), which is considered as a fingerprint of amorphous materials. The glass transition is a thermal event influenced by kinetic factors and therefore occurs over a range of temperatures. $T_g$ is thus dependent on operating conditions (heating/cooling rates), thermal history and purity of the sample[14].

In Figure 1-3, it can also be seen that there is a thermodynamic requirement for the supercooled liquid to undergo the glass transition. Otherwise, the supercooled liquid would attain an even lower enthalpy and volume than crystalline materials below a certain critical temperature. This would be paradoxical. This virtual temperature is known as Kauzmann temperature ($T_k$). It represents the lower limit for the glass transition and the point of zero configurational entropy of the system[15, 16].

The glass stability (GS) refers to the resistance of a glass to crystallize. However, this property is often determined by measuring the crystallization tendency in the supercooled region above $T_g$, which reflects the stability of the supercooled liquid rather than that of the glass. Therefore, the term GS is often a misnomer[17].

The glass forming ability (GFA) is defined as the ease of a material to be vitrified from the melt upon cooling. A common parameter to evaluate a material's GFA is the critical cooling rate ($R_{crit}$), defined as the minimum cooling rate needed for vitrification. High $R_{crit}$ values imply poor glass forming ability, whereas low $R_{crit}$ values indicate facile glass formation. Another important parameter determining GFA is the fragility[9]. It refers to the temperature dependence of a liquid to undergo physical changes above $T_g$. It is related to the structural relaxation kinetics and mechanisms of amorphous materials. The temperature dependence is described by the Vogel-Tammann-Fulcher (VTF equation):

$$\tau = \tau_0 \exp\left(\frac{DT_0}{T - T_0}\right) \qquad \text{1-8}$$

Where, $\tau$ is the mean molecular relaxation time (or viscosity), T is the temperature, $T_0$ is the zero mobility temperature, and $\tau_0$ is a constant. D is the strength parameter. The temperature dependence of viscosity of amorphous materials above $T_g$, $\eta$, is described by the Williams-Landel-Ferry (WLF) equation:

$$\eta = \eta_g \exp\{C_1(T - T_g)|[C_2 + (T - T_g)]\} \qquad \text{1-9}$$

$$C_1 = DT_0/(T_g - T_0) \qquad \text{1-10}$$

$$C_2 = T_g - T_0 \qquad \text{1-11}$$

Where, $\eta_g$ is the mean viscosity at $T_g$. From a plot of viscosity ($\log\eta$) or relaxation times ($\log\tau$) versus $T_g/T$ for $T > T_g$, materials are classified into strong liquids if the plot appears linear (quasi-Arrehenius), or fragile if a non-Arrehnius behavior is observed (Figure 1-4). Strong liquids have large D values ($>30$), higher viscosity (i.e. lower mobility) at $T_m$, and hence are more resistant to structural changes. Also, the change in heat capacity at $T_g$ is

relatively small. On the other hand, fragile liquids have lower D values (<10), lower viscosity at $T_m$, and are thus prone to structural reorganization. Many pharmaceuticals are found to be moderately fragile (D ranges from 7 to 15).

The quantity $T_b/T_m$ (where $T_b$ is the boiling temperature) is another well known predictor of glass forming ability for a given compound. As a thumb of rule, if $T_b/T_m$ is greater than 2, a glass can be formed at reasonable cooling rates, and vice versa. This is because a compound with low melting temperature tends to have weaker intermolecular force in the crystalline state whereas a high boiling point indicates stronger intermolecular forces in the liquid state. The crystallization tendency is therefore expected to be low for a compound with high $T_b/T_m$. Nevertheless, exceptions to this rule have been observed[18].

The chemical reactivity is another important factor in determining the optimal storage conditions and the shelf life for an amorphous drug product. The amorphous state of drug molecules exists at a higher energy than their respective crystalline forms, which provides sufficient free volume and molecular mobility for molecules to react as described by Arrhenius kinetics[9]:

$$k = A'exp[-\left(\frac{V^*}{V_f}\right) - \left(\frac{E_a}{kT}\right)] \qquad\qquad 1\text{-}12$$

Where $k$ is the rate constant, $A'$ a pre-exponential factor, $E_a$ is the energy of activation, $Vf$ is the free volume, and $V^*$ is the critical free volume for the molecular motion required for reactivity[9]. Indeed, when comparing the reaction rates of crystalline and amorphous forms of a drug under otherwise identical conditions, we have seen that amorphous forms have higher reaction rate than the crystalline forms in a number of systems.[19] [20]

1.4    Preparation of Amorphous Solids

Amorphous solids can be prepared in various circumstances and situations. The preparation

of an amorphous form is relatively easy for good glass formers but difficult for poor glass

formers. From a thermodynamic perspective, molecules that are poorly arranged and

contain many degrees of freedom are much more easily rendered amorphous. Kinetically,

a slow crystallization rate allows the material to become a "frozen liquid" or vitrify without

crystallization[21]. Amorphous materials might be deliberately prepared to utilize their

advantageous physicochemical or biological properties. They could also be inadvertently

induced by thermodynamic or mechanical stress in various unit operations, as shown in

Figure 1-5.

If amorphous conversion is required, there is merit in investigating the use of more than

one preparative technique since the susceptibility to amorphous conversion by mechanical

and thermal techniques is compound specific. Finally, local structure in the amorphous

phase is also a function of the preparation method and may affect the solid's physical-

chemical properties.

1.4.1    Grinding and Milling

The direct crystal to glass transformation by milling involves supplying energy to excite

an equilibrium crystal and "freeze" it in an energized metastable amorphous state. The

mechanical activation leads to disruption of the crystalline lattice and an amorphous state

is formed via a solid state transition. The effectiveness of ball milling is dependent on the

unit cell structure of the compound. Patterson et al studied the influence of ball milling on

dipyridamole, carbamazepine, glibenclamide, and indomethacin[19]. Ball milling resulted in

predominantly amorphous products for all compounds except carbamazepine. Ball milling of carbamazepine resulted in a polymorphic transition of the starting material to form III while an alternative approach of quench cooling was successful in preparing amorphous carbamazepine. The resistance to the shearing force imparted by the milling might be due to the formation of an intracellular and intermolecular hydrogen bonded dimer which is perpendicular to the other molecules in the unit cell (Figure 1-6).

Whilst milling avoids the high thermal stress of melting and quench cooling, the free excess enthalpy induced by mechanical activation has been shown to accelerate chemical degradation. Key process parameters that might affect the physical or chemical state of the ground product include: (I) Type of milling apparatus; (II) Intensity; (III) Duration; (IV) Temperature; (V) Use of excipient.

## 1.4.2   Vitrification

Vitrification, also known as quench cooling, is the most frequently used procedure of converting a material into a glass-like amorphous solid that is free from any crystalline structure, by cooling the molten phase below glass transition temperature. In melting, the amorphous state is obtained via the liquid state. If the solidification process is fast enough the molecules do not have time to rearrange themselves into a regular array and, thus, an amorphous state is formed. The drawback of this approach is its potential for chemical degradation during the melting step. Thermal degradation is compound dependent and only limited steps can be taken to overcome this problem such as heating under an inert gas. Cooling rate is critical in the preparation and is dependent on the spontaneous tendency of

the compound to crystallize, which is partially determined by the conformational diversity existing in the liquid phase[20].

### 1.4.3    Lyophilization

Lyophilization, also known as freeze drying, works by freezing the material and then reducing the surrounding pressure and adding enough heat to allow the frozen water in the material to sublime directly from the solid phase to gas. In freeze drying, as well as in spray drying, an amorphous phase is created through a solution state. Fast evaporation of the solvent can lead to formation of amorphous particles. There are three stages in the complete freeze-drying process: freezing, primary drying, and secondary drying. Amorphization is more likely to occur when the freezing step is rapid and performed at liquid nitrogen temperature to prevent nucleation. Another critical step is the secondary drying, since crystallization is likely to occur in the presence of residual solvent when the temperature is high enough.

### 1.4.4    Spray Drying

By exposure to a heated atmosphere, materials are rapidly dried from a concentrated solution or a suspension. A liquid phase is first atomized to obtain a maximal surface area in contact with the drying gas since drying occurs within seconds. Spray drying can alter biopharmaceutically relevant drug properties. It differs from lyophillization in that spray drying could produce uniform spherical particles of desired size. As a result, the powder obtained usually has good flow properties. However, an amorphous solid obtained from spray drying may be unstable and prone to crystallization. Savolainena et al[22] examined

molecular-level differences in the amorphous state of indomethacin prepared from both α and γ polymorphs using various preparative techniques: milling, quench cooling of a melt, slow cooling of a melt and spray drying. According to the X-ray powder diffraction (XRPD) and polarized light microscopy (PLM) measurements, all samples except the spray dried indomethacin were amorphous after preparation. Spray dried indomethacin had some residual crystallinity.

## 1.5 Characterization of Amorphous Material

There are many methods to analyze amorphous and crystalline materials. Powder x-ray diffraction (PXRD), differential scanning calorimetry (DSC), Fourier transform infrared spectroscopy (FTIR), solid-state nuclear magnetic resonance (ssNMR) are some of the most popular ones. The basic principles of these methods will not be discussed, however information about how some of these methods can be applied will be provided, using an example where DSC has been employed to study the molecular mobility and the relative stability of the amorphous material. Another method discussed is the use of Raman Microscopy to evaluate surface amorphization.

It has been observed that the $T_g$ occurs in a temperature range that is about 2/3 of the melting point in Kelvin. This observation can be used to estimate $T_g$ from $T_m$ or vice versa. If both these values are known then one can estimate the deviation from this rule, which reflects the temperature dependence of molecular motions in the region just above $T_g$. If the $T_g/T_m$ is significantly greater than 2/3, then the material is likely to have a greater than average temperature dependence of its molecular mobility in the region of $T_g$ and vice versa. Conventional DSC can be used to construct a semi-quantitative diagram of the

excess enthalpy versus temperature. $T_m$, $T_g$, $\Delta H_f$ and $T_g$ can be obtained from DSC measurements. In addition, modulated DSC facilitates the measurement of heat capacities (which, is a measure of molecular motions). Shamblin et al[23] found that the $\Delta C_p^{Tg}$ increased significantly as the material was heated through its $T_g$ (Figure 1-7). This is significant in studying disorder created from different processes as they have shown for freeze dried and quenched cooled sucrose.

Therefore the temperature dependence of key thermodynamic properties can be determined for new materials. These plots will indicate whether the amorphous material has $T_g$ above or below the normal storage and processing temperature. Hence for materials where the $T_g$ is significantly above normal operating temperatures, there should be a reasonable chance of being able to produce and retain a stable amorphous material. On the other hand, materials which have $T_g$ values below ambient temperature are often hard to produce and maintain in an amorphous state[23].

Sometimes the undesirable characteristics introduced by the amorphous phase are due to modifications of interfacial properties[24]. Inhalation devices provide an important example in which amorphous material at the surface of an active or excipient causes alteration of adhesion and cohesion, thus changing performance[24]. In addition, it seems likely that surface amorphous material may be less stable due to its exposure to moisture and the atmosphere, further adding to the importance of detecting its presence.

Vibrational spectroscopy such as Raman Microscopy provides information on the depth of amorphous material present through peak broadening /shifts in the spectra. In one study, Raman spectra of crystalline and glassy, quench cooled sorbitol were analyzed (Figure 1-8). The glassy state is characterized by broader peaks and loss of fine spectral structure[24]. In

particular, the broadening of the peak at 878 cm$^{-1}$ assigned to the C-C-O stretch showed an increase in full-width at half maximum from 15 (crystalline) to 34 cm$^{-1}$ (glassy) and so provided an intensity-independent method of mapping for sorbitol degree of crystallinity.

### 1.6 Solubility Advantage of Amorphous Solids

The excess internal energy and volume of the amorphous state as opposed to the crystalline state can lead to enhanced dissolution and bioavailability. According to Lipinski et al[25], the solubility (s) of a solid solute is a function of three basic quantities:

$$s = f\ (Crystal\ Packing\ Energy + Cavitation\ Energy + Solvation\ Energy) \tag{1-13}$$

The first major huddle for solubilization of crystalline solid is the energy required to disrupt molecular packing. On the other hand, amorphous solid exhibit no long range order packing, and hence no such energy barrier. For this reason, amorphous solid often show higher solubility than crystalline solid. For the same compound, the solubility ratio between amorphous solid and crystalline solid (4-14) is much higher than that between the crystalline polymorphs (2-3)[26]. Some well-known examples of amorphous to crystalline solubility ratios are nefidipine (~6)[27], ritonavir (~10)[28], and tolbutamide (4-6)[29]. Theoretically, the free energy difference ($\Delta$G) between the amorphous and crystalline forms can be calculated by the Hoffman equation[30]:

$$\Delta G = \Delta H_f \frac{(T_m - T)T}{T_m^2} \tag{1-14}$$

Where $\Delta H_f$ is the enthalpy of fusion, $T_m$ is the melting temperature, and T is the temperature of interest. The solubility advantage of the amorphous form can then be estimated by the following equation:

$$\frac{\sigma^{amorph}}{\sigma^{crystal}} = e^{\frac{\Delta G}{RT}}$$

1-15

Where $\sigma^{amorph}/\sigma^{crystal}$ represents the ratio of amorphous solubility to crystalline solubility. Hancock et al[31] predicted that amorphous materials can be 10-1600 times as soluble as their crystalline counterparts. Experimental determination of the solubility advantage of amorphous solids is impeded due to the frequent rapid conversion to crystalline state upon dissolution. Furthermore, it has been pointed out[32] that this model did not take into account either the effect of ionization of the drug or water sorption by the amorphous material on the free energy difference. Once correction factors are incorporated into the equation, a good agreement can be sometimes attained between the prediction and measured ratios.

For indomethacin[31], the solubility ratios predicted are listed in Table 1-2. The experimental solubility of amorphous indomethacin is consistently higher than that of the crystalline γ form at room temperature as shown in Figure 1-9. Maximum solubility is achieved at about 10 minutes, and this value is about 5 times the solubility of the γ form. The desupersaturation is attributed to the partial recrystallization of indomethacin from the metastable amorphous phase to a more stable crystalline phase. The experimental solubility ratio of amorphous versus the γ form is significantly lower than the theoretical estimate, which is due to the rapid crystallization tendency of indomethacin when exposed to the dissolution medium. Despite this discrepancy, the calculated value represents the

theoretical thermodynamic driving force for supersaturation in solution, and may be used to compare different drugs and amorphous systems.

Mullins and Macek[33] found that for novobiocin free acid, the amorphous form was at least 10 times more soluble than the crystalline counterpart when excess solids ($< 10\,\mu$m) of either form were shaken in 0.1N HCL at 25 °C. The in vivo studies (dose=12.5mg/kg) showed that novobiocin could not be detected in plasma when the crystalline form was administered. In contrast, the plasma level of novibiocin reached 40ug/ml after 1hr when administered in amorphous form. However, the amorphous novobiocin in suspension was observed to slowly crystallize and hence lost therapeutic effect. Several agents including methylcellulose, polyvinylpyrrolidone and sodium alginate were found to be able to provide adequate inhibition against crystallization over significant periods of time.

For injectable insulin, the duration of action is controlled by both the degree of crystallinity and the particle size. The amorphous insulin zinc complex is used in Prompt Insulin Suspension USP to provide immediate effects and have a short duration of action. The Extended Insulin Zinc Suspension USP is made up of a crystalline zinc complex. It is slowly absorbed and has a long duration of action. The Insulin Zinc Suspension USP contains a mixture of three parts amorphous and seven parts crystalline form to provide an intermediate duration of action. These formulations also differ in particle size. Large particles are formulated in prompt insulin whereas extended insulin is made up of small particles.

There are also advantages in using the amorphous form of a drug for toxicological studies, even if the final form used in the product is crystalline. Higher blood levels are expected from an amorphous compound. Therefore, toxicological data obtained using an amorphous

compound represent the "worst case" scenario and should be predictive of clinical toxicity independent of the solid form selected for the drug product.

Atorvastatin is a synthetic lipid-lowering agent. It is used as calcium salt to treat hypercholesterolemia. It exhibits high intestinal permeability over the physiologically relevant intestinal pH[34, 35]. Corsini et al[36] reported that the absolute bioavailability of Atorvastatin is as low as 12% after an oral dose of 40mg. The oral bioavailability is limited by its low aqueous solubility. Kim et al[37] prepared amorphous atorvastatin hemicalcium by spray drying and supercritical anti-solvent process (SAS). They exhibit similar maximum supersaturated concentrations (460~480 μg/ml), followed by a gradual decrease until a plateau is reached (~200 μg/ml) due to solvent mediated phase transformation. In contrast, the unprocessed crystalline particles reached its equilibrium solubility (only 140 μg/ml) rapidly. This is consistent with the intrinsic dissolution results where the spay-dried and SAS processed drug exhibit similar intrinsic dissolution values (both initial phase and late phase), much higher than that of unprocessed drug. This is because there is no particle size effect in intrinsic dissolution testing. Assuming hydrodynamic conditions are identical, the intrinsic dissolution rate is proportional to the solubility of each form. In the powder dissolution test, enhanced dissolution rate is observed for all processed particles as compared to unprocessed atorvastatin (Figure 1-10). In addition, the SAS processed particles exhibited superior dissolution performance to that of spray-dried particles, which was attributed to difference in their particle size, as summarized in Table 1-3[37].

In good agreement with the results from in vitro study, the rank order of the AUC under the plasma concentration-time curve is: SAS processed particles >spray dried particles>unprocessed particles (Figure 1-11). Therefore, the improvement of

bioavailability by SAS process is a consequence of combined benefits of high energy amorphous form and increased surface area.

### 1.7 Structural Relaxation and Crystallization from Amorphous Solids

Despite its higher dissolution rate and kinetic solubility, the amorphous state is inherently unstable due to its excess internal energy. The energy excess can be either partially relieved through the mechanism of irreversible structural relaxation or completely released by converting back to the thermodynamically stable crystalline counterpart (i.e.devitrification)[32]. Molecular mobility is an important factor that determines the physical stability of the amorphous material. It is often related to the viscosity of the system by the Stokes-Einstein equation:

$$D = \frac{kT}{6\pi\eta a}; D = \frac{x^2}{2\tau}$$  1-16

Where T is temperature, D is the translational diffusion coefficient at that temperature, k is the Boltzmann constant, $\eta$ is viscosity, a is the hydrodynamic radius of the diffusing species, x is the so called "jump distance" and $\tau$ is the diffusion correlation time. As temperature decreases, the viscosity increases. This results in a smaller D, which means a slower molecular diffusion. The time for molecules to diffuse a certain path length, x, increases. Any physical changes, be it crystallization or structural relaxation, requires molecules to go through a few diffusional jumps of those path lengths[32]. Hence a slower molecular motion leads to better physical stability and vice versa. Figure 1-12 illustrates different types of physical changes undergone by amorphous materials on annealing. Molecules may diffuse in the material to arrange themselves to a less chaotic amorphous state (Glass 2)

over a long period of time. This state has a lower volume, lower entropy and enthalpy than the original amorphous state (Glass 1), and hence is more stable and relatively more difficult to crystallize. Alternatively, molecules may move throughout the entire system and rearrange into a highly ordered crystalline lattice structure. It is also possible for molecules to have different substates and level of mobility (Figure 1-2), which depends on how they were configured initially during preparation. This may result in a localized crystallization from regions where molecules are highly mobile.

Devitrification consists of two sequential steps: (1) stable nuclei are formed after certain lag time, (2) these nuclei grow into crystals. Despite the difficulties of achieving homogeneous nucleation in large volumes of a sample, the Classical Nucleation Theory remains the first estimation of nucleation kinetics. The thermodynamic driving force for nucleation is the free energy difference of the liquid phase and the crystalline phase:

$$\Delta\mu(T) = \int_{T}^{Tm} \left[\frac{\partial \Delta\mu(T)}{\partial T}\right] dT = -\int_{T}^{Tm} \Delta S(T) dT \qquad \text{1-17}$$

Where $\Delta\mu$ is the difference in the chemical potential between the crystalline and the liquid phase, $\Delta S(T)$ is the difference in the molar entropies between the crystal and the supercooled melt and the T is the temperature in Kelvin. The clusters may aggregate or decay until a stable nucleus of critical radius ($r_c$) is formed:

$$r_c = \frac{2\gamma T^*}{\Delta H_f \Delta T} \qquad \text{1-18}$$

Where, $T^*$ is the solid/liquid equilibrium temperature in Kelvin, $\gamma$ is the interfacial tension at the nucleus-liquid interface. $\Delta T$ (=T*-T) is the degree of supercooling, and $\Delta H_f$ is the

latell heat of fusion. The critical overall excess free energy (including both the surface and bulk contribution) needed to form a stable nucleus is:

$$\Delta G_{cr} = \frac{4}{3}\pi\gamma r_c^2$$

<div align="right">1-19</div>

The rate of nucleation is:

$$J = Aexp(\frac{-16\pi\gamma^3}{3KT * \Delta H_f^2 T_r (\Delta T_r)^2} - \frac{\Delta G'}{kT})$$

<div align="right">1-20</div>

Where, J is often denoted as $I_{ss}$, the nucleation rate at steady state. A is the frequency factor independent of temperature, $T_r = (T/T^*)$, $\Delta T_r = (\Delta T/T^*) = 1 - T_r$. $\Delta G'$ is the kinetic barrier for nucleation. It is the activation free energy for molecules to diffuse in the matrix, and is related to the viscosity of the system.

Nucleation is thermodynamically favorable at low temperatures (i.e. higher degree of supercooling) while kinetically favored at higher temperature due to greater molecular mobility (lower viscosity). The shape of the curve for nucleation rate ($I_0$) clearly demonstrates this balancing effect of temperature (Figure 1-14)

A limitation of CNT is its assumption of constant nucleation rate for spontaneous nucleation. New models have been developed to account for the time dependent nature of nucleation rate as shown in Figure 1-13. There is a lag time before a steady state distribution of clusters of critical size $j_c$ is reached. During that lag time, the nucleation rate for the formation of clusters of critical size $j_c$ is time dependent, and is always slower than the steady state nucleation rate that is time independent. Nevertheless, there will be an inevitable decrease of nucleation rate at a certain time after steady state is reached. It occurs when most of the system has become nucleated. This applies to not only the nucleation

kinetics of glasses during storage, but also to that of a supersaturated solution. More specifically, as nucleation proceeds in a supersaturated solution, the degree of supersaturation decreases, which in turn results in a decrease in nucleation rate.

Once the nucleation barrier is surmounted, the nuclei so formed grow into macroscopic crystals. Whereas the presence of nuclei cannot be easily detected experimentally, the growth kinetics can be readily determined based on observations from a microscope. The growth rate of a crystal, U, is described in the following equation[11]:

$$U = \frac{CTw}{\eta}\left[1 - \exp(-\frac{\Delta G_v}{kT})\right]$$
<div style="text-align:right">1-21</div>

Where C is a constant, T is the temperature in Kelvin, and $\eta$ is the viscosity, which indicates molecular mobility. $\Delta G_v$ is the free energy difference between the amorphous and the crystalline phase, w is a constant that describes the growth mechanism, and k is Boltzmann constant. For a typical glass former[38], the temperature dependence of nucleation ($I_0$), crystal growth (G), non-steady state lag time for nucleation ($\tau$) is shown in Figure 1-14. Equation 1-20 and 1-21 suggest different temperature dependencies of nucleation and growth. Thermodynamically, nucleation is favorable at lower temperature (i.e. high degree of supercooling), whereas crystal growth is favorable at higher temperature (i.e. low degree of supercooling). Significant crystallization can only occur in a temperature zone located between $T_g$ and $T_m$ where the two processes overlap.

For many amorphous materials, significant crystallization is observed above $T_g$. However, it has also been shown that crystallization can occur below $T_g$[39, 40]. It has been recommended that a storage temperature of at least 50 °C below $T_g$ is used for amorphous drugs to minimize risks of phase conversion. Determining $T_g$ is advisable for designing a

crystallization protocol as well as for preventing the occurrence of phase transformation. For binary mixtures, the $T_g$ of the mixture ($T_{g,mix}$) can be estimated by the Gordon Taylor equation[41]:

$$T_{g,mix} = \frac{w_1 T_{g,1} + k w_2 T_{g,2}}{w_1 + k w_2} \qquad 1\text{-}22$$

Where w is the weight fraction, and the constant k can be calculated by the Simha-Boyer rule[42]:

$$k = \frac{\rho_1 T_{g,1}}{\rho_2 T_{g,2}} \qquad 1\text{-}23$$

Where, $\rho$ stands for the density of individual component. The Gordon Taylor equation assumes no specific interactions between the two components. Deviation from prediction often indicates non-ideal mixing that results from complex formation[43]. The Couchman-Karasz model is equivalent to Gordon-Taylor equation, where k is replaced by:

$$k = \frac{\Delta C_{p2}}{\Delta C_{p1}} \qquad 1\text{-}24$$

where $\Delta C_{pi}$ is the change in heat capacity at glass transition events for pure component i. Therefore, equation 1-22 becomes:

$$T_{g,mix} = \frac{w_1 \Delta C_{p1} T_{g1} + w_2 \Delta C_{p2} T_{g2}}{w_1 \Delta C_{p1} + w_2 \Delta C_{p2}} \qquad 1\text{-}25$$

Baird et al[17] observed the presence or absence of crystallization during cooling and reheating for 51 organic molecules from undercooled melt state. These compounds were classified into several categories with the rank order of crystallization tendency: IA>IB>II>III. Specifically, class IA compounds crystallize at both a moderate cooling rate

by DSC and a rapid cooling rate by immersion in liquid $N_2$. Class IB compounds can crystallize on moderate cooling, but can also be kinetically frozen in the amorphous state (at least partially) by rapid cooling. It has been hypothesized that a higher cooling rate would result in a larger degree of undercooling before crystallization is observed, and the $R_{crit}$ can be estimated by the Barandiaran and Colmenero (BC)[44] and Cabral[45] methods. It turns out that this model works for some of the class I compounds ($r^2>0.7$). However, for some other class I molecules tested, the degree of super-cooling did not show such dependency on their range of cooling rate (from 5 ℃ /min to 20 ℃ /min) applied by DSC. This was attributed to the stochastic nature of nucleation process and the inevitable occurrence of heterogeneous nucleation. Class II compounds do not crystallize upon cooling to below $T_g$, but were able to crystallize when subsequently reheated to above $T_g$. Class III compounds fail to crystallize either on cooling to below $T_g$ or on reheating to $T_m$ at 10 ℃ /min. No $R_{crit}$ could be estimated for Class II or III compounds since they do not crystallize on cooling. Not unexpectedly, all of the class II and III compounds are moderately fragile or fragile liquids (D ranges from 1 to 11). The fact that class I compounds have a higher tendency to crystallize upon cooling from the undercooled melt state indicates its lower GFA than class II and III compounds. Glass stability was evaluated by observing the crystallization of the amorphous samples of several selected molecules of each class stored below their $T_g$s. The cross-polarized light optical images of those samples indicate class I has the lowest GS, class III has the highest GS, and the GS of class II falls in between. The GS also correlated well with the stability of samples when reheated above $T_g$. Moreover, there seems to be a positive relationship between the GS and GFA. For class II and class III molecules, it is thought that their nucleation zone and growth zone are more

separated[46], whereas there is a large overlap of the two zones for class I molecules (Figure 1-15)

This explains why only class I molecules crystallize on moderate cooling. The fact that class IB and class II molecules are able to crystallize upon reheating whereas class III molecules are not can be explained as following. The nucleation process is inherently a much faster process than crystal growth. If the cooling rate is higher than the $R_{crit}$, but lower than the minimum cooling rate required to inhibit the formation of nuclei ($R_{Ncrit}$) , the nuclei will be quenched in the "glassy" material during cooling and only able to grow when reheated to the growth zone where there is sufficient molecular mobility. Whereas it is not easy to detect the formation of nuclei experimentally, the overall crystallization upon reheating can be analyzed without difficulty.  Finally, the magnitude of the nucleation and growth zone and the extent of their overlap might be cooling rate dependent. Class IA compounds have a higher $R_{crit}$ than Class IB compounds. The cooling rate achievable by DSC is slower than the $R_{crit}$ and $R_{Ncrit}$ of both class IA and class IB. However, cooling by liquid $N_2$ is slower than the $R_{crit}$ and $R_{Ncrit}$ for class IA, but larger than $R_{crit}$ and less than $R_{Ncrit}$ for class IB.

In order to investigate the relationship between the physicochemical properties of the compounds with the observed crystallization tendency of each class, a principal component analysis (PCA) was performed. They found that larger and more flexible molecules tend to be in class III, whereas smaller and more rigid molecules tend to be in class I. During cooling from the undercooled melt state, it is relatively difficult and therefore takes more time for class III molecules to find the right conformer out of all the conformers in the amorphous matrix and arrange them into the ordered crystalline lattice structure. Hence,

those molecules can be easily trapped in the glassy state. The structural difference of different classes is also reflected in the measured thermodynamic parameters. Class III molecules on average tend to have a lower melting temperature which means lower energy is needed for disrupting the crystal lattice. They also have a lower heat of fusion and entropy of fusion implying lower energy difference between the crystalline and the amorphous state and thus a lower thermodynamic driving force for crystallization.

Trasi et al[46] showed how to experimentally determine the nucleation zone of a class II compound, acetaminophen. In that study, samples were heated to just above the melting temperature of the drug and subsequently cooled to different temperatures. The upper limit of the nucleation zone was taken as the highest temperature to which the sample was cooled when recrystallization was observed upon reheating. It was expected that the number of quenched nuclei in the amorphous sample will affect the recrystallization temperature. Hence the temperature, cooling below which, no significant change in peak recrystallization temperature was observed, was considered as the lower limit of the nucleation zone (Figure 1-16). The relative height of the nucleation zone was determined by visually counting the number of crystal growth spots in a specified volume of the sample. The nucleation zone of acetaminophen was 50-60 ℃, and the recrystallization exotherm was not observed until the temperature reaches around 80 ℃ in the reheating step. Hence for acetaminophen, the nucleation zone and growth zone appear to be well separated.

## 1.8    Amorphous Solid Dispersions

Amorphous materials can be single chemical entities (e.g. an API or an excipient) or molecular-level binary mixtures (e.g., drug-polymer solid dispersions), as illustrated in

Figure 1-17. As compared to single component amorphous drugs, solid dispersions may exhibit optimum stability and dissolution profiles.

Polymers are often incorporated into the amorphous matrix to stabilize amorphous drugs. They have been extensively used in amorphous formulations. Several well known examples are cellulosic polymers such as hydroxypropyl methylcellulose (HPMC), and water soluble synthetic polymers such as polyethylene glycol (PEG) and polyvinylpyrrolidone (PVP). Selecting the optimal polymer is vital for the success of a solid dispersion strategy. Janssens et al[6] summarized several important criteria for carrier selection, given in Table 1-4. A list of commercially available solid dispersions and the polymers used is given in Table 1-5.

Currently, the methods for manufacturing solid dispersions can be generally divided into two categories:

1. Hot melt extrusion

A twin-screw extruder is typically used for hot melt extrusion (Figure 1-18)[6]. A physical mixture of drug and carrier is melted together, homogenized and then extruded and shaped into pellets, granules and sheets. Conventional tablets can be produced after further processing these intermediates. Hot melt extrusion method offers considerable advantages over the solvent based methods. First, processing in the absence of solvents and water is beneficial for both economic and ecologic reasons. Second, realization of a continuous process reduces the number of unit operations and the production time. Better content uniformity can be obtained by further processing granules of different size ranges. There are also several disadvantages associated with this method. The miscibility of the API and the carrier in the molten state is a prerequisite to the manufacture of amorphous solid

dispersions by hot melt extrusion. In addition, the flowability of the polymer is essential to processing. Another important limitation is that it cannot be applied heat-labile drugs owing to the elevated temperature involved.

2. Solvent method

The drug and the carrier are dissolved in a common solvent, which are then removed by spray drying or freeze drying, resulting in a solid dispersion. A prerequisite for the application of this method is that both components are sufficiently soluble in the solvent. Polymers that cannot be utilized in hot melt extrusion due to their high melting point (e.g. PVP) can now be considered in the solvent based methods. The typical temperature range of solvent evaporation is 23-65 ℃[48, 49]. The complete removal of organic solvent is critical due to the toxicity concerns.

## 1.9  Crystallization Inhibition by Polymers during Storage

The amorphous drug may undergo irreversible crystallization during storage, and thereby negating its solubility advantages over the crystalline form. However, presenting the compound as a molecular dispersion by addition of a polymeric carrier may significantly postpone this process.  Several mechanisms have been proposed to be responsible for crystallization inhibition by polymers, and no consensus has been reached thus far. Amorphous polymers have high $T_g$s relative to small molecule drugs, and therefore are considered as anti-plasticizers. The molecular mobility of the mixture is decreased, as reflected in an increase of the $T_g$ of the mixture, and thereby crystallization is delayed. Yoshioka et al[43] found that amorphous indomethacin ($T_g$=50 ℃) crystallizes rapidly at temperatures above 30 ℃. In contrast, when indomethacin is dispersed with a low level of

PVP (5%) and stored at up to 50 °C, an induction period of more than 20 days is required for crystallization to initiate. The contribution of any anti-plasticizing effect is minimal, as reflected by only a 5 °C increase in $T_g$. There might be other mechanism(s) responsible for crystallization inhibition. This postulation was further supported by a case[50] of reduced tendency of the amorphous drug in the solid dispersion to crystallize where the $T_g$ of the dispersion is lower than that of the drug alone. In this study, the $COO^-Na^+$ group of the drug was found to form an ion-dipole interaction with the cyclic amide group of PVP. Taylor et al[10] investigated the intermolecular interactions between PVP and indomethacin using vibrational spectroscopy. The γ form of indomethacin consists of cyclic dimers due to the formation of hydrogen bonding between carboxylic acid groups. In α form, however, the carboxylic acid groups hydrogen bond to form a chain structure. The amorphous form mainly consists of cyclic dimers and a small fraction free groups. In the solid dispersions, the amide carbonyl group of PVP could hydrogen bond with the acid group of indomethacin (Figure 1-19). Therefore, dimer formation in indomethacin, a prerequisite for nucleation, is effectively blocked. In contrast, in a physical mixture of amorphous indomethacin and PVP, no such interaction was found. Similarly, Gupta et al[51] have shown that hydrogen bonding interactions exists between celecoxib and PVP in solid dispersions using computer simulation.

Miyazaki et al[52] investigated the crystallization of amorphous acetaminophen (ACTA) and solid dispersions of ACTA with PVP and with PAA. In the non-isothermal DSC experiments, ACTA does not crystallize when dispersed in 5% PAA whereas crystallization occurs even in the presence of 10% PVP. In the isothermal studies, samples were stored at 40 °C. In the dry state, it takes more time for 10% of ACTA to crystallize

($t_{90}$) when ACTA is dispersed in either polymer than pure amorphous ACTA. The $t_{90}$ increases as the mass fraction of polymer increases. At the same mass fraction, PAA is more effective in raising $t_{90}$ than PVP. The enthalpy relaxation time is also prolonged due to the presence of polymer: 247hr for ACTA/PAA (9:1), 84hr for ACTA/PVP (9:1), and 47hr for ACTA, indicating the effect of polymer on reducing molecular mobility. The fact that ACTA crystallizes faster in PVP than PAA with a similar $T_g$ suggests that in addition to decreasing molecular ability, polymers may interact with ACTA. The interaction between the carbonyl group of PVP and the hydroxyl group of ACTA is weaker than the interaction between the carboxyl group of PAA and the hydroxyl group of ACTA. However, in the case of ketoconazole dispersed in PVP-K25[53], FT-IR and C13 NMR results indicated no interaction between the drug and polymer. The crystallization inhibition was solely attributed to anti-plasticizing effect of the polymer.

Konno et al[54] measured the nucleation rate of amorphous felodipine dispersed in PVP, HPMC, and HPMCAS, respectively. In this study, water was rigorously excluded from the system during sample preparation as well as storage. Thermal analysis suggests that the $T_g$ of PVP dispersions increases as the polymer fractions increases, close to what is predicted by the Gordon Taylor equation. In contrast, there were negative deviations from predictions of this equation for HPMC and HPMCAS dispersions, which implies that the polymer-drug interaction is weaker than the sum of the drug-drug interaction and polymer-polymer interaction in HPMC and HPMCAS dispersions. Spectroscopic analysis proves that the rank order of hydrogen bond strength between the polymer and drug were stronger in PVP dispersions than in HPMC and HPMCAS dispersions. There was essentially no change of $T_g$ for the HPMC or HPMAS dispersions at the polymer compositions employed for the

nucleation rate experiments (0 to 25% w/w). However, the abilities of all three polymers to inhibit nucleation were similar, which indicates that an anti-plasticizing effect is not the only factor that comes into play.

Instead, the change in nucleation rate was attributed to the ability of polymers to raise the kinetic barrier to nucleation ($\Delta G'$ in equation 1-20). Polymers may act as diluents to slow the diffusion of drug molecules, which is evidenced by a decrease in nucleation rate as the polymer fraction in the solid dispersions is increased. However, the disproportional change (1.5 orders of reduction in nucleation rate at only 3% as compared to 2.5 orders of reduction at 25%) indicates that the diluent effect is not the only mechanism (Figure 1-20). In addition, they suggested that polymers are excluded as felodipine crystallizes and thus accumulates to form a layer surrounding the growing crystal. Drug concentration in this layer is low, and hence an increase in $T_g$ occurs. A reduction in molecular mobility results in slower mass transport of drug molecules to the crystal. Finally, the presence of such a polymer rich layer may also raise the energy required to form new surface.

Trasi et al[46] studied the relative impact of selected polymers on nucleation versus crystal growth of the supercooled melt of acetaminophen. At the composition (10%) of polymer used in the study, all polymers had little effect on raising $T_g$. However, these polymers had differing levels of impact on crystal growth (Figure 1-21). Therefore an anti-plasticizing effect, again, is not required for growth inhibition and does not correlate with growth rate data. Interestingly, the most effective polymer in reducing the nucleation rate, HPMCAS, was found to be the worst growth inhibitor. On the other hand, the best crystal growth inhibitor PAA significantly increased the nucleation rate. However, PAA was the most effective polymer in lowering the temperature where nucleation occurred (Figure 1-22).

These results demonstrate that polymers may stabilize amorphous drugs by selectively inhibiting nucleation or growth or both. A better understanding and differentiation might potentially facilitate the development of a more robust amorphous formulation.

Moisture is ubiquitous and water is always the third component in any solid dispersions. Crystalline solids adsorb water by a surface adsorption mechanism[55]. Amorphous solids are more hygroscopic than their crystalline counterparts due to their disordered structure and free volume. In addition to surface adsorption, water may penetrate into the bulk of amorphous materials. The $T_g$ of water is as low as 136K. When absorbed by amorphous solids, water acts as a strong plasticizer, effectively lowering the $T_g$ of the system. For example, it has been shown that 1% water lowers the $T_g$ of indomethacin by 10 ℃ [56]. A reduction in $T_g$ increases the molecular mobility and free volume, and hence destabilizes amorphous materials[57]. Polymers used in solid dispersions are typically much more hydrophilic in nature than the API. They tend to have more polar groups to interact with water (i.e. hydrogen bonding). In solid dispersions, the amount of water sorbed by the system is mainly dependent on polymer chemistry/hygroscopicity. Therefore, it is of interest to investigate when a solid dispersion is exposed to moisture, the competing effect of polymers as anti-plasticizers to inhibit crystallization and the plasticizing effect due to the ability of polymers in the dispersion to sorb water. It was found that even though amorphous felodipine is not very hygroscopic, a small amount of sorbed water still caused significant increase in nucleation rate[58]. When dispersed in polymeric carriers, hygroscopicity of the system increased and the $T_g$ decreased as expected. Despite the increased moisture uptake, a reduction in nucleation is still observed as compared to drug

alone. Nevertheless, the ability of the polymers to inhibit nucleation is weaker in the presence of moisture than at dry conditions.

## 1.10 Crystallization from Solution: Theory

Crystallization in solution is a complex process involving several steps. First, a supersaturated solution is formed and the system is in a non-equilibrium state. Then solute molecules diffuse through bulk solution, collide with each other to form clusters, which is accompanied with a concentration (density) fluctuation. These clusters increase their size by addition of one monomer at a time. This eventually leads to the formation of nuclei, defined as the minimum amount of new phase that could exist independently inside a large volume of the old phase. Indeed, nucleation is a decisive step that determines the structure and size distribution of the crystals.

From a thermodynamic point of view, the free energy of the initial solution phase exceeds the sum of the free energy of crystalline phase and final solution phase. In terms of nucleation, the free energy change required for the formation of clusters is:

$$\Delta G = \Delta G_v + \Delta G_s$$

1-26

Where $\Delta G_v$ is the volume free energy change associated with phase transformation. It represents the spontaneous tendency for desupersaturation. It is a negative quantity and reduces the free energy of the system. $\Delta G_s$ is the free energy change due to the formation of a solid/liquid interface. It is a positive quantity and increases the free energy of the system. The growth of the clusters depends on the competition between $\Delta G_v$ which favors growth, and $\Delta G_s$ which favors dissolution. This can be understood by the diagram shown below.

Initially, as clusters of small radii are formed, the surface contribution dominates. This causes an increase in the total free energy change. Hence the smallest clusters usually dissolve. There exists a critical cluster radius where the total free energy change goes through a maximum (activation energy, $\Delta G^*$):

$$\Delta G^* = \pi\upsilon^2\gamma_{ns}^3/3\left(k_b T \ln(S)\right)^2 \qquad \text{1-27}$$

Where $\upsilon$ is the frequency of molecular transport at the nucleus/liquid interface, which is inversely related to viscosity $\eta$, $\gamma$ is the interfacial energy per unit area between the medium and the nucleating cluster, $k_b$ is the Boltzmann constant, and T is the absolute temperature. The mechanism of nucleation[59] can be divided into two categories: homogeneous nucleation and surface induced nucleation (Figure 1-24). Homogeneous nucleation occurs in the interior of a uniform substance. It rarely takes place in large volume ($>100\,\mu$l) due to the presence of impurities in solution. Surface catalyzed nucleation, instead, is more frequently encountered. It can be further divided into two subcategories: Nucleation facilitated by the seed crystals of the solute is known as secondary nucleation. Or nuclei may preferentially form at surface of the containers or random impurities because of improved wetting. This mechanism is referred to as heterogeneous nucleation.

Despite being more practically important, heterogeneous nucleation is much more difficult to model. For both homogeneous and heterogeneous nucleation, the volume free energy change is:

$$\Delta G_v = -\alpha l^3 v^{-1} k_B T \ln\left(\frac{c}{s}\right) \qquad \text{1-28}$$

Where α is the volume-shape factor, l is the characteristic length, v is the molecular volume of the crystallizing solute, $K_B$ is the Boltzmann constant, T is temperature, c is solute concentration, and s is solubility. The equation above indicates higher supersaturation decreases the free energy barrier for nucleation.

For homogeneous nucleation:

$$\Delta G_s = \beta l^2 \gamma_{12}$$

1-29

Where β is the area shape factor and γ is the interfacial energy per unit area between the crystallization medium, 1, and the nucleating cluster, 2. This equation suggests that the free energy barrier for homogenous nucleation can be reduced when the interfacial energy decreases.

For heterogeneous nucleation,

$$\Delta G_s = \gamma_{12} A_{12} + (\gamma_{23} - \gamma_{13}) A_{23}$$

1-30

Where A is the surface area of the interfaces, and subscript 3 represents the substrate. The first term in the equation is the same as that of homogeneous nucleation. The second term says that the surface free energy change can be reduced if the interfacial energy between the nucleating cluster and substrate is less than that between the substrate and the medium. This will in turn diminish the total free energy barrier and facilitate nucleation. Nevertheless, the critical radius remains unchanged (Figure 1-25).

Heterogeneous nucleation mechanism may have profound impact on the dissolution of metastable forms due to the reduced energy barrier for nucleation. Preparation of a high energy amorphous form with higher solubility is aimed at achieving faster dissolution and

higher concentration in solution, achievement of this may not be successful in the presence of substantial surface catalyzed nucleation

The nucleation rate for homogeneous nucleation of spherical molecular assemblies is given by the following equation[59]:

$$J = N_0 \upsilon \exp\left(\frac{-16\pi\upsilon^2\gamma_{12}^3}{3(k_B T)^3 \left(\ln\left(\frac{c}{s}\right)\right)^2}\right) \qquad \text{1-31}$$

Where J is the number of nuclei formed per unit time per unit volume, $N_0$ is the number of molecules of the crystallizing phase in a unit volume, and $\nu$ is the frequency of atomic or molecular transport at the nucleus-liquid interface. This equation suggests that the nucleation rate is increased when supersaturation increases or the interfacial energy decreases. Some excipients in the formulation (e.g., polymers, surfactants) might alter the nucleation rate by changing the viscosity of the solution and the rate of molecular transport[6]. For non-surface active compounds, increasing solubility will decrease nucleation rate. However, adding surfactants at a concentration above the critical micelle concentration (CMC) may solubilize surface active drugs, causing them to partition into the micellar phase. The overall solubility of the drug is increased. However, the supersaturation is relieved since the solubility of drug in water phase remains unchanged. On the other hand, surfactants may lower the interfacial energy between the nucleating clusters and the medium. Therefore, the influence of surfactants on nucleation rate is dependent on the competition of their relative contribution on supersaturation and wetting.

Nucleation rate is inversely proportional to the induction time, $t_{ind}$, of nucleation, which is the time elapsed from when a supersaturated solution is created to the appearance of a solid phase[59]:

$$t_{ind} = t_r + t_n + t_g$$

1-32

Where $t_r$ is the relaxation time required to reach a quasi steady state distribution of molecular clusters, $t_n$ is the time necessary for the formation of a stable nucleus, and $t_g$ is the time needed for the nucleus to grow to an experimentally detectable size. Figure 1-26 illustrates how the induction time varies with supersaturation.

The growth stage occurs immediately after nucleation. It involves two steps: where growth units diffuse from the bulk solution to the crystal/solution interface and are then integrated into the ordered crystal lattice, accompanied by desolvation. The increase in crystal radius, r, is calculated using the following equation[6]:

$$\frac{dr}{dt} = \left[ D\nu N_A / (r + \frac{D}{k_+}) \right] (C - C_{eq})$$

1-33

Where D is the diffusion coefficient of the compound, $k_+$ is the surface integration factor, $N_A$ is Avogadro's constant, and $(C-C_{eq})$ is the concentration difference between the bulk solution and the boundary liquid layer between the growing crystal and the bulk solution. Careful inspection of this equation reveals that crystal growth is controlled by the rate of diffusion if $r \gg D/k_+$, and by the rate of surface integration if $r \ll D/k_+$. Similar to nucleation, the presence of certain excipients may alter the viscosity, and thereby change D and $\nu$. The surface integration factor can be modified by adding excipients that are able to adsorb on to the surface of crystal[61].

The surface-integration controlled growth can be subdivided into continuous growth and layer growth mechanisms. Continuous growth occurs on relatively rough surfaces whereas the layer growth occurs on relatively smooth surfaces. The layers (also referred to as steps) can be formed by two different mechanisms: 2-D nucleation which takes place at high supersaturation and screw dislocation which dominates at intermediate and low supersaturation (Figure 1-27).

Volmer postulated that layers are formed when solute molecules adsorb onto an existing crystallizing surface (Figure 1-28)[60]. The surface consists of terraces which are flat and steps which are raised partial layers. The steps contain kink sites where molecules can make more bonds with neighboring molecules than on terraces or flat step edges. On the other hand, molecules detach from kinks more easily than from either complete step edges or terraces. Therefore, the rate of addition of molecules to a crystal is proportional to the kink density. Consequently, crystal growth rates can be altered through either roughening steps or blocking kink sites. The flux of molecules detaching from the surface is dependent on the bond strength of a molecule to its neighbors, which is a function of temperature rather than solute concentration. The flux of molecules attaching to the crystallizing surface is proportional to the concentration (or activity). Therefore, assuming all other factors are equal, crystals of higher solubility compound will grow faster than a sparingly soluble compound, even at equivalent supersaturation. Hence, crystal growth rates may also be modified by shifting the solubility[62]. The entire layer is formed once the pre-existing steps grow out to the edge of the crystal, leaving a featureless terrace. To enable further growth, a new source of steps must be generated. This is accomplished through the formation of two dimensional islands of molecules, which may then spread out. For these islands to

form, a free energy barrier has to be overcome. The overall excess free energy for 2-D nucleation[59] consists of a surface component and a volume component, as given by the following equation:

$$\Delta G = a\gamma + v\Delta G_v$$

1-34

Where, a and v are the surface area and volume of the nucleus, respectively. $\gamma$ is the surface tension.

Assuming a circular disc nucleus, where r is the radius and h is the height:

$$\Delta G = 2\pi r h\gamma + \pi r^2 h\Delta G_v$$

1-35

The critical nucleus ($r_c$) can be found by taking the derivative:

$$\frac{d\Delta G}{dr} = 2\pi h\gamma + 2\pi r h\Delta G_v = 0$$

1-36

$$r_c = -\frac{\gamma}{\Delta G_v}$$

1-37

The critical free energy is given by:

$$\Delta G_{crit} = \frac{\pi h\gamma^2 v}{kT\ln S}$$

1-38

And the 2-D nucleation rate is :

$$J = B \cdot \exp[-\frac{\pi h\gamma^2 v}{k^2 T^2 \ln S}]$$

1-39

Figure 1-29 shows examples of crystal surfaces that do grow by 2-D nucleation mechanism at sufficiently high supersaturations. However, the critical size is large at low supersaturation, and hence the odds of obtaining the islands are prohibitively small.

Frank[63] suggested that crystals are imperfect, containing edge dislocations and/or screw dislocations upon which permanent sources of steps are generated (Figure 1-30). This mechanism accounts for the crystal growth observed at low supersaturations. In this case, interesting spiral arrangements of steps are generated by dislocation growth sources. This feature is often referred to as growth hillocks (Figure 1-31). The equilibrium shape (i.e. spiral staircase, pyramids, cubic spirals etc) is the one that possess minimum total surface free energy and the radius of the curvature is dependent upon the critical radius.

The growth hillocks can be modified by impurities through four mechanisms (Figure 1-32). Growth inhibition by impurities for each mechanism exhibits a different dependence of step kinetics on impurity concentration, supersaturation and temperature[64, 65].

1) Step pinning: Adsorption of impurities may block the attachment of molecules to the step edges. In this case, steps can only proceed by growing around the blocked sites.

2) Incorporation: Impurities maybe captured and incorporated into the kinks and become part of the growing crystals.

3) Kink blocking: Kink density is temporarily reduced[66] due to the adsorption of impurities to kinks for very short residence time. In this case, step advancement is not permanently stopped at the kink site, just kink propagation.

4) Surfactants: The adsorption of impurities could lower the interfacial energy of the step edge, and thereby modify the shape of the growth hillocks and the resulting crystals.

For 2-D nucleation, the effect of impurities on crystal growth in a supersaturated solution by the step pinning mechanism can be quantified by the Kubota and Mullin model[65]. Assuming a constant step height for each layer, the relationship between the growth rate of a single step V and that of the crystal face containing a step V is given by:

$$\frac{V}{V_0} = \frac{G}{G_0}$$

1-40

Where, the numerator is the growth rate in the presence of impurities and the denominator is the growth rate in the absence of impurities.

If steady state adsorption is assumed, (i.e., the adsorption equilibrium is reached instantaneously, and the surface coverage of active sites by an impurity is independent of time), then

$$\frac{V}{V_0} = 1 - \alpha\theta_{eq}$$

1-41

Where, $\theta_{eq}$ is the equilibrium surface coverage of active sites by an impurity. Assuming the Langmuir adsorption isotherm, then

$$\theta_{eq} = \frac{Kc}{1 + Kc}$$

1-42

Where K is the Langmuir constant, c is the impurity concentration, and $\alpha$ is the impurity effectiveness factor. Combining equation 1-41 and 1-42 gives:

$$\frac{V}{V_0} = 1 - \frac{\alpha Kc}{1 + Kc}$$
<div align="right">1-43</div>

This equation is shown in Figure 1-33 where the dimensionless relative step velocity ($V/V_0$) is plotted against the dimensionless impurity concentration with the effectiveness factor as a parameter.

It can be seen that the ability of an impurity to inhibit step growth decreases as the effectiveness factor decreases. If this value is less than unity, the step advancement will not be completely arrested, even at high impurity concentration. Instead, plateau regions are observed where relative step velocity is independent of dimensionless impurity concentration when the impurity concentration is high.

The impurity effectiveness factor $\alpha$ is given by:

$$\alpha = \frac{\gamma a}{kT\sigma L}$$
<div align="right">1-44</div>

Where L is the separation of sites available for impurity adsorption, $\gamma$ is the surface tension, a is the surface area occupied by one crystallizing molecule and k is the Boltzmann constant, T is the temperature, and $\sigma$ is the degree of supersaturation. This equation implies that for any given temperature, the effectiveness of the impurity on growth rate inhibition decreases as the degree of supersaturation increases.

Combining equation 1-40, 1-43 and 1-44 gives:

$$\frac{G}{G_0} = 1 - \frac{\sigma_c}{\sigma} \quad (\text{for } \sigma_c < \sigma)$$
<div align="right">1-45</div>

Where, $\sigma_c$ is the critical supersaturation, defined as the supersaturation below which G=0 (dead zone):

$$\frac{G}{G_0} = 0 = 1 - \left(\frac{\gamma a}{kT\sigma_c L}\right)\left(\frac{Kc}{1+Kc}\right)$$ 1-46

$$\sigma_c = \frac{\gamma a Kc}{kTL(1+Kc)}$$ 1-47

Equation 1-47 can be rewritten in the form of

$$\frac{1}{\sigma_c} = \frac{C_1}{c} + C_2$$ 1-48

Where $C_1 = kTL/\gamma aK$, and $C_2 = kTL/\gamma a$. This equation indicates a linear relationship exists between the reciprocal of the critical supersaturation $1/\sigma_c$ and the reciprocal of impurity concentration $1/c$

If a second order growth law is applied:

$$G_0 = k\sigma^2$$ 1-49

By normalizing with $k\sigma_c^2$, we obtain:

$$\frac{G_0}{k\sigma_c^2} = \left(\frac{\sigma}{\sigma_c}\right)^2$$ 1-50

Combining equation 1-45 and 1-49 gives:

$$\frac{G}{k\sigma_c^2} = \left(\frac{\sigma}{\sigma_c}\right)\left[\left(\frac{\sigma}{\sigma_c}\right) - 1\right]$$ 1-51

This equation is shown in Figure 1-34, where crystal growth inhibition by the impurity is apparent. There also exists a supersaturation range ($0 < \sigma < \sigma_c$), where the crystal does not grow in the presence of impurity.

## 1.11 Crystallization during Dissolution of Amorphous Solids

Amorphous solids have drawn much research interest today due to their capability of increasing bioavailability by enhancing the solubility/dissolution characteristics of poorly water soluble compounds. However, amorphous solids are inherently unstable and tend to convert to less soluble crystalline forms, which negates such benefits. To fully take advantage of amorphous materials, it is not enough just to ensure that drug remains amorphous during the entire period of storage, preventing crystallization during dissolution of amorphous solids is equally important[67]. While a plethora of investigations have been conducted on the physical stability of amorphous solids during storage, there is a lack of fundamental understanding around the underlying factors influencing phase transformation during dissolution of amorphous pharmaceuticals.

A supersaturated solution has higher chemical potential ($\mu$) as compared to saturated solution ($\mu_{eq}$). The difference in chemical potential is the thermodynamic driving force for crystallization.

$$\Delta\mu = \mu - \mu_{eq} = RTln\left(\frac{a}{a_{eq}}\right) = RT\left(\frac{\gamma C}{\gamma_{eq}C_{eq}}\right) \qquad 1\text{-}52$$

Where a is the activity of the solute in supersaturated state, and $a_{eq}$ is the activity of the solute in saturated state, and $\gamma$ is the activity coefficient. Assuming the activity coefficient is independent of concentration, then

$$\Delta\mu = RTln\left(\frac{C}{C_{eq}}\right) = RTlnS \qquad 1\text{-}53$$

Therefore, the higher the degree of supersaturation, the larger thermodynamic driving force for crystallization of solute from solution. However, as mentioned previously, even if

supersaturation is achieved, the activation energy barrier for nucleation has to be surmounted. Otherwise, nucleation is suppressed, at least during a certain time frame.

There are several domains in the concentration versus temperature diagram as shown in Figure 1-35. Solutions with concentrations lower than the solubility curve are considered undersaturated ($\Delta\mu<0$), and no crystallization will be observed. In the metastable region, it is difficult for spontaneous nucleation to occur. However, crystals may grow rapidly if added to the solution. In the labile zone, nucleation is spontaneous followed by rapid crystal growth.

Solubilization formulation strategies aim at reducing the degree of supersaturation by decreasing the free drug concentration in the aqueous phase (e.g. self emulsifying drug delivery systems, surfactants above CMC, cyclodextrins). Hence, the distance between the system and the saturation curve in the diagram is reduced and the thermodynamic driving force for crystallization ($\Delta\mu$) decreases. In contrast, during the dissolution of amorphous solids, the presence of polymers sustains supersaturated concentrations of the solute and in the meantime prolongs the time for the nucleating clusters to grow to the critical radius. The high concentration of drug in the lumen results in enhanced flux acrossed the GI wall. In this scenario, $\Delta\mu$ does not change significantly, at least during that time frame. Therefore, this approach can be conceptually considered as increasing the metastable zone width[68].

Raghavan et al[69] studied the influence of selected polymers on the crystallization during dissolution of amorphous hydrocotisone acetate (HA). Crystallization was spontaneous for solutions at all levels of supersaturation investigated in the absence of polymers, indicating that these concentrations were in the labile zone. Nucleation time was inversely related to the degree of supersaturation at all the polymer concentrations studied.

Nucleation time was prolonged in the presence of polymers and the effect was more pronounced as the polymer content increased. In the absence of polymers, spontaneous nucleation indicated that nucleation is not diffusion controlled. Polymers may associate with HA to form hydrogen bonds in solution. Such bonds have to be broken before HA molecules can diffuse and collide to form a nuclei of critical size. Cellulosic polymers have more functional groups to hydrogen bond with HA than PVP or PEG, and hence a longer nuleation time is expected. Unfortunately, only the nucleation times in the presence of HPMC were shown in their paper. Crystals grown in the presence of any of the polymers were smaller than crystals grown without polymer. They suggested that once nuclei are formed, there will be competitions between HA growth units and polymers for growth sites on the crystal surface. Due to size and structure considerations, polymers will be excluded as the HA growth units are incorporated into the crystal lattice. However, the excluded polymer molecules do not leave immediately. Instead, they may adsorb and accumulate on the boundary region between the crystal surface and solution due to their ability to form hydrogen bond with HA molecules (Figure 1-36).

This layer provides a mechanical barrier to retard the diffusion of HA molecules from solution to the crystal surface. In addition to growth inhibition, cellulosic polymers were able to modify the crystal habit of HA: from a well-faceted polar prismatic morphology to a boomerang morphology with very rough surfaces and edges. In contrast, PVP and PEG do not have such effect. A change in crystal morphology suggests that cellulose polymers may preferentially adsorb on the surface where HA molecules have more functional groups for hydrogen bonding. The growth of these faces are delayed. The fact that the

morphology of HA crystal is less affected by PVP and PEG is perhaps because these polymers do not have as many functional groups per monomer unit as cellulose polymers. When introduced to the aqueous medium, amorphous solids have a tendency to convert to a thermodynamically stable, less soluble crystalline state directly from the amorphous matrix. Water is absorbed by the amorphous material upon exposure and causes a substantial reduction of $T_g$ at the surface of the solids. This will increase molecular mobility, and may lead to crystallization at the surface of the solid. If the solid to solid conversion is extremely rapid, then the concentration-time profile of the amorphous solids will mimic that of the crystalline form because it is essentially the transformed crystalline material that is dissolving. If the solid state transition is relatively slow as compared to the dissolution of the amorphous material, a supersaturated solution will be attained. Once the solution concentration exceeds the metastable zone, the solute will crystallize spontaneously, whereby the nucleation and growth rate are propotional to the degree of supersaturation (Figure 1-37). Eventually, the solution will attain thermodynamic equilibrium as the solute is depleted. Based on the above considerations, Alonzo et al[67] hypothesized that the level of supersaturation achieved during dissolution of amorphous materials depends on the kinetics of solid state crystallization as well as solution crystallization. Polymers may reduce crystallization tendency of either or both routes. They compared the dissolution behavior of amorphous felodipine and indomethacin in the presence/absence of predissolved PVP, HPMC and HPMCAS. At 25 ℃, dissolution of amorphous felodipine resulted in a small extent of supersaturation, followed by desupersaturation due to solution crystallization. At 37 ℃, however, the dissolution profile of amorphous felodipine looked very similar to that of the crystalline solid. A slurry experiment with Raman analysis

showed that powdered felodipine commenced crystallization immediately upon contact with the medium and proceeded rapidly at 37 ℃. The phase transformation kinetics were relatively slower at 25 ℃. All three polymers were able to delay solid state crystallization of amorphous felodipine, and therefore higher levels of maximum supersaturation were observed at 37 ℃. It was suggested that the polymers interact with the surface of the amorphous drug and thereby inhibit surface crystallization.  HPMC and HPMCAS were able to effectively inhibit crystallization from solution and maintain the supersaturation. PVP, however, was a poor inhibitor of solution crystallization. In the case of indomethacin, high maximum supersaturations were observed at both temperatures because the solid state crystallization of indomethacin was much slower as compared to felodipine. In the absence of polymers, desupersaturation occurred at both temperatures. Hence, for indomethacin, solution crystallization was the predominant mechanism of negating the solubility advantage of amorphous solids. Similar to the felodipine case, polymeric additives were able to stabilize the supersaturation by inhibiting solution crystallization. At 25 ℃, the presence of PVP and HPMC yielded a similar maximum concentration consistent with the value estimated using the Hoffman equation. Interestingly, at 37 ℃, the same maximum concentration was achieved in the presence of PVP, followed by significant desupersaturation.  A lower maximum concentration was achieved in the presence of HPMC. However, no desupersaturation was observed. To conclude, the kinetics of both crystallization pathways determine the overall shape of concentration-time profiles for amorphous solids. The maximum solution concentration observed will be close to the estimated amorphous solubility only when both the metastable amorphous solid and the supersaturated solution are stabilized against crystallization. Assessment of the ability of

different polymers in inhibiting each route could lead to rational design of amorphous formulation. Multiple polymers can be incorporated into a single formulation, with one optimized for solid state crystallization inhibition and the other for solution crystallization inhibition.

With respect to solution crystallization, a follow up study[70] was conducted to quantify the relative impact of pre-dissolved HPMC on nucleation versus growth kinetics of felodipine from supersaturated solution. Growth inhibition by the polymer was quantified by measuring the desupersaturation rate in the presence of seed crystals. At low levels of initial supersaturation ($S \leq 6$), the presence of HPMC at all concentrations investigated (from 0.2ug/ml to 3.5ug/ml) resulted in measurable reduction of the desupersaturation rate and consequently the growth rate. At high levels of initial supersaturation ($S \geq 8$), HPMC present at the lowest concentration (0.2ug/ml) was not able to decrease desupersaturation and growth rate. As supersaturation increased, the rate of growth increased no matter whether HPMC was present or not, indicating there is a certain limit of growth inhibition that HPMC can provide at a given S. In other words, HPMC became less effective in inhibiting crystal growth as initial supersaturation was increased. At a given S, as polymer concentration increases, more polymer molecules are available to be adsorbed onto the surface of the crystal, and hence have a more profound impact on growth rate. However, there is a limit of surface area on the crystal that can be covered by the polymer. The adsorption isotherm suggested that maximum coverage was attained when polymer was present at 1ug/ml. This was consistent with the finding that there was no further increase in the extent of growth rate inhibition by increasing polymer concentration beyond 1ug/ml. In the absence of HPMC, the growth of crystals was controlled by both diffusion and

integration. The presence of HPMC reduced the rate at which the growth units were incorporated into the lattice while not affecting the diffusion of growth units from bulk solution into the incorporated site. Nucleation inhibition by HPMC was quantified from measurement of the desupersaturation rate in seedless solution. At an S of 10 (high level of supersaturation), the presence of HPMC at 1ug/ml resulted in an approximately 1000 fold reduction in nucleation rate. In contrast, there was only a 2 fold reduction in growth rate at the same S and HPMC concentration.

Figure 1-38 clearly shows that the pre-dissolved HPMC has a much more significant effect on nucleation than on crystal growth[70]. Hence for felodipine, preventing nucleation from solution and minimizing residual crystallinity in the formulation are extremely important for maintaining supersaturation.

## 1.12 Drug-Polymer Solubility and Miscibility

In small molecule solutions, the chemical potential of the solute in the solid phase equals the chemical potential of the solute in the liquid phase when the solution concentration reaches the equilibrium solubility at a given temperature. This concept can be extended to crystalline drug-polymer mixtures, where the composition of drug in the polymer at equilibrium is the solubility. In other words, it refers to the ability of a polymer to play the role of solvent to dissolve a crystalline API. On the other hand, miscibility refers to the property of liquids to mix in all proportions, forming a homogeneous solution. For polymer blends, miscibility can be well characterized since the amorphous polymer components are stable. In binary solid dispersions, the liquid components to be mixed are the amorphous drug and the amorphous polymer, respectively. In this case, complexity around the

miscibility arises because as compared to polymers, small molecule drugs have greater tendency to crystallize due to the relative ease of molecular rearrangement in the amorphous matrix and subsequently form an ordered lattice structure. Eventually, equilibrium will be attained with respect to crystalline drug in the amorphous polymer. The mixture composition at this equilibrium would be the solubility of the crystalline drug in the polymer. Therefore, the term miscibility is meaningful only if the drug can maintain the supercooled liquid state in the dispersion within the experimental timeframe well above or close to $T_g$. Below or close to $T_g$, however, the material become too viscous ($>10^{12}$ Pa S) for the system to reach equilibrium, which involves the kinetics of physical aging as well as phase separation. Hence miscibility is only "apparent" in this case.

Achieving and maintaining molecular level mixing is important for two reasons. First, regardless of the specific mechanism, the ability a polymer to inhibit crystallization relies on the ability of the polymer to interact with the API and thereby change its local environment. In a well mixed binary system, only a single amorphous phase exists. If the two components are immiscible, regions with different API-to-polymer ratio will be present in the system. It can be understood intuitively that crystallization will initiate from the drug rich phase where the availability and thus the influence of polymer is minimal. Second, if the drug is intimately mixed with the polymer at the molecular level, the chemical potential of the API in the dispersion will be lower as compared to the pure amorphous API. The lower chemical potential infers a reduced thermodynamic driving force for crystallization as well. That is why crystallization inhibition was not observed in the physical mixtures of indomethacin-PVP and sucrose-PVP[71, 72] , where only macroscopic mixing were achieved.

Feng et al[73] proposed a hypothetical working diagram defined by drug loading in polymer and temperature as shown in Figure 1-39. This diagram consists of six different domains (labeled I-VI) that are separated by three curves: crystalline drug-polymer solubility, amorphous drug-polymer miscibility, and $T_g$ of a solid dispersion system. The goal is to find a domain in which the solid dispersion is physically stable while maximizing the drug loading in polymer to reduce the pill burden for patients.

As described by the Gordon-Taylor equation, the $T_g$ of a binary solid dispersion decreases as the drug loading increases. This curve represents a kinetic boundary, to the left of which an amorphous solid become a highly viscous glass, and hence has very low molecular mobility. Below $T_g$, the system is kinetically stabilized against phase separation and/or crystallization, if any. For simplicity, the miscibility can be considered as the "solubility" of an amorphous API in a polymer, since drug to polymer ratio is usually much less than unity in a typical solid dispersion formulation. It follows that the amorphous drug-polymer miscibility curve must be higher than the crystalline drug-polymer curve due to the higher chemical potential of amorphous state as compared to the crystalline state. Below the crystalline curve, there is no risk of destabilization of the system. If drug loading is above the crystalline-drug solubility curve, the polymer solvent is supersaturated with respect to crystalline drug. There is a potential risk of crystallization of the API from a thermodynamic perspective. However, if the amorphous drug is relatively stable without crystallization, the miscibility curve represents the boundary for destabilization of the system. Above that curve, the free energy of mixing will become positive, resulting in spontaneous phase separation. Crystallization would preferentially initiate in the drug-rich

region. The thermodynamic nature and destabilization driving force for solid dispersion in different domains[73] are summarized in Table 1-6

Determination of domain III is of interest because in this region the solid dispersion is stabilized both kinetically (limited molecular mobility below $T_g$) and thermodynamically (below miscibility). In the meantime, a higher drug loading in polymer is achieved as compared to domain I and II. If an even higher drug loading is required (above miscibility), it is recommended to work in domain V to kinetically stabilize the system. Domain VI should be avoided at any time based on similar arguments.

Thermodynamically, whether the formation of a homogeneous single phase mixture is successful is governed by the Gibbs free energy of mixing of the system:

$$\Delta G_{mix} = \Delta H_{mix} - T \Delta S_{mix}$$

1-54

Where, $\Delta G_{mix}$ is the free energy of mixing, $\Delta H_{mix}$ is the enthalpy of mixing, T is temperature, and $\Delta S_{mix}$ is the entropy of mixing. Mixing of the two components is thermodynamically favorable if $\Delta G_{mix}$ is negative. When $\Delta G_{mix}$ is positive, mixing is considered unfavorable.

The entropy of mixing is defined as the increase in the total entropy of a system, when different and chemically non-reacting components are mixed by removing partition(s) between the system's initially separate volumes. Assuming ideality, the entropy of mixing for two components is given by:

$$\Delta S_{mix} = -nR(X_u ln X_u + X_v ln X_v)$$

1-55

$$X_u = 1 - X_v$$

1-56

In this equation, n is the total number of moles. $X_i$s are the mole fractions of component i, which are less than unity, and thus the natural logarithm is always negative. Upon removal of the partition, $nX_i$ moles of component i will explore the combined volume which is not initially accessible to it, resulting in an increase in $\Delta S_{mix}$ by $nRX_i \ln X_i$. Mixing as ideal solutions is always spontaneous, and there is no heat transfer involved or work is done. The enthalpy of mixing is the heat taken up or released during mixing of the chemically non-reacting pure components. It is given by:

$$\Delta H_{mix} = (H_{uu} + H_{vv}) - H_{uv}$$

1-57

Where $H_{uu}$, $H_{vv}$ are the enthalpies of the pure components and $H_{uv}$ is the enthalpy of the mixture. $\Delta H_{mix}$ depends upon the interactions between the molecules, which may include van der Waals force, hydrogen bonding interactions, charge transfer complexation, and ionic interactions. The energy change during mixing can be regarded as being made of three parts, the endothermic breaking of interactions within the two pure components, and the exothermic formation of attractions between them. An ideal mixture is one in which the interactions in the mixture are the same as for the two pure components. Hence the process is athermal (i.e. $\Delta H_{mix}=0$). If the adhesive interactions are weaker than the sum of cohesive interactions, $\Delta H_{mix}$ will be positive (endothermic mixing), resulting in an increase in $\Delta G_{mix}$, and vice versa.

From the discussion above, it follows that mixing is always entropically favored. A certain level of unfavorable enthalpy interactions could be tolerated while molecular level mixing is still achieved[74]. Therefore, a quantitative assessment of both enthalpic and entropic contributions to the mixing free energy is advisable to enable an unequivocal prediction of the miscibility.

Originally developed for polymer-solvent systems, the Flory-Huggins lattice theory was adapted by Marsac et al[74] to estimate the free energy of mixing for drug-polymer system by assuming that the drug behaves similarly to a solvent:

$$\frac{\Delta G_{mix}}{RT} = n_{drug}ln\Phi_{drug} + n_{polymer}ln\Phi_{polymer} + n_{drug}\Phi_{polymer}\chi \qquad \text{1-58}$$

Where $n_{drug}$ is the number of moles of drug, $n_{polymer}$ is the number of moles of polymer, $\Phi_{drug}$ is the volume fraction of the drug, $\Phi_{polymer}$ is the volume fraction of polymer. The first two terms in the equation accounts for the entropy of mixing, which is similar to equation 1-55. However, the mole fractions are replaced by the volume fractions. This is attributed to the reduced $\Delta S_{mix}$ for large molecular weight materials caused by the reduced number of possible configurations of the two components in a binary mixture. $\chi$ is the Florry-Huggins interaction parameter which accounts for the enthalpy of mixing, which is a measure of the relative strength of cohesive and adhesive interactions. Positive interaction parameter indicates stronger cohesive interactions than adhesive interactions in the system and mixing is enthalpically unfavorable whereas a system with a negative interaction parameter is characterized by extensive adhesive interactions and hence favorable mixing. For a typical small molecule API (MW between 200 to 600)-polymer (MW between 10,000 to 1,500,000) system, the contribution of entropy term to the free energy of mixing was determined to be relative constant by simulation (assuming $\chi=0$). Whether a system is miscible or not is essentially determined by the sign and magnitude of $\chi$. Negative interaction parameters were obtained by the melting point depression method for both felodipine-PVP and nifedipine-PVP mixtures, and hence miscibility was predicted. A

limitation to the melting point depression approach is that the $\chi$ estimated is only applicable within a small temperature range close to melting point and at low polymer weight fractions. Finally, a model was developed[74] based on Flory-Huggins theory to predict the solubility of a crystalline drug in a glassy polymer:

$$ln\gamma_{drug}x_{drug} = -\frac{\Delta H_{fus}}{RT}\left[1 - \frac{T}{T_m}\right] - \frac{1}{RT}\int_{T_m}^{T}\Delta C_p{}^{config}\,dT$$

$$+\frac{1}{R}\int_{T_m}^{T}\frac{\Delta C_p{}^{config}}{T}\,dT$$

1-59

where, $x_{drug}$ is the mole fraction, $\Delta H_{fus}$ is the enthalpy of fusion, $T_m$ is the melting temperature of the drug, and $\Delta C_p{}^{config}$ is the configurational heat capacity. $\gamma_{drug}$ is the activity coefficient, which reflects non-ideality, and is given by:

$$ln\gamma_{drug} = \ln\left(\Phi_{\text{drug}}/x_{drug}\right) + (1 - 1/m)\Phi_{\text{polymer}} + \chi\Phi_{\text{polymer}}^2$$

1-60

Where, m is the ratio of the volume of the polymer to the molecular volume of the drug. The solubility of nifedipine in PVP was determined to be very low (6~7%). This would require at least 90% of polymer present in the formulation to ensure that the drug does not crystallize due to supersaturation. In this case, the system is considered to be thermodynamically stabilized. However, if a high drug loading is required, stabilization of the amorphous nifedipine would mainly rely on the ability of polymer to retard the kinetics of crystallization as discussed previously. By comparing felodipine and nifedipine, the authors pointed out that the solubility of an API in a polymer increases as the melting point and the heat of fusion increases and/or with a more negative enthalpy of mixing.

For a binary amorphous mixture, the compositional dependence of $\Delta G_{mix}$ can be described by the following equation, which is originally developed for liquid mixtures[75]:

$$\Delta G_{mix} = x_A(\mu_A - \mu_A^*) + x_B(\mu_B - \mu_B^*) \qquad \text{1-61}$$

Figure 1-40 is the plot of free energy as a function of composition for binary systems with different types of miscibility behavior[76]. If the two components are completely miscible at any composition, a concave shaped curve with only one energy minimum will be observed. Normally, immiscibility only occurs when the $\Delta G_{mix}$ is positive, which is characterized by a convex shaped curve over the complete range of compositions. However, some binary systems may exhibit partial miscibility, that is, only a certain amount of one component can be mixed with the other to form a homogeneous phase at a given temperature and pressure. Above that concentration, however, the component in excess will phase separate, even though the $\Delta G_{mix}$ is negative with respect to the unmixed components. This is illustrated in the red curve in Figure 1-40 and more details are given in Figure 1-41. It can be seen that $\Delta G_{mix}$ is negative at all compositions. Nevertheless, two minima are observed at composition $x_{AB}$ and $x_{BA}$, resulting in a miscibility gap. At these compositions, $\Delta G_{mix}$ is lower as compared to that of any compositions in between them. They are called binodal points, at which the chemical potential of each component is equal in both phases. Any composition below $x_{AB}$ or above $x_{BA}$ is stable and does not phase separate. The inflection points between the binodal points and the point of maximum $\Delta G_{mix}$ are known as spinodal points ($x^*_{AB}$ and $x^*_{BA}$). Mathematically, the spinodal points can be found by setting the second derivative of $\Delta G_{mix}$ with respect to concentration equal to zero. Between $x_{AB}$ and $x^*_{AB}$ and $x_{BA}$ and $x^*_{BA}$ is the metastable region, where phase separation can occur after

overcoming an energy barrier. The spinodal points envelope the unstable region, where phase separation occurs spontaneously. This process is also referred to as spinodal decomposition where a new phase is initiated without any thermodynamic barrier. The resulting two liquid phases have equal chemical potential. Partial immiscibility is a function of temperature. The degree of immiscibility decreases as temperature increases in some systems. The temperature at which complete miscibility is observed is known as upper consolute temperature (UCT).

If immiscibility occurs, different phases with varying composition of the components will be present in the system. Such difference will be reflected in the measured physical properties. DSC is the standard method to characterize the number of phases present in amorphous mixtures. For a miscible system, a single $T_g$ is expected. Conversely, the presence of multiple $T_g$s is indicative of a phase separated system. Despite its straightforwardness and hence popularity, the DSC method has several inherent limitations in evaluating miscibility. First, if the $T_g$s of individual components are very similar, identification of multiple $T_g$s in a phase separated system can be difficult. Second, a minimum domain size (10-50nm for polymeric blends) [77] containing more than one phase is required for $T_g$ events to be detected. Third, the heat capacity change in glass transition maybe too broad or weak to allow unambiguous identification. Fourth, multiple $T_g$s have been reported for miscible polymer blends recently[78]. Last but not least, when a sample is heated, there might be a shift in the miscibility behavior of the system due to the increase in temperature. Techniques such as atomic force microscopy (AFM) and scanning/transmission electron microscopy (SEM/TEM) are able to achieve nanoscale resolution. However, they cannot characterize the chemical compositions of different

phases in the system. On the other hand, mid-infrared (MID-IR) and Raman mapping could interrogate the chemical information, but suffer from limited spatial resolution as imposed by the diffraction limit of light. Nanoscale mid-IR is a promising technique to bridge this gap in that it provides the chemical information from mid-IR analysis with high spatial resolution (submicrometer) thanks to the implementation of an AFM probe.

Eerdenbrugh et al[79] explored this technique to evaluate the miscibility of felodipine and PAA dispersions. The chemical structures of both components are shown in Figure 1-42. Standard topolographical AFM imaging indicates miscibility at 25:75 (w/w) drug to polymer ratio. The formation of discrete domains in a continuous phase was observed in a 50:50 (w/w) ratio dispersion. Further increasing the drug content to 75:25 (w/w) resulted in apparent phase separation. The discrete domains began to dominate the image with the compensating reduction of the continuous phase. Nevertheless, it was hard to determine the chemical content in each domain. Therefore, a 50:50 (w/w) sample was then subject to nanoscale mid-IR spectroscopy for this purpose. Reference nanoscale mid-IR spectra of pure amorphous PAA, amorphous felodipine, and crystalline felodipine are shown in Figure 1-43. It can be seen that both PAA and felodipine show a strong response at around $1700cm^{-1}$. As compared to pure PAA, the pure amorphous or crystalline felodipine has a characteristic peak at approximately $1500cm^{-1}$, which was assigned to N-H bending coupled with $CH_2$ vibrations. Localized nanoscale mid-IR spectra are shown in Figure 1-44. It can be seen that the spectra corresponding to discrete domains (marked in red) is dominated by the peaks at $1700cm^{-1}$, and the peak at $1500cm^{-1}$ was much weaker. In the spectra corresponding to the continuous phase (green marked), the peaks at $1500cm^{-1}$ were stronger than at $1700cm^{-1}$. Such results verified the occurrence of phase separation, with

the discrete domains being richer in drug while the continuous phase was richer in polymer. The presence of felodipine in the continuous phase and polymer in the discrete phase is inferred by the spectral contribution of their characteristic peaks. The system is hence considered partially miscible at 50 (w/w) drug loading, in agreement with a previous study[76]. Moreover, by comparing the localized spectra of the mixture with those of pure crystalline and amorphous felodipine, it can be deduced that felodipine did not crystallize during the experimental timeframe. This is consistent with the fact that felodipine is a slow crystallizing compound[17].

Marsac et al[80] assessed the impact of environmental stresses on the miscibility of amorphous dispersions of felodipine and PVP. Briefly, at room temperature, the drug-drug cohesive hydrogen bonding is associated with an NH peak centered at $3341cm^{-1}$, whereas the drug-polymer adhesive hydrogen bonding is related to an NH peak at $3290^{-1}$. The drug-drug interaction is gradually weakening for pure amorphous felodipine on heating, as reflected by an increase in the corresponding NH peak position. Similar trend was observed in the solid dispersions as well. Moreover, the drug-polymer interaction is also weakening, but persisted up to the melting temperature of the drug, indicating that the miscibility of the solid dispersions is retained. From Figure 1-45, we can see that the effect of temperature on the intermolecular interactions is reversible[80]. Another interesting observation is that the slope of peak positions versus temperature changes near the $T_g$ of each system.

Upon exposure to moisture for short periods of time (2-24hr), the drug-polymer hydrogen bonding is disrupted while the number of drug-drug interaction is increasingly numerous and the resulting IR spectra increasingly resemble that of the pure amorphous drug[80] (Figure 1-46). This change is most exaggerated at above 75% RH due to a dramatic increase

in water uptake when the relative humidity exceeds 75%. This is indicative of moisture induced phase separation to a drug-rich amorphous phase and a polymer rich amorphous phase, and is later confirmed by the DSC, AFM and TEM (transmission election microscopy) results. Moreover, the spectroscopic change persisted after drying over phosphorous pentoxide at room temperature for 1 week, suggesting that the moisture induced immiscibility is irreversible. Similar spectroscopic change was observed for solid dispersions of felodipine and PVP prepared with water added to the solvent during production as compared to those prepared from the dry solvent. The moisture/liquid water induced phase separation was explained by the asymmetry of interactions of the two components with the water, which is reflected by the large difference in the Flory-Huggins parameter of water with PVP ($\chi_{12}$=0.5) and water with felodipine ($\chi_{13}$=3.3). This is known as the $\Delta\chi$ effect (where $\Delta\chi= |\chi_{12}-\chi_{13}|$)[81, 82]. In addition, molecular mobility is also increased due to water sorption, which enables faster diffusion of molecules to form drug-rich and polymer-rich domains. As water is subsequently removed by heating at 125 °C, however, remixing of felodipine and PVP gradually proceeded and completed within approximately 24 hrs[80] (Figure 1-47). The occurrence of remixing at high temperature (well above the $T_g$ of felodipine and that of the corresponding one phase solid dispersion) is dictated by the thermodynamic driving force for mixing in the absence of moisture. However, the fact that remixing was not observed after drying at room temperature is a consequence of the prohibitively slow kinetics. This is because both meta-stable phases are in the glassy regime (high viscosity and hence slow molecular diffusion) at room temperature. The implication from this study is that the water content of solvents has to be rigorously

controlled and the exposure of the solid dispersions to high relative humidity needs to be avoided so as to prevent water induced phase separation.

### 1.13 Drug Release Mechanisms from Solid Dispersions

To facilitate the design of a solid dispersion with optimal dissolution performance, a fundamental appreciation of the underpinning mechanisms and complexities associated with the release process is required. These factors may include the method of preparation, weight fraction of the carrier used, the solubility/dissolution rate difference between the drug and the carrier, crystallization tendency of the drug during dissolution, etc.

There are two types of release behavior of drug from solid dispersions reported in the literatures. A carrier-controlled dissolution mechanism was proposed by Corrigan et al[83, 84] who found that the dissolution rate of the drug in the polymeric carrier is equal to that of the polymer alone. Support for this hypothesis was provided by Dubois and Ford[85] who showed that the release rates of different drugs in a single polymer were similar, indicating the release behavior is dependent on the properties of the polymer rather than the drug. Contradictory results were found in a Sjokvist and Nystrom[86] report that the dissolution rate enhancement was dependent on the particle size of the griseofulvin released from the dispersions. In these cases, a drug-controlled dissolution mechanism is manifested.

Higuchi et al[87, 88] developed a mathematical model to describe the dissolution of binary systems. According to the Noyes Whitney equation, the dissolution rates of the both components are proportional to their respective product of solubilities (Cs) and diffusion coefficient (D). After a short period of time, one component (for example, B) will dissolve into the bulk phase from the surface of the solid mass if the following condition is met:

$$\frac{N_A}{N_B} > \frac{D_A C_{sA}}{D_B C_{sB}} \qquad 1\text{-}62$$

Where, $N_A$ and $N_B$ are the amounts of A and B in the binary mixture, respectively. As a result, an interfacial layer rich in A is left behind, through which B has to diffuse before releasing into the bulk solution (Figure 1-48).

In this case, the dissolution rate of A is given by:

$$G_A = \frac{D_A C_A}{h} \qquad 1\text{-}63$$

Where, h is the effective diffusion layer thickness. The dissolution rate of B is determined by that of A, as shown in the equation below:

$$G_B = \frac{N_B}{N_A} G_A \qquad 1\text{-}64$$

It follows that a drug controlled dissolution mechanism is expected at high drug loading whereas drug release from the dispersion is regulated by the dissolution rate of the polymer at low drug loading. The condition at which dominance changes is given by:

$$\frac{N_A}{N_B} = \frac{D_A C_{sA}}{D_B C_{sB}} \qquad 1\text{-}65$$

If similar diffusion coefficients are assumed, the drug loading up to which carrier-controlled release is anticipated will be lower for low solubility drugs than for more soluble drugs. Contradictorily, Dubois et al[85] observed a more limited range of drug loadings that exhibit carrier-controlled release for a more soluble drug phenacetin (up to 5%) than for a much less soluble drug indomethacin (up to 10%). However, this may be accounted for by the difference in distribution of two drugs in their respective dispersions or the difference

in diffusion coefficients. Sjokvist and Craig[89] reported that the aqueous solubilities decreased logarithmically with the molecular weight of PABAs. A linear relationship exists between the initial intrinsic dissolution rate of the dispersions and the aqueous solubility of para-aminobenzoates (PABAs), indicating a drug-controlled dissolution mechanism. In addition they found that the dissolution rate of PABAs from the dispersions was similar to that of the drug alone, independent of composition when the concentration of drug in the dispersion exceeds 20% (Figure 1-49). This is consistent with Higuchi's model. On the other hand, at low drug loadings, a carrier-controlled release is expected according to Higuchi. However, a positive interrelationship is apparent between the initial intrinsic dissolution rate and the solubilities of the PABAs at drug concentrations below 20%.

To reconcile such contradictions, Corrigan et al[83] provided an explanation for the dual observations of carrier–controlled and drug-controlled dissolution at low drug loadings (Figure 1-50), where a concentrated carrier layer is formed at the dissolving surface according to Higuchi. In the first scenario (a), that of the carrier-controlled mechanism, the dissolution of drug particles in the carrier layer is rapid as compared to the drug diffusion through this layer. As a result, the rate determining step of drug release into the bulk phase becomes the release of the carrier. In the second scenario (b), the dissolution of drug in the carrier layer is much slower than the diffusion rate, which allows the drug to be released effectively intact into the bulk phase. In this case, the dissolution rate of drug becomes dominated by the properties of the drug, such as particle size and/or physical form. Nevertheless, an enhanced release as compared to conventional dosage forms is still expected because the polymer carrier diffusion layer may provide the improved wetting and decreased agglomeration as the drug diffuses through. Overall, factors that may play a

role in determining the dissolution mechanism include the solubility of the drug in the polymer layer, the viscosity of the polymer, and the hydrodynamics of the medium.

Konno et al[90] compared the effect of different polymers (PVP, HPMC, and HPMCAS) on the dissolution rate of felodipine from solid dispersions. These dispersions were prepared at different polymer to drug ratio. They found that supersaturation was achieved for the majority of the dispersions prepared, with the exception of 10% to 50% w/w PVP dispersion. At each given polymer to drug ratio, HPMCAS dispersions generated the highest extent of supersaturation, while PVP turns out to be the least effective. This was attributed to the different magnitude of polymers' ability to inhibit solution crystallization, as has been discussed previously. Moreover, the extent of supersaturation observed increased as the polymer to drug ratio increased. This dependence was strongest in HPMCAS dispersions whereas PVP dispersions only shown limited increase in solution concentration as a function of polymer concentration. For the majority of the release profiles, a plateau region was observed which roughly equals the maximum solution concentrations achieved. 75% HPMCAS dispersion were able to achieve the highest solution concentration of $14\,\mu g/ml$, as compared to only $0.9\,\mu g/ml$ equilibrium crystalline solubility. However, desupersaturation occurs at the late stage of the experimental timeframe. This finding, again, exemplified the increased thermodynamic driving force for crystallization at high supersaturation. Finally, it was found that crystalline felodipine solubility did not change whether those polymers were present or absent in the dissolution medium tested. Therefore, any supersaturation attained during dissolution of solid dispersions could not be accounted for by solubilization effect of polymers, which have been reported in several literatures[91-93].

Alonzo et al[94] investigated the dissolution and precipitation behavior of HPMC and PVP amorphous solid dispersions (ASDs). Felodipine and indomethacin were selected as model compounds. They found that at moderate drug loading (50%), the maximum solution concentrations generated were similar to the predicted amorphous solubility (5-6 μg/ml for felodipine at 25 ℃) using the Hoffman equation, despite there being more drug in the systems (Figure 1-51). In this case, the dissolution behavior of the ASDs was controlled by a pure layer of amorphous drug, which was left behind after the polymer entered the bulk solution. Therefore, the maximum solution concentration cannot exceed that of the pure amorphous drug. At low drug loading (10%), however, the initial dissolution rates were much faster than that of the 50% dispersions, resulting in very high apparent peak concentrations. In this scenario, the drug loading was not sufficient to allow the formation of a drug rich layer limiting dissolution. Instead, the dissolution rate of the drug was controlled by the rapid dissolution of the polymer. Hence, very high supersaturation was generated. Another interesting observation is that the solutions became uniformly cloudy upon dissolution of the 90:10 ASDs whereas cloudiness was not observed during dissolution of the 50:50 ASDs.

Shown in Figure 1-52 are the cross-polarized microscope images of the ASDs exposed to phosphate buffer, which provides a qualitative assessment of the dissolution behavior. It can be seen that the particles of the 50:50 HPMC-felodipine dispersion were able to maintain their size and shape for at least 30 minutes whereas particles of the 90:10 HPMC-felodipine dispersion lost their integrity within 5 minutes of exposure.

Dynamic light scattering (DLS) experiments were performed to monitor the particle size generated during the dissolution of ASDs. It can be seen from Figure 1-53 that particles of

submicron scale were detected during dissolution of 90:10 solid dispersions, which then gradually increase in size. It is also apparent that PVP was less effective in inhibiting the growth of the particles. The growth of particles from artificially supersaturated solution in the absence of any polymer was much more rapid. At 7 minutes, the average particle diameter was slightly below 1 micron. This size is enough for significant precipitation to occur.

## 1.14    Research Overview

The overall goal of this research is to improve the physical stability and dissolution performance of amorphous solid dispersions (ASDs) by using a combination of polymers, whereby one polymer is included to inhibit crystallization during dissolution, whereas a second polymer is used to achieve another key property such as rapid release or enhanced storage stability.  Before this strategy can be implemented, research is necessary to determine factors such as miscibility in the ternary systems, as well as the optimum level of the solution stabilizing polymer, since it is clear that an additional polymer cannot be added at the expense of drug loading.

In this chapter, the thermodynamics with respect to the miscibility of amorphous materials are discussed. The mechanisms of polymeric additives in inhibiting nucleation and growth of drugs from both solid and solution phase are examined. The impact of polymers in modifying drug release from ASDs are also discussed. In chapter 2, efforts were made to probe the relative effectiveness of various polymers in inhibiting matrix crystallization of ASDs of CEX upon exposure to aqueous medium versus crystallization from supersturated solutions generated during dissolution of the ASDs. In chpater 3, the strength of

intermolecular interaction and miscibilty of polymer blends and CEX with polymer(s) and are investigated, directed towards obtaining a better mechanistic understanding on the stability of the CEX ASDs during storage at different environmental conditions. Chapter 4 showcased an example where both the drug release rate and supersaturation behavior can be optimized in a ternary ASD, so long as the relevant properties of polymeric carriers are appreciated.

Table 1-1 Biopharmaceutics classification system of drugs and recommended formulation strategies

| BCS CLASS | SOLUBILITY | PERMEABILITY | % OF PRODUCTS ON THE MARKET | % OF DRUG CANDIDATES | FORMULATION APPROACH |
|---|---|---|---|---|---|
| I | High | High | 35% | 5–10% | Tablet or capsule |
| II | Low | High | 30 | 60–70 | Particle-size reduction, salt formation, self-emulsifying systems, nanoparticles, solid dispersions, surfactants |
| III | High | Low | 25 | 5–10 | Absorption and permeability enhancers, lipids |
| IV | Low | Low | 10 | 10–20 | Combination of Class II and III approaches |

BCS = Biopharmaceutics Classification System from FDA. **SOURCE:** Company information

Table 1-2 Experimental Solubility Ratios for indomethacin

| Compound | Forms | Solubility ratio | Comments |
|---|---|---|---|
| This work: | | | |
| Indomethacin | $\alpha$-crystal/$\gamma$-crystal | 1.1 | 45°C, water |
| Indomethacin | amorphous/$\gamma$-crystal | 4.4 | 5°C, water |
| | | 4.5 | 25°C, water |
| | | 2.8 | 45°C, water |

Table 1-3 Intrinsic Dissolution Rate and Solubility of Crystalline and Amorphous Atorvastatin Calcium in Water at 37 ℃.

| form | intrinsic dissolution rate $\mu g/(min/cm^2)$ | | solubility $\mu g/mL$ | mean particle size |
|---|---|---|---|---|
| crystalline | 84.9 | | 142.2 | $3.83 \pm 0.08\,\mu m$ |
| amorphous | early phase (10 min) | late phase | | |
| SASA[b] | 288.5 ($\times$ 3.4) | 179.5 ($\times$ 2.1) | 483.2 ($\times$ 3.4) | $68.7 \pm 15.8$ nm |
| SDA[c] | 280.1 ($\times$ 3.3) | 175.5 ($\times$ 2.1) | 469.1 ($\times$ 3.3) | $3.62 \pm 0.15\,\mu m$ |

Increase in IDR and solubility compared to the crystalline form is given as (_ times). SASA: supercritical antisolvent amorphous from acetone. SDA: spray-dried amorphous from acetone

Table 1-4  Desired carrier properties for solid dispersion formulation

| | |
|---|---|
| Safety | Inert |
| | GRAS (generally recognized as safe) |
| Preparation | Melting methods: |
| |     Thermally stable |
| |     Thermoplasticity (hot melt extrusion) |
| | Solvent methods: |
| |     Soluble in organic solvents |
| Release | Water soluble |
| | Solubilizing properties |
| | Stabilizing properties |
| Stability | High Tg |
| | High fragility |
| | Hydrogen donors/acceptors |

Table 1-5 Examples of commercially available solid dispersions

| Brand name | Manufacturer | Drug | Carrier |
|---|---|---|---|
| Gris-PEG | Pedinol Pharmacal Inc. | Griseofulvin | PEG6000 |
| Cesamet | Valeant Pharmaceuticals | Nabilone | PVP |
| Kaletra | Abbott | Lopinavir, ritonavir | PVPVA |
| Sporanox | Janssen Pharmaceutica | Itraconazole | HPMC |
| Intelence | Tibotec | Etravirin | HPMC |
| Certican | Novartis | Everolimus | HPMC |
| Isoptin SR-E | Abbott | Verapamil | HPC/HPMC |
| Nivadil | Fujisawa Pharmaceutical Co., Ltd | Nivaldipine | HPMC |
| Prograf | Fujisawa Pharmaceutical Co., Ltd | Tacrolimus | HPMC |
| Rezulin | Developed by Sankyo, manufactured by Parke-Davis division of Warner-Lambert | Troglitazone | PVP |

HPMC, hydroxypropylmethylcellulose; HPC, hydroxypropyl cellulose; PVP, polyvinylpyrrolidone; PVPVA, polyvinylpyrrolidone-co-vinylacetate.

Table 1-6 Thermodynamic nature and destabilization driving force for solid dispersions in zone I-VI Assuming all solid dispersions were homogeneously mixed initially.

| Zone | Thermodynamic Nature | Destabilization Driving Force |
|---|---|---|
| I | Thermodynamically stable glass | None |
| II | Thermodynamically stable liquid | None |
| III | Supersaturated glass | Crystallization of supersaturated drug |
| IV | Supersaturated liquid | Crystallization of supersaturated drug |
| V | Supersaturated and immiscible glass | Amorphous phase separation, crystallization of supersaturated drug |
| VI | Supersaturated and immiscible liquid | Amorphous phase separation, crystallization of supersaturated drug |
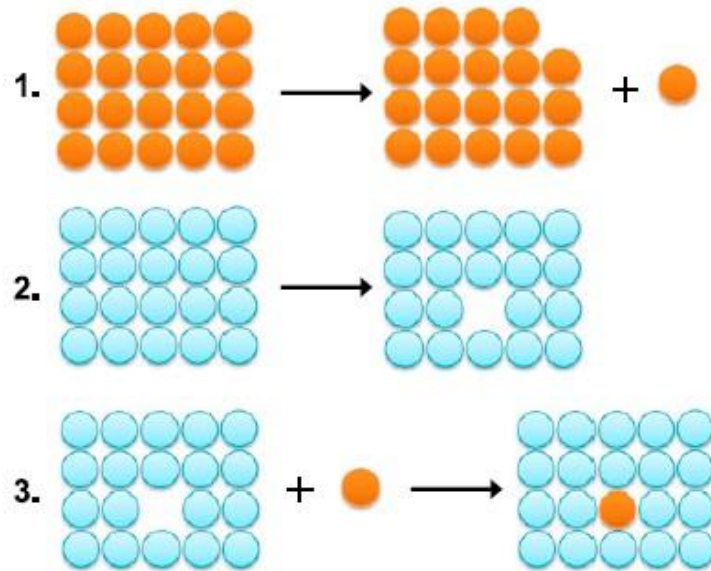
Figure 1-1 Three steps required for a solute to be displaced from solid state and to enter solution[5]



100% crystalline                                          100% amorphous
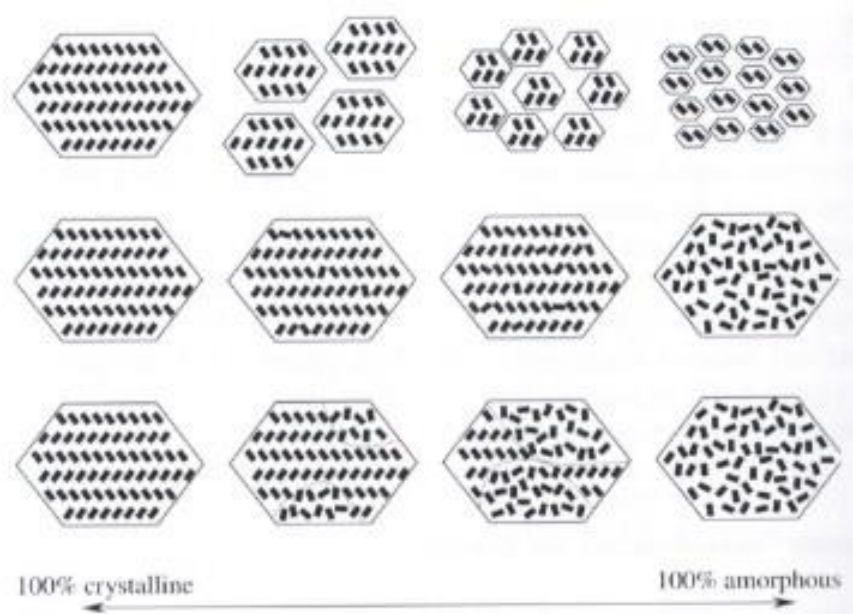
Figure 1-2 Schematic Representation of the three types of continuity between 100% crystalline and 100% amorphous solids[13]
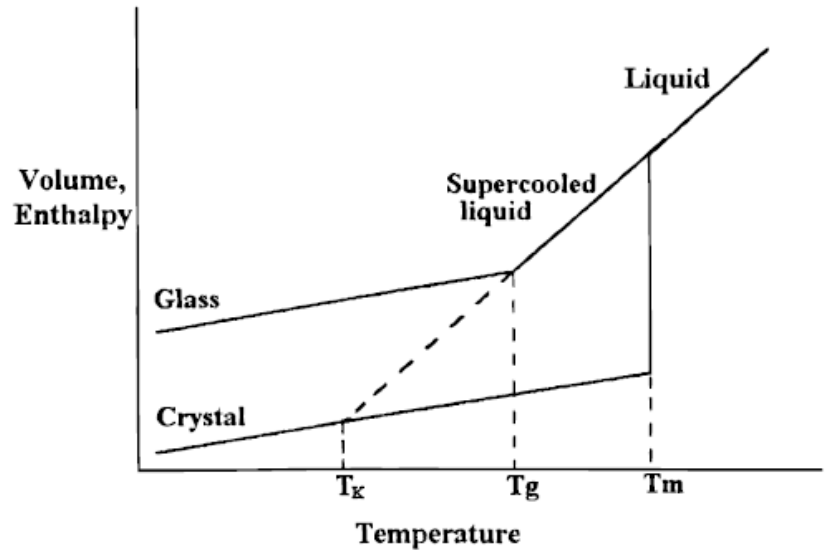
Figure 1-3  Schematic depiction of change in volume and enthalpy with temperature[9].
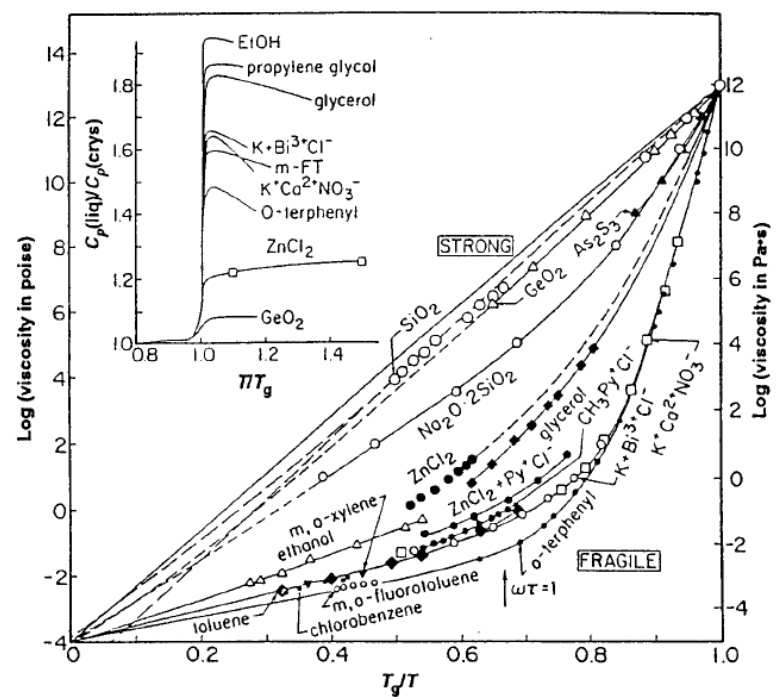


Figure 1-4 Molecular mobility/viscosity of amorphous materials as a function of normalized temperature above $T_g$.[9]
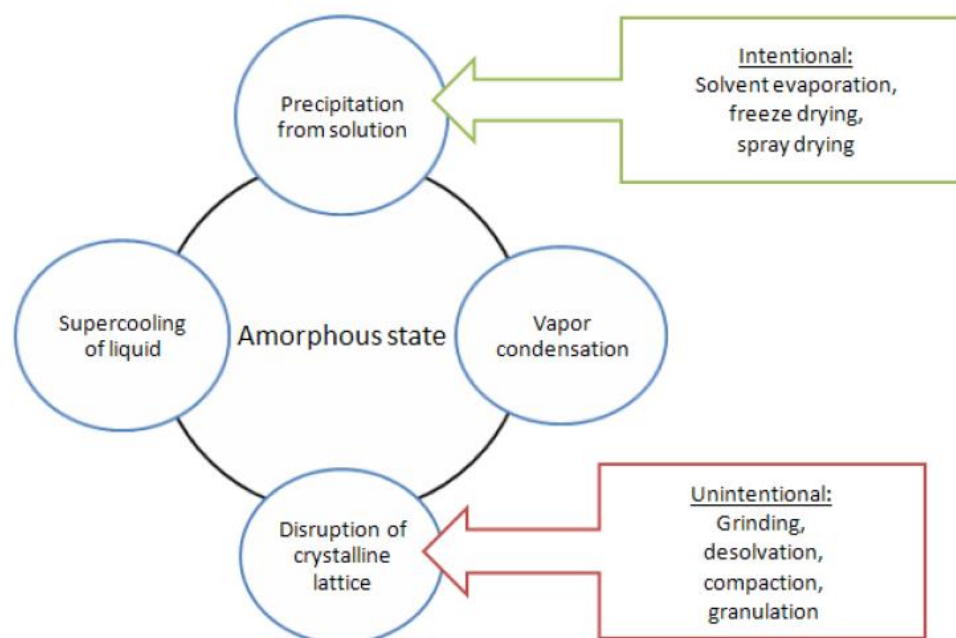
Figure 1-5 Amorphous state produced in typical pharmaceutical unit operations.
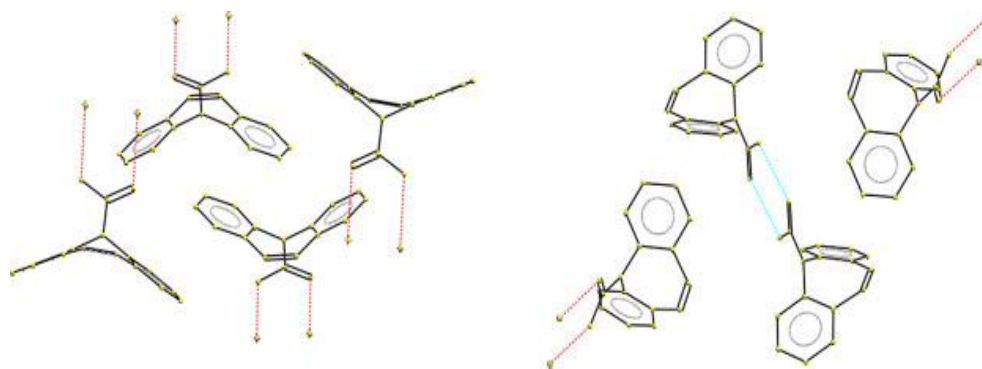


Figure 1-6 On Left-Packing diagrams of carbamazepine form I (N2-O1 intermolecular hydrogen bond length 2.929A ̊). On Right: Carbamazepine form III (N2-O1 intermolecular hydrogen bond length 2.928 A ̊)[19]
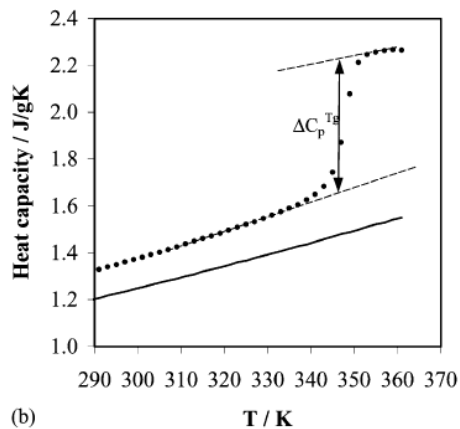
Figure 1-7 Heat Capacity Vs Temperature for Sucrose.
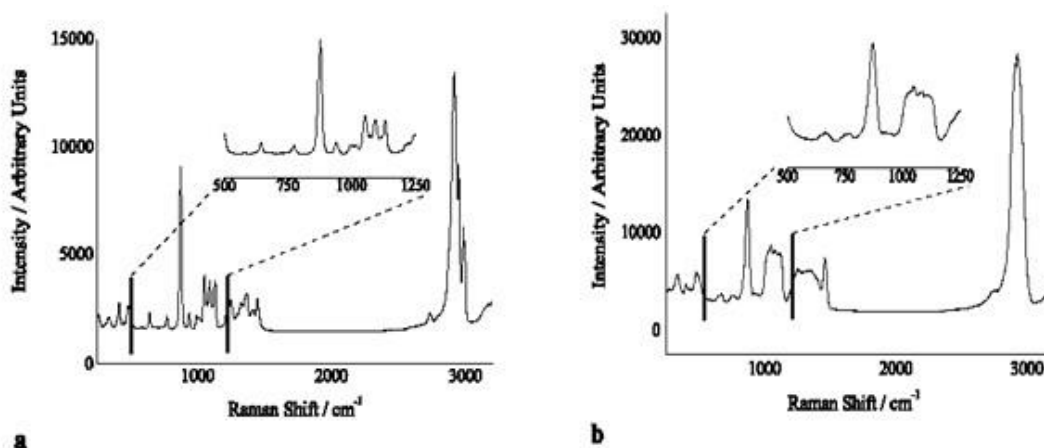


Figure 1-8 Raman Spectra: (a) crystalline sorbitol and (b) quench cooled glassy sorbitol.
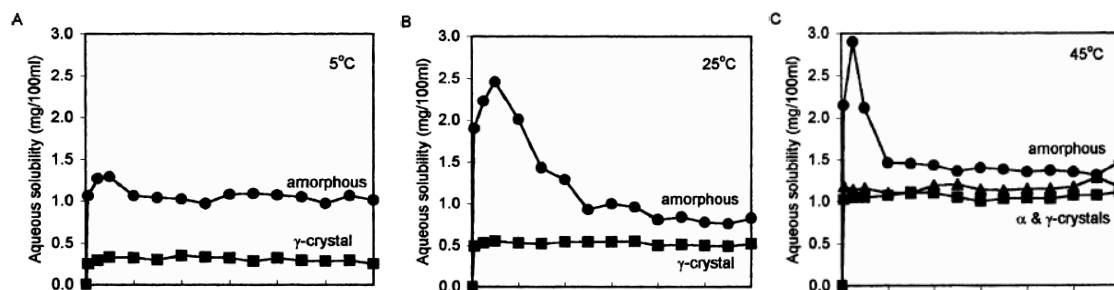


Figure 1-9 Experimental aqueous solubility profiles for amorphous and crystalline indomethacin ( ● ) amorphous; (■) γ-crystal; and ( ▲ ) α-crystal (A) at 5 ℃ (B) at 25 ℃ (C) at 45 ℃.[31]
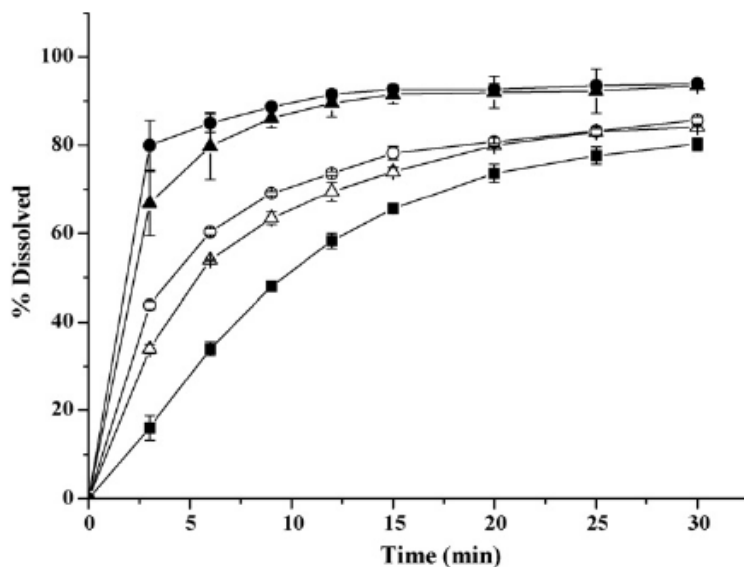
Figure 1-10 Powder dissolution profiles of unprocessed atorvastatin particles ( ■ ), SAS processed amorphous atorvastatin calcium precipitated from an acetone solution (●), SAS processed amorphous atorvastatin calcium precipitated from a tetrahydrofuran solution (▲), spray-dried amorphous atorvastatin calcium from an acetone solution (○) and spray-dried amorphous atorvastatin calcium from a tetrahydrofuran solution (□) ($n = 3$, mean±S.D.).[37]
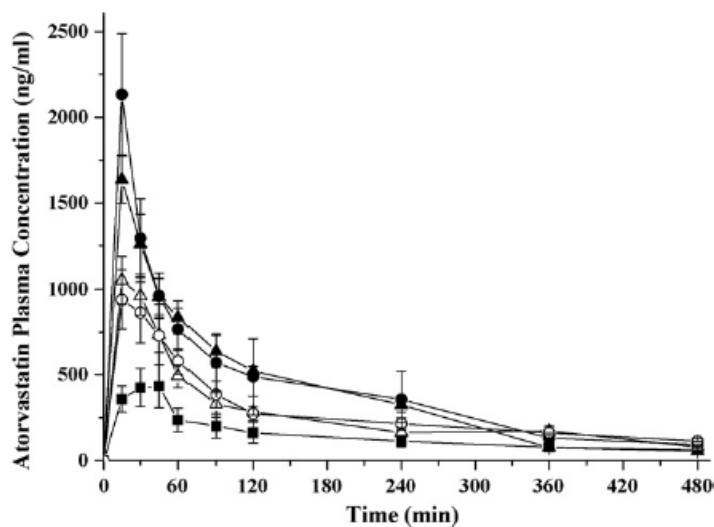


Figure 1-11 Plasma concentration–time curves of unprocessed atorvastatin particles (■), SAS processed amorphous atorvastatin calcium precipitated from an acetone solution (●), SAS processed amorphous atorvastatin calcium precipitated from a tetrahydrofuran solution (▲), spray-dried amorphous atorvastatin calcium from an acetone solution (○) and spray-dried amorphous atorvastatin calcium from a tetrahydrofuran solution (□) ($n = 5$, mean±S.D.). [37]
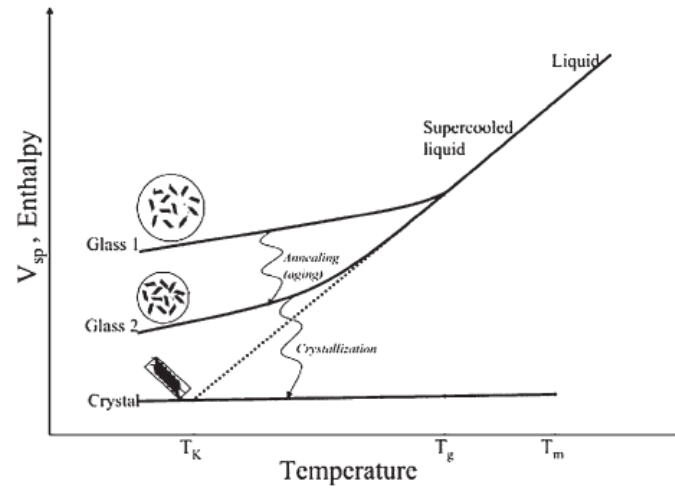
Figure 1-12 Enthalpy and specific volume change of amorphous materials during annealing[32]
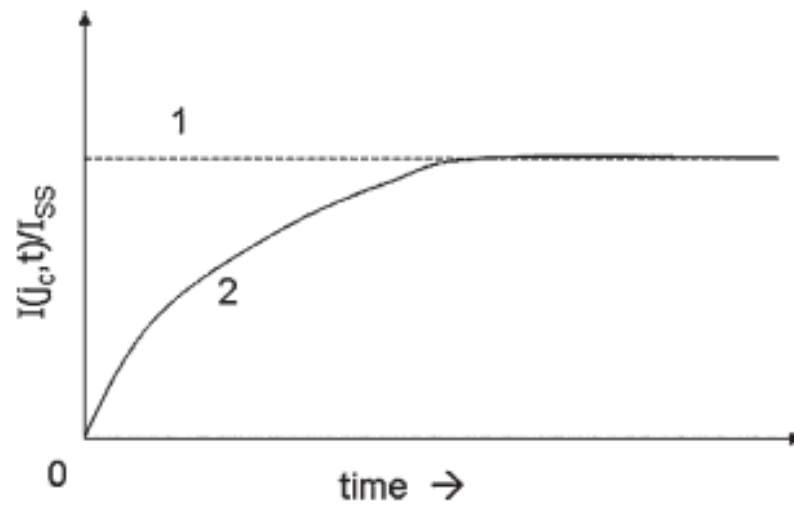


Figure 1-13 Time dependence of nucleation rate I ($j_c$,t): (1) steady state nucleation; (2) non-steady state nucleation rate[32].
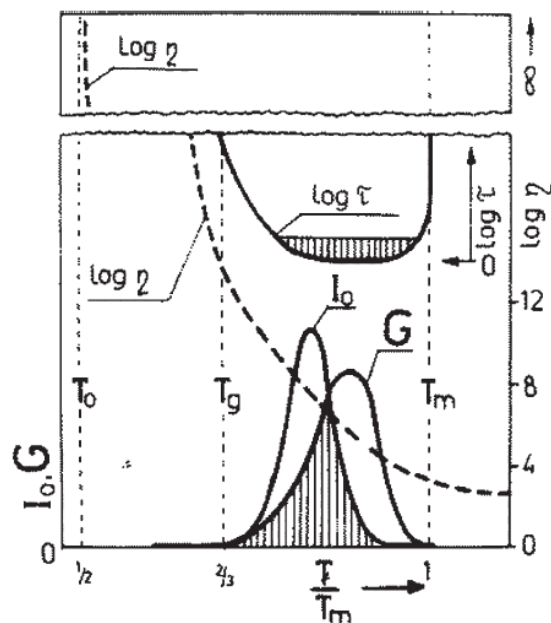
Figure 1-14 Schematic of nucleation rate ($I_0$),crystal growth rate(G), non-steady state lag time for crystallization ($\tau$), and viscosity ($\eta$) in a supercooled liquid. $T_0$ is the VTF zero mobility temperature, $T_g$ is the glass transition temperature, and $T_m$ is the melting temperature. Shaded region is where the nucleation and growth overlap[32]
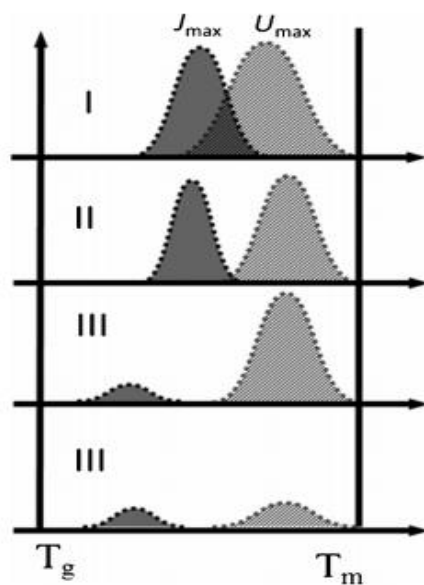


Figure 1-15 Schematic diagram of the temperature dependence of nucleation rate (J) and growth rate (U)[46].
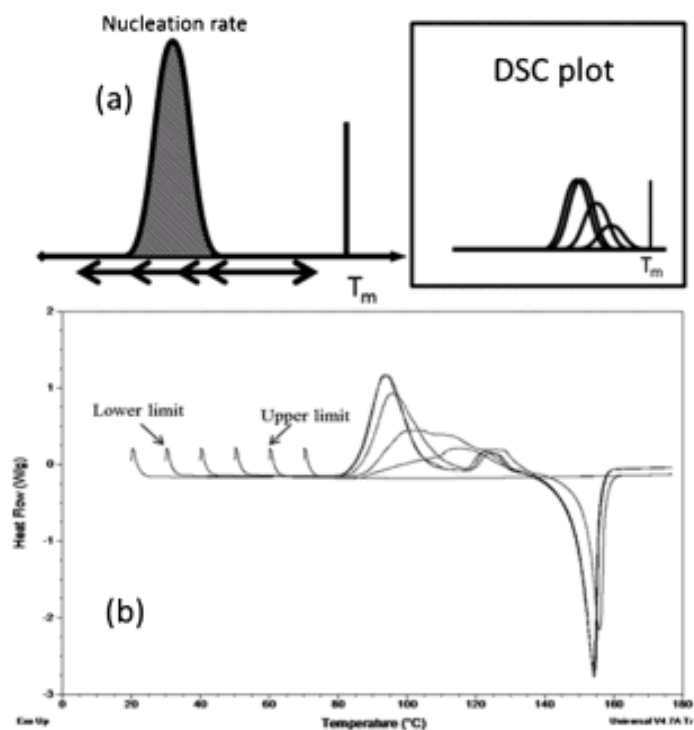
Figure 1-16 (a) A schematic of the expected DSC plot when the sample is cooled to different regions of the nucleation temperature zone. (b) An actual example of a nucleation zone experiment for APAP-PVPVA (10%w/w) showing that the recrystallization peak temperature does not change when cooled below 30 °C.
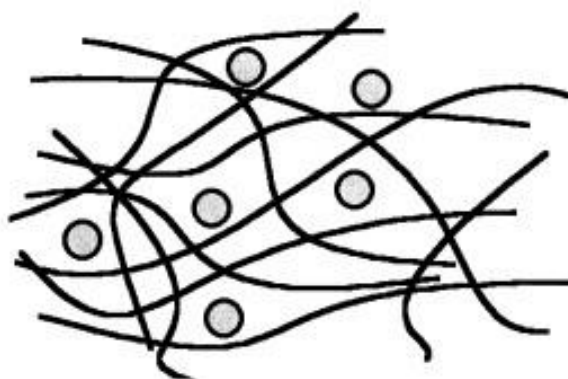


Figure 1-17 Amorphous solid solution: solute molecules are dispersed molecularly but irregularly in an amorphous solvent[47]
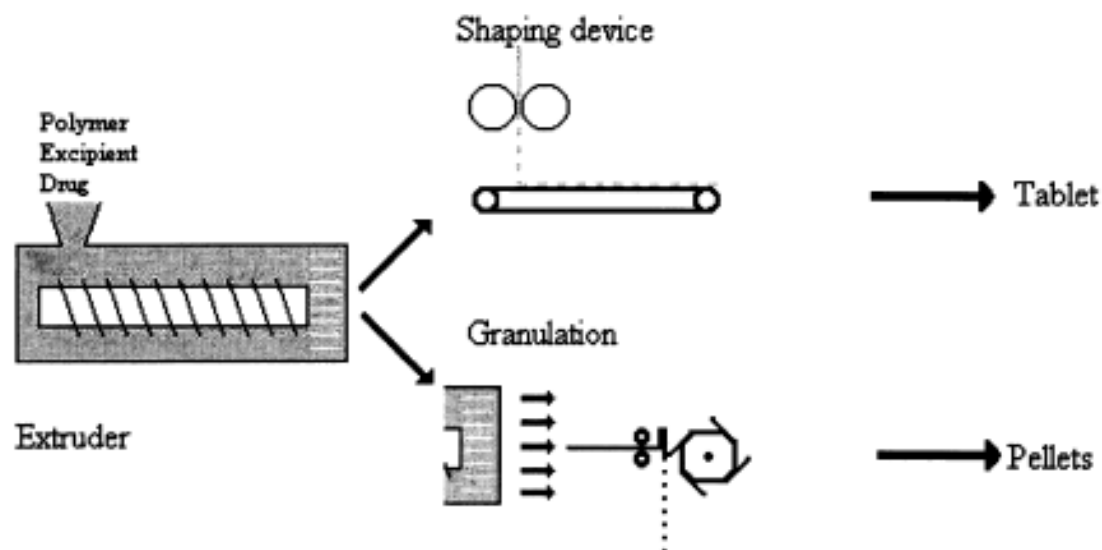
Figure 1-18 Scheme of a hot melt extruder.
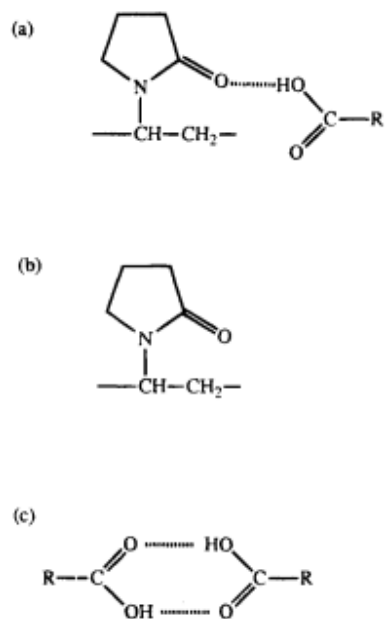


Figure 1-19 Species proposed to be present in indomethacin-PVP solid dispersions. a) hydrogen bonded indomethacin-PVP species, b) non hydrogen bonded PVP and c) indomethacin symmetric dimer[10].
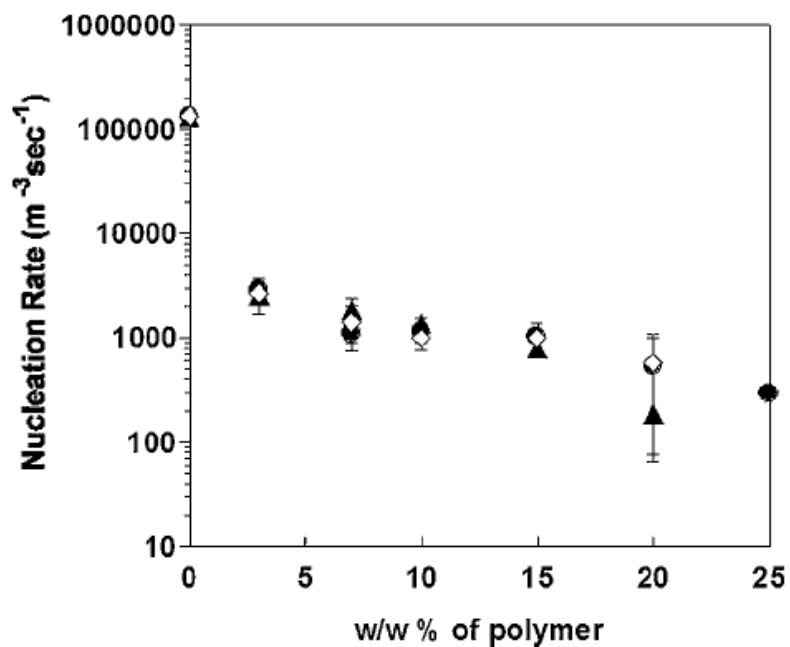
Figure 1-20 Nucleation as a function of polymer concentration at 0% RH. Symbols represent data for felodipine with HPMCAS (▲), PVP (●), and HPMC (◊)[54]
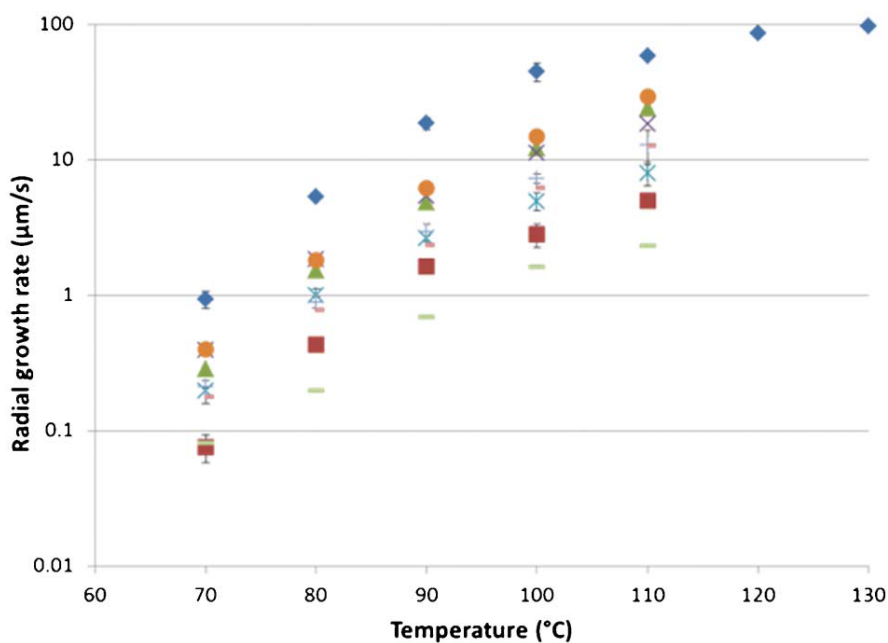


Figure 1-21 Radial growth rate of the spherulite of APAP (◆) and in the presence of HPMCAS (●), E100 (▲), HPMC (×), PVP (✳), PVPh (▬), PVPVA (+), PAA 1800 (■), and PAA (450 K) (▬)[46]
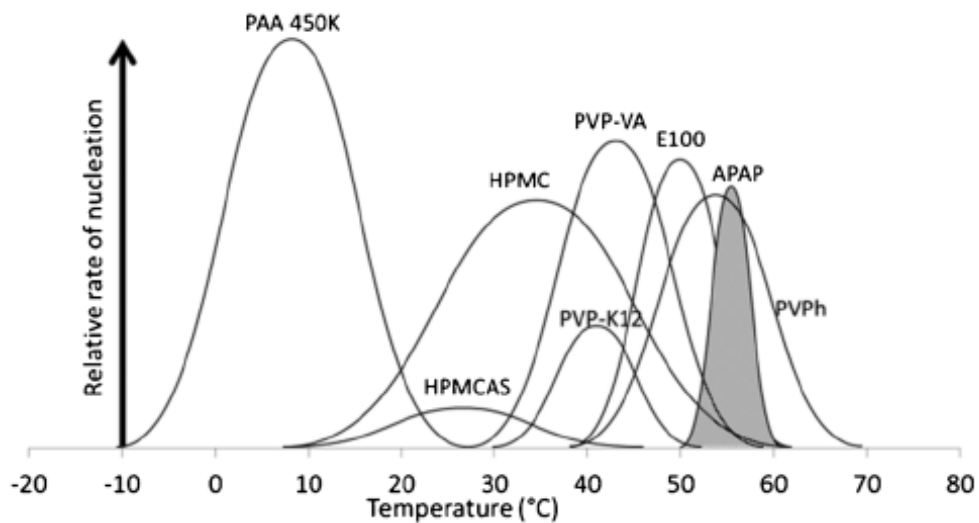
Figure 1-22 A semi quantitative representation of the nucleation temperature zones and relative nucleation rates of pure APAP (shaded region) and APAP in the presence of 10% w/w polymer[46].
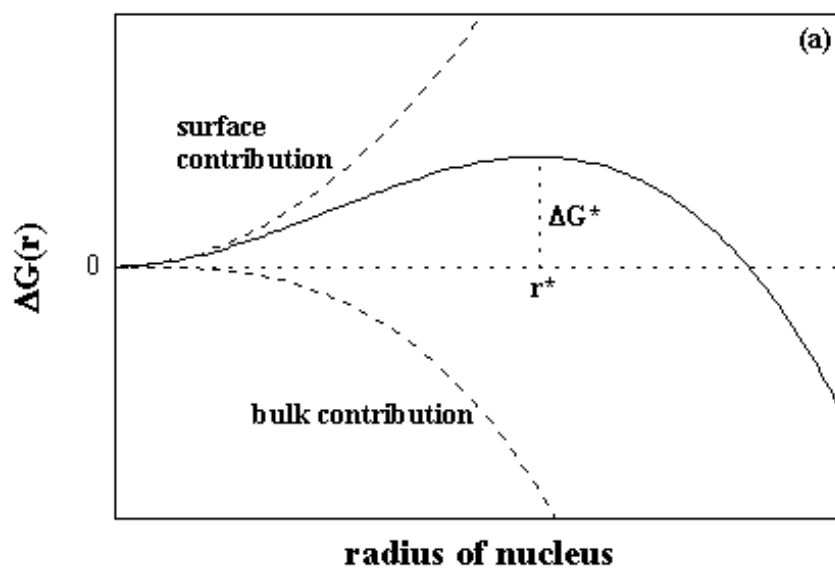


Figure 1-23 Nucleation free energy change as a function of the clusters radius r.
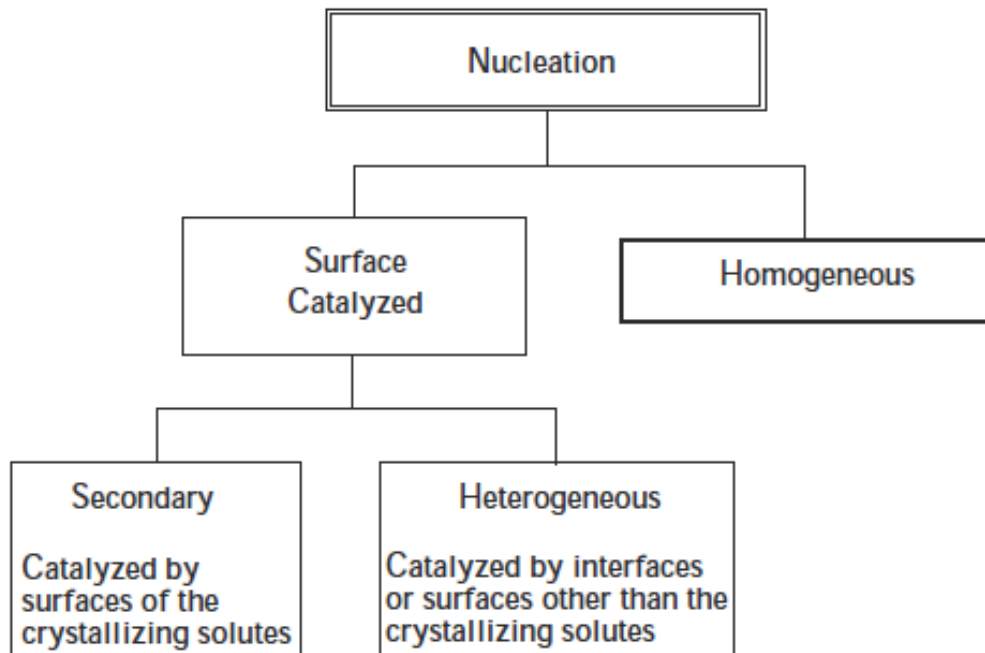
Figure 1-24 Mechanisms for crystal nucleation
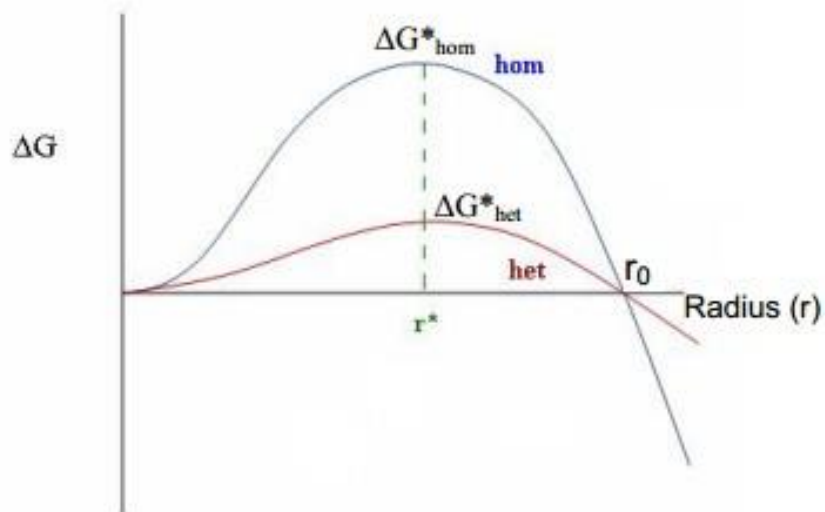


Figure 1-25 Free energy barrier for homogeneous nucleation and heterogeneous nucleation
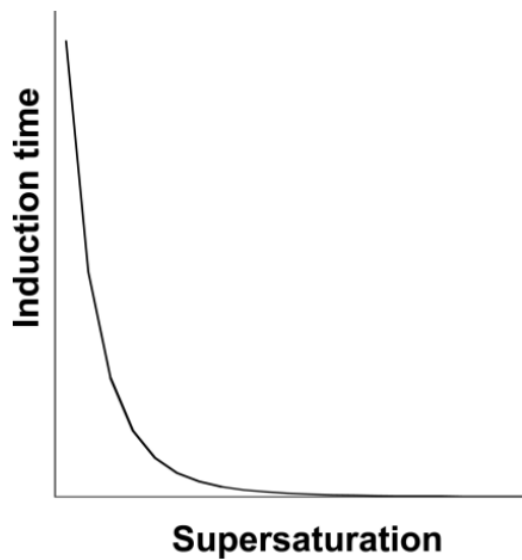
Figure 1-26 The induction time for nucleation as a function of supersaturation[60]
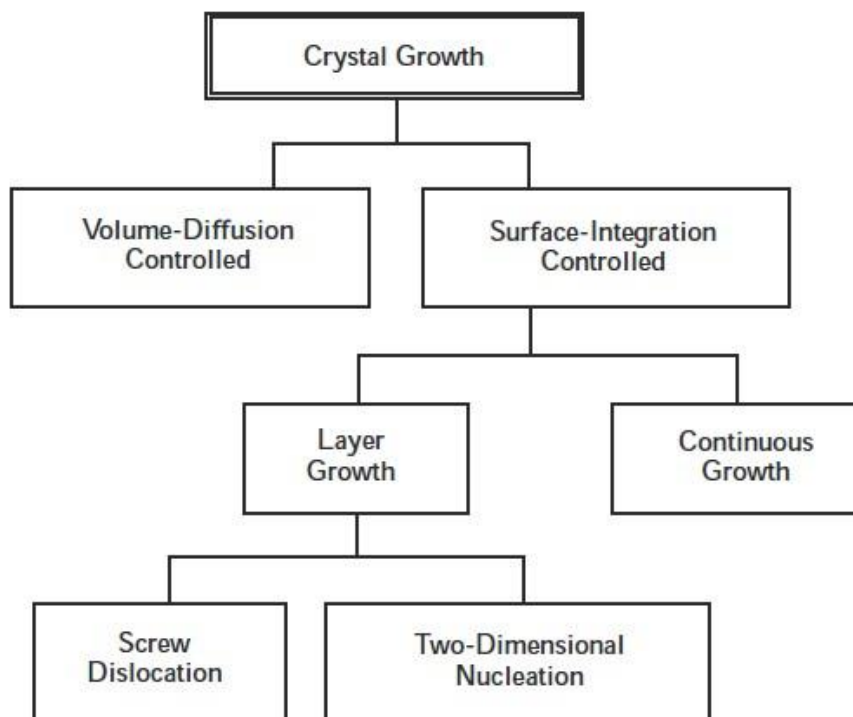


Figure 1-27 Mechanisms for crystal growth.[59]
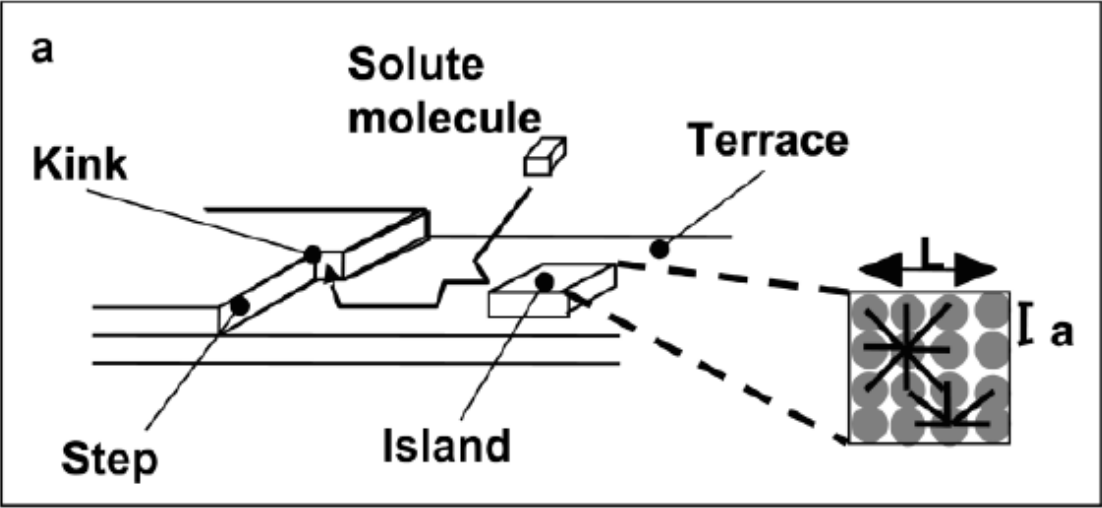
Figure 1-28 Surface layer adsorption of solute molecules onto the growing crystal surface
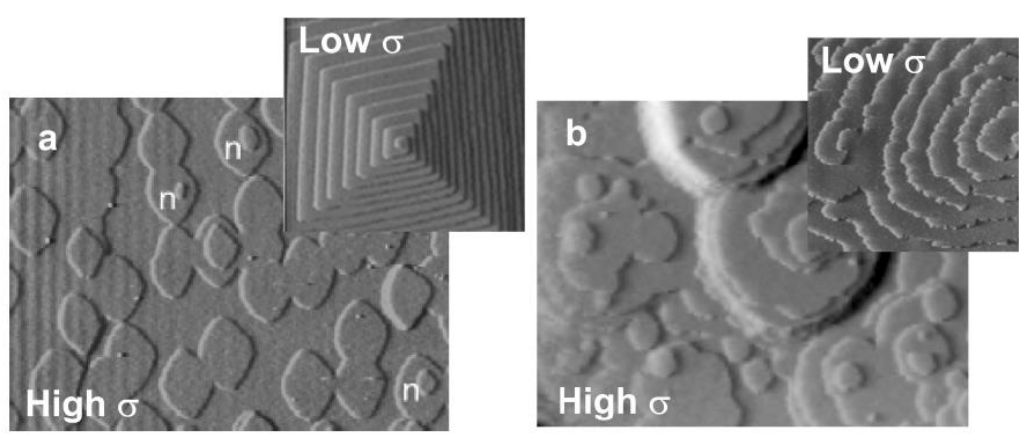


Figure 1-29 AFM images showing examples of 2D nucleation at high supersaturation for (a) calcite and (b) canavalin. N-locations where islands have nucleated on top of other islands[60]
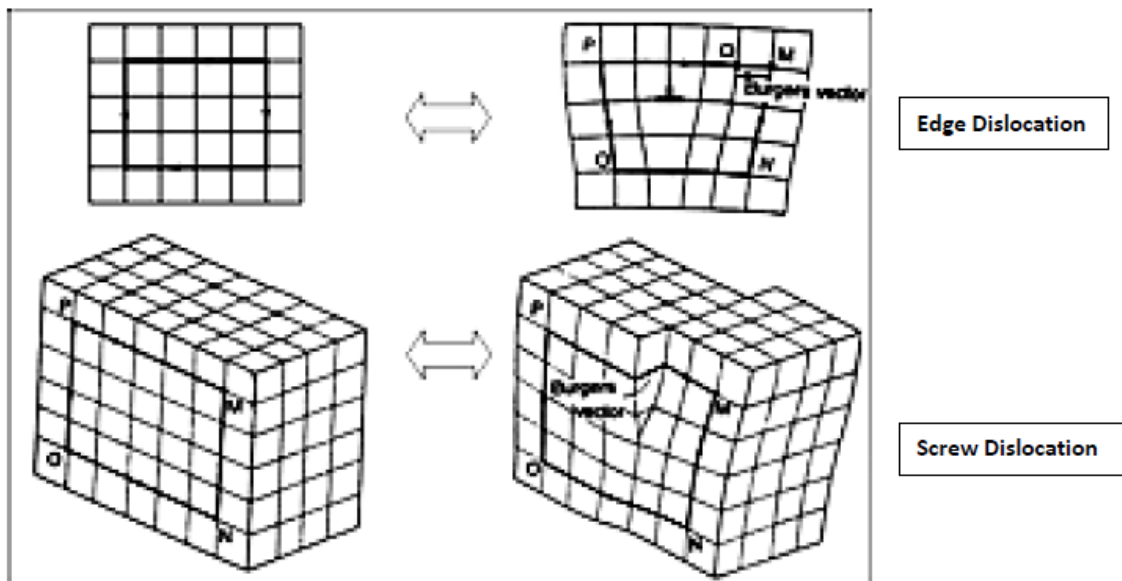
Figure 1-30 Edge dislocation and screw dislocation
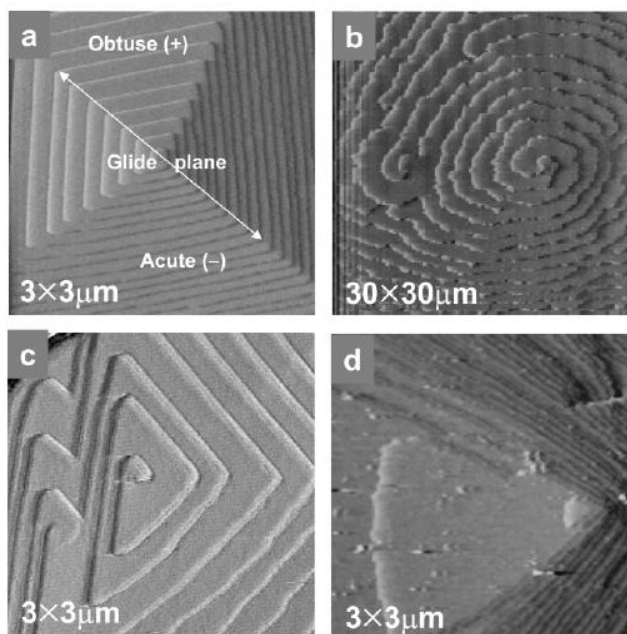


Figure 1-31 AFM images of dislocation hillocks on (a) calcite, (b) canavalin, (c) brushite and (d) calcium oxalate monohydrate[60]
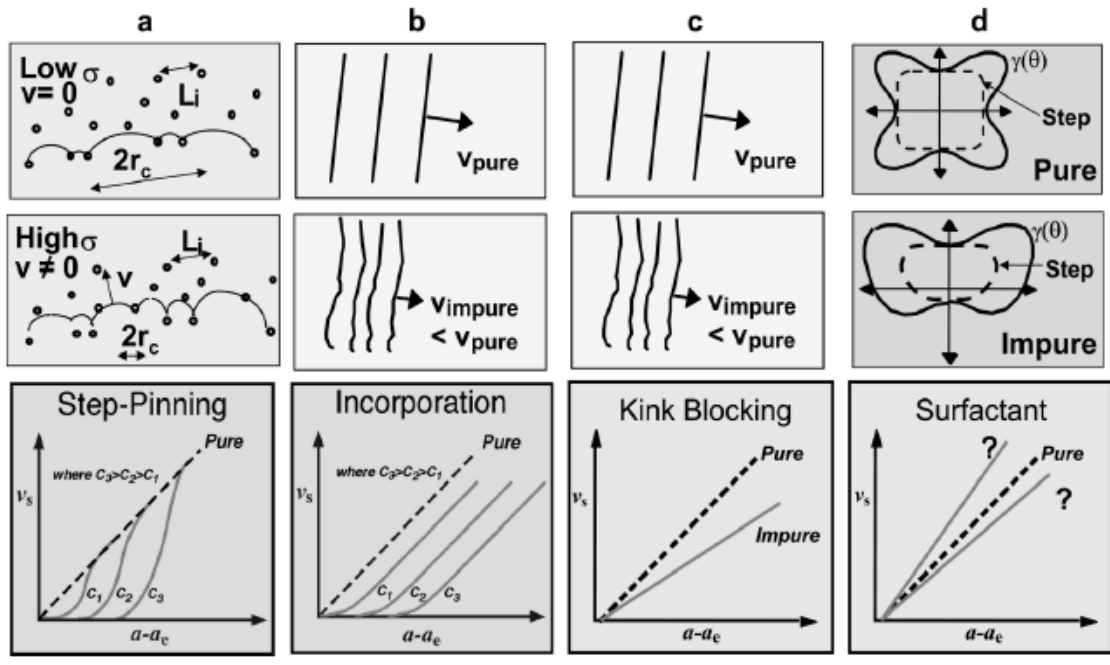
Figure 1-32 Four models for impurity interactions and their effect on step kinetics: (a) step pinning, (b) incorporation. (c) kink blocking, and (d) surface action[64].
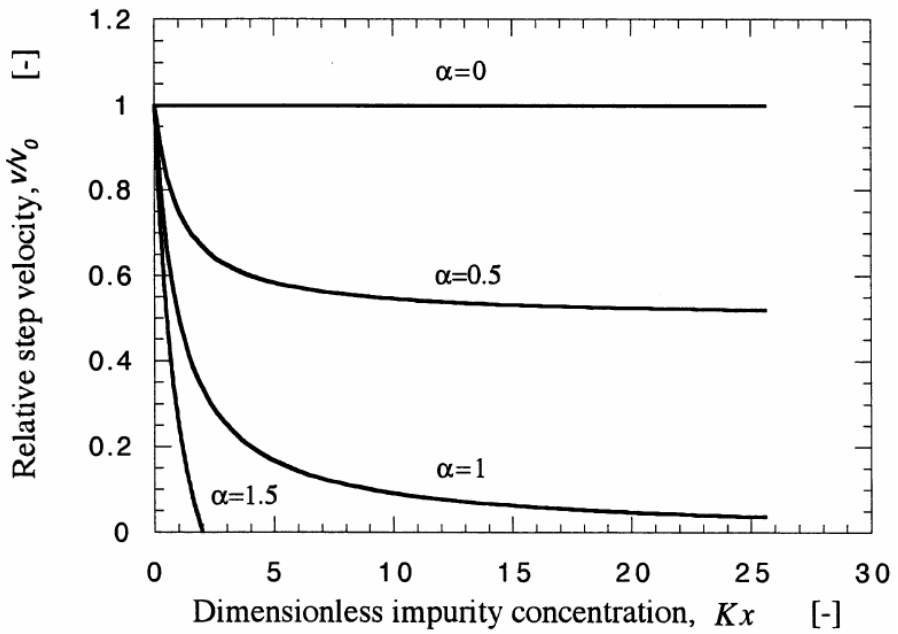


Figure 1-33 Theoretical relationship between the relative step velocity and the dimensionless impurity concentration Kc for different values of the impurity effectiveness factor α[65].
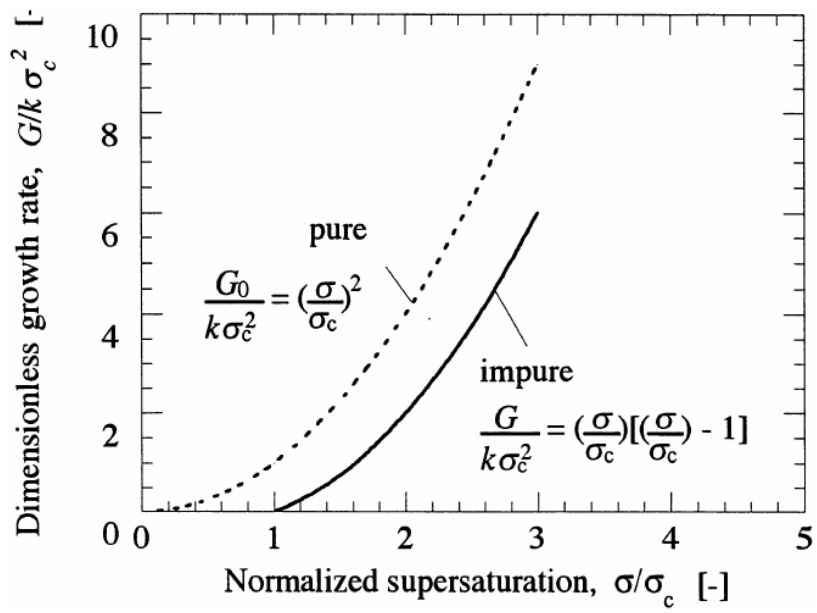
Figure 1-34 Theoretical normalized face growth rate $G/k\,\sigma_c^2$ as a function of normalized relative supersaturation $\sigma/\sigma_c$ for the second order growth law $G_0 = k\,\sigma^2$. The face growth rate is suppressed over a wide range of relative supersaturation in this steady state impurity action.[65]
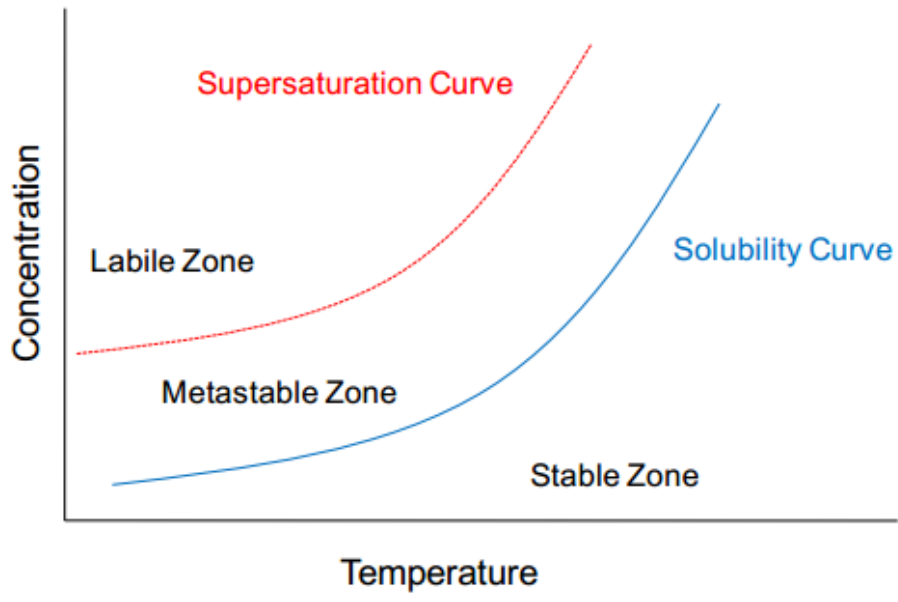


Figure 1-35 Regions of solution stability
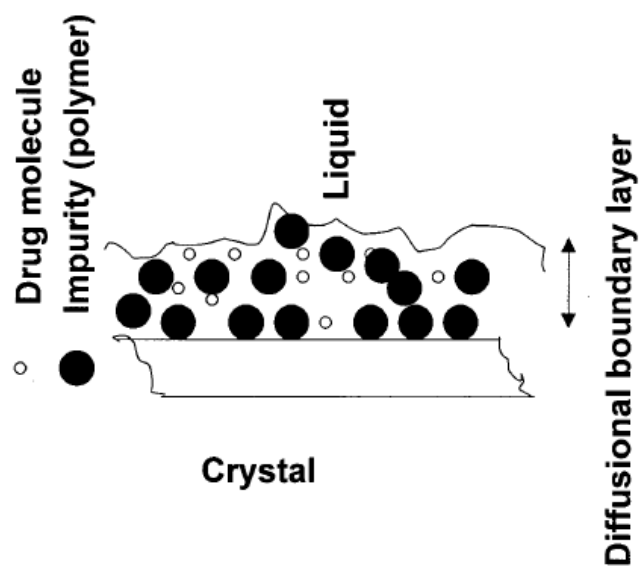
Figure 1-36 Schematic diagram showing the mechanism of growth inhibition and habit modification of HA crystals by polymers[69].
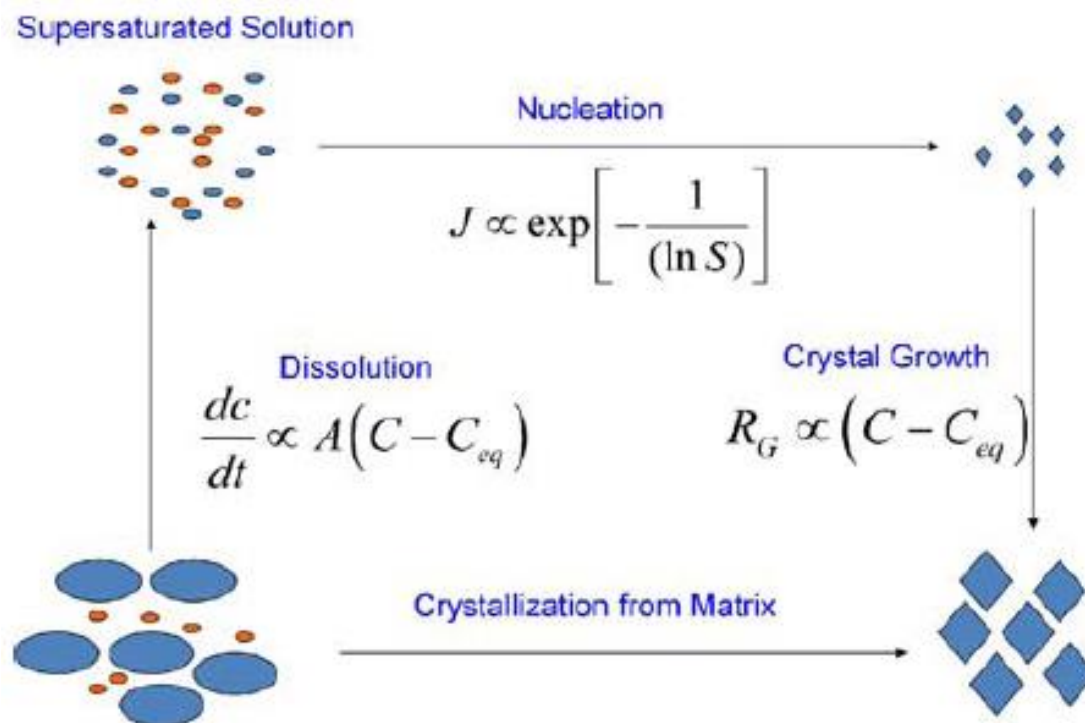


Figure 1-37 Schematic illustrating the competition between dissolution and crystallization via the solid or solution state for amorphous systems[67].
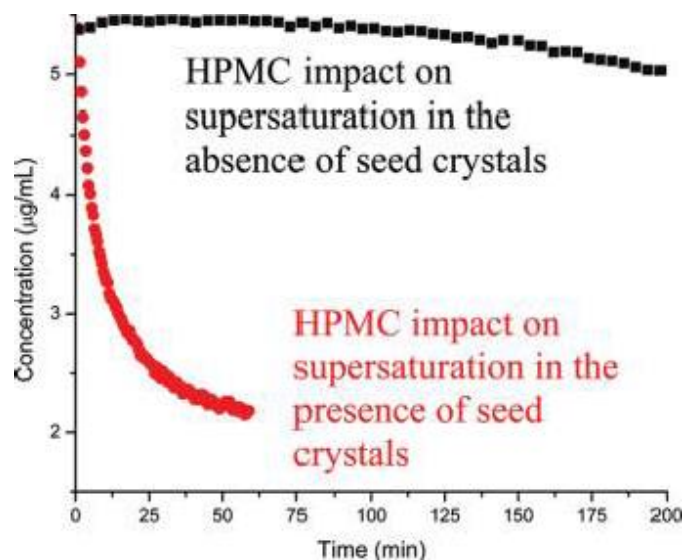
Figure 1-38 Unseeded and seeded desupersaturation of felodipine (S of 10) in the presence of 1ug/ml HPMC.
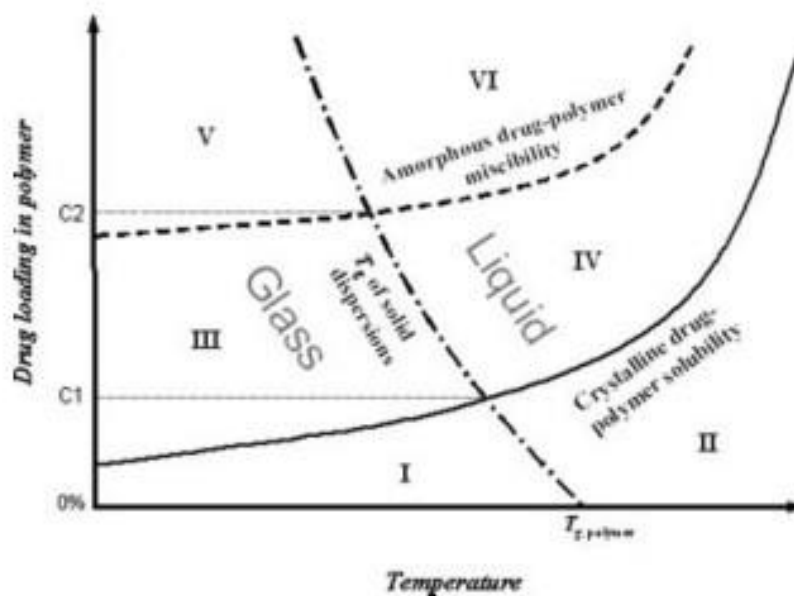


Figure 1-39 A hypothetical diagram consists of drug-polymer solubility, miscibility, and glass transition temperatures of a solid dispersion system[73].
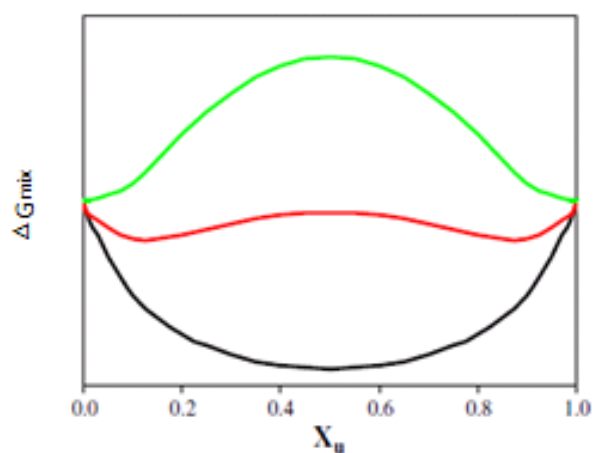
Figure 1-40 composition dependence of free energy of mixing ($\Delta G_{mix}$) for a binary hypothetical mixture, showing complete immiscibility (green), partial immiscibility (red), and complete miscibility behaviors (black)[76].
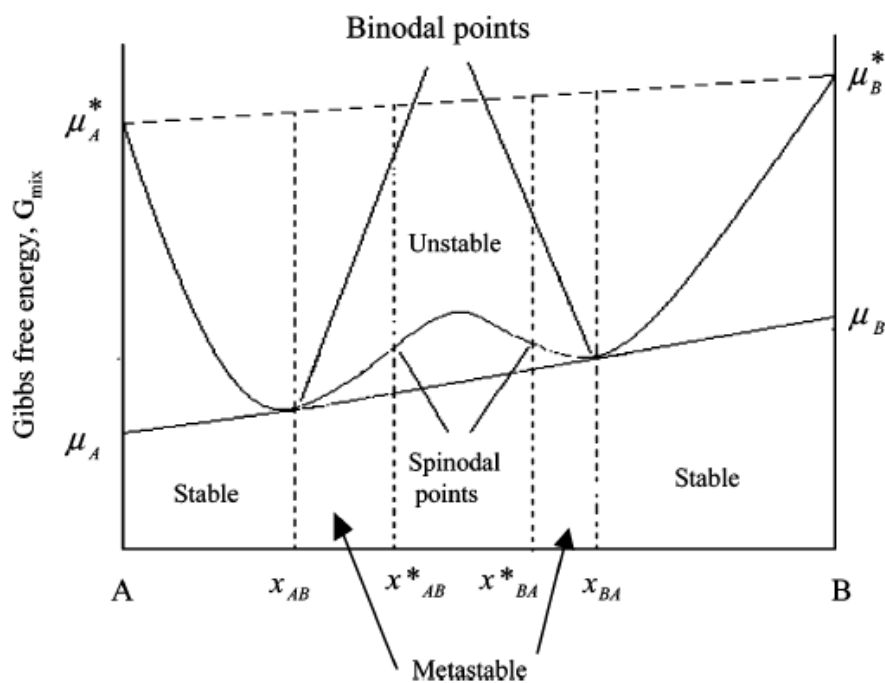


Figure 1-41 Gibbs free energy function exhibiting liquid-liquid miscibility gap[75].

Figure 1-42 Chemical structure of felodipine (left) and PAA (right).



Figure 1-43 Reference mid-IR spectra (1200–1800 cm$^{-1}$): Average local nanoscale mid-IR spectra ($n = 10$, normalized and offset). From top to bottom: pure PAA, pure amorphous felodipine, and pure crystalline felodipine[79].
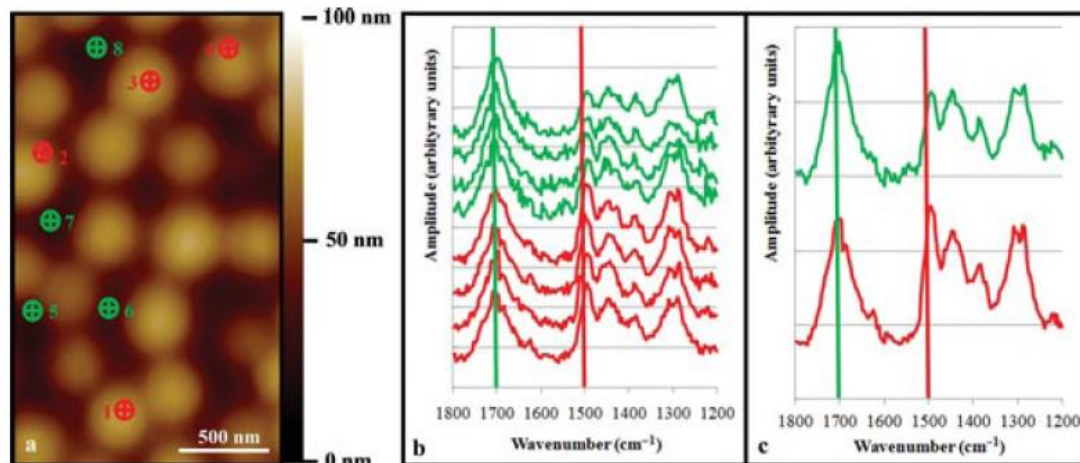
Figure 1-44 Localized nanoscale mid-IR spectra of a 50:50 (w/w) felodipine–PAA system obtained at discrete domains (1–4) and in the continuous phase (5–8): (a) topographical image (1.5 ×2.5 μm², color scale is 100 nm, the positions of the spectral measurements are marked), (b) nanoscale mid-IR spectra (1200–1800 cm⁻¹, spectra from bottom to top corresponds to locations 1–8, normalized and offset), and (c) average spectra of both phases (1–4 bottom, 5–8 top, $n = 4$, normalized and offset)[79].
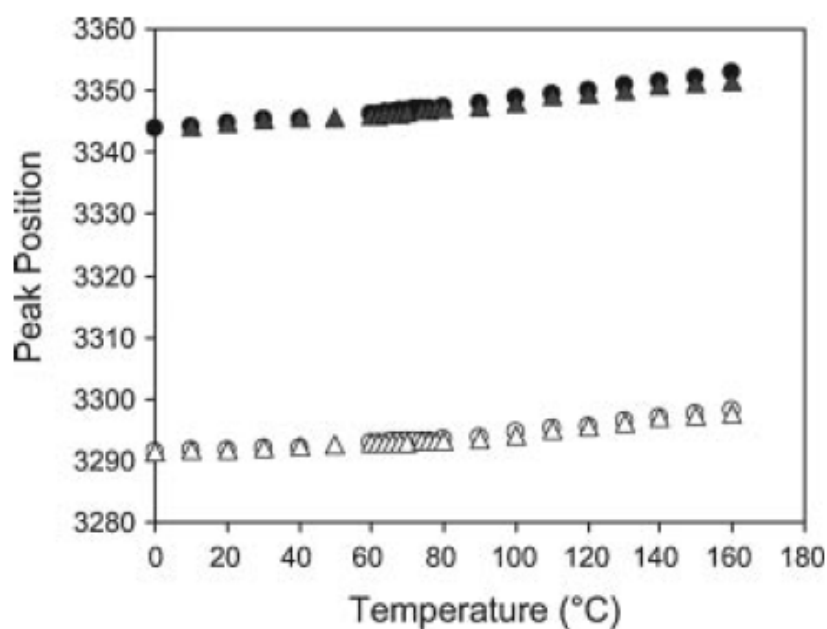


Figure 1-45 Peak position associated with drug-drug hydrogen bond interactions (closed symbols) and drug-polymer hydrogen bond interactions (open symbols) for the amorphous molecular level solid dispersions of felodipine with 37 wt% PVP as a function of increasing temperature ( ▲ ) and decreasing temperature (●).
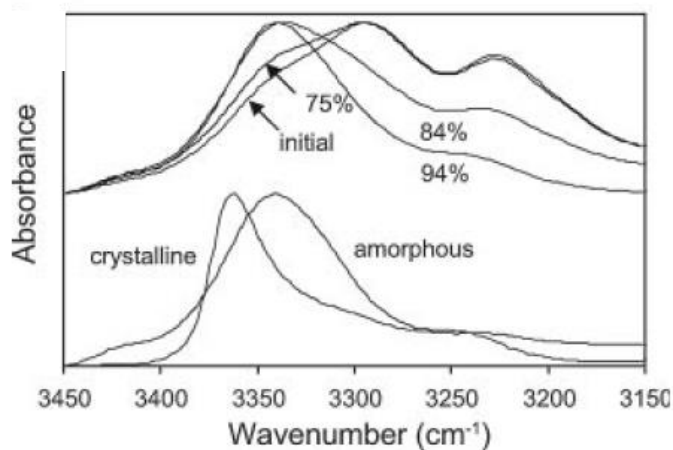
Figure 1-46 Amorphous molecular level solid dispersions of felodipine and 46.4 wt% PVP immediately after sample preparation and after storage at 75, 84, and 94% RH for 1 day. Also shown for comparison are the amorphous and crystalline spectra of felodipine. PVP does not exhibit any significant absorption in this region.
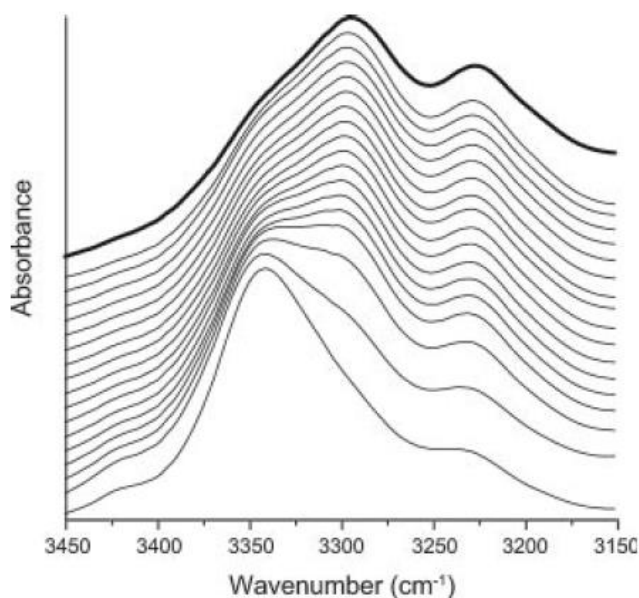


Figure 1-47 FT-IR spectra of NH stretching region of amorphous solid dispersion of felodipine with 50% PVP. The sample was stored at 94% RH for approximately 4 h, then dried using a dry air purge for an hour. Subsequently, the sample was heated to 125 °C, and the infrared spectra collected; they are (bottom to top): initial, and after 5, 10, 15, 20, 25, 30, 45, 60, 90, 120, 150, 240, 300, 360, 420, and 1500 min. The top-most spectrum (thicker line) shows a solid dispersion sample at the same drug-to-polymer ratio that was never exposed to moisture.

Component A dominates dissolving surface

$$\frac{N_A}{N_B} \rangle \frac{D_A C_{SA}}{D_B C_{SB}}$$

Component B dominates dissolving surface

$$\frac{N_A}{N_B} \langle \frac{D_A C_{SA}}{D_B C_{SB}}$$

Both components codissolve in proportion to their initial concentrations

$$\frac{N_A}{N_B} = \frac{D_A C_{SA}}{D_B C_{SB}}$$
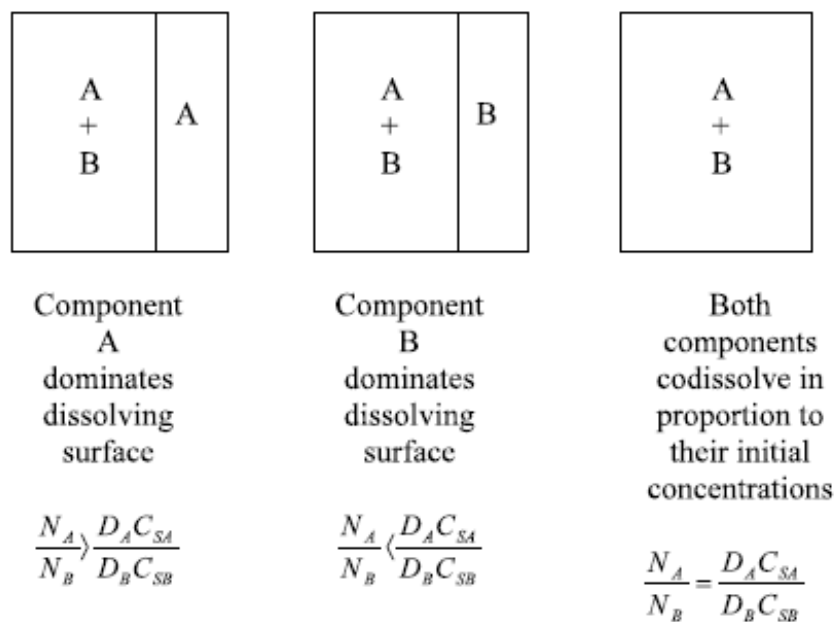
Figure 1-48 Dissolution behavior of two-phase mixture of A and B. In case A, phase B dissolves fast enough to leave a layer of pure A behind; in case B, the reverse is true; while in case C, dissolution rates of A and B are proportional to their relative amounts in the mixture[83].
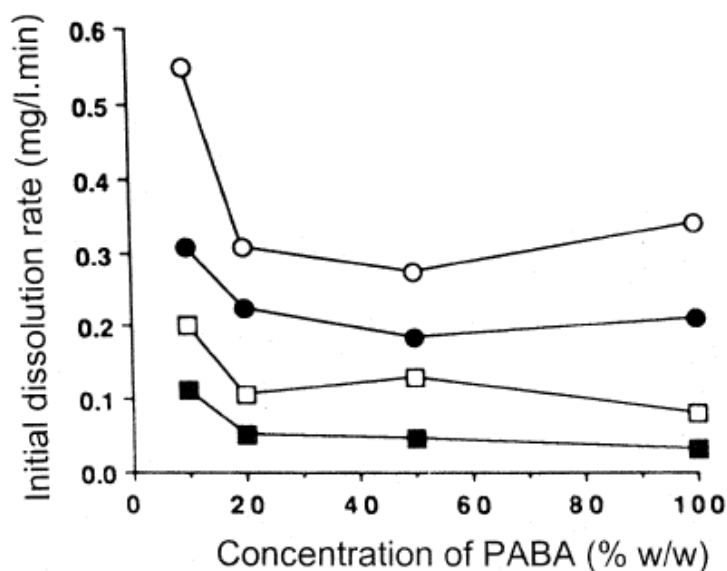


Figure 1-49 Relationship between initial intrinsic dissolution rate and concentration of para-aminobenzoic acid (PABA) in PEG 4000 solid dispersions. (○) Methyl PABA; (●) ethyl PABA; (□)propyl PABA; (■)butylPABA[89].
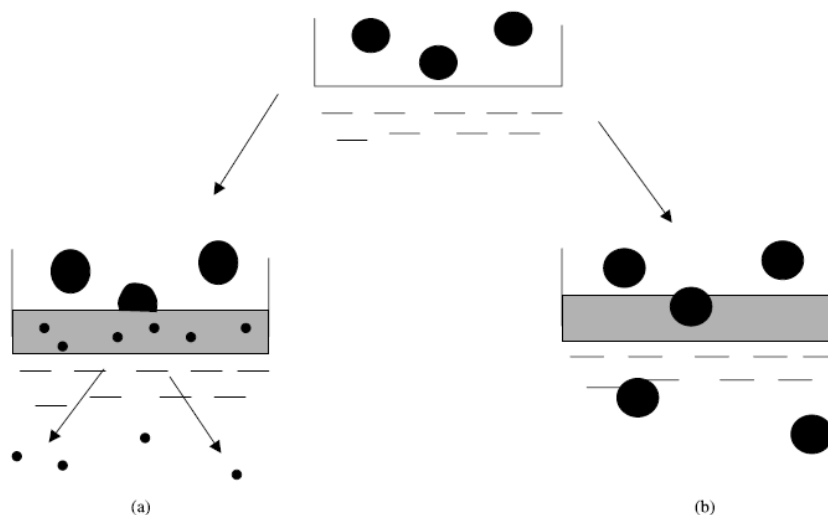
Figure 1-50 Schematic diagram showing the fate of drug particle during the dissolution process. (a) Carrier-controlled dissolution, wherby the drug dissolves into the concentrated carrier layer prior to release and (b) drug-controlled dissolution whereby the drug is released effectively intact into the dissolution medium. Large spheres represent undissolved drug particles, small spheres partially dissolved drug particles, shaded region correspond to hydrated material.
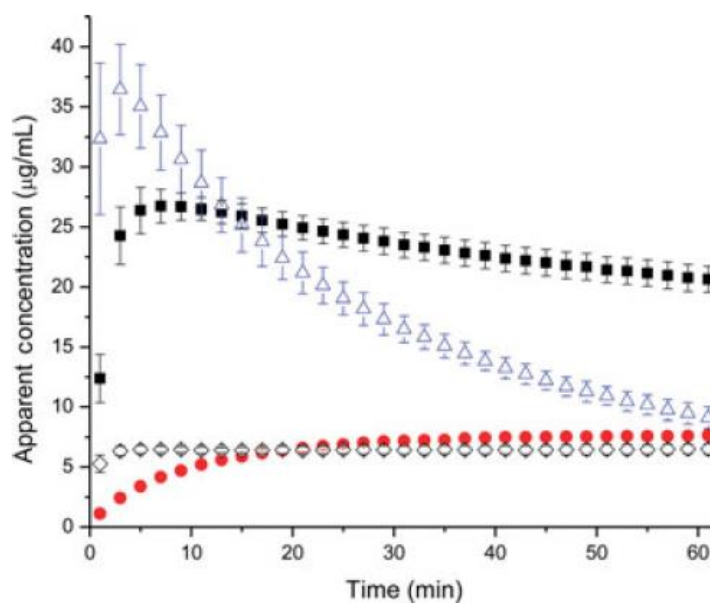


Figure 1-51 Apparent dissolution profiles of 90:10 HPMC–felodipine (■), 50:50 HPMC–felodipine (●), 90:10 PVP–felodipine (Δ), and 50:50 PVP–felodipine (◊) solid dispersions at 25 ℃. Error bars represent 1 standard deviation ($n = 3$). Error bars for the 50:50 data are smaller than the symbols[94].
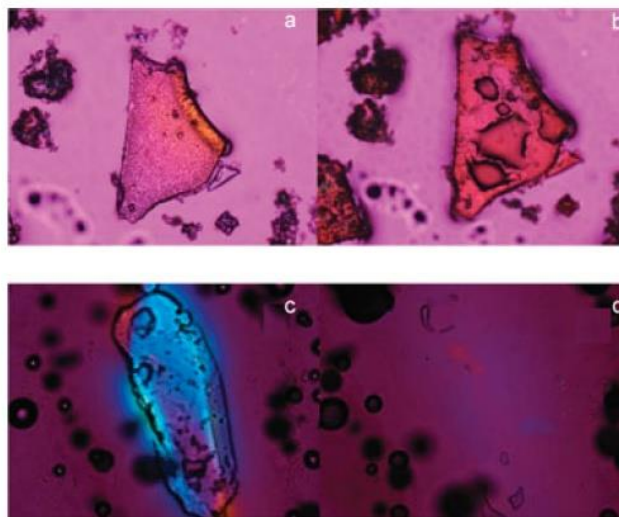
Figure 1-52 Solid dispersion microscope images under cross-polarized light: 50:50 HPMC–felodipine (10×magnification) initial (a) and 30min after exposure (b), and 90:10 HPMC–felodipine (20×magnification) initial (c) and 5min (d) after exposure[94]
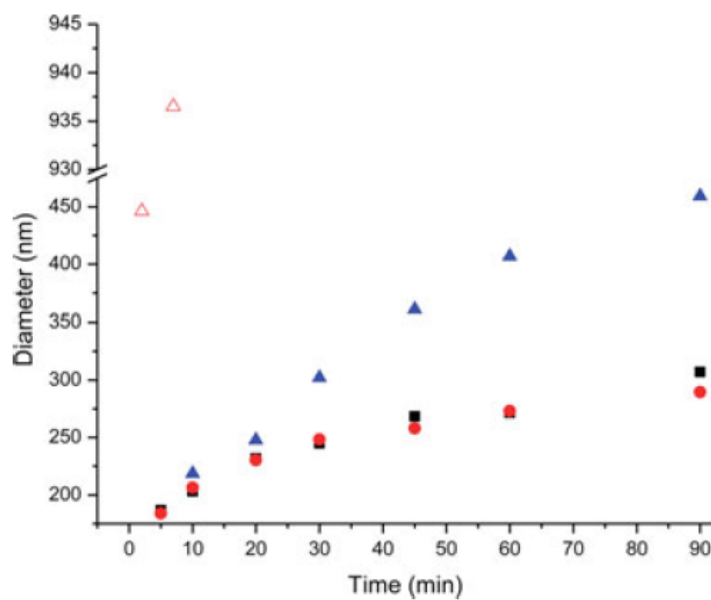


Figure 1-53 Average particle diameter generated by a 90:10 HPMC–felodipine solid dispersion at 30 (■) and 50(●) μg/mL, a 90:10 PVP–felodipine solid dispersion at 40 μg/mL (▲), and an artificial supersaturation in the absence of polymer at 30 μg/mL ( Δ) at 25∘C. All concentrations refer to the nominal amount of felodipine in the system[94].

## 1.15 References

1. Amidon, G.; Lennernäs, H.; Shah, V.; Crison, J. A Theoretical Basis for a Biopharmaceutic Drug Classification: The Correlation of in Vitro Drug Product Dissolution and in Vivo Bioavailability. *Pharm Res-Dordr* **1995,** *12*, (3), 413-420.

2. Benet, L.; Broccatelli, F.; Oprea, T. BDDCS Applied to Over 900 Drugs. *AAPS J* **2011,** *13*, (4), 519-547.

3. Thayer, A. M. FINDING SOLUTIONS. *Chemical & Engineering News Archive* **2010,** *88*, (22), 13-18.

4. Florence, A. T.; Attwood, D., *Physicochemical principles of pharmacy*. pharmaceutical press: 2011.

5. Williams, H. D.; Trevaskis, N. L.; Charman, S. A.; Shanker, R. M.; Charman, W. N.; Pouton, C. W.; Porter, C. J. H. Strategies to Address Low Drug Solubility in Discovery and Development. *Pharmacological Reviews* **2013,** *65*, (1), 315-499.

6. Janssens, S.; Van den Mooter, G. Review: physical chemistry of solid dispersions. *Journal of Pharmacy and Pharmacology* **2009,** *61*, (12), 1571-1586.

7. Matteucci, M. E.; Brettmann, B. K.; Rogers, T. L.; Elder, E. J.; Williams, R. O.; Johnston, K. P. Design of Potent Amorphous Drug Nanoparticles for Rapid Generation of Highly Supersaturated Media. *Mol Pharmaceut* **2007,** *4*, (5), 782-793.

8. Greco, K.; Bogner, R. Solution-mediated phase transformation: Significance during dissolution and implications for bioavailability. *Journal of Pharmaceutical Sciences* **2012,** *101*, (9), 2996-3018.

9. Hancock, B. C.; Zografi, G. Characteristics and significance of the amorphous state in pharmaceutical systems. *Journal of Pharmaceutical Sciences* **1997,** *86*, (1), 1-12.

10. Taylor, L.; Zografi, G. Spectroscopic Characterization of Interactions Between PVP and Indomethacin in Amorphous Molecular Dispersions. *Pharm Res-Dordr* **1997,** *14*, (12), 1691-1698.

11. Andronis, V.; Zografi, G. Crystal nucleation and growth of indomethacin polymorphs from the amorphous state. *Journal of Non-Crystalline Solids* **2000,** *271*, (3), 236-248.

12. Rodríguez-Spong, B.; Price, C. P.; Jayasankar, A.; Matzger, A. J.; Rodríguez-Hornedo, N. r. General principles of pharmaceutical solid polymorphism: A supramolecular perspective. *Advanced Drug Delivery Reviews* **2004,** *56*, (3), 241-274.

13. Hilfiker, R., *Polymorphism: in the pharmaceutical industry*. John Wiley & Sons: 2006.

14. Her, L.-M.; Deras, M.; Nail, S. L. Electrolyte-induced changes in glass transition temperatures of freeze-concentrated solutes. *Pharm Res-Dordr* **1995,** *12*, (5), 768-772.

15. Ediger, M. D.; Angell, C.; Nagel, S. R. Supercooled liquids and glasses. *The journal of physical chemistry* **1996,** *100*, (31), 13200-13212.

16. Angell, C.; MacFarlane, D.; Oguni, M. The Kauzmann paradox, metastable liquids, and ideal glasses. *Ann. NY Acad. Sci* **1986,** *484*, 241-247.

17. Baird, J. A.; Van Eerdenbrugh, B.; Taylor, L. S. A classification system to assess the crystallization tendency of organic molecules from undercooled melts. *Journal of pharmaceutical sciences* **2010,** *99*, (9), 3787-3806.

18.     Alba-Simionesco, C.; Fan, J.; Angell, C.  Thermodynamic aspects of the glass transition phenomenon. II. Molecular liquids with variable interactions. *The Journal of chemical physics* **1999,** *110*, (11), 5262-5272.

19.     Patterson, J. E.; James, M. B.; Forster, A. H.; Lancaster, R. W.; Butler, J. M.; Rades, T.  The influence of thermal and mechanical preparative techniques on the amorphous state of four poorly soluble compounds. *Journal of pharmaceutical sciences* **2005,** *94*, (9), 1998-2012.

20.     Yu, L.; Reutzel-Edens, S. M.; Mitchell, C. A.  Crystallization and Polymorphism of Conformationally Flexible Molecules:  Problems, Patterns, and Strategies. *Organic Process Research & Development* **2000,** *4*, (5), 396-402.

21.     Yu, L.  Amorphous pharmaceutical solids: preparation, characterization and stabilization. *Advanced drug delivery reviews* **2001,** *48*, (1), 27-42.

22.     Savolainen, M.; Heinz, A.; Strachan, C.; Gordon, K. C.; Yliruusi, J.; Rades, T.; Sandler, N.  Screening for differences in the amorphous state of indomethacin using multivariate visualization. *Eur J Pharm Sci* **2007,** *30*, (2), 113-123.

23.     Shamblin, S. L.; Tang, X.; Chang, L.; Hancock, B. C.; Pikal, M. J.  Characterization of the time scales of molecular motion in pharmaceutically important glasses. *The Journal of Physical Chemistry B* **1999,** *103*, (20), 4113-4121.

24.     Ward, S.; Perkins, M.; Zhang, J.; Roberts, C. J.; Madden, C. E.; Luk, S. Y.; Patel, N.; Ebbens, S. J.  Identifying and mapping surface amorphous domains. *Pharm Res-Dordr* **2005,** *22*, (7), 1195-1202.

25.     Lipinski, C. A.; Lombardo, F.; Dominy, B. W.; Feeney, P. J.  Experimental and computational approaches to estimate solubility and permeability in drug discovery and development settings. *Advanced drug delivery reviews* **2012,** *64*, 4-17.

26.     Pudipeddi, M.; Serajuddin, A.  Trends in solubility of polymorphs. *Journal of pharmaceutical sciences* **2005,** *94*, (5), 929-939.

27.     Caira, M. R.; Robbertse, Y.; Bergh, J. J.; Song, M.; De Villiers, M. M.  Structural characterization, physicochemical properties, and thermal stability of three crystal forms of nifedipine. *Journal of pharmaceutical sciences* **2003,** *92*, (12), 2519-2533.

28.     Law, D.; Schmitt, E. A.; Marsh, K. C.; Everitt, E. A.; Wang, W.; Fort, J. J.; Krill, S. L.; Qiu, Y.  Ritonavir–PEG 8000 amorphous solid dispersions: in vitro and in vivo evaluations. *Journal of pharmaceutical sciences* **2004,** *93*, (3), 563-570.

29.     KiMURA, K.; Hirayama, F.; Arima, H.; UEKAMA, K.  Effects of Aging on Crystallization, Dissolution and Absorption Characteristics of Amorphous Tolbutamide-2-Hydroxypropyl-. BETA.-cyclodextrin Complex. *Chemical and pharmaceutical bulletin* **2000,** *48*, (5), 646-650.

30.     Hoffman, J. D.  Thermodynamic driving force in nucleation and growth processes. *The Journal of Chemical Physics* **1958,** *29*, (5), 1192-1193.

31.     Hancock, B. C.; Parks, M.  What is the true solubility advantage for amorphous pharmaceuticals? *Pharm Res-Dordr* **2000,** *17*, (4), 397-404.

32.     Bhugra, C.; Pikal, M. J.  Role of thermodynamic, molecular, and kinetic factors in crystallization from the amorphous state. *Journal of pharmaceutical sciences* **2008,** *97*, (4), 1329-1349.

33.     Mullins, J. D.; Macek, T. J.  SOME PHARMACEUTICAL PROPERTIES OF NOVOBIOCIN. *Journal of the American Pharmaceutical Association* **1960,** *49*, (4), 245-248.

34.     LENNERNÄS, H.  Human jejunal effective permeability and its correlation with preclinical drug absorption models. *Journal of pharmacy and pharmacology* **1997,** *49*, (7), 627-638.

35.     Wu, X.; Whitfield, L. R.; Stewart, B. H.  Atorvastatin transport in the Caco-2 cell model: contributions of P-glycoprotein and the proton-monocarboxylic acid co-transporter. *Pharm Res-Dordr* **2000,** *17*, (2), 209-215.

36.     Corsini, A.; Bellosta, S.; Baetta, R.; Fumagalli, R.; Paoletti, R.; Bernini, F.  New insights into the pharmacodynamic and pharmacokinetic properties of statins. *Pharmacology & therapeutics* **1999,** *84*, (3), 413-428.

37.     Kim, J.-S.; Kim, M.-S.; Park, H. J.; Jin, S.-J.; Lee, S.; Hwang, S.-J.  Physicochemical properties and oral bioavailability of amorphous atorvastatin hemi-calcium using spray-drying and SAS process. *International journal of pharmaceutics* **2008,** *359*, (1), 211-219.

38.     Gutzow, I.; Avramov, I.; Kästner, K.  Glass formation and crystallization. *Journal of Non-Crystalline Solids* **1990,** *123*, (1), 97-113.

39.     Yoshioka, M.; Hancock, B. C.; Zografi, G.  Crystallization of indomethacin from the amorphous state below and above its glass transition temperature. *Journal of pharmaceutical sciences* **1994,** *83*, (12), 1700-1705.

40.     ABE, Y.; ARAHORI, T.; NARUSE, A.  Crystallization of Ca (PO3) 2 glass below the glass transition temperature. *Journal of the American Ceramic Society* **1976,** *59*, (11-12), 487-490.

41.     Gordon, M.; Taylor, J. S.  Ideal copolymers and the second-order transitions of synthetic rubbers. i. non-crystalline copolymers. *Journal of Applied Chemistry* **1952,** *2*, (9), 493-500.

42.     Simha, R.; Boyer, R.  On a general relation involving the glass temperature and coefficients of expansion of polymers. *The Journal of Chemical Physics* **1962,** *37*, (5), 1003-1007.

43.     Yoshioka, M.; Hancock, B. C.; Zografi, G.  Inhibition of indomethacin crystallization in poly (vinylpyrrolidone) coprecipitates. *Journal of pharmaceutical sciences* **1995,** *84*, (8), 983-986.

44.     Barandiaran, J.; Colmenero, J.  Continuous cooling approximation for the formation of a glass. *Journal of Non-Crystalline Solids* **1981,** *46*, (3), 277-287.

45.     Cabral, A.; Cardoso, A.; Zanotto, E.  Glass-forming ability versus stability of silicate glasses. I. Experimental test. *Journal of Non-Crystalline Solids* **2003,** *320*, (1), 1-8.

46.     Trasi, N. S.; Taylor, L. S.  Effect of polymers on nucleation and crystal growth of amorphous acetaminophen. *Crystengcomm* **2012,** *14*, (16), 5188-5197.

47.     Leuner, C.; Dressman, J.  Improving drug solubility for oral delivery using solid dispersions. *Eur J Pharm Biopharm* **2000,** *50*, (1), 47-60.

48.     Kearney, A. S.; Gabriel, D. L.; Mehta, S. C.; Radebaugh, G. W.  Effect of polyvinylpyrrolidone on the crystallinity and dissolution rate of solid dispersions of the antiinflammatory CI-987. *International journal of pharmaceutics* **1994,** *104*, (2), 169-174.

49.     El-Zein, H.; Riad, L.; El-Bary, A. A.  Enhancement of carbamazepine dissolution: in vitro and in vivo evaluation. *International journal of pharmaceutics* **1998,** *168*, (2), 209-220.
50.     Khougaz, K.; Clas, S. D.  Crystallization inhibition in solid dispersions of MK-0591 and poly (vinylpyrrolidone) polymers. *Journal of pharmaceutical sciences* **2000,** *89*, (10), 1325-1334.
51.     Gupta, P.; Thilagavathi, R.; Chakraborti, A. K.; Bansal, A. K.  Role of molecular interaction in stability of celecoxib-PVP amorphous systems. *Mol Pharmaceut* **2005,** *2*, (5), 384-391.
52.     Miyazaki, T.; Yoshioka, S.; Aso, Y.; Kojima, S.  Ability of polyvinylpyrrolidone and polyacrylic acid to inhibit the crystallization of amorphous acetaminophen. *Journal of pharmaceutical sciences* **2004,** *93*, (11), 2710-2717.
53.     Van den Mooter, G.; Wuyts, M.; Blaton, N.; Busson, R.; Grobet, P.; Augustijns, P.; Kinget, R.  Physical stabilisation of amorphous ketoconazole in solid dispersions with polyvinylpyrrolidone K25. *Eur J Pharm Sci* **2001,** *12*, (3), 261-269.
54.     Konno, H.; Taylor, L. S.  Influence of different polymers on the crystallization tendency of molecularly dispersed amorphous felodipine. *J Pharm Sci-Us* **2006,** *95*, (12), 2692-2705.
55.     Zografi, G.  States of water associated with solids. *Drug Development and Industrial Pharmacy* **1988,** *14*, (14), 1905-1926.
56.     Andronis, V.; Yoshioka, M.; Zografi, G.  Effects of sorbed water on the crystallization of indomethacin from the amorphous state. *Journal of pharmaceutical sciences* **1997,** *86*, (3), 346-351.
57.     Levine, H.; Slade, L.  Water as a plasticizer: physico-chemical aspects of low-moisture polymeric systems. *Water science reviews* **1988,** *3*, 79-185.
58.     Konno, H.; Taylor, L. S.  Ability of different polymers to inhibit the crystallization of amorphous felodipine in the presence of moisture. *Pharm Res-Dordr* **2008,** *25*, (4), 969-978.
59.     Rodrıguez-Hornedo, N.; Kelly, R. C.; Sinclair, B.; Miller, J., Crystallization: general principles and significance on product development. Taylor & Francis: 2006.
60.     De Yoreo, J. J.; Vekilov, P. G.  Principles of crystal nucleation and growth. *Reviews in mineralogy and geochemistry* **2003,** *54*, (1), 57-93.
61.     Lindfors, L.; Forssén, S.; Westergren, J.; Olsson, U.  Nucleation and crystal growth in supersaturated solutions of a model drug. *J Colloid Interf Sci* **2008,** *325*, (2), 404-413.
62.     Davis, K.; Dove, P.; De Yoreo, J.  Resolving the controversial role of Mg2 in calcite biomineral formation. *Science* **2000,** *290*, 1134-1137C.
63.     Frank, F.  The influence of dislocations on crystal growth. *Discuss. Faraday Soc.* **1949,** *5*, 48-54.
64.     Dove, P. M.; De Yoreo, J. J.; Davis, K. J.  Inhibition of CaCO3 crystallization by small molecules: the magnesium example. *Solid-fluid interfaces to nanostructural engineering* **2004**, 55-82.
65.     Kubota, N.  Effect of impurities on the growth kinetics of crystals. *Crystal Research and Technology* **2001,** *36*, (8-10), 749-769.
66.     Chernov, A.  The spiral growth of crystals. *Physics-Uspekhi* **1961,** *4*, (1), 116-148.

67.     Alonzo, D. E.; Zhang, G. G. Z.; Zhou, D. L.; Gao, Y.; Taylor, L. S. Understanding the Behavior of Amorphous Pharmaceutical Systems during Dissolution. *Pharm Res-Dordr* **2010,** *27*, (4), 608-618.

68.     Brouwers, J.; Brewster, M. E.; Augustijns, P. Supersaturating drug delivery systems: The answer to solubility-limited oral bioavailability? *Journal of pharmaceutical sciences* **2009,** *98*, (8), 2549-2572.

69.     Raghavan, S.; Trividic, A.; Davis, A.; Hadgraft, J. Crystallization of hydrocortisone acetate: influence of polymers. *International journal of pharmaceutics* **2001,** *212*, (2), 213-221.

70.     Alonzo, D. E.; Raina, S.; Zhou, D.; Gao, Y.; Zhang, G. G.; Taylor, L. S. Characterizing the impact of hydroxypropylmethyl cellulose on the growth and nucleation kinetics of felodipine from supersaturated solutions. *Cryst Growth Des* **2012,** *12*, (3), 1538-1547.

71.     Matsumoto, T.; Zografi, G. Physical properties of solid molecular dispersions of indomethacin with poly(vinylpyrrolidone) and poly(vinylpyrrolidone-co-vinylacetate) in relation to indomethacin crystallization. *Pharm Res-Dordr* **1999,** *16*, (11), 1722-1728.

72.     Shamblin, S. L.; Zografi, G. The effects of absorbed water on the properties of amorphous mixtures containing sucrose. *Pharm Res-Dordr* **1999,** *16*, (7), 1119-1124.

73.     Qian, F.; Huang, J.; Hussain, M. A. Drug–polymer solubility and miscibility: Stability consideration and practical challenges in amorphous solid dispersion development. *J Pharm Sci-Us* **2010,** *99*, (7), 2941-2947.

74.     Marsac, P. J.; Shamblin, S. L.; Taylor, L. S. Theoretical and practical approaches for prediction of drug–polymer miscibility and solubility. *Pharm Res-Dordr* **2006,** *23*, (10), 2417-2426.

75.     Deneau, E.; Steele, G. An in-line study of oiling out and crystallization. *Organic process research & development* **2005,** *9*, (6), 943-950.

76.     Rumondor, A. C.; Ivanisevic, I.; Bates, S.; Alonzo, D. E.; Taylor, L. S. Evaluation of drug-polymer miscibility in amorphous solid dispersion systems. *Pharm Res-Dordr* **2009,** *26*, (11), 2523-2534.

77.     Utracki, L. Glass transition temperature in polymer blends. *Advances in Polymer Technology* **1985,** *5*, (1), 33-39.

78.     Sakaguchi, T.; Taniguchi, N.; Urakawa, O.; Adachi, K. Calorimetric study of dynamical heterogeneity in blends of polyisoprene and poly (vinylethylene). *Macromolecules* **2005,** *38*, (2), 422-428.

79.     Van Eerdenbrugh, B.; Lo, M.; Kjoller, K.; Marcott, C.; Taylor, L. S. Nanoscale mid-infrared imaging of phase separation in a drug–polymer blend. *Journal of pharmaceutical sciences* **2012,** *101*, (6), 2066-2073.

80.     Marsac, P. J.; Rumondor, A. C.; Nivens, D. E.; Kestur, U. S.; Stanciu, L.; Taylor, L. S. Effect of temperature and moisture on the miscibility of amorphous dispersions of felodipine and poly (vinyl pyrrolidone). *Journal of pharmaceutical sciences* **2010,** *99*, (1), 169-185.

81.     Pouchlý, J.; Patterson, D. Polymers in mixed solvents. *Macromolecules* **1976,** *9*, (4), 574-579.

82.     Robard, A.; Patterson, D.; Delmas, G. The" Δη Effect" and Polystyrene-Poly (vinyl methyl ether) Compatibility in Solution. *Macromolecules* **1977,** *10*, (3), 706-708.

83.     Corrigan, O. I.  Mechanisms of Dissolution of Fast Release Solid Dispersions. *Drug Development and Industrial Pharmacy* **1985,** *11*, (2-3), 697-724.

84.     Corrigan, O. I.  Retardation of polymeric carrier dissolution by dispersed drugs: Factors influencing the dissolution of solid dispersions containing polyethlene glycols. *Drug Development and Industrial Pharmacy* **1986,** *12*, (11-13), 1777-1793.

85.     Dubois, J. L.; Ford, J. L.  Similarities in the release rates of different drugs from polyethylene glycol 6000 solid dispersions. *Journal of pharmacy and pharmacology* **1985,** *37*, (7), 494-495.

86.     Sjökvist, E.; Nyström, C.  Physicochemical aspects of drug release. VI. Drug dissolution rate from solid particulate dispersions and the importance of carrier and drug particle properties. *International journal of pharmaceutics* **1988,** *47*, (1), 51-66.

87.     Higuchi, W. I.  Diffusional models useful in biopharmaceutics. Drug release rate processes. *J Pharm Sci-Us* **1967,** *56*, (3), 315-324.

88.     Higuchi, W.; Mir, N.; Desai, S.  Dissolution rates of polyphase mixtures. *J Pharm Sci-Us* **1965,** *54*, (10), 1405-1410.

89.     Saers, E. S.; Craig, D. Q.  An investigation into the mechanisms of dissolution of alkyl p-aminobenzoates from polyethylene glycol solid dispersions. *International journal of pharmaceutics* **1992,** *83*, (1), 211-219.

90.     Konno, H.; Handa, T.; Alonzo, D. E.; Taylor, L. S.  Effect of polymer type on the dissolution profile of amorphous solid dispersions containing felodipine. *Eur J Pharm Biopharm* **2008,** *70*, (2), 493-499.

91.     Usui, F.; Maeda, K.; Kusai, A.; Nishimura, K.; Yamamoto, K.  Inhibitory effects of water-soluble polymers on precipitation of RS-8359. *International Journal of Pharmaceutics* **1997,** *154*, (1), 59-66.

92.     Acartürk, F.; Kişlal, Ö.; Celebi, N.  The effect of some natural polymers on the solubility and dissolution characteristics of nifedipine. *International journal of pharmaceutics* **1992,** *85*, (1), 1-6.

93.     Loftsson, T.; Fri, H.; Gu, T. K.  The effect of water-soluble polymers on aqueous solubility of drugs. *International journal of pharmaceutics* **1996,** *127*, (2), 293-296.

94.     Alonzo, D. E.; Gao, Y.; Zhou, D.; Mo, H.; Zhang, G. G. Z.; Taylor, L. S.  Dissolution and precipitation behavior of amorphous solid dispersions. *J Pharm Sci-Us* **2011,** *100*, (8), 3316-3331.

# CHAPTER 2. DISSOLUTION PERFORMANCE OF HIGH DRUG LOADING CELECOXIB AMORPHOUS SOLID DISPERSIONS FORMULATED WITH POLYMER COMBINATIONS

## 2.1 Abstract

The aims of this study were twofold. First, to evaluate the effectiveness of selected polymers in inhibiting solution crystallization of celecoxib. Second, to compare the release rate and crystallization tendency of celecoxib amorphous solid dispersions (ASDs) formulated with a single polymer, or binary polymer combinations. The effectiveness of polymers, polyvinylpyrrolidone (PVP), hydroxypropylmethyl cellulose (HPMC) or HPMC acetate succinate (HPMCAS), in maintaining supersaturation of celecoxib solutions was evaluated by performing nucleation induction time measurements. Crystallization kinetics of ASD suspensions were monitored using Raman spectroscopy. Dissolution experiments were carried out under non-sink conditions. Pure amorphous celecoxib was found to crystallize rapidly through both matrix and solution pathways. Matrix and solution crystallization was inhibited when celecoxib was molecularly mixed with a polymer, resulting in release of the drug to form supersaturated solutions. Cellulosic polymers were more effective than PVP in maintaining supersaturation. Combining a cellulosic polymer and PVP enabled improved drug release and stability to crystallization. Inclusion of an effective solution crystallization inhibitor as a minor component in ternary dispersions resulted in prolonged supersaturation following dissolution.

This study shows the feasibility of formulation strategies for ASDs where a major polymer component is used to achieve one key property e.g. release, while a minor polymer component is added to prevent crystallization.

## 2.2 Introduction

It has been suggested that up to 80% of new molecular entities have sub-optimum aqueous solubility[1] which can lead to solubility-limited bioavailability. The low aqueous solubility of many new compounds can be attributed in part to the nature of contemporary drug discovery methodologies. Formulations containing amorphous drug are promising for the oral delivery of poorly water-soluble drugs since the amorphous form of a compound has higher free energy as compared to the crystalline counterparts, which may give rise to higher apparent solubility and dissolution rates[2]. This in turn may lead to improved drug absorption and increased bioavailability relative to the crystalline counterpart. Despite the potential benefit, the application of formulation containing pure amorphous drug remains limited primarily because of their higher instability: the thermodynamic driving force always favors a transformation towards a lower energy crystalline state[3].

Polymers are often employed to form amorphous solid dispersions (ASDs) with a drug to improve the physical stability during processing and storage[4]. Polymers are thought to inhibit crystallization through a number of mechanisms including reducing the drug molecular mobility, by increasing the glass transition temperature ($T_g$) of the system [5], and/or forming hydrogen bonds with the drug[6, 7].

While it is obviously critical to stabilize the amorphous drug in the solid state, it is of equal importance to prevent crystallization during dissolution of the ASD. Nevertheless, some of

the fundamental processes underlying the concentration-time profiles attained during dissolution are poorly understood, in particular due to the tendency to run dissolution studies under sink conditions, which are unlikely to be found *in vivo* for many poorly water soluble compounds. A number of factors need to be considered when evaluating the dissolution behavior of ASDs including the amount of ASD introduced to the medium, the drug loading, the relative dissolution rates of the individual components, the equilibrium solubility of drug, the degree of supersaturation achieved, and the crystallization kinetics of the drug. Alonzo *et. al.* demonstrated two pathways through which crystallization could occur during the dissolution process [8]. Nucleation and crystal growth could commence at the surface of the amorphous solid matrix upon contact with dissolution medium due to a reduction in $T_g$ by the absorbed water. In this case, only a small extent of supersaturation can be generated. Alternatively, if the dissolution rate of drug is fast relative to matrix crystallization, drug may crystallize from the supersaturated solution, resulting in desupersaturation at some point following dissolution. The more supersaturated the solution is, the more prone it will be to crystallize. While it has been demonstrated that polymers, when pre-dissolved in buffer, may inhibit either or both routes of crystallization for pure amorphous compounds [8], little is known regarding the role of polymer during dissolution of ASDs.

The aims of the current study were to evaluate the crystallization propensity of the pure amorphous form of the poorly soluble anti-inflammatory agent, celecoxib (CEX), and to compare the impact of various polymers, alone and in combination, on the route and kinetics of crystallization and their impact on the dissolution rate of CEX from ASDs. It was also of interest to determine the feasibility of using polymer combinations to improve

the performance of ASDs with high drug loadings, hence the dispersions studied herein had a 50% drug loading.

## 2.3 Materials

CEX was purchased from Attix Pharmaceuticals (Toronto, Ontario, Canada). Polyvinylpyrrolidone (PVP) (Grade K12: Mw 2000–3000 g mol$^{-1}$) was provided by BASF (Ludwigshafen, Germany) and polyvinylpyrrolidone (PVP) (Grade K29/32: Mw 58,000 g mol$^{-1}$ ) was purchased from ISP Technologies, INC (Wayne, NJ, USA). Hydroxypropylmethylcellulose acetate succinate (HPMCAS, Type AS-MF), and hydroxypropyl methylcellulose (HPMC, Grade 606) were supplied by Shin-Etsu Chemical Co. (Tokyo, Japan). The molecular structures are shown in Figure 2-1.

## 2.4 Methods

### 2.4.1 Preparation of Bulk Amorphous Materials

CEX and the polymer(s) were dissolved in a 50:50 v/v solution of ethanol and dichloromethane. Solvent removal was achieved by rotary evaporation. The ASDs (Table 2-1) were subsequently dried in a vacuum oven overnight to remove any residual solvent. Pure amorphous CEX was prepared by melting crystalline CEX at approximately 180 ℃ on aluminum foil using a hot plate, followed by quench cooling. Based on analysis using high performance liquid chromatography, no degradation was observed using this procedure. Both ASDs and pure amorphous CEX were ground using a mortar and pestle and sieved to obtain particle size fraction of 106-250 μm. The solids were then stored in a

desiccator containing phosphorous pentoxide at room temperature. The amorphous nature of the ASDs and the pure CEX were verified by powder X-ray diffraction prior to use.

### 2.4.2    Phase transformation of slurred ASDs

ASD (200 mg) was slurred in 2 mL pH 6.8 100 mM sodium phosphate buffer (SPB) in a scintillation vial equilibrated at 37 °C and stirred at a constant rate. The kinetics of phase transformation was monitored using a RamanRxn-785 Raman Spectrometer (Kaiser Optical Systems, Inc., Ann Arbor, MI, USA) with a laser wavelength of 785 nm. Spectra were collected every 15 minutes for 7 hours. Data were analyzed with OPUS software (Version 7.2, Bruker Optics Inc, Billerica, Massachusetts, USA).

### 2.4.3    Inhibitory effectiveness of polymers on solution crystallization

275 μL of a 4 mg/mL methanol solution of CEX was pipetted into 50 mL pH 6.8 100 mM SPB with and without 5 μg/mL pre-dissolved polymer. The solution was equilibrated at 37 °C and stirred at 300rpm (+shaped magnetic stirrer, 0.75 inch diameter). Solution concentrations were measured as a function of time using a SI photonics UV-Vis spectrometer coupled with a fiber optic probe (SI Photonics Inc, Tuscon, Arizona, USA). Wavelength scans (200-450nm) were performed at 1min interval for 8 hours. The absorption peak at 249 nm was used to monitor solution concentration. Light scattering was detected by monitoring the extinction at 350 nm at which the drug has no absorbance. All measurements were performed in triplicate.

### 2.4.4    Dissolution study of ASDs

8.8 mg crystalline or amorphous CEX or 17.6 mg of ASD was added to 400 mL pH 6.8 100 mM SPB, equilibrated at 37 ℃ and stirred at 300 rpm with a stir bar (+shaped, 0.75 inch diameter). Solution concentration evolution as a function of time was measured using the SI photonics system. Wavelength scans (200-450nm) were performed at 1min time intervals for 16 hours. The absorption peak at 249 nm was used to monitor solution concentration. Calibration solutions of CEX were prepared in methanol. All measurements were performed in triplicate.

### 2.4.5    Effect of Polymer on the Equilibrium Solubility of CEX

The equilibrium solubility of CEX was determined by adding an excess amount of crystalline CEX to 20 mL pH 6.8 100mM SPB with the absence/presence of 22 μg/ml pre-dissolved polymer in scintillation vials. The vials were equilibrated at 37 ℃ for 48h in an agitating water bath (Dubnoff metallic shaking incubator; PGC Scientific, Palm Desert, CA, USA). Samples were then subject to ultracentrifugation to separate excess crystalline CEX particles from the supernatant. Ultracentrifugation was performed at 35000 rpm for 30 minutes in an Optima L-100XP ultracentrifuge equipped with Swinging-Bucket Rotor SW 41 Ti (Beckman Coulter, Inc., Brea, CA, USA). HPLC analysis were carried out with an Agilent HPLC 1260 Infinity system (Agilent Technologies, Santa Clara, California, USA). The chromatographic separation was performed by an XTerra Shield RP18 Column (125Å, 3.5 μm, 3.9 mm X 100 mm) (Waters Cooperation, Milford, MA, USA). Water (20%) and acetonitrile (80%) mixture was used as mobile phase and the flow rate was

0.25mL/min. The ultraviolet detection wavelength was 250nm. All measurements were performed in triplicate at room temperature.

### 2.4.6   Polarized Light Microscopy

The crystallization behavior of the pure amorphous CEX was observed using a Nikon Eclipse E600 Pol microscope with 10x objective (Nikon Company, Tokyo, Japan). The pulverized samples (106-250um) were placed on a microscope slide containing a depression. 3-4 drops of pH 6.8 100 mM SPB with or without a pre-dissolved polymer were then added to the particles. Images were processed by NIS-Elements software package (Version 2.3; Nikon Company, Tokyo, Japan).

### 2.5   Results

### 2.5.1   Nucleation Induction Time

The effectiveness of the polymers in inhibiting crystallization from supersaturated solution was assessed by performing nucleation induction time measurements. The experimental nucleation induction time, $t_{ind}$, can be defined as the sum of the time for critical nucleus formation (true nucleation time, $t_n$), and growth to detectable size, $t_g$.[9]

$$t_{ind} = t_n + t_g \qquad (1)$$

The initial solution concentration generated was 22 μg/mL, which was approximately the calculated "amorphous solubility" of CEX [10] [11], and therefore the maximum theoretical concentration of free drug that can be achieved by dissolving an ASD. The onset of crystallization was determined as a sudden increase of light scattering at 350 nm concomitant with a rapid decrease in absorbance at 249nm [12]. As shown in Figure 2-2, in

the absence of any polymer, the drug concentration decreased rapidly and crystallization commenced within 5 minutes. The solution became increasingly turbid with the development of macroscopic crystals. Nucleation induction times extended to approximately 1hr in the presence of PVP-K12 and 2hrs with PVP-K29/32. It was noteworthy that the rate of desupersaturation following nucleation induction was slower in the presence of PVP-K29/32 than in the presence of PVP-K12 and slower in the presence of both of these polymers relative to in the absence of a polymer. In the case of HPMCAS and HPMC, however, no substantial nucleation/crystal growth occurred and the initial level of supersaturation was maintained for more than 8 hours. Furthermore, when combinations of HPMCAS with PVP-K12 or PVP-K29 were evaluated, no significant desupersaturation occurred, indicating that the effectiveness of HPMCAS in maintaining supersaturation was not impaired by the presence of PVP.

### 2.5.2 Crystallization Kinetics of Slurred ASDs

The tendency of pulverized amorphous CEX and ASDs formulated with a 50% drug loading to crystallize when added to aqueous media (SPB at 37 ℃) was evaluated using Raman spectroscopy and results for the various systems summarized in Figure 2-4. The crystalline and amorphous CEX reference spectra show distinct differences in peak position, intensity and width, which can be used to monitor the phase transformation from the amorphous to the crystalline form. For example, the crystalline form spectrum has a peak at 1614 cm$^{-1}$ with a small shoulder at 1596 cm$^{-1}$, whereas the reference amorphous CEX spectrum shows a peak at 1611 cm$^{-1}$ with a much more pronounced shoulder at approximately 1598 cm$^{-1}$ (Figure 2-3).

By monitoring the decrease in intensity of the 1598 cm$^{-1}$ shoulder as a function of time, it can be seen that the CEX:PVP-K12 ASD crystallized within 4 hours, as shown in Figure 4. When a small amount of the PVP was replaced with HPMCAS, to form a ternary dispersion (consisting of 50% CEX, 40% PVP-K12 and 10% HPMCAS), the dispersion remained amorphous for the duration of the experiment (7 hours). Increasing the molecular weight grade of PVP used to form the dispersion, improved resistance to crystallization; the shoulder at 1598 cm$^{-1}$ (indicative of the amorphous form) persisted for 7 hours when CEX:PVP-K29/32 ASDs were slurried.  Both the CEX: HPMCAS ASD and the CEX: PVP-K29/32: HPMCAS ternary ASD remained amorphous over this time frame.

Pure amorphous CEX crystallized rapidly during slurrying, whereby crystallization was complete within an hour. Furthermore, it was found that the polymer needed to be present in the dispersion to be an effective crystallization inhibitor; adding the polymer in pre-dissolved form (22µg/ml) to the buffer did not substantially retard the crystallization kinetics of the pure amorphous CEX (data not shown).

### 2.5.3   Dissolution Behavior of CEX ASDs

Figure 2-5 shows the dissolution profiles of ASDs of CEX formulated with different polymers and polymer combinations at a drug loading of 50% (w/w). The maximum apparent solution concentration of CEX achieved by dissolving the ASDs was between 21-22 µg/ml in all cases except for the dispersions that contained HPMC, which equals 100% release of the CEX in the ASDs; the amount of ASD added was selected so that theoretical concentration of CEX was equivalent to the reported amorphous solubility [10, 11]. Thus the

dissolution conditions are at-sink with respect to amorphous solubility and non-sink with respect to crystalline solubility.

While the maximum concentration achieved was the same for these dispersions, considerable differences in the time to achieve the maximum concentration and the longevity of the achieved supersaturation can be noted between the different formulations. Binary dispersions with either PVP-K12 or PVP-K29/32 showed faster dissolution rates than the corresponding dispersions with HPMCAS or HPMC (Figure 2-5). However, PVP-K12 was the least effective polymer at maintaining the generated supersaturation, with desupersaturation being observed about 2hrs after all the CEX had dissolved. Interestingly, the peak CEX concentration achieved by dissolving the PVP-K29/32 ASD was maintained for approximately twice as long as that of the PVP-K12 ASD, although the initial dissolution rates for the two systems were very similar. Dispersions with HPMCAS dissolved more slowly, but did not desupersaturate over the experimental timeframe. Dispersions with HPMC exhibited the slowest dissolution rate, the maximum concentration achieved was only 16 μg/ml and was still increasing by the end of the experiment.

Replacing 20% of the PVP-K12 with HPMCAS led to two major changes in the dissolution behavior of the dispersion (Figure 2-6). First, the dissolution rate was much slower, being more similar in profile to that of the binary dispersion containing HPMCAS. Second, no desupersaturation was observed and thus the ternary ASD has improved stability against crystallization relative to the binary dispersion with PVP-K12. A similar profile was observed for a ternary dispersion with PVP-K29/32 and HPMCAS. Replacing 20% of the PVP-K12 or PVP-K29/32 with HPMC also resulted slower dissolution rates relative to the

PVP only dispersion, albeit to different extents depending on the grade of PVP. Again, no desupersaturation was observed in either case. Interestingly, the dissolution rate of the ternary dispersion containing PVP-K12 with HPMC was much slower than for PVP-K29; this difference between the PVP grades was not observed with the other ternary dispersions. Additionally, it was found that pre-dissolved cellulosic polymers present in the dissolution medium slightly reduced the dissolution rate of the CEX: PVP-K12 ASD, resulting in a longer time period to achieve complete release, but were able to prevent desupersaturation (Figure 2-7). In contrast to the dispersions, the solution concentration time profile achieved by dissolving amorphous CEX was similar to that obtained by dissolving crystalline CEX, despite a faster initial release rate. Dissolution of amorphous CEX into buffer containing 5 μg/ml pre-dissolved HPMCAS or HPMC resulted in only a slightly higher final concentration, as shown in Figure 2-8.

### 2.5.4   Polarized Light Microscopy

Figure 2-9 shows that when neat amorphous CEX was exposed to phosphate buffer, the material appears to undergo rapid crystallization from the amorphous particles. In addition, some crystallization from the solution phase was also observed. When a cellulosic polymer was present in the buffer, solution crystallization was not observed whereas matrix crystallization was still evident, albeit proceeding at a much slower rate (Figure 2-10 and Figure 2-11).

### 2.5.5 Equilibrium Solubility of CEX

The measured equilibrium solubility of crystalline CEX was 1.5µg/mL. Polymers, when present at a concentration of 22µg/ml in SPB, did not substantially impact the crystalline solubility of CEX, as demonstrated by the results summarized in Table 2-2.

### 2.6 Discussion

For ASD formulations, it is essential to prevent crystallization (either nucleation and/or growth) both in the solid formulation during storage, as well as during the dissolution process, either from the dissolving amorphous matrix, or from the supersaturated solution generated by dissolution under non-sink conditions. However, the polymer that is the best crystallization inhibitor in the solid formulation, may not be effective in preventing crystallization from aqueous solution and vice versa. For example, it was observed that polyacrylic acid was very effective at inhibiting the crystal growth of acetaminophen from supercooled liquids[13], and hence retarded crystallization from amorphous solid dispersions, but was ineffective in preventing either nucleation or crystal growth from aqueous solutions[14]. Other systems show similar types of behavior[6, 15-17]. Therefore, it may be appropriate to use combinations of polymers [18] to ensure adequate stability during storage and optimum performance during dissolution. Although ternary dispersions have been used to improve dissolution rates, [19 20], as well as to improve physical stability in the solid dispersion[21], there is relatively little work evaluating the impact of binary polymer combinations on crystallization kinetics during ASD dissolution.

Crystallization during dissolution of amorphous materials can occur through surface/bulk crystallization of the solid matrix upon contact with the dissolution medium or from the

supersaturated solution generated upon dissolution [8, 22]. The former process impacts the achievable extent of supersaturation, because any crystals formed will act as seeds, growing rapidly and depleting the supersaturation. If no crystallization from the matrix occurs, solution crystallization will govern the longevity of the supersaturated solution formed by dissolution of amorphous material; once nucleation from the solution phase commences, desupersaturation will be observed shortly thereafter due to growth of the nuclei. Ideally, matrix crystallization should be inhibited during the dissolution process, in order to achieve a higher level of supersaturation [8].

The microscope images and the Raman spectra revealed that pure amorphous CEX crystallized rapidly and primarily via the matrix route upon contact with buffer. Absorption of water will decrease the glass transition temperature, leading to increased molecular mobility and hence rapid crystallization. Polymers, when pre-dissolved in buffer, were not able to substantially impede the onset of crystallization, although their presence did extend the time needed to complete crystallization during the slurry experiment. Correspondingly, little supersaturation was generated during the dissolution of pure amorphous CEX in buffer or buffer containing a pre-dissolved polymer (Figure 2-8). This indicates either that complete matrix crystallization is rapid, or that the seed crystals formed grow rapidly under these conditions, depleting the supersaturation produced by dissolution of any residual amorphous material. Furthermore, polymers dissolved in solution are clearly unable to inhibit the formation of crystals in the amorphous matrix. These observations confirm the need to prevent matrix crystallization in order generate supersaturated solutions.

When formulated as an ASD, even at drug loadings as high as 50%, CEX stability to crystallization upon exposure to buffer is considerably improved, although some

differences are seen depending on the polymer used to form the ASD. The Raman data indicate that the CEX: PVP-K12 ASD is more prone to crystallization in the slurry experiments as compared to other ASDs which didn't crystallize over the timeframe of the experiment. Raman spectroscopy alone does not enable us to identify the pathway through which crystallization occurred. However, since all binary and ternary ASDs gave complete release of the drug during the dissolution experiments, achieving the 21-22 µg/ml targeted CEX concentration and yielding supersaturated solutions, it is apparent that matrix crystallization was completely inhibited. Therefore, any difference in dissolution performance for the different ASDs can be attributed to the impact of a specific polymer or polymer combination on crystallization from the solution phase.

The overall desupersaturation profile observed following complete release of the drug will depend on the impact of the polymer on both nucleation and growth kinetics from the solution phase. Since growth cannot occur until nuclei have formed, the impact of polymers on crystal nucleation is of paramount importance. Nucleation kinetics are often inferred from measurement of the induction time, which is defined as the time required for stable nuclei to form and grow to a detectable size (equation 1). If it is assumed that steady-state nucleation is achieved quickly and that $t_n \gg t_g$, then the induction time for the formation of a critical nucleus[9] can be expressed as:

$$t_{ind} \propto J^{-1} \qquad (2)$$

Where $J$ is the nucleation rate, which is given by classical nucleation theory (CNT) as:

$$J = A exp \left[ -\frac{16\pi\gamma^3 v^2}{3k^3 T^3 (\ln S)^2} \right] \qquad (3)$$

Where $\gamma$ is the interfacial tension, $v$ is the molecular volume of the crystallizing solute, $k$ is the Boltzmann constant, $T$ is the temperature, and $S$ is supersaturation[23]. S can be expressed[24] in terms of chemical potential differences as:

$$ln\ S = \frac{\mu - \mu^*}{RT} \qquad (4)$$

where $\mu$ is the solute chemical potential, and $\mu^*$ is the chemical potential of a solute in a saturated solution, and $R$ is the gas constant. In dilute solutions, S can be determined from the ratio, c/c*, where c is the solute concentration in the supersaturated solution and c is the crystal solubility. From equation 3 it is apparent that the main factors influencing the nucleation rate (and hence induction time) are temperature (a constant in our studies), supersaturation and interfacial tension. In the presence of the polymers, experimental induction times are extended indicating that the nucleation rate is decreased, with differences being observed between the polymers. PVP-K12 is the least effective polymer (Figure 2-2) with desupersaturation commencing after 60 min whereas in the presence of HPMCAS or HPMC, no discernable nucleation or crystal growth can be observed for 8 hrs. These differences between polymer effectiveness cannot be explained based on changes in supersaturation (the supersaturation is the same for all solutions containing polymers based on consideration of solution concentration values and equilibrium solubilities; see Table 1) or interfacial tension. Adsorption of a polymer to the nucleus would lead to a decrease in interfacial tension, leading to an expected increase in nucleation rate based on equation 3, rather than the decrease observed in this study. Although CNT is the main framework for understanding nucleation phenomena, it is apparent that this theory does not readily allow for obvious mechanistic insights into how polymers extend induction times. Computer

simulations have suggested that nucleation occurs via a two-step process, whereby the first step is the formation of a dense liquid cluster, followed by structural rearrangement of this cluster to an ordered state[25]. Additives are proposed to interfere with the rearrangement process depending on their relative affinity for the solute cluster and the solvent, as well as some geometric considerations. The greater effectiveness of the cellulose derivatives as nucleation inhibitors in comparison to either PVP grade may therefore relate to a greater ability to interact with a dense liquid cluster of celecoxib, relative to the more hydrophilic PVP which will also have a competing interaction with the solvent phase. This is in accordance with previous studies where more hydrophilic polymers were found to have a smaller impact on nucleation induction times of relatively lipophilic drugs relative to more amphiphilic polymers (including many cellulose derivatives) which extended the longevity of supersaturated solutions to a greater extent[10, 26].

The induction time values are quite predictive of the dissolution performance, whereby the dispersions formulated with PVP-K12 also undergo desupersaturation at the earliest time point following dissolution. Interestingly, the higher tendency of the PVP-K12 dispersions to undergo crystallization from solution can be mitigated by adding a small amount of an effective crystallization inhibitor, either HPMCAS or HPMC, to the dispersion. Thus the cellulose polymers dissolve sufficiently rapidly from the ternary dispersion to be effective solution nucleation inhibitors and are able to inhibit CEX nucleation in the presence of PVP. This strategy might be useful *in vivo* to improve the performance of a dispersion, by combining a polymer that rapid releases the drug, but is a poor solution crystallization inhibitor, with a small quantity of a polymer that is a good inhibitor. The induction time experiments (Figure 2) confirm that the effectiveness of HPMCAS or HPMC in inhibiting

solution nucleation was not impaired by the presence of PVP. These observations open up a strategy of utilizing more than one polymer in an ASD formulation in order to improve performance and also show that only very low polymer concentrations are required to inhibit solution nucleation (only 5 μg/mL of polymer was used for the induction time experiments shown in Figure 2). In the current study, high drug loading ASDs formulated with PVP and HPMC or HPMCAS show enhanced stability against crystallization. Furthermore, the ternary CEX: PVP-K29/32: HPMC dispersions have enhanced release relative to the binary CEX: HPMC dispersions, from which the drug is released very slowly. However, it is important to note that relative to the binary CEX: PVP-K12 dispersion, somewhat surprisingly, release is delayed when a small quantity of either HPMCAS or HPMC is added to matrix. This reduced release rate clearly may not be desirable. However, based on the evidence shown in Figure 7, it is apparent that the additional polymer added to improve stability against crystallization need not be present in the dispersion itself. Here it can be seen that trace amounts (5 μg/mL) of both HPMC and HPMCAS effectively inhibit crystallization from the CEX: PVP-K12 dispersions when pre-dissolved in buffer. Thus, they could be potentially added to the formulation as a separate component from the ASD matrix. Given the wide array of available polymers, as well as the current interest in increasing drug loading, using very hydrophilic polymers to ensure rapid drug release, combined with a small amount of an effective crystallization inhibitory polymer, is an approach that should be investigated further based on the promising results shown in this study.

## 2.7 Conclusions

High drug loading amorphous solid dispersions of celecoxib formulated with different polymers led to supersaturated solutions, but showed dramatically different release profiles and solution crystallization behavior. Using a combination of polymers, where an effective crystallization inhibition polymer was present as a minor component, led to the formation of supersaturated solutions upon solid dispersion dissolution that had improved stability against crystallization. These findings open up new formulation approaches for amorphous solid dispersions, whereby one polymer is included to inhibit crystallization during dissolution, whereas a second polymer is used to achieve another key property such as rapid release, or enhanced storage stability.

Table 2-1. Summary of the various ASDs prepared with different weight ratios

| Drug-Polymer(s) System | w:w |
|---|---|
| CEX: PVP-K12 | 5:5 |
| CEX: PVP-K29/32 | 5:5 |
| CEX: HPMC | 5:5 |
| CEX: HPMCAS | 5:5 |
| CEX: PVP-K12: HPMC | 5:4:1 |
| CEX: PVP-K12: HPMCAS | 5:4:1 |
| CEX: PVP-K29/32: HPMC | 5:4:1 |
| CEX: PVP-K29/32: HPMCAS | 5:4:1 |

Table 2-2 Crystalline CEX solubility in the absence/presence of pre-dissolved polymers

| | No polymer | PVP-K12 | PVP-K29/32 | HPMCAS | HPMC |
|---|---|---|---|---|---|
| CEX solubility (μg/mL) | $1.5 \pm 0.1$ | $2.14 \pm 0.05$ | $2.11 \pm 0.08$ | $1.89 \pm 0.02$ | $2.05 \pm 0.03$ |
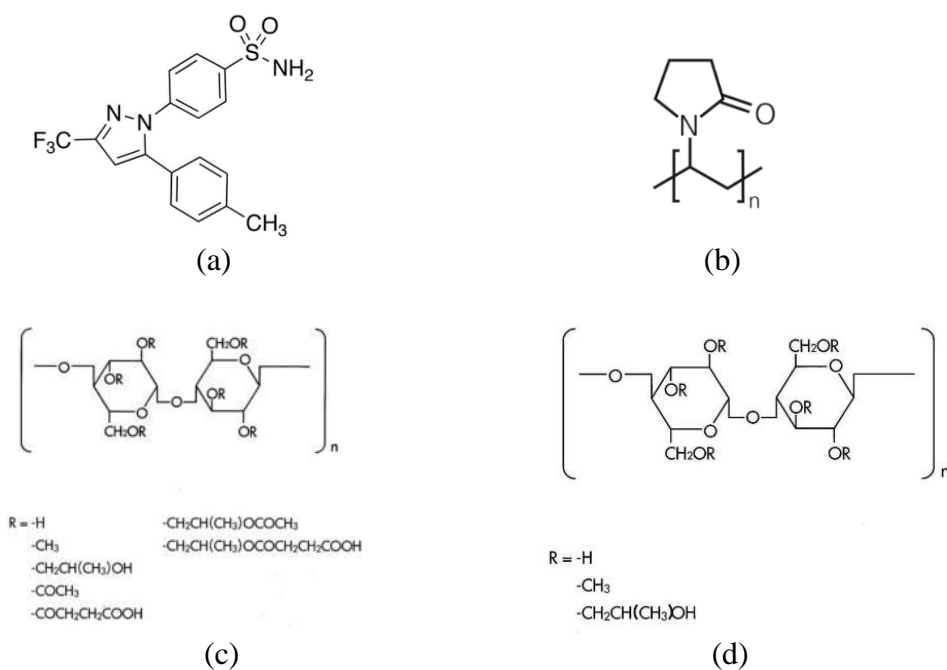
Figure 2-1. Chemical structures of CEX (a), PVP (b), HPMCAS(c), and HPMC (d)
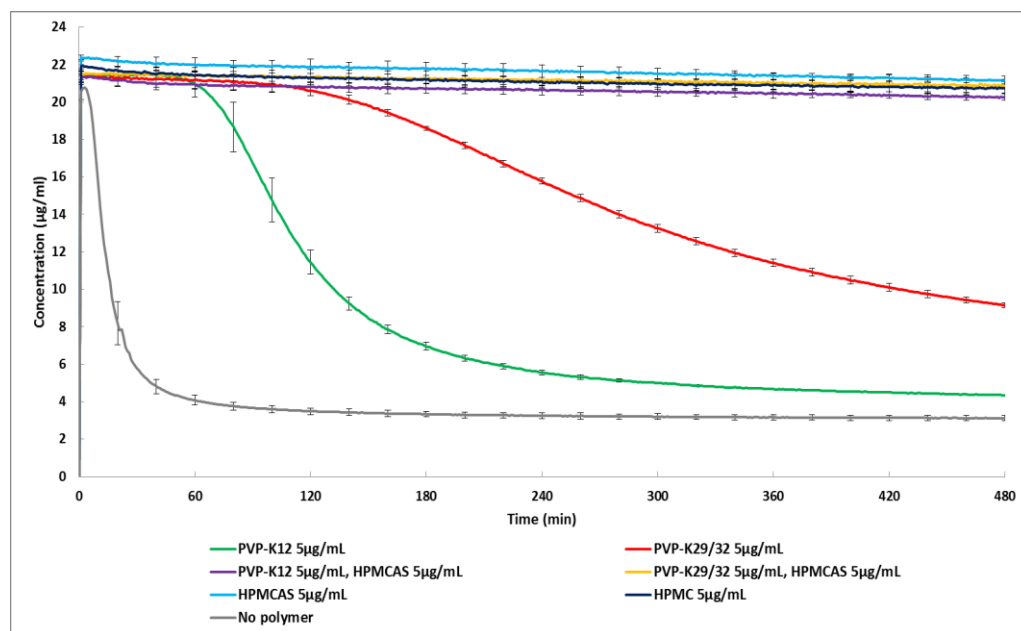


Figure 2-2. Induction time measurements of CEX in the presence and absence of different polymers.
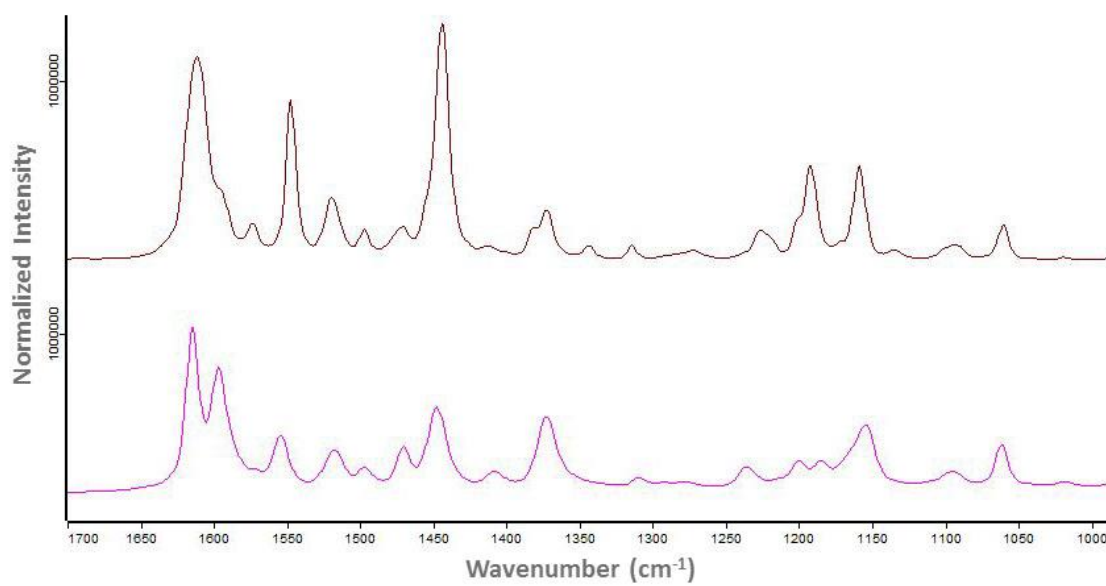
Figure 2-3. Raman spectra of pure crystalline (top) and amorphous (bottom) CEX over the wavenumber range 1700-1000 cm$^{-1}$
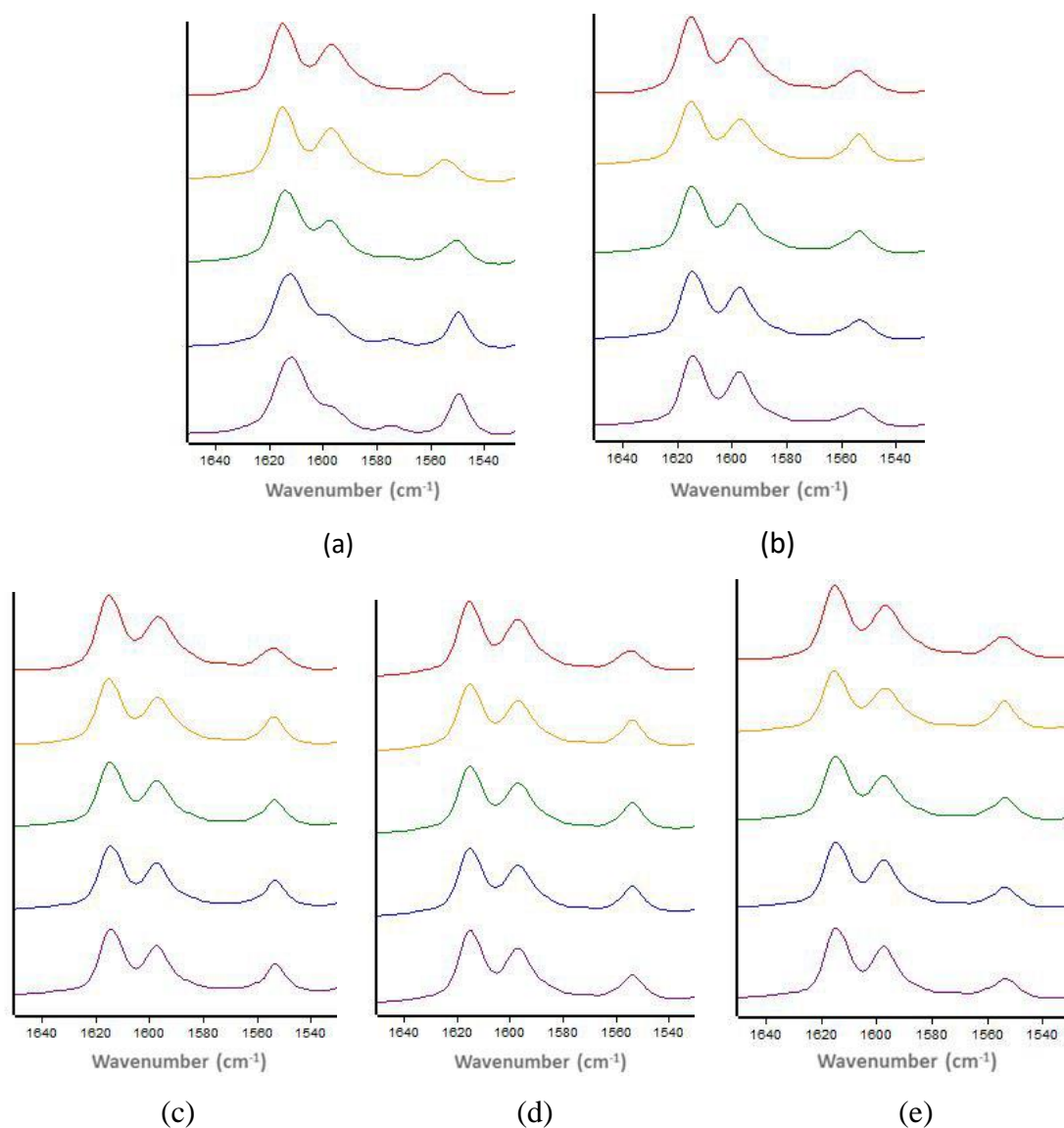
Figure 2-4 Normalized intensities (y-axis) of CEX peaks in ASDs slurried in buffer for different time periods: (a) CEX: PVP-K12 5:5 (b) CEX: PVP-K12: HPMCAS 5:4:1, (c) CEX: PVP-K29/32 5:5, (d) CEX: HPMCAS 5:5, (e) CEX-PVP-K29/32: HPMCAS 5:4:1. All ratios are on a weight basis. The wavenumber range shown 1640-1540 cm$^{-1}$(x-axis). From top to bottom: unexposed ASD, and after 0.5hr, 2.5hrs, 4hrs, and 7hrs exposure to buffer, respectively.
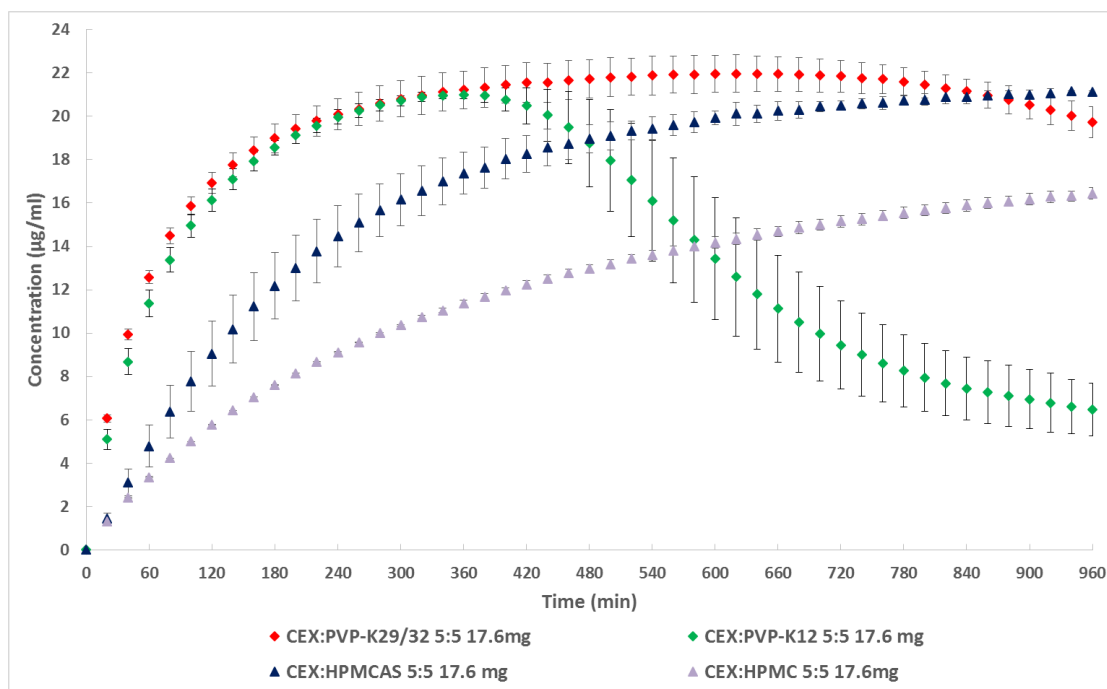
Figure 2-5 Dissolution profiles of binary ASDs
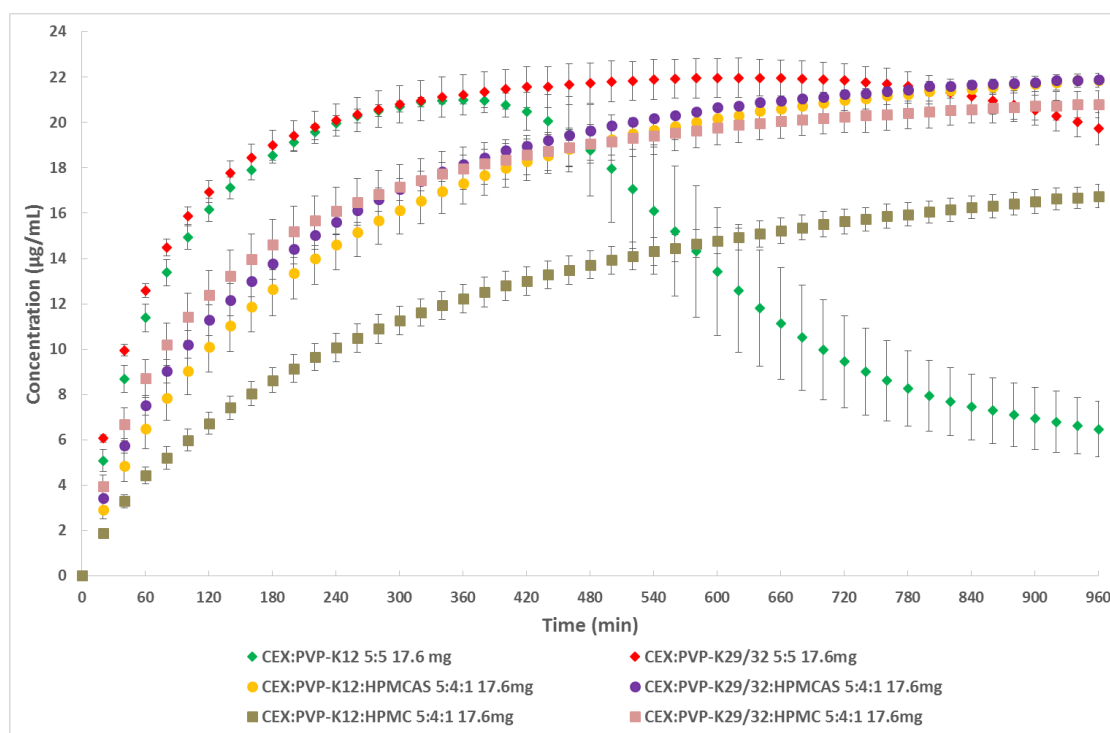


Figure 2-6 Dissolution profiles of binary and ternary ASDs
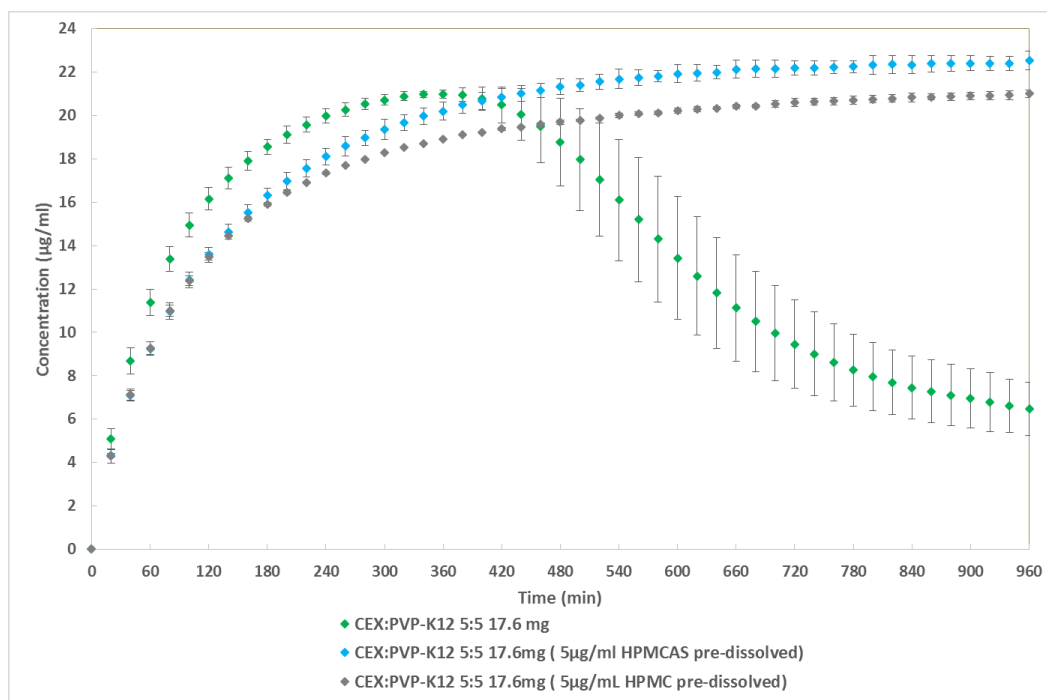
Figure 2-7 Dissolution profiles of CEX: PVP-K12 ASDs in pure SPB with and without a pre-dissolved polymer
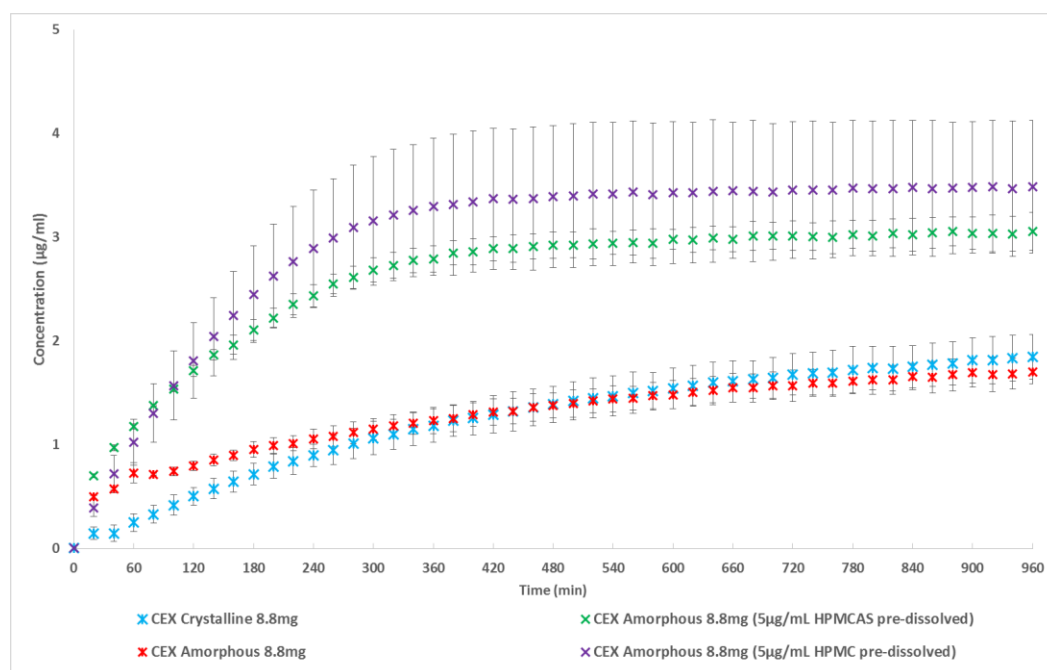


Figure 2-8 Dissolution profiles of crystalline and amorphous CEX in SPB with and without a pre-dissolved polymer

(a)        (b)        (c)
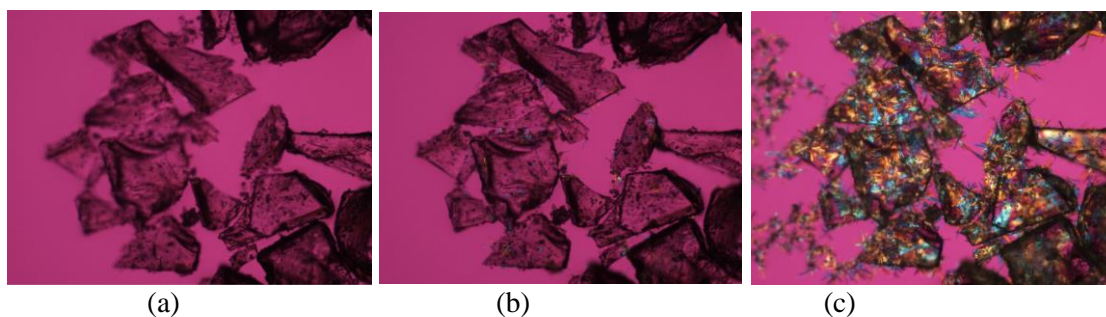
Figure 2-9 Polarized light microscope images of neat amorphous CEX exposed to pure SPB. (a) Unexposed, (b) 2mins, (c) 10mins.



(a)        (b)        (c)
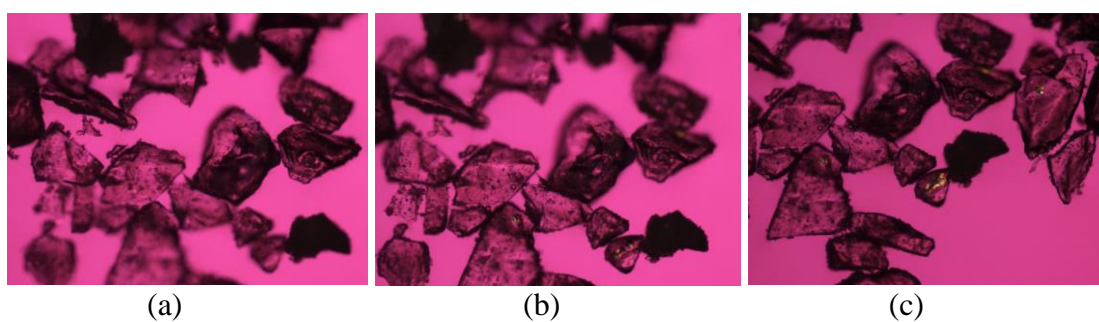
Figure 2-10 Polarized light microscope images of neat amorphous CEX exposed to SPB with 5 μg/mL pre-dissolved HPMC. (a) Unexposed, (b) 20mins, and (c) 60mins.



(a)        (b)        (c)
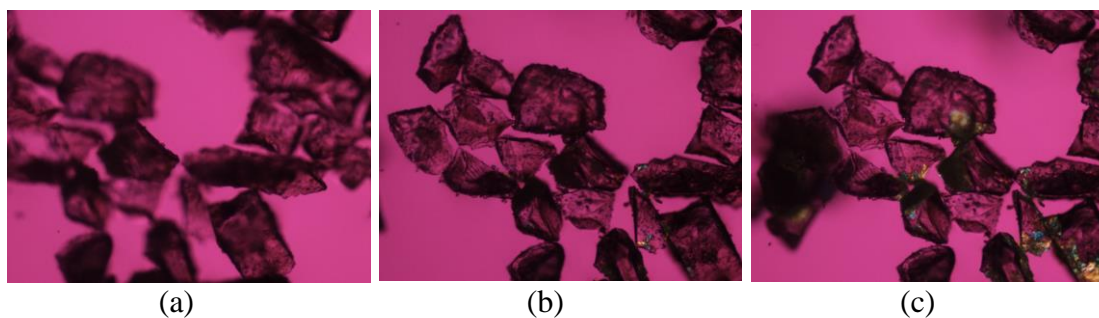
Figure 2-11 Polarized light microscope images of neat amorphous CEX exposed to SPB with 5 μg/mL pre-dissolved HPMCAS. (a) unexposed, (b) 5mins, and (c) 60mins.

## 2.8    References

1.    Fahr, A.; Liu, X.  Drug delivery strategies for poorly water-soluble drugs. *Expert Opin Drug Deliv* **2007,** *4*, (4), 403-16.

2.    Hancock, B. C.; Parks, M.  What is the true solubility advantage for amorphous pharmaceuticals? *Pharm. Res.* **2000,** *17*, (4), 397-404.

3.    Baird, J. A.; Van Eerdenbrugh, B.; Taylor, L. S.  A Classification System to Assess the Crystallization Tendency of Organic Molecules from Undercooled Melts. *J Pharm Sci-Us* **2010,** *99*, (9), 3787-3806.

4.    Trasi, N. S.; Taylor, L. S.  Effect of Additives on Crystal Growth and Nucleation of Amorphous Flutamide. *Cryst Growth Des* **2012,** *12*, (6), 3221-3230.

5.    Van den Mooter, G.; Wuyts, M.; Blaton, N.; Busson, R.; Grobet, P.; Augustijns, P.; Kinget, R.  Physical stabilisation of amorphous ketoconazole in solid dispersions with polyvinylpyrrolidone K25. *Eur J Pharm Sci* **2001,** *12*, (3), 261-269.

6.    Kestur, U. S.; Taylor, L. S.  Role of polymer chemistry in influencing crystal growth rates from amorphous felodipine. *Crystengcomm* **2010,** *12*, (8), 2390-2397.

7.    Kestur, U. S.; Van Eerdenbrugh, B.; Taylor, L. S.  Influence of polymer chemistry on crystal growth inhibition of two chemically diverse organic molecules. *Crystengcomm* **2011,** *13*, (22), 6712-6718.

8.    Alonzo, D. E.; Zhang, G. G. Z.; Zhou, D. L.; Gao, Y.; Taylor, L. S.  Understanding the Behavior of Amorphous Pharmaceutical Systems during Dissolution. *Pharm Res-Dordr* **2010,** *27*, (4), 608-618.

9.    Sohnel, O.; Mullin, J. W.  Interpretation of Crystallization Induction Periods. *J Colloid Interf Sci* **1988,** *123*, (1), 43-50.

10.    Ilevbare, G. A.; Liu, H. Y.; Edgar, K. J.; Taylor, L. S.  Maintaining Supersaturation in Aqueous Drug Solutions: Impact of Different Polymers on Induction Times. *Cryst Growth Des* **2013,** *13*, (2), 740-751.

11.    Abu-Diak, O. A.; Jones, D. S.; Andrews, G. P.  An Investigation into the Dissolution Properties of Celecoxib Melt Extrudates: Understanding the Role of Polymer Type and Concentration in Stabilizing Supersaturated Drug Concentrations. *Mol Pharmaceut* **2011,** *8*, (4), 1362-1371.

12.    Chen, J.; Ormes, J. D.; Higgins, J. D.; Taylor, L. S.  Impact of Surfactants on the Crystallization of Aqueous Suspensions of Celecoxib Amorphous Solid Dispersion Spray Dried Particles. *Mol Pharmaceut* **2015,** *12*, (2), 533-541.

13.    Trasi, N. S.; Taylor, L. S.  Effect of polymers on nucleation and crystal growth of amorphous acetaminophen. *Crystengcomm* **2012,** *14*, (16), 5188-5197.

14.    Trasi, N. S.; Oucherif, K. A.; Litster, J. D.; Taylor, L. S.  Evaluating the influence of polymers on nucleation and growth in supersaturated solutions of acetaminophen. *Crystengcomm* **2015,** *17*, (6), 1242-1248.

15.    Konno, H.; Handa, T.; Alonzo, D. E.; Taylor, L. S.  Effect of polymer type on the dissolution profile of amorphous solid dispersions containing felodipine. *Eur J Pharm Biopharm* **2008,** *70*, (2), 493-499.

16.    Konno, H.; Taylor, L. S.  Influence of different polymers on the crystallization tendency of molecularly dispersed amorphous felodipine. *J Pharm Sci-Us* **2006,** *95*, (12), 2692-2705.

17.      Rumondor, A. C. F.; Stanford, L. A.; Taylor, L. S.  Effects of Polymer Type and Storage Relative Humidity on the Kinetics of Felodipine Crystallization from Amorphous Solid Dispersions. *Pharm Res-Dordr* **2009,** *26*, (12), 2599-2606.

18.      Marks, J. A.; Wegiel, L. A.; Taylor, L. S.; Edgar, K. J.  Pairwise Polymer Blends for Oral Drug Delivery. *J Pharm Sci-Us* **2014,** *103*, (9), 2871-2883.

19.      Goddeeris, C.; Willems, T.; Van den Mooter, G.  Formulation of fast disintegrating tablets of ternary solid dispersions consisting of TPGS 1000 and HPMC 2910 or PVPVA 64 to improve the dissolution of the anti-HIV drug UC 781. *Eur J Pharm Sci* **2008,** *34*, (4-5), 293-302.

20.      Janssens, S.; De Armas, H. N.; Roberts, C. J.; Van Den Mooter, G.  Characterization of ternary solid dispersions of itraconazole, PEG 6000, and HPMC 2910 E5. *J Pharm Sci-Us* **2008,** *97*, (6), 2110-2120.

21.      Al-Obaidi, H.; Ke, P.; Brocchini, S.; Buckton, G.  Characterization and stability of ternary solid dispersions with PVP and PHPMA. *International Journal of Pharmaceutics* **2011,** *419*, (1-2), 20-27.

22.      Raina, S. A.; Alonzo, D. E.; Zhang, G. G. Z.; Gao, Y.; Taylor, L. S.  Impact of Polymers on the Crystallization and Phase Transition Kinetics of Amorphous Nifedipine during Dissolution in Aqueous Media. *Mol Pharmaceut* **2014,** *11*, (10), 3565-3576.

23.      Mullin, J. W., *Crystallization*. Butterworth-Heinemann: 2001.

24.      Myerson, A., *Handbook of industrial crystallization*. Butterworth-Heinemann: 2002.

25.      Anwar, J.; Boateng, P. K.; Tamaki, R.; Odedra, S.  Mode of Action and Design Rules for Additives That Modulate Crystal Nucleation. *Angewandte Chemie International Edition* **2009,** *48*, (9), 1596-1600.

26.      Warren, D. B.; Benameur, H.; Porter, C. J. H.; Pouton, C. W.  Using polymeric precipitation inhibitors to improve the absorption of poorly water-soluble drugs: A mechanistic basis for utility. *Journal of Drug Targeting* **2010,** *18*, (10), 704-731.

# CHAPTER 3. EFFECT OF TEMPERATURE AND MOISTRUE ON THE SOLID STATE STABILITY OF BINARY AND TERNARY AMORPHOUS SOLID DISPERSIONS OF CELECOXIB

## 3.1    Abstract

The effectiveness of different polymers, alone or in combination, in inhibting crystallization of amorphous solid dispersions of CEX was evaluated. It was found that PVP and PVP-VA formed stronger hydrogen bonding with CEX than cellulose based polymers. This, combined with their better effectiveness in raising the glass transition temperatures (Tgs) of the dispersions, provided better physical stabilization of amorphous CEX against crystallization in the absence of moisture. PVP was found to be miscible with both CEX and HPMCAS. The presence of HPMCAS would not result in demixing of CEX with PVP, in spite of a stronger hydrogen bonding between PVP and HPMCAS than that between PVP and CEX. Consequently, the physical stability is minimally impaired by the presence of HPMCAS when the major polymer present in the ternary dispersion is PVP. The results of crystal growth rate measurements was predictive of the relative stability of bulk ASDs. In the presence of moisture, the physical stability of CEX ASDs are strongly affected by both the hygrocopicity and the strength of intermolecular interactions. PVP ASDs was more susceptible than PVP/VA ASDs to moisture induced amorphous-amorphous phase separation, followed by crystallization HPMC ASDs are less stable than HPMCAS ASDs owing to higher amount of water uptake.

## 3.2    Introduction

Drugs formulated as the amorphous form can provide advantages over their crystalline counterparts by offering increased kinetic solubility and a faster dissolution rate, contributing to improved absorption *in vivo*. However, such improvements in delivery are inevitably accompanied with an increased risk of product instability, due to the intrinsic tendency of an amorphous compound to crystallize during storage.

A polymer is often mixed with the amorphous drug at the molecular level to inhibit solid state crystallization. The stabilizing effect of polymers is multifaceted. Polymers are thought to reduce the molecular mobility of the amorphous drug at the storage temperature by increasing the glass transition temperature (Tg) of the system [1], typically referred to as an anti-plasticization effect. However, other studies have revealed that crystallization inhibition by a polymer cannot always be rationalized based on Tg changes [2, 3]. Nifedipine was found to crystallize more readily than felodipine both from the pure amorphous form and amorphous solid dispersions (ASDs) with polyvinylpyrrolidone (PVP) in spite of a similar $T_g$ and molecular mobility. The greater ease of nifedipine to crystallize was attributed to a lower nucleation activation energy and a larger enthalpic crystallization driving force[4]. Polymers may also contribute to the physical stabilization of amorphous drug by forming specific inter-species interactions with the drug, such as hydrogen bonding[5] or ionic interactions[6, 7]. The strength of such interactions, as inferred using mid-infrared spectroscopy, appears to be in-line with the relative effectiveness of polymers as crystallization inhibitors for naringenin and quercetin[8]. Furthermore, the nature of the drug-polymer interactions formed in the amorphous systems were found to be much more critical

for rapidly crystallizing systems, whereby less discrimination is seen for more slowly crystallizing compounds, at least over shorter timeframes[9].

Crystalline solids adsorb water by a surface adsorption mechanism[10]. Amorphous solids are more hygroscopic than their crystalline counterparts due to their disordered structure and higher free volume. In addition to surface adsorption, water may penetrate into the bulk of amorphous materials. The moisture absorbed can be detrimental to the stability of amorphous solid dispersions (ASDs) for several reasons. As an effective plasticizer with a Tg as low as -137 ℃[11], water can effectively reduce the $T_g$ of the ASD and thereby increase the molecular mobility at the storage temperature[12] It has been shown that 1% water lowers the $T_g$ of indomethacin by 10 ℃[13]. Water can also irreversibly disrupt the drug-polymer interactions by competitively forming hydrogen bonds with a hydrophilic polymer[14]. Both factors [15] may induce amorphous-amorphous phase separation [16] in the ASDs with subsequent crystallization that preferentially occur in the drug-rich domains[17].

If crystallization during storage can be avoided, then dissolution of the solid dispersion can potentially yield a supersaturated solution of the drug with a substantially elevated solution concentration relative to that obtained from the crystalline material. While it is obviously vital to ensure that the drug remains amorphous during the product shelf life, it is of equal significance to inhibit crystallization during dissolution over pharmaceutically relevant timeframes. Unfortunately, choosing the optimum pharmaceutically acceptable inhibitor for each of these crystallization pathways is largely empirical. Furthermore, the polymer that is the best solid state inhibitor [18] may be ineffective as a solution crystallization inhibitor [19] and vice versa. For example, it was observed that polyacrylic acid (PAA) was very effective at inhibiting the crystal growth of acetaminophen from supercooled liquids[5,]

[20], and hence prevented crystallization from amorphous solid dispersions, but was ineffective at preventing either nucleation or crystal growth from aqueous solutions[21]. Similarly, PVP reduces both the crystal nucleation and growth rates from amorphous felodipine[18, 22], and in the absence of water, dispersions prepared with this polymer are stable to crystallization[23]. However, PVP does not inhibit crystallization from supersaturated felodipine solutions and the dissolution performance of felodipine-PVP dispersions is relatively poor [19].

Therefore, an important advance in ASD formulation could be to incorporate combinations of polymers, chosen to maximize crystallization inhibition in both the solid and solution phases [24-26]. Before this strategy can be implemented, however, it is necessary to determine factors such as miscibility of the ternary systems. If the polymers are miscible, it should be relatively straightforward to determine if a one phase amorphous system is produced when the drug is added. However, if the polymers are immiscible/partially immiscible, it will be important to determine how the drug is distributed between the two polymer phases. It is expected that the drug will preferentially mix with the polymer chosen as the solid state stabilizer, since the formation of inter-species interactions will promote miscibility, but to the best of our knowledge, these issues have not been probed to date. By studying the miscibility in a ternary system, we will also be able to evaluate if the polymer pair miscibility influences the miscibility of the drug with either polymer.

It has been well documented that the solid state stability of ASDs are improved when the polymer loading is increased. Therefore, for the strategy to be successful, it is also necessary to determine the optimum level of solution stabilizing polymer, since it is clear that an additional polymer cannot be added at the expense of drug loading.

Herein, we evaluated the solid state stability of celecoxib (CEX), a poorly soluble anti-inflammatory agent, when formulated in ASDs with different polymer combinations and exposed to high stress storage conditions of elevated temperature and/or relative humidity. Previously, we reported that the dissolution performance of high drug loading ASDs of CEX formulated with polyvinylpyrrolidone (PVP) were improved when 20% of the PVP was replaced by a strong solution crystallization inhibiting polymer: either hydroxypropyl methyl cellulose (HPMC) or HPMC acetate succinate (HPMCAS)[27]. It was therefore also of interest to evaluate the solid state stability of ternary ASDs relative to the corresponding binary ASDs.

## 3.3    Materials

CEX was purchased from Attix Pharmaceuticals (Toronto, Ontario, Canada). Polyvinylpyrrolidone (PVP) (K29/32: Mw 58,000 g mol$^{-1}$) was purchased from ISP Technologies, INC (Wayne, NJ, USA). PVP (K12: MW 2000-3000g mol$^{-1}$) and vinylpyrrolidone-vinyl acetate copolymer (PVP/VA) (Kollidon VA64, Mw 45,000-47,000g mol$^{-1}$) were provided by BASF Corporation (Ludwigshafen, Germany). Hydroxypropylmethylcellulose acetate succinate (HPMCAS, Type AS-MF: Mw 17,000g mol$^{-1}$) and hydroxypropyl methylcellulose (HPMC, Type 606: Mw 35,600g mol$^{-1}$) were supplied by Shin-Etsu Chemical Co. (Tokyo, Japan). The molecular structures are shown in Figure 3-1.

## 3.4    Methods

### 3.4.1    Preparation of Bulk Amorphous Materials

CEX and the polymer(s) at different dry weight ratios were dissolved in a mixture of ethanol and dichloromethane. Solvent removal was achieved by rotary evaporation. The ASDs of the drug or polymer blends were subsequently dried in a vacuum oven overnight to remove any residual solvent.  They were then ground using a mortar and pestle and sieved to obtain a particle size fraction of 106-250μm. They were then stored in a desiccator containing phosphorous pentoxide at room temperature prior to use.

### 3.4.2    Infrared (IR) Spectroscopy

Solutions of drug and polymer mixtures at different dry weight ratios or single component polymers were dissolved in a mixture of ethanol and dichloromethane. The solutions were then dipped onto thallium bromoiodide (KRS-5) optical crystals and rotated on a KW-4A spin coater (Chemat Technology, Inc, Northridge, CA, USA). IR spectra of the resulting thin films were obtained on a Bruker Vertex 70 (Bruker, Billerica, MA, USA).  64 scans were collected with a 4 cm$^{-1}$ resolution for each sample over the wavenumber range from 4000cm$^{-1}$ to 500 cm$^{-1}$. Dry air was purged into the sampling and optical compartment to prevent spectral interference from water vapor. Pure amorphous CEX was prepared by melting the drug on an aluminum foil at approximately 180°C and quenched to room temperature on a flat metal surface and gently ground by a mortar and pestle. No diffraction peaks was observed in the powder x-ray diffraction pattern.  Pure crystalline CEX was used as is. The pure amorphous or crystalline CEX was placed in an attenuated total reflectance

(ATR) attachment and the IR spectra was obtained using the same Bruker instrument. The Opus 7.2 software (Bruker, Billerica, MA, USA) was used to analyze the spectra.

### 3.4.3 Thermal Analysis

Thermal analysis was carried out using a TA Q2000 DSC with a cooling refrigerator system (TA Instruments, New Castle, DE, USA). Indium and tin was used for calibration of temperature and indium was used for calibration of enthalpy. Dry nitrogen was purged at a rate of 50mL min$^{-1}$. 3-5mg of the samples were weighed into an aluminum T zero sample pan and sealed using a hermetic T zero lid with a pinhole. The glass transition temperature was determined by heating the sample at approximately 20°C min$^{-1}$ to approximately 30°C above $T_g$, followed by cooling and reheating at 20°C min$^{-1}$. The onset temperature of the second heating scan was reported.

### 3.4.4 Dynamic Vapor Sorption

Moisture sorption isotherms of the ASDs and pure polymers were measured by a Symmetrical Gravimetric Analyzer (SGA-100) (VTI Corporation, Hialeah, FL, USA). Samples were dried at 45°C with dry nitrogen purged into the sorption analyzer prior to exposure to increasing RH. The equilibrium criterion for the drying step was less than 0.01% w/w change within 2 min with a maximum drying time of 60min. The sample was then exposed to RH from 5 to 95% with 10% step increase at 25 ℃. The maximum time for equilibration in each step was 180 min.

### 3.4.5   Crystal Growth Rate Measurements

Physical mixtures were prepared by mixing the crystalline drug and the polymer(s) in a cryogenic mill (6750 freezer mill, Spex Sampleprep, Metuchen, New Jersey, USA). The mixture were then melted between two cover slips on a hot plate and quench cooled to room temperature on a flat metal surface. The coverslips were then stored in an oven at 80°C until small nuclei were formed and became visible. The increase in diameter of the crystal nuclei with time on a hot stage set at the temperature of interest were measured using a polarizing microscope as described previously[18].

### 3.4.6   Storage Conditions and Powder X-ray Diffraction

ASDs of CEX were stored in 20ml open scintillation vials in a dessicator, and then subject to different environmental conditions for long term stability studies: 80°C/0%RH (Drierite®), room temperature (22-25°C) /94%RH (saturated solution of potassium nitrate), and 40°C/75%RH (saturated solution of sodium chloride). Powder X-ray diffraction (PXRD) pattern were taken periodically to evaluate the crystallization kinetics using a Rigaku SmartLab diffractometer (Rigaku Cooperation, The Woodlands, TX, USA). The patterns were collected in step scan mode with a scan range from 5° to 35° and a scan speed of 4°/min. The tube voltage and current were 44kV and 40mA, respectively. A silicon standard was used to calibrate the instrument.

### 3.5   Results

### 3.5.1   Fourier Transform Infrared Spectroscopy

Figure 3-2 shows the IR spectra of crystalline and amorphous forms of the pure drug,

focusing on the high wavenumber region. Crystalline CEX show a doublet at 3225cm$^{-1}$ and 3322cm$^{-1}$, which arise from N-H stretching vibrations associated with the asymmetric and symmetric motions respectively of the NH$_2$ of the sulfonamide group (Figure 1). These peaks shifted to 3268cm$^{-1}$ and 3351cm$^{-1}$ for amorphous CEX. These values are very close to those reported by Chawla et al[28]. It has been established that a lower peak frequency of the N-H group is typically associated with a shorter hydrogen bond distance[29]. Therefore, the hydrogen bonding in the pure amorphous form of CEX appears weaker than in the crystalline form.

In amorphous mixtures of CEX and PVP, a peak at 3196cm$^{-1}$ emerged and increased in intensity at the expense of the 3268cm$^{-1}$ peak as the polymer loading increased (Figure 3-3). Correspondingly, the C=O peak of PVP at 1682cm$^{-1}$ developed a shoulder at approximately 1661cm$^{-1}$ (the drug has no absorbance at this wavenumber), increasing in dominance as the drug to polymer ratio increased. The spectra suggest that an increasing fraction of the drug NH$_2$ groups was involved in hydrogen bonding with the C=O of PVP as the polymer loading increased. For CEX-HPMCAS ASDs, the NH peak of CEX at 3268cm$^{-1}$ gradually shifted towards 3237cm$^{-1}$ as the polymer loading increased, whereas the HPMCAS's ester carbonyl peak[15] shifted from 1743cm$^{-1}$ to 1734cm$^{-1}$ (Figure 3-4). Therefore, compared to the dispersion with PVP and based on the relative extent of the peak shifts in the presence of the polymer, the hydrogen bonding between CEX and HPMCAS was found to be much weaker.

For the PVP: HPMCAS films, the peak at 1682cm$^{-1}$ showed a shoulder at 1643cm$^{-1}$, and can be assigned to the C=O of PVP hydrogen bonded to the OH group of HPMCAS (Figure 3-5). This shoulder was lower in wavenumber than that observed in CEX: PVP films,

indicating that the hydrogen bonding between the two polymers was stronger than that between the drug and PVP. Furthermore, the fact that the peak at $1682cm^{-1}$ persists and was dominant in the binary polymer blend spectra indicates that not all PVP monomers were involved in hydrogen bonding with HPMCAS even when HPMCAS was present at very high weight fraction.

For ternary mixtures where HPMCAS was present as a minor fraction, the spectra (Figure 3-6) were similar to those obtained from a binary mixture of CEX and PVP, and no shoulder at $1643cm^{-1}$ (characteristic of PVP-HPMCAS interactions) can be observed. It is unclear whether hydrogen bonding between CEX and HPMCAS exists in the ternary systems and whether it will form at the cost of reduced hydrogen bonding between CEX and PVP, which might potentially substantially impair the solid state stability of the ternary ASDs relative to the corresponding CEX: PVP binary ASDs.

To further evaluate this, the HPMCAS loading was increased up to 40%, and it can be deduced that the hydrogen bonding between CEX and PVP persist in this dispersion (Figure 3-7). The shoulder at $1643cm^{-1}$, indicative of hydrogen bonding between PVP and HPMCAS, eventually emerged when the HPMCAS loading was increased to 60% (Figure 3-8). Furthermore, distinct spectral differences between the ternary mixture at a ratio of 1:3:6 and the binary mixture of PVP: HPMCAS 3:7 were observed in the $1630cm^{-1}$ to $1670cm^{-1}$ region. This suggests that hydrogen bonding between CEX and PVP persists in the ternary mixture even when a high weight fraction of HPMCAS is present in the ternary mixture.

PVP/VA is a copolymer of vinylpyrrolidone and vinylacetate, and hence it has two types of C=O group, pyrrolidone and acetate with characteristic peaks at $1684cm^{-1}$ and $1737cm^{-}$

[1], respectively. Similar to the case of CEX: PVP films, the C=O peak at 1684cm^{-1} showed a shoulder at 1662cm^{-1} when PVP/VA was mixed with CEX. Correspondingly, the NH peak of CEX shifted from 3268cm^{-1} to approximately 3198cm^{-1}. This indicates that the hydrogen bonding strength between the C=O group of the vinylpyrrolidone monomer of PVP/VA and the $NH_2$ group of CEX was comparable to that observed in CEX: PVP dispersions. Interestingly, at high drug loadings (70% and 90%), the C=O of the vinylacetate group of PVP/VA showed a shoulder at lower wavenumber, indicating a potential weak hydrogen bonding interaction with CEX. When the spectra of CEX: PVP/VA and CEX: PVP-K29/32 films were compared at the same drug loading (70%), based on the $NH_2$ stretching region, it appears that a larger fraction of drug molecules was involved in hydrogen bonding in the case of CEX: PVP-K29/32 than in CEX: PVP/VA. This can be presumably attributed to the dilution effect due to the presence of the vinylacetate monomer in PVP/VA which is a weaker hydrogen bond acceptor than the vinylpyrrolidone carbonyl. The difference in the carbonyl stretching region indicates that most of PVP/VA pyrrolidone monomers have engaged in hydrogen bonding with CEX, in contrast to the PVP system, where there was a larger fraction of PVP with free C=O remaining at the same 70% drug loading.

To investigate the potential impact of environmental moisture on the miscibility and stability of mixtures during storage, spin coated films were exposed to high relative humidity (94%RH). Moisture was then removed by purging dry air into the chamber of the IR spectrometer prior spectral acquisition. For CEX: PVP-K29/32 films (Figure 3-11-13), the peak at 3196cm^{-1} decreased in intensity whereas the peak at 3268 cm^{-1} increased in intensity. Correspondingly, there was a slight but discernable decrease in C=O shoulder at 1661cm^{-1}. This suggests that water irreversibly disrupts the hydrogen bonding of PVP with

CEX and induced amorphous-amorphous phase separation to some extent. This phenomenon appears more pronounced in films with higher polymer loading due to a higher amount of water uptake by the hygroscopic polymer. Subsequently, the amorphous CEX partially crystallized as indicated by the appearance of peak at about 3236 cm$^{-1}$ in CEX: PVP 7:3 within 18 days of storage. Crystallization was also evident by visual inspection in the form of white opaque spots appearing on the initially transparent film. The faster crystallization at higher drug loading is expected since at high drug loadings there was a higher fraction of CEX that is not hydrogen bonded with PVP to begin with, despite a smaller extent of moisture induced amorphous-amorphous phase separation. Similarly, for felodipine and PVP system that undergoes moisture induced drug-polymer demixing[14], it was found that at higher drug loading, crystallization was faster even though the amount of water uptake by the ASD was reduced[30].

In contrast, CEX: HPMCAS and CEX: PVP/VA spin coated films (Figure 3-14 and Figure 3-15) were more resistant to amorphous-amorphous phase separation and/or crystallization as they showed no notable changes in the spectra following exposure to moisture over 18days. After storage for more than a month, crystallization mainly occurred on the edges of the IR substrates for both CEX: HPMCAS and CEX: PVP/VA spin coated films at high drug loadings (7:3 and 9:1).

The changes in spectra of the ternary films (Figure 3-16) were similar to those observed for the binary CEX: PVP films owing to the fact that PVP was present in a larger fraction than HPMCAS. In addition, PVP may phase separate from HPMCAS due to moisture sorption, as indicated in Figure 3-17, since the small shoulder at 1643cm$^{-1}$ is lost following exposure to moisture and drying.

### 3.5.2 Isothermal Moisture Sorption

To understand the impact of moisture on the solid state stability of ASDs, it is necessary to quantify the amount of water absorbed by each pure component as a function of relative humidity. As shown in Figure 3-18, pure amorphous CEX was very hydrophobic with only 2 wt. % water absorbed at 95%RH. Particles were retrieved after the experiment and observed under the polarized microscope (images not shown). Partial crystallization occurred in this case despite relatively low moisture sorption by the pure drug. The pure polymers differ substantially in hygroscopicity, with the order from highest to lowest moisture sorption being PVP>PVP/VA>HPMC>HPMCAS. Moreover, the amount of water absorbed by PVP was minimally affected by the molecular weight grade.

The binary ASD at 50% drug loading absorbs much less moisture than the corresponding pure polymer. This is expected considering the hydrophobicity of the drug[30]. The ASDs shows the same rank order of hygroscopicity as the corresponding pure polymer in terms of moisture sorption profiles with the exception of CEX: PVP/VA ASD whose moisture sorption isotherm was similar to that of the CEX: HPMC ASD.  Furthermore, it was found that the binary ASDs showed a dramatic increase when the relative humidity was increased to above 85% with the exception of the CEX: HPMCAS ASD. This effect was the more pronounced in ASDs with PVP than with PVP/VA or HPMC. When the calculated moisture sorption profiles based on the water uptake and the weight fraction of each component were plotted against the experimental profiles (Figure 3-20), it is clear that water uptake is largely suppressed in CEX:PVP/VA but dramatically increased in CEX:PVP system at 95%RH. This agrees with the IR results that CEX: PVP undergoes moisture induced partial demixing whereas CEX: PVP/VA does not. In a phase separated

system, the moisture sorption of the binary system is expected to be additive whereas a negative deviation from the calculated values is expected for a miscible system.

The moisture sorption profiles of the ternary ASDs where PVP was in excess (Figure 3-21) exhibited a similar pattern to the corresponding binary CEX: PVP ASDs. However, it is also apparent that replacing PVP with a less hygroscopic cellulosic polymer did result in a slight reductions in water uptake.

### 3.5.3   Thermal Analysis

Despite some practical limitations[31], DSC analysis remains the most frequently used method to probe the mixing state of a drug with a polymer[32]. To this end, $T_g$ as a function of composition was measured and results are shown in Figure 3-22. The drug alone has a Tg of approximately 55°C, which is substantially lower than the Tg values observed for the polymers. For binary ASDs of the drug with different polymers, a single $T_g$ value was obtained for each composition, suggesting that only a single amorphous phase was present. In other words, the drug appears to be miscible with these polymers. PVP-K12 and PVP/VA have lower $T_g$ values than HPMCAS and HPMC, but apparently they were much more effective in raising the $T_g$ values of the ASDs.

Similarly, Sakurai et al [24] reported that the Tg values of solid dispersions of a BCS class II drug prepared with PVP or PVP/VA were close to the predicted values using Gordon Taylor equation, whereas a negative deviation was observed in the dispersions with HPMC. Consequently, the ternary solid dispersions prepared with both HPMC and PVP/VA or PVP provided better resistance to crystallization than the dispersions with HPMC alone at 40°C /75%RH, presumably due to reduced molecular mobility.

Polymer-polymer blends are frequently largely immiscible due to the low entropy of mixing for two large molecules[33]. Consequently, miscibility between polymers can only be anticipated when they can form specific interactions and hence have a favorable enthalpic contribution to the free energy of mixing[34]. For binary polymer blends of PVP and HPMCAS, a single $T_g$ value was obtained for each composition (Figure 3-23), indicating that only a single amorphous phase was present. This agrees with the IR results that PVP can form strong hydrogen bonds with HPMCAS (Figure 3-5).

With three components, the phase behavior in the solid state immediately becomes very complex. Understanding the miscibility of the ternary system is of crucial importance, since it is desirable that the solid state stabilizing polymer is in the same amorphous phase as the drug. Nevertheless, it is also expected that the final concentration of the solution stabilizing polymer (HPMCAS or HPMC) will be low[27], and therefore it should at least not interfere with the miscibility of the drug and the solid state stabilizing polymer (PVP). The IR results suggest that CEX has a higher affinity with PVP than HPMCAS, which is not impaired by the competition from HPMCAS for hydrogen bonding with PVP. Hence, a miscible ternary system is expected. This is further supported by the single Tg values obtained for CEX: PVP: HPMCAS ASDs at 8:1.6:0.4 and 5:4:1 ratios (Figure 3-24). Moreover, the ternary ASD's $T_g$ values were close to, but slightly lower than that of the CEX: PVP binary ASDs due to the fact that PVP was present as the major component in the ternary ASDs.

### 3.5.4 Crystal Growth Rate

To quantitatively evaluate the impact of the polymers, crystal growth rate measurements in the presence and absence of the polymers were determined. As shown in Figure 3-25, CEX has the highest growth rate in the absence of any polymer. Crystal growth was much faster in the presence of HPMCAS than in the presence of PVP at an equivalent weight percent of polymer. Increasing the molecular weight of PVP only slightly reduced the growth rate. The crystal growth rate of CEX in the presence of PVP/VA was slightly faster than that in the presence of PVP. This may be because more vinylpyrrolidone carbonyl groups are present in PVP than in PVP/VA at the same polymer loading, though the hydrogen bonding strength of the PVP/VA's vinyl pyrrolidone group with CEX was comparable to that between PVP and CEX. Replacing a minor proportion of PVP with HPMCAS led to a small increase in crystal growth rate, although the growth rate remained substantially lower than the for the CEX:HPMCAS dispersion.

### 3.5.5 Solid State Stability during Storage

Figure 3-26 shows PXRD patterns of the binary and ternary ASDs which were stored at 80°C/0%RH. At 80% drug loading, the crystallization kinetics of the ternary ASD where HPMCAS was present in minor fraction was comparable to that of the binary CEX: PVP/VA ASDs, both of which crystallized slightly faster than that of the binary CEX: PVP-K29/32 ASD. In contrast, CEX: HPMCAS ASD crystallized the fastest. These trends are in good agreement the crystal growth rate measurements from the melt quenched films, implying that the solid state properties of the ternary ASD could be largely predicted by the corresponding binary ASD closest to the ternary composition. Similarly, CEX: HPMC

ASD was found to crystallize much faster than the corresponding ternary ASD containing both PVP and HPMC. The poor solid state stabilizing capability of cellulose derivatives can be attributed to weak hydrogen bonding with CEX (HPMC does not have carbonyl group to form hydrogen bonding with CEX at all) and/or their lower effectiveness in increasing the Tg of ASDs.

For ASDs with 60% drug loading stored at RT (~20°C)/94%RH, CEX: PVP/VA was the most stable binary ASD remaining amorphous for up to 150 days and crystallized thereafter. CEX: HPMCAS was stable for up to 115 days and crystallized thereafter. The binary ASDs with HPMC or PVP and the ternary ASDs where PVP was the major polymer was relatively unstable, with some diffraction peaks observed within a month. Similarly, at an 80% drug loading under the same storage condition, the ranking order of solid state stability was CEX:PVP/VA>CEX:HPMCAS>CEX:PVP-K29/32:HPMCAS>CEX:PVP-K29/32 (data not shown).

For pure amorphous CEX, the PXRD pattern after 3 days of storage closely resembled that of the pure crystalline form. This suggests that although the addition of hygroscopic polymers increased the water uptake of the system, the tendency of the drug in ASD matrix to crystallize is reduced relative to pure amorphous form at high storage relative humidity[35]. At 40°C/75%RH where both the temperature and humidity were elevated relative to the ambient conditions, CEX: PVP/VA 8:2 ASD remained amorphous for up to 4 months. CEX:HPMCAS dispersion was stable for up to 45days and crystallization was detected thereafter. Interestingly, at the same drug loading, CEX: PVP-K29/32 and the corresponding ternary ASD outperform CEX: HPMCAS at this storage condition. While the ASD with PVP absorbs more water at all relative humidities than ASD with HPMCAS,

these difference are less pronounced at or below 75%RH. Hence, the drug-polymer interaction strength may become the dominant factor determining the stability of ASDs.

From the results above, it is clear that PVP/VA was very effective in stabilizing the amorphous CEX at both elevated temperature and humidity. We also found that PVP/VA was a good solution crystallization inhibitor for CEX from nucleation inhibition measurements (unpublished data). Therefore, it appears that instead of using 2 different polymers, the same goal might be reached by using a single polymer: PVP/VA, with multiple functional groups on this single polymer. However, the dissolution rate of CEX: PVP/VA ASD was much slower than the CEX: PVP: HPMCAS ternary ASDs[27] with a smaller extent of supersaturation was generated under the same experimental setting (unpublished data). This maybe undesirable for drugs such as CEX which is mainly used for pain management[36]. Similarly, Six et al[25] found that itraconazole was miscible with PVP/VA and the dispersion was stable against crystallization. But the dissolution rate was slow, with only 45% drug release after 3h. In contrast, Eudragit E100 was miscible with itraconazole only up to 13% w/w drug loading and failed to provide adequate physical stabilization. However, the release of the drug was relatively fast. The ternary ASD of itraconazole exhibited both fast dissolution and improved physical stability relative to the corresponding binary ASDs

## 3.6    Discussion

Crystallization from the amorphous state is complicated. Quantitative prediction based on a single variable maybe inappropriate in many cases.  Instead, a qualitative appreciation of different factors may be useful, as reviewed by Bhugra et al[37]. There are two types of

mobility associated with amorphous material. The α mobility is considered as global mobility associated with the glass transition temperature, and is often assessed by measuring the structural relaxation time[38]. Above Tg, the viscosity is relatively low, and hence the slow diffusion of molecules over a large length scale is less restricted. Therefore, the difference between the storage temperature and the glass transition temperature is often used as a crude approximation of the stability of amorphous materials. At temperature below Tg, the material become highly viscous and hence the translational (or diffusive) and rotational motions (α mobility) are substantially suppressed. In such case, higher frequency local motions (β mobility) may become critical in determining crystallization rate[38]. Yoshioka et al[39, 40] found that the dry amorphous indomethacin (Tg=50 ℃) crystallized completely within 3 weeks at 30 ℃ and the rate greatly increased when the temperature was increased, presumably due to the increase in molecular mobility. In contrast, when indomethacin was dispersed with a low level of PVP (5%) and stored at up to 50 ℃, an induction period of more than 20 days was required for crystallization to initiate. Hancock and Zografi[41] found that the temperature dependence of molecular motions below Tg differed considerably than that above Tg, and was rapidly changing. The authors suggested that amorphous materials should be stored at least 50°C below the glass transition temperature so as to minimize the risk of crystallization over shelf life. In this study, we found that PVP and PVP/VA are more effective in raising Tg of ASDs than cellulosic derivatives, which contribute to the difference in the crystallization kinetics. This is perhaps, at least intuitively, consistent with the existence of strong hydrogen bonding between CEX and PVP or PVP/VA which may restrict the diffusive motion and hence self-association of the drug molecules in the dispersions. Similarly, Miyazaki et al[5] found that

PAA provided better physical stabilization for amorphous acetaminophen than PVP by forming a stronger hydrogen bonding interaction with the drug and a larger decrease in molecular mobility as indicated by the longer enthalpy relaxation time, despite a similar Tg value. The hydrogen bonding between CEX and HPMCAS is very weak, and the increase in Tg is minimal at high drug loading. However, a dramatic decrease in crystal growth rate and much slower crystallization kinetics of ASDs relative to pure amorphous CEX were observed even at very low polymer loading. HPMC does not have a carbonyl to form hydrogen bonding with CEX and the difference in Tg between CEX: HPMC and CEX: HPMCAS is small. Yet the crystallization kinetics of CEX: HPMC ASD is comparable to that of CEX: HPMCAS ASD. Therefore, the improved stability of CEX when molecularly mixed with a cellulosic derivative cannot be solely attributed to these two factors. Bhugra suggested[37] that polymeric additives impact drug diffusion by at least three mechanisms: (1) polymers may act as a diluent to reduce the chemical potential of the drug. In this case, a proportional decrease in crystallization rate is envisaged. (2) Through drug-polymer interactions to restrict the local mobility[42]. (3) Impede the drug transport to the growing crystals by accumulating on the amorphous-crystal interface. This mechanism may be critical at high drug loadings[22] and help explain our results.

Crystallization is a sequential process involving both nucleation and growth. The temperature range where nucleation is favored is expected to be lower than where crystal growth is favored[43, 44]. Significant crystallization occurs where the nucleation zone and growth zone overlap[20, 37]. It has been reported in several studies[18, 20] that slower crystal growth rate is often associated with stronger hydrogen bonding. While it is anticipated that a reduced crystal growth rate could translate to a slower overall crystallization kinetics of

bulk ASDs, no direct evidence of such correlation, to the best of our knowledge, has been reported. For acetaminophen[20], the most effective polymer in reducing the nucleation rate, HPMCAS, was found to be the worst growth inhibitor. Conversely, one of the best crystal growth inhibitor, PAA, significantly increased the nucleation rate. This demonstrates that polymers may stabilize amorphous drugs by selectively inhibiting nucleation or growth or both. In that study, the authors also highlighted a good correlation between hydrogen bonding strength with crystal growth but a lack of correlation between this factor and nucleation rate. In the current study, the temperature dependence of the nucleation rate is not investigated. Yet, a good correlation between the growth rate and crystallization kinetics of the bulk ASDs has been established, at least qualitatively. This indicates either that polymers effective in inhibiting crystal growth of CEX are also effective in inhibiting nucleation or that inhibiting nucleation is less important than inhibiting crystal growth in retarding overall crystallization.

In a study by Curatolo et al[45], 41 small and polymeric molecules were tested for their effectiveness in initiation and maintaining supersaturation for each of 9 structurally diverse low solubility drugs, HPMCAS was found to be the most effective precipitation inhibitor. Consequently, spray dried dispersions (SDDs) prepared with HPMCAS were consistently superior to SDDs formulated with other polymers in both achieving and maintaining supersaturation during in vitro dissolution studies. Warren et al[46] tested the precipitation inhibition behavior of 53 polymeric materials for supersaturated solution of danazol, the majority of superior precipitation inhibitor were cellulose based. While the mechanisms of superiority of cellulosic polymers as solution state inhibitor are not clearly understood, these studies nevertheless indicate the necessity of incorporating them into ASD

formulations to ensure adequate dissolution performance for many poorly water soluble drugs[26]. The utility of PVP as a good hydrogen bond donor to stabilize ASDs has been reported in numerous studies (add ref). Wegiel et al[47] found that due to a stronger hydrogen bonding interaction, a relatively small amount of PVP is required to successfully produce amorphous solid dispersion of resveratrol as compared to HPMC, HPMCAS, carboxymethyl cellulose acetate butyrate (CMCAB), and PAA. At the same drug loading, PVP dispersions were more stable than dispersions formulated with those polymers in the absence of moisture. In that study, it was also revealed that inter-species ionic interactions between Eudragit® E100 provided even better physical stabilization. Nevertheless, such type of interaction is less frequently observed in the literatures and is relatively hard to be predicted *a priori*. From the discussion above, it is speculated that using the PVP and HPMCAS polymer blend may potentially have a broad applicability as a strategy for ASD formulation, and the need for further investigation is clearly warranted. It is anticipated that such polymer pair could be used to produce high drug loading ASDs of drugs with low Tg and difficult to be rendered amorphous with satisfactory solid state stability as well as dissolution performance. Last but not least, PVP is found to be miscible with HPMCAS at all proportions, and the addition of HPMCAS will not impair the miscibility of PVP with CEX even at high HPMCAS loading. This observation maybe of practical significance in scenarios where the composition of ASDs needs to be balanced for optimum outcome.

To understand the impact of water on the solid state stability of ASDs, the hydrophobicity/hydrophilicity of the individual component, the strength of drug-polymer interaction and water uptake by ASDs need to be taken into account. As compared to CEX: PVP-K29/32, CEX: PVP/VA absorbs much less water and hence is more resistant to

amorphous-amorphous phase separation and plasticization induced crystallization during storage at high relative humidity. Similarly, Rumondor et al[15] found that for both felodipine and quinidine, the strength of hydrogen bonding the drugs with PVP/VA was comparable to that with PVP, but the PVP/VA containing mixture experienced smaller extent of moisture induced phase separation than PVP containing mixture, attributed to a reduced amount of water uptake. In contrast, moisture induced drug-polymer demixing was absent in both indomethacin:PVP[48] and indomethacin:PVP/VA systems. Such difference was attributed to a stronger hydrogen bonding between indomethacin's COOH and C=O of PVP than that between OH of felodipine or NH of quinidine and C=O of PVP. Interestingly, while HPMCAS dispersion of CEX absorbs less water than PVP/VA dispersion, CEX: PVP/VA still outperforms CEX: HPMCAS at 94%RH, most likely due to the stronger drug-polymer interaction strength as evidenced by both the IR spectra and $T_g$ values. By the same argument, CEX: PVP/VA was more stable than CEX: HPMC despite a similar moisture sorption profile. Finally, while replacing a small amount of more hygroscopic PVP with a less hygroscopic cellulose derivative did resulted in reduced water uptake in ternary ASDs relative to the corresponding binary ASD with PVP, this reduction was not large enough to result in a discernable difference in the solid state stability.

## 3.7    Conclusion

Polymers that can form stronger hydrogen bonding and more effective in reducing molecular mobility of CEX are found to be more effective in inhibiting crystallization in the absence of moisture. The measured crystal growth rate can be used to predict the relative crystallization kinetics of bulk ASDs formulated with different polymers. This

might potentially reduce the time and cost associated with long term physical stability studies. This study also demonstrated proof of concept for the approach of using miscible binary polymers to maximize crystallization inhibition in both the solid and solution phases and provided greater confidence in the use of solid dispersion strategies. When subject to high relative humidity, ASDs of CEX with stronger drug-polymer interaction and lower hygroscopicity will be less susceptible to moisture induced phase separation and crystallization.

(A)     (B)     (C)

(D)     (E)

R = H, CH$_3$, CH$_2$CH(OH)CH$_3$,
COCH$_3$, COCH$_2$CH$_2$COOH,
CH$_2$CH(OCOCH$_3$)CH$_3$,
CH$_2$CH(OCOCH$_2$CH$_2$COOH)CH$_3$

R = –H, –CH$_3$, –CH$_2$–CHOH–CH$_3$
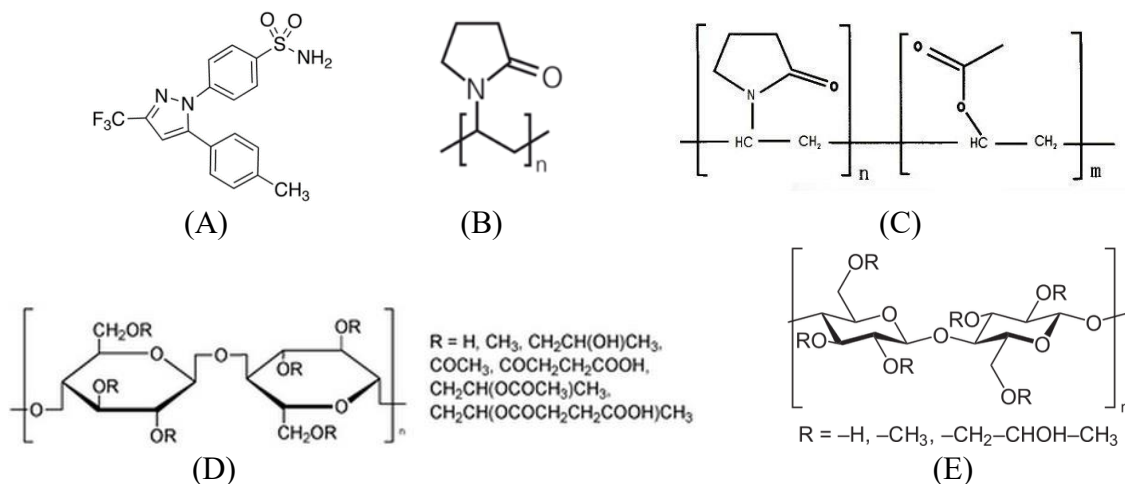
Figure 3-1. Chemical structures of CEX (A), PVP (B), PVP/VA (C), HPMCAS (D), and HPMC (E).
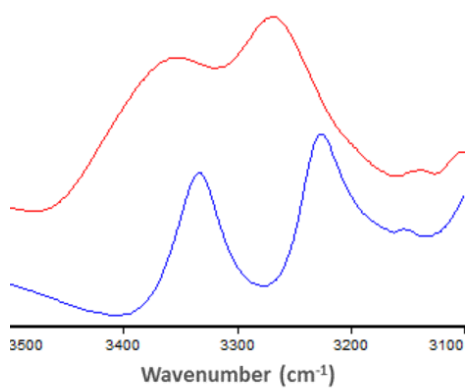


Wavenumber (cm$^{-1}$)

Figure 3-2 FT-IR spectra of pure amorphous CEX (red) and pure crystalline CEX (blue) showing the wavenumber range from 3100cm$^{-1}$ to 3500cm$^{-1}$.
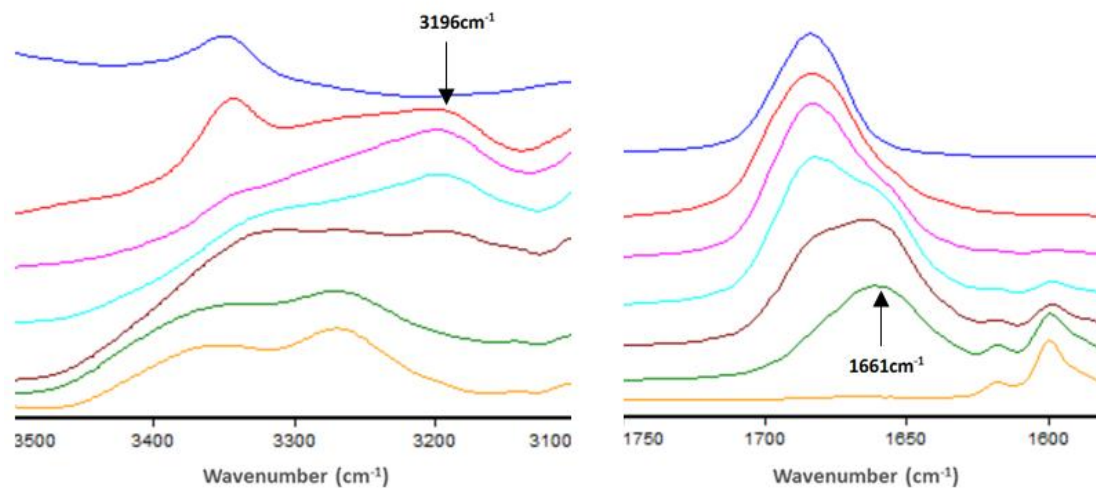
Figure 3-3 FT-IR spectra of CEX:PVP-K29/32 spin coated films (From top to bottom: pure PVP (blue), drug:polymer ratios of 1:9 (red), 3:7 (pink), 5:5 (cyan), 7:3 (brown), 9:1 (green), and pure amorphous CEX (orange), respectively) showing the wavenumber range from $3100cm^{-1}$ to $3500cm^{-1}$ and from $1550cm^{-1}$ to $1750cm^{-1}$. The arrows show the emergence of peaks indicating hydrogen bonding between the celecoxib $NH_2$ group and the PVP carbonyl group.



Figure 3-4 FT-IR spectra of CEX:HPMCAS spin coated films (From top to bottom: pure HPMCAS (blue), 1:9 (red), 3:7 (pink), 5:5 (cyan), 7:3 (brown), 9:1 (green), and pure amorphous CEX (orange), respectively) showing the wavenumber range from $3100cm^{-1}$ to $3500cm^{-1}$ and from $1550cm^{-1}$ to $1850cm^{-1}$

Figure 3-5 FT-IR spectra of PVP: HPMCAS spin coated films showing the wavenumber range from 1600cm$^{-1}$ to 1800cm$^{-1}$
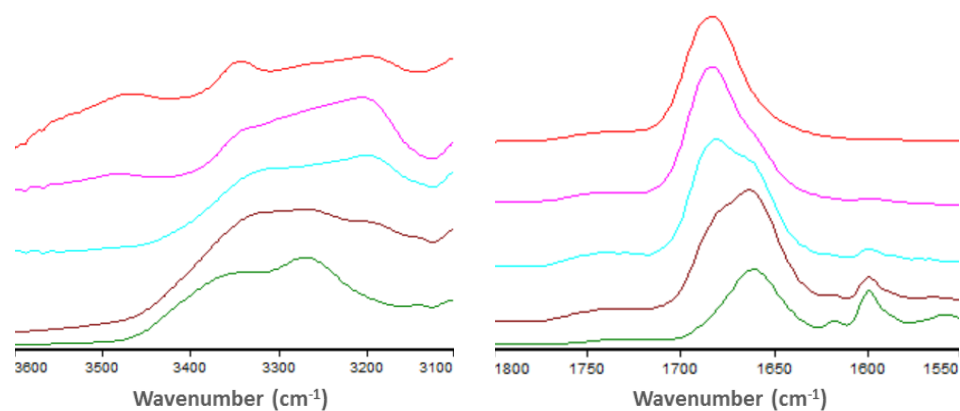


Figure 3-6 FT-IR spectra of CEX: PVP-K29/32: HPMCAS spin coated films (From top to bottom: 1:8:1 (red), 3:6:1 (pink), 5:4:1 (cyan), 70:25:5 (brown), 90:8:2 (green), respectively) showing the wavenumber range from 3100cm$^{-1}$ to 3600cm$^{-1}$ and from 1550cm$^{-1}$ to 1800cm$^{-1}$
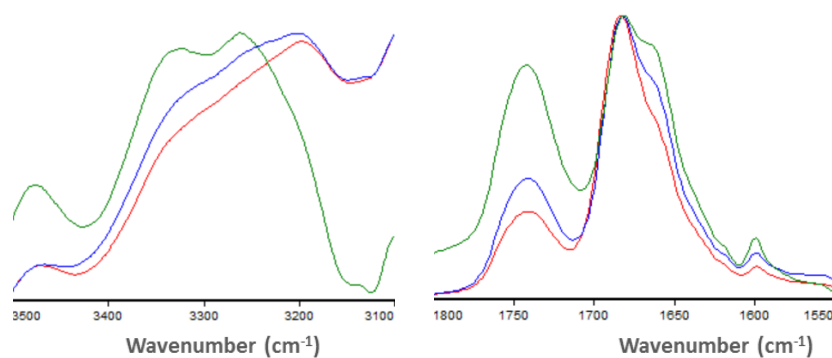
Figure 3-7 FT-IR spectra of CEX: PVP-K29/32: HPMCAS spin coated films: 3:4:3 (red), 35:30:35 (blue), and 4:2:4 (green) showing the wavenumber range from 3100cm$^{-1}$ to 3500cm$^{-1}$ and from 1550cm$^{-1}$ to 1800cm$^{-1}$.
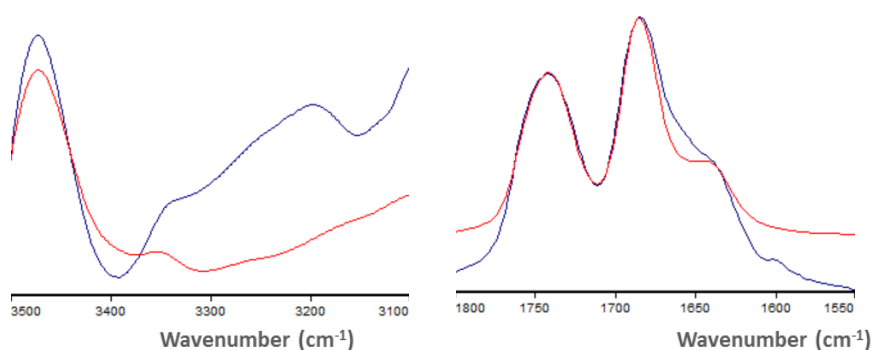


Figure 3-8 FT-IR spectra of CEX: PVP-K29/32: HPMCAS 1:3:6 (blue) and PVP: HPMCAS 3:7 (red) spin coated films showing the wavenumber range from 3100cm$^{-1}$ to 3500cm$^{-1}$ and from 1550cm$^{-1}$ to 1800cm$^{-1}$.
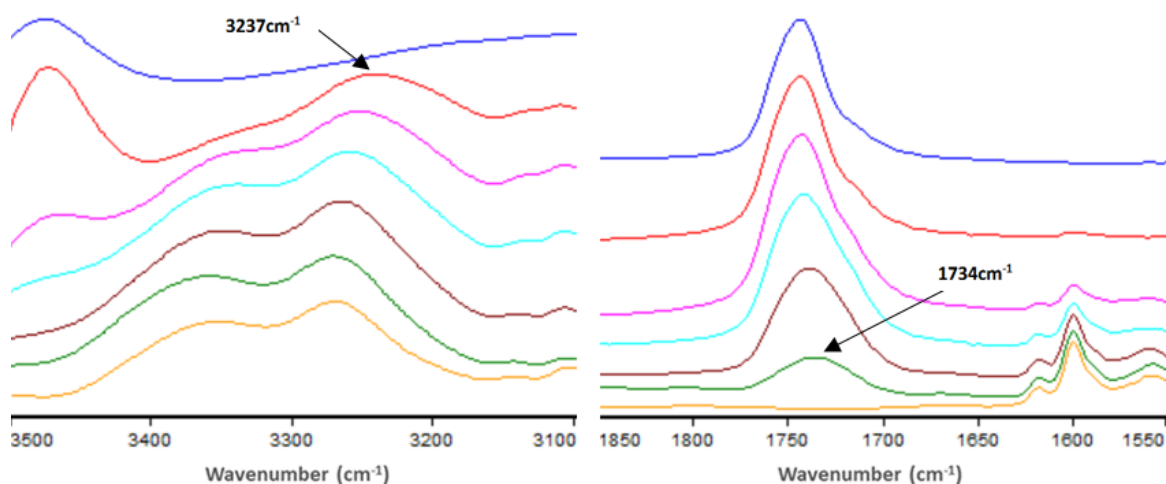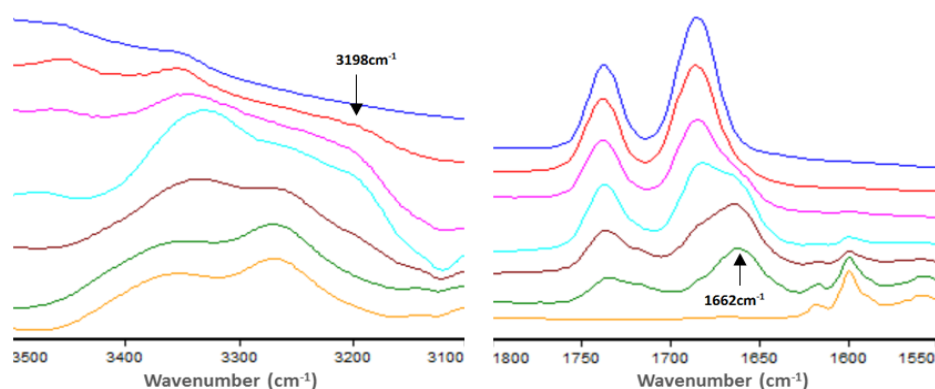


Figure 3-9 FT-IR spectra of CEX: PVP/VA spin coated films (From top to bottom: pure PVP/VA (blue), 1:9 (red), 3:7 (magenta), 5:5 (cyan), 7:3 (brown), 9:1 (green), and pure amorphous CEX (orange), respectively) showing the wavenumber range from 3100cm$^{-1}$ to 3500cm$^{-1}$ and from 1550cm$^{-1}$ to 1800cm$^{-1}$.
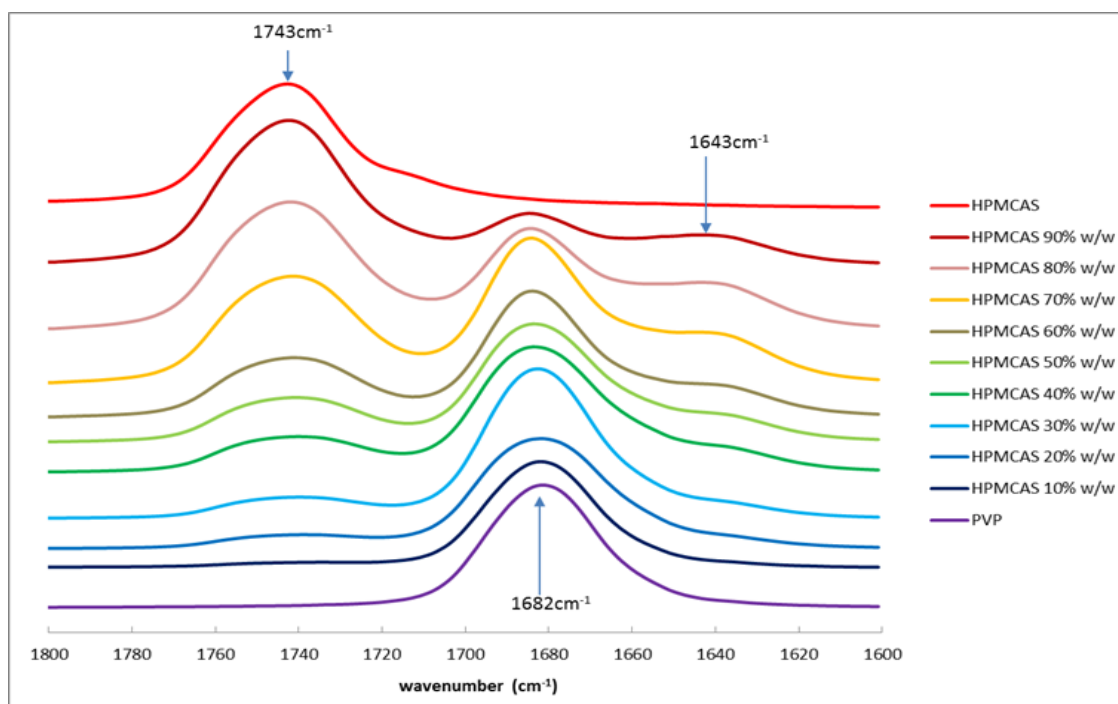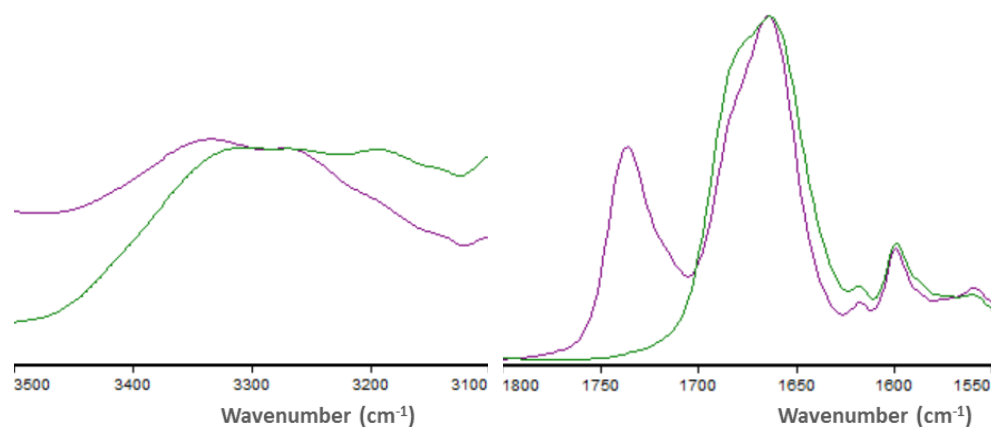
Figure 3-10 FT-IR spectra of CEX: PVP/VA 7:3 (purple) and CEX: PVP-K29/32 7:3 (green) spin coated films showing the wavenumber range from 3100cm$^{-1}$ to 3500cm$^{-1}$ and from 1550cm$^{-1}$ to 1800cm$^{-1}$.
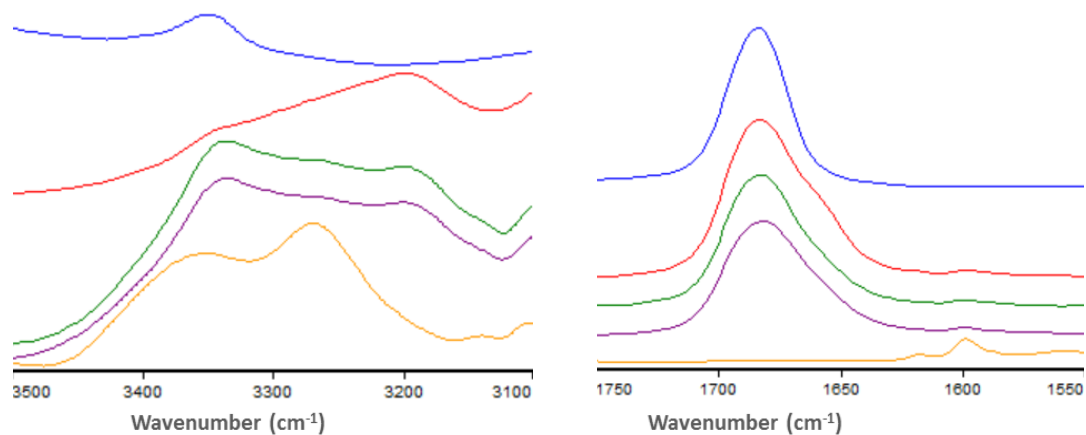


Figure 3-11  FT-IR spectra of pure PVP(blue), CEX: PVP 3:7 unexposed (red), 1day(green), 18days(purple), and amorphous CEX(orange) spin coated films showing the wavenumber range from 3100cm$^{-1}$ to 3500cm$^{-1}$ and from 1550cm$^{-1}$ to 1800cm$^{-1}$.
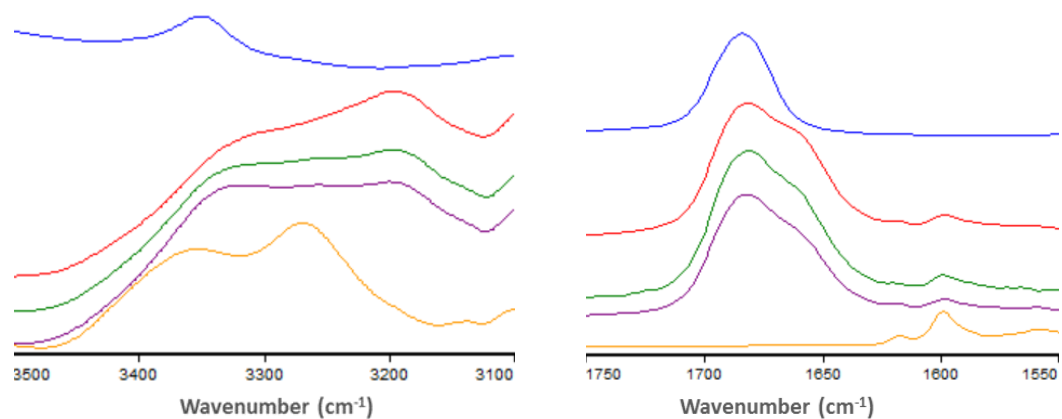
Figure 3-12 FT-IR spectra of PVP(blue), CEX: PVP 5:5 unexposed (red), 1day(green), 18days(purple), and amorphous CEX(orange) spin coated films showing the wavenumber range from $3100cm^{-1}$ to $3500cm^{-1}$ and from $1550cm^{-1}$ to $1800cm^{-1}$.
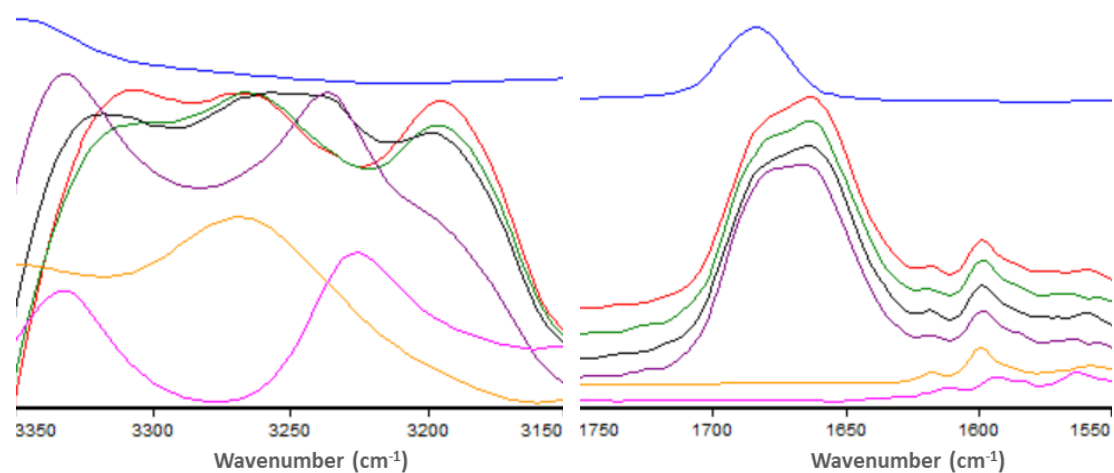


Figure 3-13 FT-IR spectra of PVP(blue), CEX: PVP 7:3 unexposed (red), 1day(green), 4days (black), 18days(purple), amorphous CEX(orange), and crystalline CEX (pink) spin coated films showing the wavenumber range from $3150cm^{-1}$ to $3350cm^{-1}$ and from $1550cm^{-1}$ to $1800cm^{-1}$.
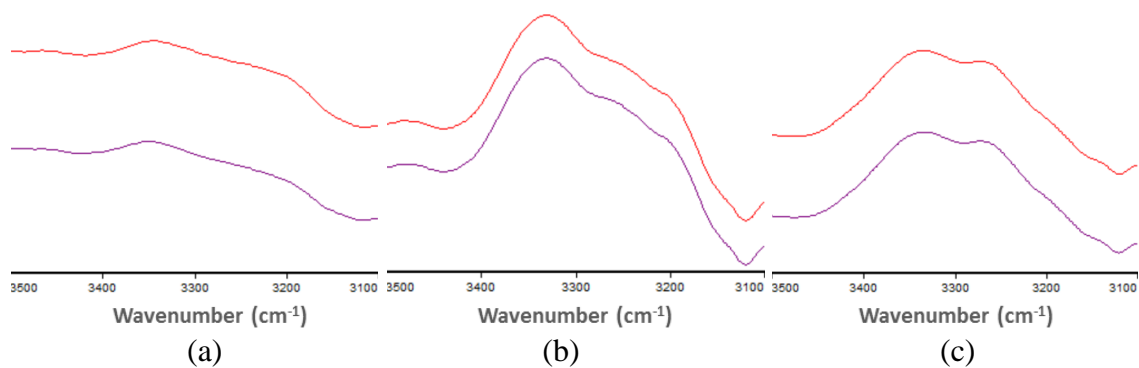
Figure 3-14 FT-IR spectra of CEX: PVP/VA 3:7(a) 5:5 (b) and 7:3 (c) spin coated films before (red) and after 18days (purple) of storage at 94%RH/RT showing the wavenumber range from 3100cm$^{-1}$ to 3500cm$^{-1}$
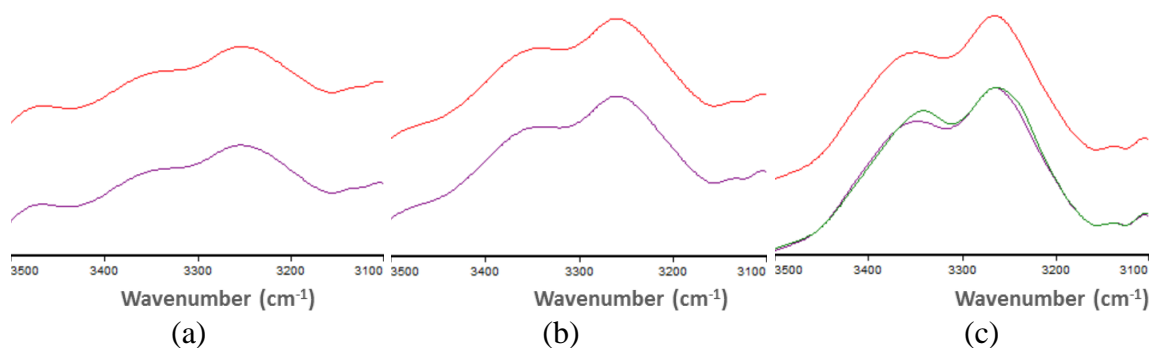


Figure 3-15 FT-IR spectra of CEX: HPMCAS 3:7(a) 5:5 (b) and 7:3 (c) spin coated films before (red) and after 18days (purple) and 2 months (green) of storage at 94%RH/RT showing the wavenumber range from 3100cm$^{-1}$ to 3500cm$^{-1}$
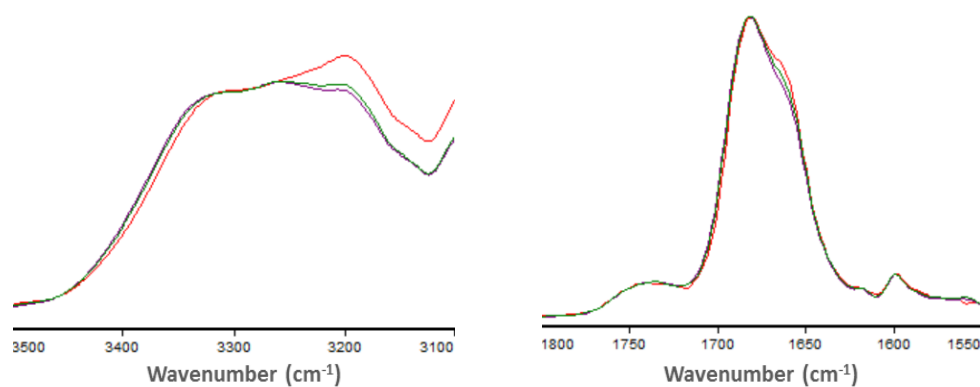


Figure 3-16 CEX: PVP-K29/32: HPMCAS 5:4:1 before (red) and after 1days (green) and 18days (purple) of storage at 94%RH/RT showing the wavenumber range from 3100cm$^{-1}$ to 3500cm$^{-1}$ and from 1550cm$^{-1}$ to 1800cm$^{-1}$
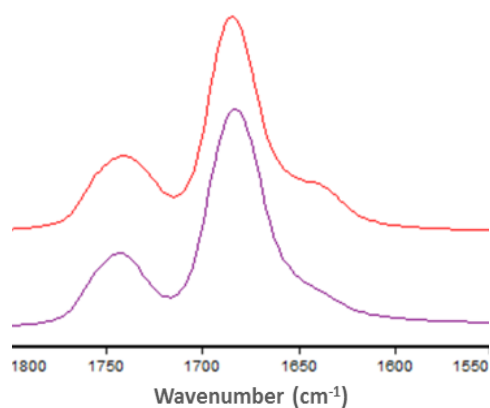
Figure 3-17 PVP: HPMCAS 1:1 spincoated films before (red) and after 1 day storage (purple) at 94%RH/RT showing the wavenumber range from 1550cm$^{-1}$ to 1800cm$^{-1}$
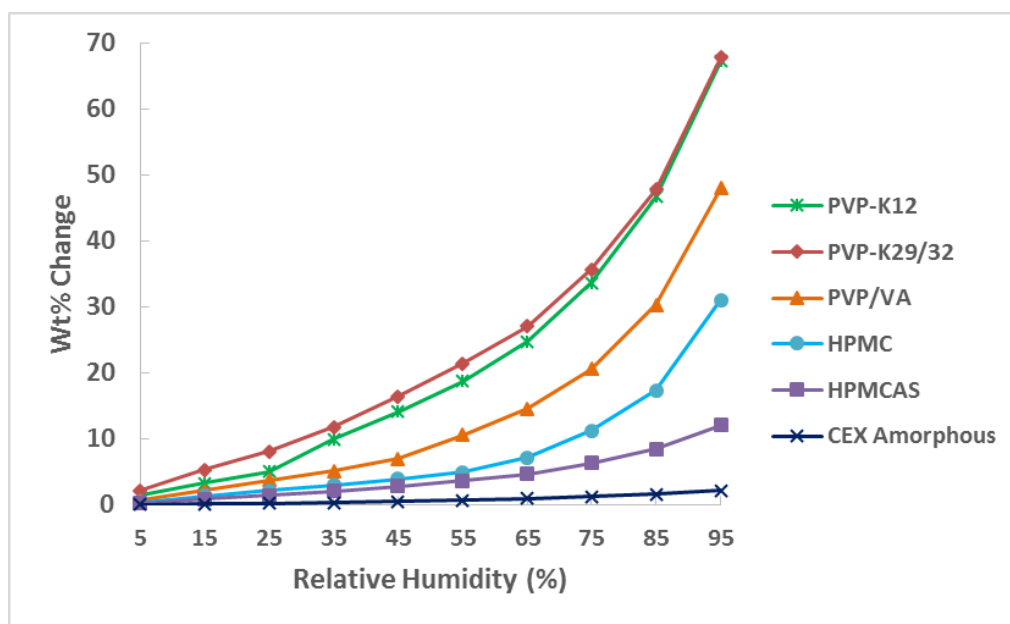


Figure 3-18 Moisture sorption isotherms of pure amorphous CEX and polymers
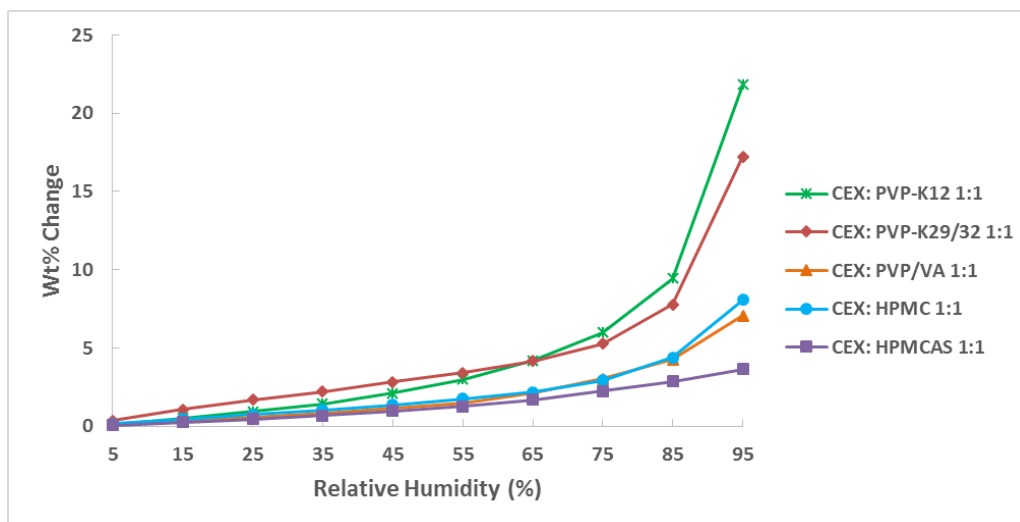
Figure 3-19 Moisture sorption isotherms of binary ASDs of CEX with different polymers
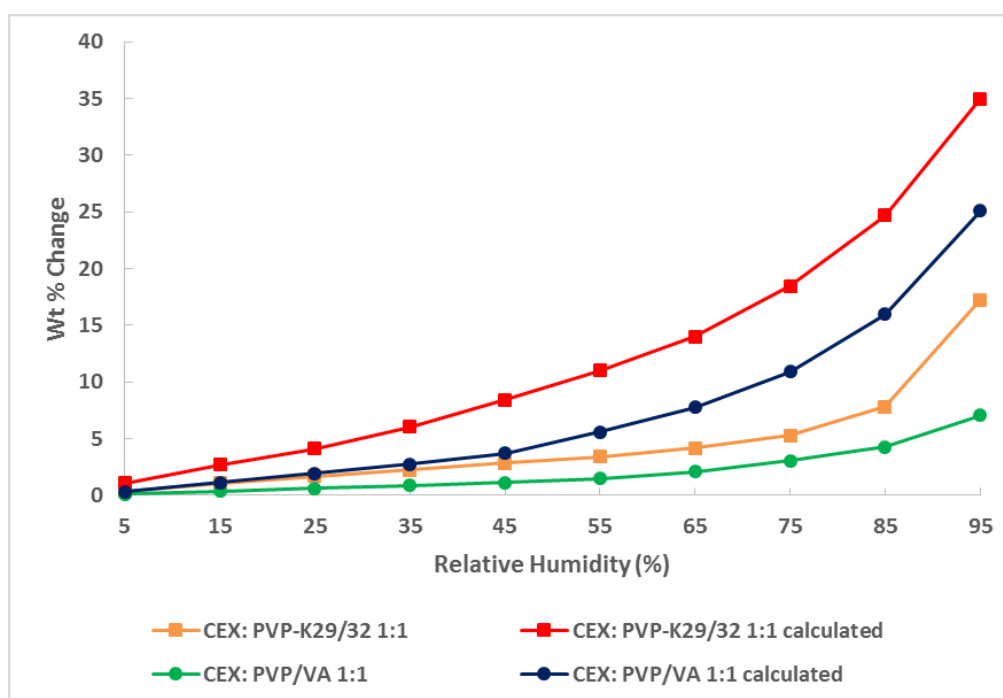


Figure 3-20 Experimental and calculated moisture sorption isotherms of binary ASDs of CEX with PVP-K29/32 or PVP/VA
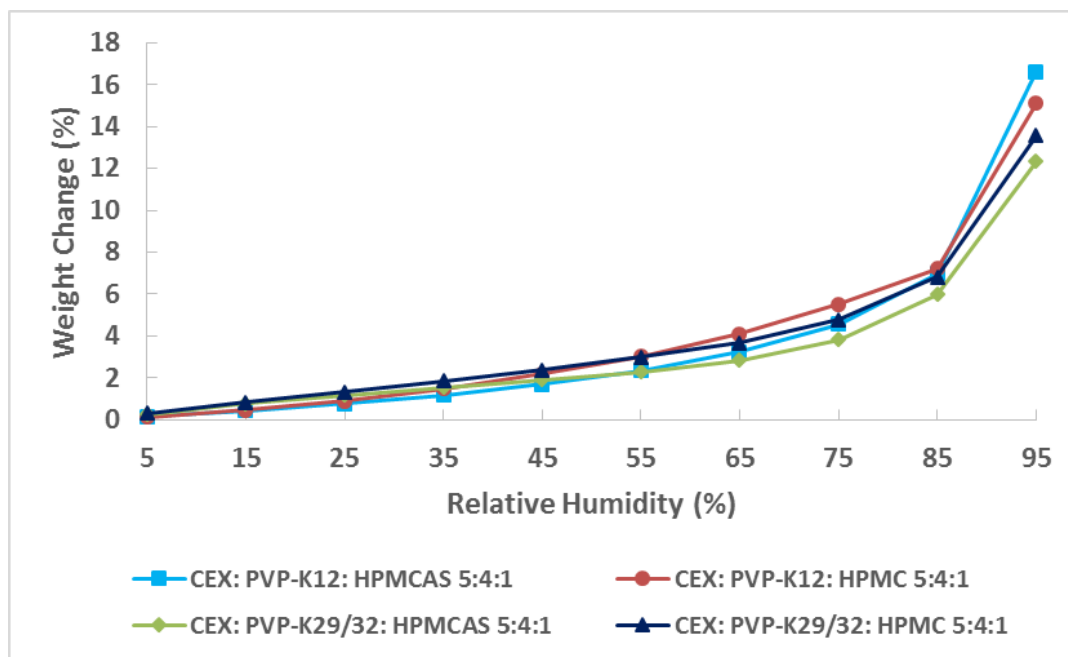
Figure 3-21 Moisture sorption isotherms of the ternary ASDs
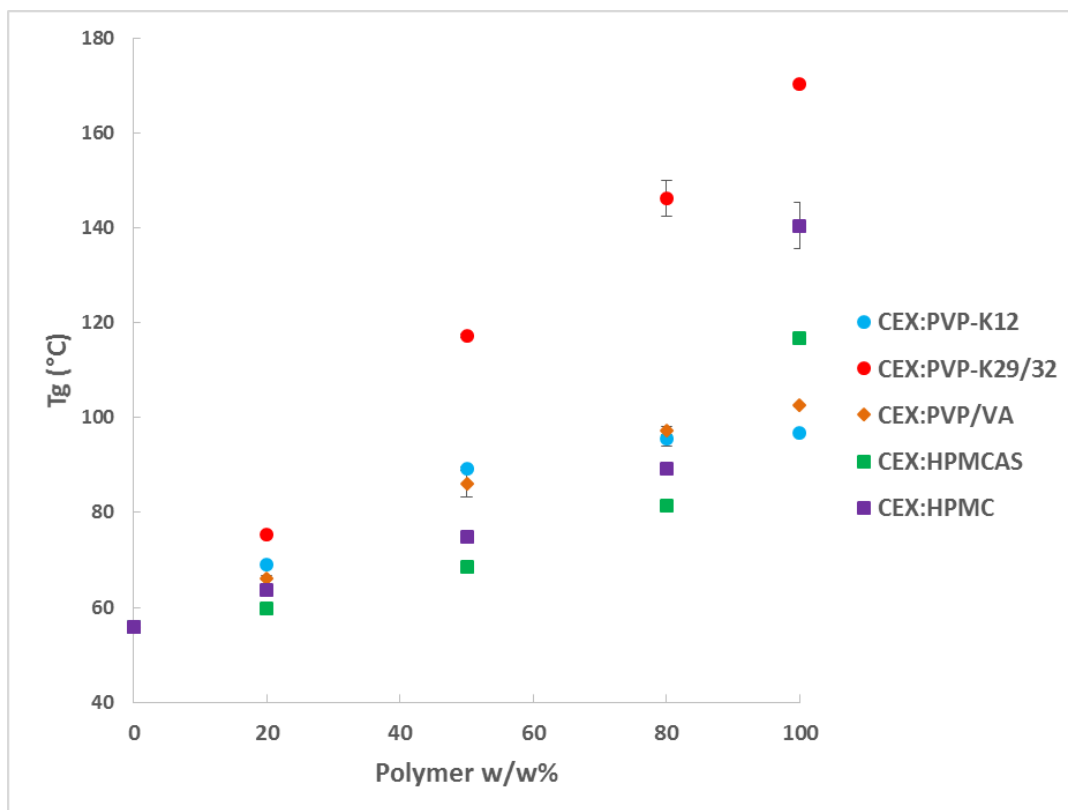


Figure 3-22 Tg values of ASDs of CEX with a single polymer
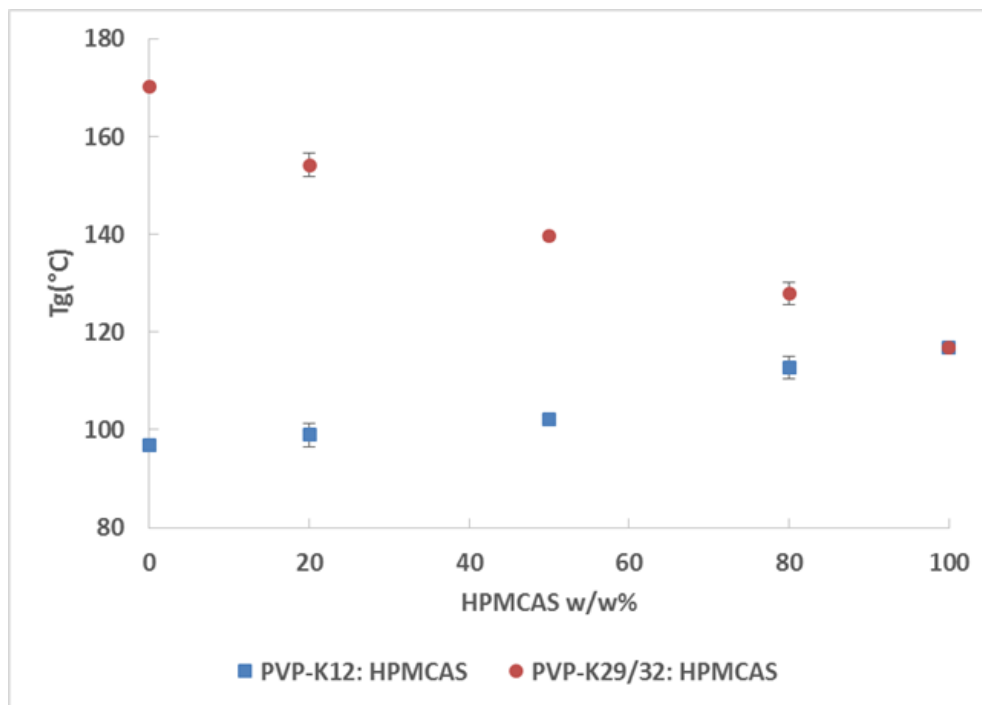
Figure 3-23 Tg values of PVP and HPMCAS blends
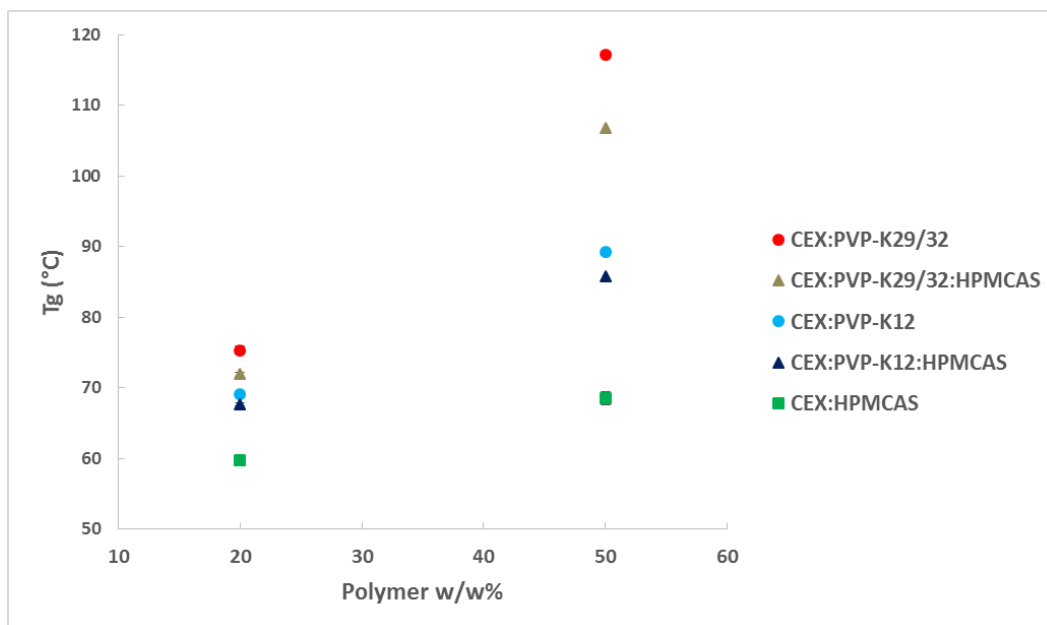


Figure 3-24 Tg values of CEX: PVP (8:2 and 5:5), CEX: HPMCAS (8:2 and 5:5) and CEX:PVP:HPMCAS (8:1.6:0.4 and 5:4:1) ASDs
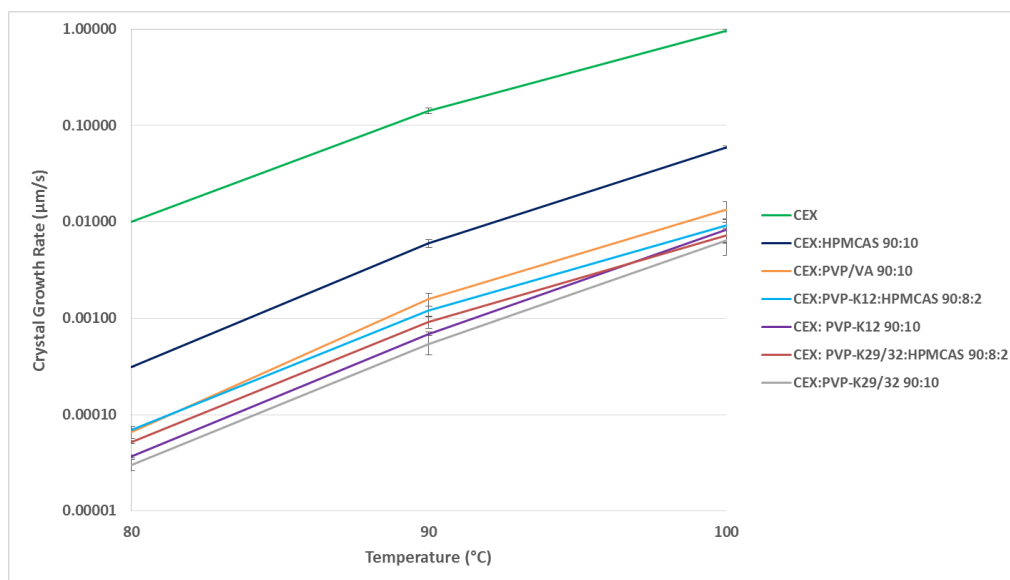
Figure 3-25. Crystal growth rate of CEX in the absence and presence of polymers.
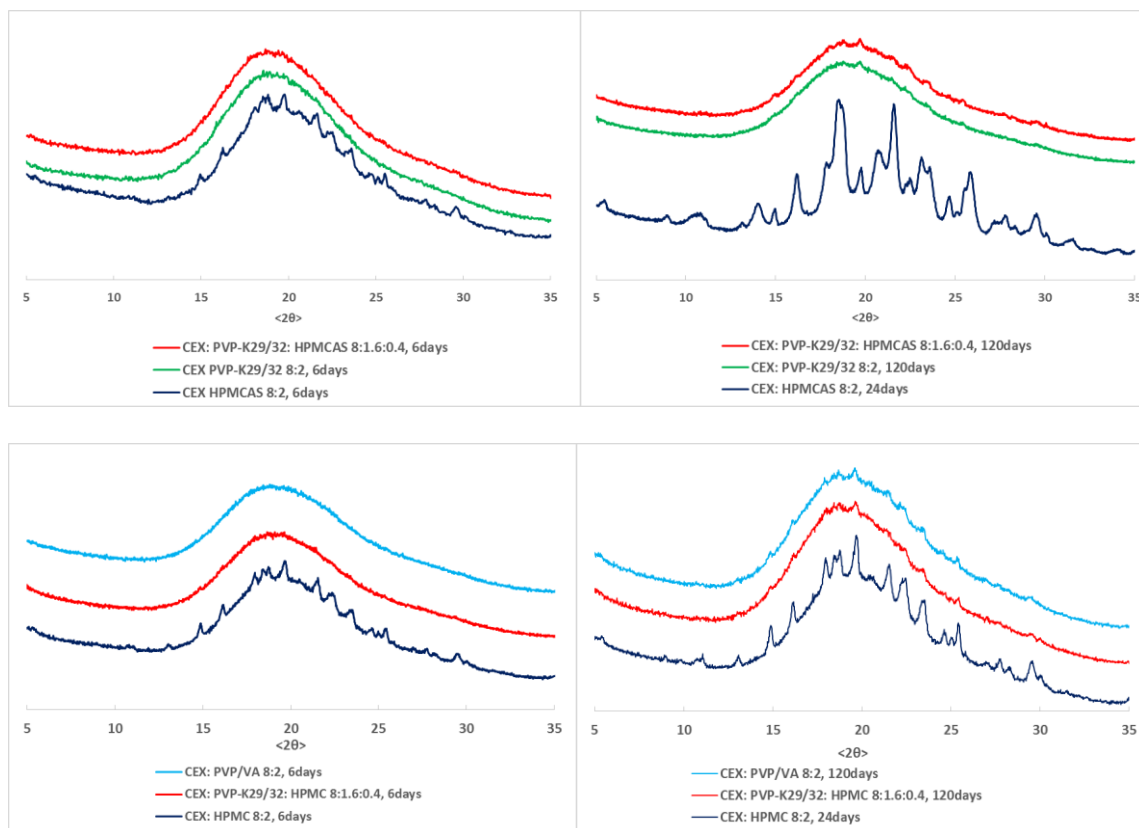


Figure 3-26. PXRD of ASDs stored at 80 ℃/0%RH.
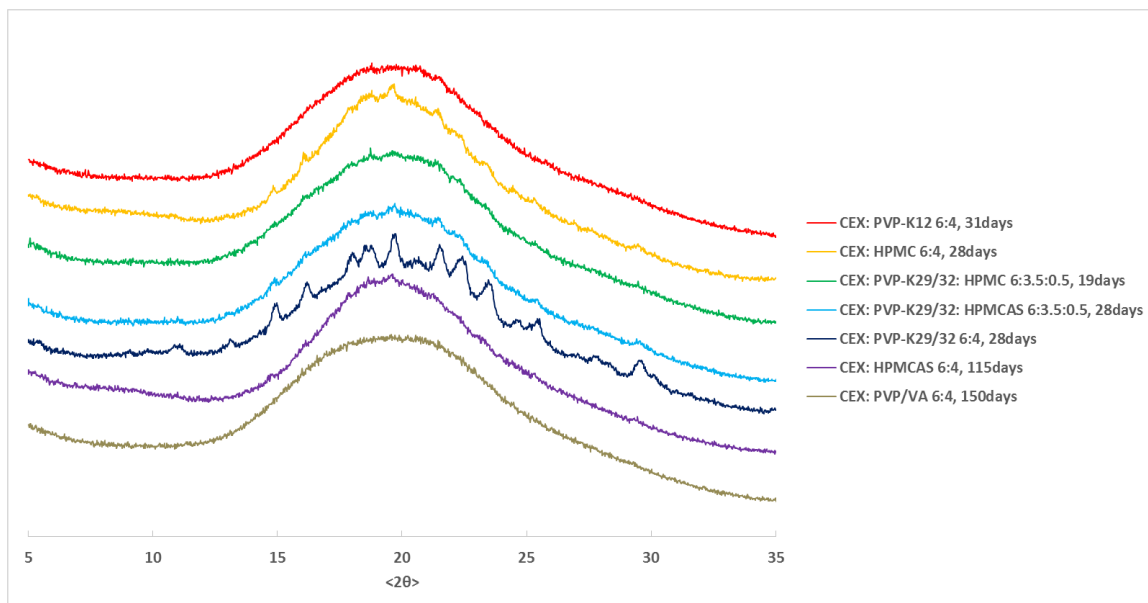
Figure 3-27 PXRD of ASDs stored at RT/94%RH
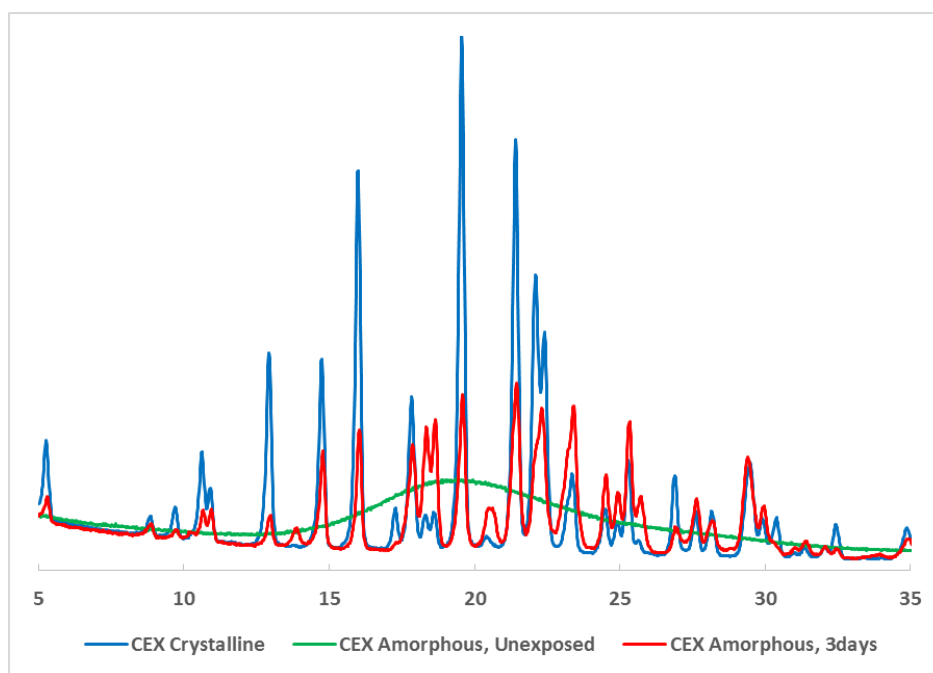


Figure 3-28 PXRD of pure crystalline CEX, and pure amorphous CEX before and after storage at RT/94%RH
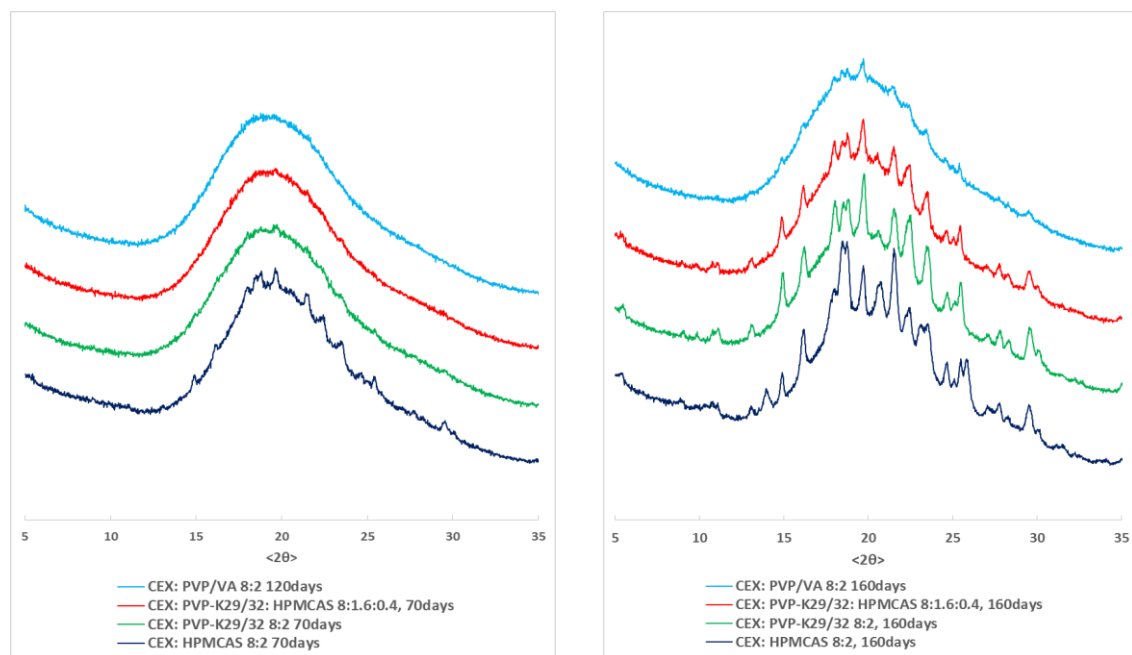
Figure 3-29 PXRD of ASDs stored at 40°C /75%RH

## 3.8    References

1.       Van den Mooter, G.; Wuyts, M.; Blaton, N.; Busson, R.; Grobet, P.; Augustijns, P.; Kinget, R.  Physical stabilisation of amorphous ketoconazole in solid dispersions with polyvinylpyrrolidone K25. *Eur J Pharm Sci* **2001,** *12*, (3), 261-269.

2.       Khougaz, K.; Clas, S.-D.  Crystallization inhibition in solid dispersions of MK-0591 and poly(vinylpyrrolidone) polymers. *Journal of Pharmaceutical Sciences* **2000,** *89*, (10), 1325-1334.

3.       Matsumoto, T.; Zografi, G.  Physical properties of solid molecular dispersions of indomethacin with poly(vinylpyrrolidone) and poly(vinylpyrrolidone-co-vinylacetate) in relation to indomethacin crystallization. *Pharm Res* **1999,** *16*, (11), 1722-1728.

4.       Marsac, P.; Konno, H.; Taylor, L.  A Comparison of the Physical Stability of Amorphous Felodipine and Nifedipine Systems. *Pharm Res* **2006,** *23*, (10), 2306-2316.

5.       Miyazaki, T.; Yoshioka, S.; Aso, Y.; Kojima, S.  Ability of polyvinylpyrrolidone and polyacrylic acid to inhibit the crystallization of amorphous acetaminophen. *Journal of pharmaceutical sciences* **2004,** *93*, (11), 2710-2717.

6.       Guzmán, M. L.; Manzo, R. H.; Olivera, M. E.  Eudragit E100 as a Drug Carrier: The Remarkable Affinity of Phosphate Ester for Dimethylamine. *Mol Pharmaceut* **2012,** *9*, (9), 2424-2433.

7.       Quinteros, D. A.; Rigo, V. R.; Kairuz, A. F. J.; Olivera, M. E.; Manzo, R. H.; Allemandi, D. A.  Interaction between a cationic polymethacrylate (Eudragit E100) and anionic drugs. *Eur J Pharm Sci* **2008,** *33*, (1), 72-79.

8.       Wegiel, L. A.; Mauer, L. J.; Edgar, K. J.; Taylor, L. S.  Mid-infrared spectroscopy as a polymer selection tool for formulating amorphous solid dispersions. *Journal of Pharmacy and Pharmacology* **2014,** *66*, (2), 244-255.

9.       Van Eerdenbrugh, B.; Taylor, L. S.  An ab initio polymer selection methodology to prevent crystallization in amorphous solid dispersions by application of crystal engineering principles. *Crystengcomm* **2011,** *13*, (20), 6171-6178.

10.      Zografi, G.  States of water associated with solids. *Drug Development and Industrial Pharmacy* **1988,** *14*, (14), 1905-1926.

11.      Katkov, I. I.; Levine, F.  Prediction of the glass transition temperature of water solutions: comparison of different models. *Cryobiology* **2004,** *49*, (1), 62-82.

12.      Hancock, B. C.; Zografi, G.  The relationship between the glass transition temperature and the water content of amorphous pharmaceutical solids. *Pharm Res-Dordr* **1994,** *11*, (4), 471-477.

13.      Andronis, V.; Yoshioka, M.; Zografi, G.  Effects of sorbed water on the crystallization of indomethacin from the amorphous state. *Journal of pharmaceutical sciences* **1997,** *86*, (3), 346-351.

14.      Marsac, P. J.; Rumondor, A. C.; Nivens, D. E.; Kestur, U. S.; Stanciu, L.; Taylor, L. S.  Effect of temperature and moisture on the miscibility of amorphous dispersions of felodipine and poly (vinyl pyrrolidone). *Journal of pharmaceutical sciences* **2010,** *99*, (1), 169-185.

15.      Rumondor, A. C. F.; Taylor, L. S.  Effect of Polymer Hygroscopicity on the Phase Behavior of Amorphous Solid Dispersions in the Presence of Moisture. *Mol Pharmaceut* **2010,** *7*, (2), 477-490.

16.     Purohit, H. S.; Taylor, L. S.  Phase Separation Kinetics in Amorphous Solid Dispersions Upon Exposure to Water. *Mol Pharmaceut* **2015,** *12*, (5), 1623-1635.

17.     Williams, H. D.; Trevaskis, N. L.; Charman, S. A.; Shanker, R. M.; Charman, W. N.; Pouton, C. W.; Porter, C. J. H.  Strategies to Address Low Drug Solubility in Discovery and Development. *Pharmacological Reviews* **2013,** *65*, (1), 315-499.

18.     Kestur, U. S.; Taylor, L. S.  Role of polymer chemistry in influencing crystal growth rates from amorphous felodipine. *Crystengcomm* **2010,** *12*, (8), 2390-2397.

19.     Konno, H.; Handa, T.; Alonzo, D. E.; Taylor, L. S.  Effect of polymer type on the dissolution profile of amorphous solid dispersions containing felodipine. *Eur J Pharm Biopharm* **2008,** *70*, (2), 493-499.

20.     Trasi, N. S.; Taylor, L. S.  Effect of polymers on nucleation and crystal growth of amorphous acetaminophen. *Crystengcomm* **2012,** *14*, (16), 5188-5197.

21.     Trasi, N. S.; Oucherif, K. A.; Litster, J. D.; Taylor, L. S.  Evaluating the influence of polymers on nucleation and growth in supersaturated solutions of acetaminophen. *Crystengcomm* **2015,** *17*, (6), 1242-1248.

22.     Konno, H.; Taylor, L. S.  Influence of different polymers on the crystallization tendency of molecularly dispersed amorphous felodipine. *J Pharm Sci-Us* **2006,** *95*, (12), 2692-2705.

23.     Rumondor, A. C. F.; Stanford, L. A.; Taylor, L. S.  Effects of Polymer Type and Storage Relative Humidity on the Kinetics of Felodipine Crystallization from Amorphous Solid Dispersions. *Pharm Res-Dordr* **2009,** *26*, (12), 2599-2606.

24.     Sakurai, A.; Sakai, T.; Sako, K.; Maitani, Y.  Polymer Combination Increased Both Physical Stability and Oral Absorption of Solid Dispersions Containing a Low Glass Transition Temperature Drug: Physicochemical Characterization and <i>in Vivo</i> Study. *Chemical and Pharmaceutical Bulletin* **2012,** *60*, (4), 459-464.

25.     Six, K.; Verreck, G.; Peeters, J.; Brewster, M.; Mooter, G. V. d.  Increased physical stability and improved dissolution properties of itraconazole, a class II drug, by solid dispersions that combine fast- and slow-dissolving polymers. *Journal of Pharmaceutical Sciences* **2004,** *93*, (1), 124-131.

26.     Paudel, A.; Worku, Z. A.; Meeus, J.; Guns, S.; Van den Mooter, G.  Manufacturing of solid dispersions of poorly water soluble drugs by spray drying: formulation and process considerations. *International journal of pharmaceutics* **2013,** *453*, (1), 253-284.

27.     Xie, T.; Taylor, L.  Dissolution Performance of High Drug Loading Celecoxib Amorphous Solid Dispersions Formulated with Polymer Combinations. *Pharm Res-Dordr* **2015**, 1-12.

28.     Chawla, G.; Gupta, P.; Thilagavathi, R.; Chakraborti, A. K.; Bansal, A. K.  Characterization of solid-state forms of celecoxib. *Eur J Pharm Sci* **2003,** *20*, (3), 305-317.

29.     Nakamoto, K.; Margoshes, M.; Rundle, R. E.  Stretching Frequencies as a Function of Distances in Hydrogen Bonds. *Journal of the American Chemical Society* **1955,** *77*, (24), 6480-6486.

30.     Konno, H.; Taylor, L.  Ability of Different Polymers to Inhibit the Crystallization of Amorphous Felodipine in the Presence of Moisture. *Pharm Res-Dordr* **2008,** *25*, (4), 969-978.

31.     Qian, F.; Huang, J.; Zhu, Q.; Haddadin, R.; Gawel, J.; Garmise, R.; Hussain, M.  Is a distinctive single T g a reliable indicator for the homogeneity of amorphous solid dispersion? *International journal of pharmaceutics* **2010,** *395*, (1), 232-235.

32.     Qian, F.; Huang, J.; Hussain, M. A.  Drug–polymer solubility and miscibility: Stability consideration and practical challenges in amorphous solid dispersion development. *J Pharm Sci-Us* **2010,** *99*, (7), 2941-2947.

33.     Coleman, M. M.; Painter, P. C.; Graf, J. F., *Specific interactions and the miscibility of polymer blends*. CRC Press: 1995.

34.     Marsac, P.; Shamblin, S.; Taylor, L.  Theoretical and Practical Approaches for Prediction of Drug–Polymer Miscibility and Solubility. *Pharm Res-Dordr* **2006,** *23*, (10), 2417-2426.

35.     Konno, H.; Taylor, L. S.  Ability of different polymers to inhibit the crystallization of amorphous felodipine in the presence of moisture. *Pharm Res-Dordr* **2008,** *25*, (4), 969-978.

36.     Paulson, S. K.; Vaughn, M. B.; Jessen, S. M.; Lawal, Y.; Gresk, C. J.; Yan, B.; Maziasz, T. J.; Cook, C. S.; Karim, A.  Pharmacokinetics of Celecoxib after Oral Administration in Dogs and Humans: Effect of Food and Site of Absorption. *Journal of Pharmacology and Experimental Therapeutics* **2001,** *297*, (2), 638-645.

37.     Bhugra, C.; Pikal, M. J.  Role of thermodynamic, molecular, and kinetic factors in crystallization from the amorphous state. *Journal of pharmaceutical sciences* **2008,** *97*, (4), 1329-1349.

38.     Bhattacharya, S.; Suryanarayanan, R.  Local mobility in amorphous pharmaceuticals—characterization and implications on stability. *Journal of pharmaceutical sciences* **2009,** *98*, (9), 2935-2953.

39.     Yoshioka, M.; Hancock, B. C.; Zografi, G.  Crystallization of indomethacin from the amorphous state below and above its glass transition temperature. *Journal of pharmaceutical sciences* **1994,** *83*, (12), 1700-1705.

40.     Yoshioka, M.; Hancock, B. C.; Zografi, G.  Inhibition of indomethacin crystallization in poly (vinylpyrrolidone) coprecipitates. *Journal of pharmaceutical sciences* **1995,** *84*, (8), 983-986.

41.     Hancock, B. C.; Zografi, G.  Characteristics and significance of the amorphous state in pharmaceutical systems. *Journal of Pharmaceutical Sciences* **1997,** *86*, (1), 1-12.

42.     Taylor, L.; Zografi, G.  Spectroscopic Characterization of Interactions Between PVP and Indomethacin in Amorphous Molecular Dispersions. *Pharm Res-Dordr* **1997,** *14*, (12), 1691-1698.

43.     Tsai, C. J.; Chen, M.; Lu, H. Y.; Chang, W. C.; Chen, C. H.  Crystal growth rates and master curves of poly (ethylene succinate) and its copolyesters using a nonisothermal method. *Journal of Polymer Science Part B: Polymer Physics* **2010,** *48*, (9), 932-939.

44.     Gutzow, I.  Induced crystallization of glass-forming systems: A case of transient heterogeneous nucleation, part 1. *Contemporary Physics* **1980,** *21*, (2), 121-137.

45.     Curatolo, W.; Nightingale, J. A.; Herbig, S. M.  Utility of hydroxypropylmethylcellulose acetate succinate (HPMCAS) for initiation and maintenance of drug supersaturation in the GI milieu. *Pharm Res-Dordr* **2009,** *26*, (6), 1419-1431.

46.     Warren, D. B.; Benameur, H.; Porter, C. J.; Pouton, C. W.  Using polymeric precipitation inhibitors to improve the absorption of poorly water-soluble drugs: A mechanistic basis for utility. *Journal of drug targeting* **2010,** *18*, (10), 704-731.

47.     Wegiel, L. A.; Mauer, L. J.; Edgar, K. J.; Taylor, L. S.  Crystallization of amorphous solid dispersions of resveratrol during preparation and storage—Impact of different polymers. *Journal of Pharmaceutical Sciences* **2013,** *102*, (1), 171-184.

48.     Rumondor, A. C.; Marsac, P. J.; Stanford, L. A.; Taylor, L. S.  Phase behavior of poly (vinylpyrrolidone) containing amorphous solid dispersions in the presence of moisture. *Mol Pharmaceut* **2009,** *6*, (5), 1492-1505.

CHAPTER 4.  IMPROVED RELEASE OF CELECOXIB FROM HIGH DRUG
LOADING AMORPHOUS SOLID DISPERSIONS FORMULATED WITH
POLYACRYLIC ACID AND CELLULOSE DERIVATIVES

## 4.1    Abstract

Amorphous solid dispersions (ASDs) have been extensively exploited as a strategy for improving the dissolution performance of poorly water-soluble drugs. However, factors underpinning the observed dissolution profiles are not clearly understood and the choice of polymeric carriers is largely empirical. In the current study, the dissolution performance of a high drug loading ASD containing the poorly water soluble, anti-inflammatory agent, celecoxib, was optimized by using binary polymers combinations. Polyacrylic acid (PAA), a highly water soluble polymer, was used to substantially increase the dissolution rate of the drug, while hydroxypropyl methyl cellulose (HPMC) or HPMC acetate succinate (HPMCAS), were added to stabilize the solid amorphous matrix against crystallization upon hydration, as well as to maintain supersaturation. Quantitative measurements of the impact of the polymers on the solution nucleation and growth rates of celecoxib revealed that, while the cellulose derivatives are effective nucleation inhibitors, it is more difficult to completely prevent crystal growth in solutions containing seed crystals, in particular at high supersaturations. Therefore, it is critical to prevent the formation of crystals in the dissolving matrix during dissolution. By using certain ratios of HPMC and PAA, both rapid release as well as crystallization inhibition could be achieved, even at high drug loadings.

Utilizing combinations of polymers may therefore be useful to tailor release profiles, while providing optimized crystallization inhibition.

## 4.2 Introduction

Pharmaceutical pipelines are currently populated with a high percentage of drug candidates which are very lipophilic, and/or have high melting points, leading to extremely low aqueous solubility[1, 2]. Strategies to improve the dissolution rate and apparent solution concentration can be divided into two main approaches[3]. The first encompasses dosage forms containing solubilizing additives whereby the equilibrium crystalline solubility of the drug is increased by processes such as binding with surfactant micelles or complexation with cyclodextrins. Dissolution rate is typically enhanced, however, the free fraction of the drug, which is in equilibrium with the solubilized fraction, remains limited[4]. The second approach involves drug delivery systems such as amorphous solid dispersions (ASDs) that generate supersaturated solutions. A supersaturated solution has a higher free drug concentration than that generated from dissolution of the crystalline form in the same medium. High energy state ASDs are thus formulated with the goal of generating and maintaining a higher free drug concentration than can be achieved with the crystal, whereby the higher concentration persists for biologically relevant timeframes. This is advantageous since the passive drug flux across the gastrointestinal wall is expected to be proportional to the free drug concentration[5, 6], and hence the degree of supersaturation. The dissolution rate of the drug when molecularly dispersed a highly soluble polymer is also typically enhance by factors such as improved particle hydrophilicity and wettability[7-10]. However, amorphous solids and supersaturated solutions are thermodynamically

metastable. Crystallization from amorphous formulations is complex and may occur either directly from the solid matrix upon contact with the dissolution medium, or from a supersaturated solution generated during dissolution under non-sink conditions [11]. Polymers play an essential role in modifying crystallization kinetics both from the matrix[12] and solution phase[13], enabling supersaturated solutions to be generated and maintained when the optimum polymer is employed in the formulation[11, 14, 15]. In order to understand the mechanisms of release from ASDs and to optimize polymer selection it is therefore essential to evaluate the polymer impact on different crystallization pathways, as well as to determine the relative impact of the polymer on crystal nucleation and growth.

Not only does the polymer play a pivotal role as a crystallization inhibitor for both the matrix and solution phases, but the release rate of the drug from the ASDs will depend on both the type and the amount of the polymer in the formulation. In their seminal work on sulfathiazole-PVP amorphous solid dispersions, Higuchi and coworkers showed that as the drug loading increased, the rate of drug release was dramatically reduced, even though there was no crystallization of the drug[16]. Corrigan reviewed mechanisms of release from solid dispersions and identified different controlling factors that depend on the drug:polymer ratio and the difference in solubility between the drug and polymer[8]. In his review, it was noted that, at low drug loadings, the drug dissolves simultaneously with the polymer. In contrast, at high drug loadings, the polymer may dissolve faster than the drug leaving behind a drug-rich layer and hence the dissolution behavior becomes drug controlled.

Corrigan [8] proposed a model suggesting that the dissolution rate of component B, $G_B$, in the ASD will be regulated by that of component A, $G_A$, as follows:

$$G_B = \frac{N_B}{N_A} G_A \qquad (1)$$

where N is the proportion of each component. Equation 1 will hold if:

$$\frac{N_A}{N_B} > \frac{D_A C_{SA}}{D_B C_{SB}} \qquad (2)$$

where D is the diffusion coefficient and Cs is the solubility of each component. This forms the theoretical basis for drug controlled release from amorphous solid dispersions at moderate to high drug loading and polymer controlled release at low drug loadings [15, 17]. The drug:polymer ratio in the ASD is an important practical consideration for all but the most potent compounds. Low drug:polymer ratios, while typically leading to enhanced release rates, result in large or even multiple dosage units, which is undesirable from a patient compliance perspective. Therefore, in order to use ASDs more broadly as an enabling strategy for poorly water soluble compounds, there is a need to increase drug loading, while maintaining the amorphous form of the drug, the supersaturated solution, and achieving an adequate rate of drug release, in particular for therapeutic indications where a rapid onset of action is required, for example pain management.

Celecoxib (CEX), a cyclooxygenase-2 inhibitor, is a poorly water soluble compound that is mainly used to treat pain arising from osteo and rheumatoid arthritis[18]. It has been widely used to explore the properties of amorphous solid dispersions and is known to crystallize rapidly from aqueous solutions when either no polymer is present[19], or if the polymeric excipient employed is a poor crystallization inhibitor[20]. A number of studies have evaluated the release rate of celecoxib from amorphous solid dispersions at high drug loading. It has been noted previously that celecoxib release rate slows considerably with an increase in drug loading[20]. Albers et al succeeded in circumventing this issue, achieving

rapid celecoxib release from an ASD prepared by hot melt extrusion and formulated with a polymethacrylate carrier, at a 50% drug loading. However, the resultant supersaturated solution was very short lived, crystallizing in less than ten minutes[21] indicating that this polymer is a poor solution crystallization inhibitor. In a clinical study[6], Morgen et al. found that amorphous nanoparticles of CEX formulated with ethylcellulose and casein were much more rapidly absorbed than a 50:50 w/w spray dried dispersion of CEX and HPMCAS, leading to a much shorter time to achieve the maximum drug concentration ($T_{max}$) and a slightly higher area under the curve (AUC) for the nanoparticles as compared to the spray dried dispersion. They suggested that the nanoparticle formulation might be useful therapeutically due to the fast onset of action.

Herein we explore an alternative approach to achieve rapid celecoxib release, and sustained supersaturation levels upon dissolution of high drug loading solid dispersions under non-sink dissolution conditions. The specific goal of this research was to combine a polymer with rapid release properties with polymers selected for their crystallization inhibitory properties, in order to attain an improved release rate at high drug loading, together with a sustained supersaturation level. To achieve this, CEX dispersions were prepared with polyacrylic acid (PAA) and either hydroxypropyl methylcellulose (HPMC) or HPMC acetate succinate (HPMCAS) and the dissolution rate and extent of supersaturation was evaluated under non-sink conditions. PAA is a highly water soluble, weakly acidic polymer that is often used in pharmaceutical applications for drug delivery[22] and was selected to facilitate rapid drug release. However, PAA has been noted to be a poor inhibitor of solution crystallization.[23, 24] HPMCAS and HPMC are both used in ASDs formulations[25, 26] and ASDs of CEX with HPMCAS have been shown previously to

improve bioavailability relative to the conventional dosage form containing crystalline drug[6]. Furthermore, HPMC and HPMCAS have been found to be good crystallization inhibitors for numerous compounds[27, 28]. The impact of the polymers on celecoxib crystallization in an aqueous environment was evaluated in order to better understand factors impacting the extent of drug release and the longevity of the supersaturated solutions generated upon dissolution. Nucleation induction times and growth rates were measured in the presence and absence of the polymers in order to compare their efficiency as crystallization inhibitors. Polarized light microscopy was used to evaluate crystallization behavior, while non-sink dissolution testing was used to evaluate the rate, extent and longevity of supersaturation following dissolution of the various ASDs.

## 4.3   Materials

CEX was purchased from Attix Pharmaceuticals (Toronto, Ontario, Canada). PAA was purchased from Sigma-Aldrich Corporation (St. Louis, Mo, USA). HPMCAS, Type AS-MF and HPMC, 606 grade were supplied by Shin-Etsu Chemical Co. (Tokyo, Japan). The molecular structures are shown in Figure 4-1

## 4.4   Methods

### 4.4.1   Preparation of Bulk Amorphous Materials

CEX and the polymer(s) with different dry weight ratios were dissolved in a mixture of ethanol and dichloromethane (50:50 v/v). Solvent removal was achieved by rotary evaporation. The ASDs were subsequently dried in a vacuum oven overnight to remove any residual solvent.  The ASDs were then ground using a mortar and pestle and sieved to

obtain a particle size fraction of 106-250µm. (Note that for CEX: HPMCAS 1:9 ASD, cryo-milling was applied to achieve particle size reduction). They were then stored in a desiccator containing phosphorous pentoxide at room temperature. A Rigaku SmartLab diffractometer (Rigaku Cooperation, The Woodlands, TX, USA) was used to confirm that the samples were amorphous prior to use. PXRD patterns were collected in step scan mode (0.02°/step) with a scan range from 5° to 35° and a scan speed of 4°/min. The tube voltage and current used to collect the pattern were 44kV and 40mA, respectively.

### 4.4.2   Nucleation Induction Time Measurements

275 µL of a 4 mg/mL or 2mg/mL methanol solution of CEX was pipetted into 50 mL pH 6.8 100 mM sodium phosphate buffer (SPB) with and without pre-dissolved polymer to create an initial CEX concentrations of 22µg/mL or 11µg/mL. The solution was equilibrated at 37°C and stirred at 300rpm (+shaped magnetic stirrer, 0.75 inch diameter). Solution concentrations were measured as a function of time using an SI photonics UV-Vis spectrometer coupled with a fiber optic probe. Wavelength scans (200-450nm) were performed at 1min intervals for 8hrs in the absence of polymers and 16hrs in the presence of polymers. The absorption peak at 249 nm was used to monitor solution concentration of CEX. Light scattering was detected by monitoring the extinction at 350 nm; the drug had no absorbance at this wavelength. All measurements were performed in triplicate.

### 4.4.3   Seeded Desupersaturation Experiments

7mg of CEX crystals were suspended in 50 mL pH 6.8 100 mM SPB. The SPB was equilibrated at 37°C and stirred at 300rpm (+shaped magnetic stirrer, 0.75 inch diameter)

in the absence or presence of pre-dissolved HPMCAS. 275 µL of a 4 mg/mL, or 2mg/mL methanol solution of CEX was pipetted into the suspension to create different initial CEX concentrations. The solution concentration as a function of time was monitored by the SI photonics UV-Vis system as described above.

### 4.4.4 Dissolution Studies of ASDs

When assessing the dissolution behavior of amorphous solid dispersions with the goal of gaining insight into the release mechanisms, it is critical to select the appropriate volume of medium. Conventionally, dissolution testing is carried out using sink conditions[3], which are unlikely to be achievable *in vivo* for poorly water-soluble drugs and does not typically allow appropriate evaluation of the crystallization behavior since the solution will not become supersaturated. Therefore, non-sink conditions are preferred when evaluating amorphous formulations mechanistically since these enable the degree of supersaturation to be evaluated. For this study, the dissolution conditions were chosen to correspond to "at sink" conditions with respect to the reported "amorphous solubility" of celecoxib. In other words, if the formulation remains amorphous during the dissolution experiment, complete drug release is expected, while if some crystallization of the drug occurs in the ASD matrix, this fraction of the drug will not be able to dissolve because the solution will be supersaturated with respect to the crystalline solubility.

An amount of ASD that contained 8.8mg CEX (see Table 4-1 for details of the total mass of ASD added) was added to 400 mL pH 6.8 100 mM SPB, equilibrated at 37°C and stirred at 300 rpm with a stir bar (+shaped, 0.75 inch diameter). These dissolution conditions should lead to the complete dissolution of amorphous CEX based on the reported

"amorphous solubility" value of approximately 22 µg/mL[20, 29]. Solution concentration evolution as a function of time was measured using the SI Photonics UV system. Wavelength scans (200-450nm) were performed at 1min time intervals for 16 hours. The absorption peak at 249 nm was used to monitor solution concentration of CEX. Calibration solutions of CEX were prepared in methanol. All measurements were performed in triplicate.

### 4.4.5 Effect of Polymer on the Equilibrium Solubility of CEX

The equilibrium solubility of CEX was determined by adding an excess amount of crystalline CEX to 20 mL pH 6.8 100mM SPB with the absence/presence of 22µg/ml pre-dissolved polymer in scintillation vials. The vials were equilibrated at 37°C for 48h in an agitating water bath (Dubnoff metallic shaking incubator; PGC Scientific, Palm Desert, CA, USA). Samples were then subject to ultracentrifugation to separate excess crystalline CEX particles from the supernatant. Ultracentrifugation was performed at 35000 rpm for 30 minutes in an Optima L-100XP ultracentrifuge equipped with Swinging-Bucket Rotor SW 41 Ti (Beckman Coulter, Inc., Brea, CA, USA). High performance liquid chromatography (HPLC) analyses were carried out with an Agilent HPLC 1260 Infinity system (Agilent Technologies, Santa Clara, California, USA). The chromatographic separation was performed by an XTerra Shield RP18 Column (125Å, 3.5 µm, 3.9 mm X 100 mm) (Waters Cooperation, Milford, MA, USA). Water (20%) and acetonitrile (80%) mixture was used as mobile phase and the flow rate was 0.25mL/min. The ultraviolet detection wavelength was 250nm. All measurements were performed in triplicate at room temperature.

#### 4.4.6   Polarized Light Microscopy

The ASDs (106-250μm) were placed on a glass slide with a depression. A few drops of pH 6.8 100 mM SPB were then added to the particles. The crystallization behavior of ASDs was observed using a Nikon Eclipse E600 Pol microscope with 10x objective (Nikon Company, Tokyo, Japan). Images were processed by NIS-Elements software package (Version 2.3; Nikon Company, Tokyo, Japan).

#### 4.4.7   Thermal Analysis

Thermal analysis was carried out using a TA Q2000 DSC with a cooling refrigerator system (TA Instruments, New Castle, DE, USA). Nitrogen was purged at a rate of 50mL min$^{-1}$. Approximately 5mg of the samples were weighed into an aluminum Tzero sample pan and sealed using a hermetic Tzero lid with a pinhole. The glass transition temperature was determined by heating the sample at approximately 20°C min$^{-1}$ to approximately 30 °C above the glass transition temperature ($T_g$), followed by cooling and reheating. The $T_g$ onset in the second heating scan was reported.

#### 4.4.8   Fourier Transform Infrared Spectroscopy

Polymer(s) was dissolved in a mixture of ethanol and dichloromethane. The resultant solution was then spin coated onto a thallium bromide (KRS-5) optical crystal. FT-IR spectra were obtained on a Bruker Vertex 70 spectrometer (Bruker, Billerica, MA, USA) in transmission mode and the spectra were subsequently converted into units of absorbance. 64 scans were collected with a 4 cm$^{-1}$ resolution for each sample over the wavenumber range from 4000cm$^{-1}$ to 500 cm$^{-1}$. Dry air was purged into the sampling and optical

compartment to prevent spectral interference from water vapor. Opus 7.2 software (Bruker, Billerica, MA, USA) was used to analyze the spectra.

## 4.5    Results and Discussion

### 4.5.1    Equilibrium Solubility of CEX

The measured equilibrium solubility of crystalline CEX was 1.5μg/mL in the absence of any polymers, and this value is in good agreement with the value reported by Abu-Diak et al[20]. Polymers, when present at a concentration of 22μg/mL in SPB, did not substantially impact the crystalline solubility of CEX, as shown in Table 4-2. Based on the solubility values of crystalline CEX in the presence and absence of the polymers, it is apparent that the polymers do not solubilize the drug, and therefore will not substantially impact the supersaturation and hence the driving force for nucleation.

### 4.5.2    Impact of Polymers on Nucleation Induction Times

The effectiveness of the polymers in inhibiting crystallization from supersaturated solution was assessed by performing nucleation induction time measurements. It is well known that the nucleation rate is highly dependent on the degree of supersaturation in the system, S, which is typically defined by[30]:

$$S = \frac{c}{c*} \qquad\qquad (3)$$

Where c is the concentration of the crystallizing solute in the solution and c* is the concentration of a saturated solution. To assess the ability of the various polymers to maintain supersaturation, a level of supersaturation close to the experimentally measured and calculated "amorphous solubility" of CEX[19, 20, 29, 31], 22 μg/mL, was generated. This

concentration is considerably higher than the measured crystalline solubility (shown in Table 4-2) and hence a large driving force for nucleation is present. It has been shown previously that the "amorphous solubility" represents the highest free drug concentration that can be achieved, and hence this is the maximum possible supersaturation[4, 31, 32]. Therefore, the effectiveness of the polymers at the maximum theoretical driving force for nucleation is being assessed.

The experimental nucleation induction time, $t_{ind}$, can be defined as the sum of the time for critical nucleus formation (true nucleation time, $t_n$), and the time for growth to detectable size, $t_g$.

$$t_{ind} = t_n + t_g \qquad (4)$$

The onset of crystallization is readily determined from the UV spectroscopic measurements from the abrupt increase in scattered light at a non-absorbing wavelength of 350 nm concomitant with rapid decrease in absorbance at 249nm, where CEX shows an absorption peak[33].

As shown in Figure 4-2, in the absence of any polymer, nucleation was rapid and the drug concentration decreased rapidly whereby crystallization commenced within 5 minutes at an initial CEX concentration of 22 μg/mL (For clarity, data points after 3hrs are not shown). This concentration represents a very high initial supersaturation and the rapid desupersaturation is consistent with previous reports that CEX is a rapid crystallizer from aqueous solutions[20, 34]. The induction time increased to approximately 20 minutes when the initial CEX concentration was reduced to 11 μg/mL, in agreement with classical nucleation theory which predicts a decrease in the nucleation rate (and hence an increase in induction time) with decreasing supersaturation[35].

The nucleation induction time and the rate of desupersaturation did not change in the presence of pre-dissolved PAA (Figure 4-3), indicating that this polymer is an ineffective crystallization inhibitor. In contrast, the initial supersaturation was effectively maintained for the duration of the experiment, 16 h, when small quantities of either HPMCAS or HPMC were dissolved in solution. When HPMCAS was used in combination with PAA, no significant desupersaturation occurred, indicating that the effectiveness of HPMCAS in maintaining supersaturation was not impaired by the presence of PAA. This result lends support to our proposed strategy of combining two polymers in an amorphous formulation, since the crystallization inhibitory properties of a given polymer are not diminished by the presence of a second polymer, at least for the system studied herein.

The remarkable increase in the induction time in the presence of HPMCAS or HPMC cannot be explained by changes to the supersaturation due to increasing the solubility of the crystalline drug, since the polymers have very little impact on the crystal solubility and must be due to subtle molecular level interactions that are difficult to probe experimentally, as with all direct investigations of the nucleation process. Nevertheless, the superiority of HPMCAS or HPMC relative to PAA is perhaps not particularly surprising. Previously, it has been suggested that for a polymer to be an effective crystallization inhibitor, it needs to have a suitable level of hydrophobicity; too hydrophilic and it will preferentially interact with the water, and too hydrophobic and it will preferentially interact with itself, rather than interacting with the nucleating drug phase[29, 36]. Warren et al[27] tested the precipitation inhibition behavior of 53 polymeric materials for supersaturated solution of danazol, and the majority of superior precipitation inhibitor were amphiphilic cellulose derivatives. On the other hand, PAA is very hydrophilic, and is expected to have a much stronger

interaction with water than with CEX in solution. Therefore, the nucleation of CEX in solution was unaffected by the presence of PAA. Previous studies have also noted that PAA is an ineffective inhibitor of nucleation[29].


### 4.5.3 Characterization of Binary Dispersions Containing PAA or HPMCAS

The dissolution rate of CEX: HPMCAS ASDs was highly dependent on the drug loading, as shown in Figure 4-4. At low drug loadings (10% drug), the initial release rate was rapid and complete release of the drug to reach the reported amorphous solubility was achieved in 4 hours whereby the supersaturation was retained for the duration of the experiment (16 h). It is of interest to note that the solution concentration achieved from the HPMCAS dispersion is similar to that reported in another study with CEX: PVP dispersions[20]. In that particular study, the authors also made note of the fact that the dispersion dissolved to reach a maximum concentration equivalent to the "amorphous solubility", even though excess drug was present. The sustained supersaturation achieved by dissolution of the HPMCAS dispersions confirms the excellent crystallization inhibitory properties of HPMCAS towards supersaturated solutions of CEX. Furthermore, the achievement of complete drug release indicates that HPMCAS inhibits matrix crystallization, enabling the drug to dissolve to the amorphous solubility. As the drug loading was increased, the release rate became much slower. For 50% drug loading, the solution concentration increased slowly and complete release was achieved only after 16 h. In a study by Curatolo et al[28], 41 small and polymeric molecules were tested for their effectiveness in initiation and maintaining supersaturation for each of 9 structurally diverse low solubility drugs, HPMCAS was found to be the most effective precipitation inhibitor. Consequently, spray dried dispersions

(SDDs) prepared with HPMCAS were consistently superior to SDDs formulated with other polymers in both achieving and maintaining supersaturation during in vitro dissolution studies.

In contrast, a high drug loading CEX: PAA 5:5 dispersion exhibited an extremely fast dissolution rate, reaching a maximum CEX concentration of 11μg/mL within 3 minutes. However, the release was incomplete and the supersaturation generated by the ASD dissolution was rapidly depleted by crystallization and the CEX concentration approached the crystalline solubility within 60 minutes. A similar profile was obtained when the drug loading was reduced to 30% or 10% (data not shown). The substantial increase in initial drug release rate can presumably be attributed to the greater hydrophilicity and complete ionization of the carrier PAA (the pKa of PAA is 4.28)[37], which result in a high polymer solubility and hence fast dissolution. The pH of the medium after dissolution was measured and was found to be unchanged. CEX is weakly acidic with a pKa of 11.1 and hence remained as the unionized form during dissolution. The rapid desupersaturation of the supersaturated CEX solutions generated by dissolution of the CEX:PAA dispersions is in excellent agreement with the nucleation-induction time results shown in Figure 2, and is consistent with the poor nucleation inhibition properties of PAA. The incomplete release from the PAA dispersions suggests either that matrix crystallization has occurred prior to complete dissolution, or that there is very rapid solution crystallization of the dissolved drug that efficiently depletes the supersaturation while the matrix may still dissolve simultaneously.

Polarized light microscopy was used as a complementary method to study the phase behavior of the CEX:PAA and CEX: HPMCAS ASDs. From Figure 4-5, it is apparent that

the CEX: PAA 5:5 ASD was amorphous following preparation with no evidence of birefringence under polarized light. The amorphous nature of the material following preparation was also verified by powder x-ray diffraction. Therefore, the incomplete release observed during dissolution is not due to some initial fraction of crystalline material. After adding a few drops of SPB, rapid dissolution from the solid matrix was observed, concomitant with the emergence of needle-shaped crystals. However, this process proceeded so rapidly that it was not possible to unambiguously differentiate matrix crystallization from solution crystallization based on these images alone. In contrast, crystallization was not observed in the case of CEX: HPMCAS 3:7 ASD, which dissolved much more slowly (Figure 4-6)

These results suggest that preparing a high drug loading dispersion with PAA, whereby drug release is fast, but supersaturation is not sustained due to the rapid drug crystallization, that also includes a polymer with good crystallization inhibition properties, could lead to improved overall dissolution performance. To test this idea, HPMCAS was pre-dissolved in the buffer and the dissolution behavior of the CEX: PAA 5:5 ASD was evaluated, and the results are shown in Figure 4-7.

For this system, the release rate was very fast, although the release was again not complete and the maximum concentration achieved was ~10 μg/mL. Different from the CEX:PAA dispersion described above (Figure 3), the supersaturation that was generated was maintained for 16 h, because there is now an effective crystallization inhibitor (i.e. HPMCAS) in solution. It therefore appears that the incomplete release is due to the crystallization of CEX in the matrix. In other words, there is a competition between matrix crystallization (which HPMCAS in the solution phase is unable to influence) and release

of CEX into solution (whereby HPMCAS is able to inhibit crystallization of dissolved CEX). Thus, once the matrix has crystallized, no further CEX release can occur because the solution is supersaturated with respect to the crystal solubility. The undissolved solids were retrieved soon after the peak concentration was reached. The polarized light microscopic images verified that those solids were needle-shaped crystals, consistent with the stable crystalline form of CEX[38] (Figure 4-8). Decreasing the drug loading to 10% did not substantially improve the extent of drug release, indicating that PAA is a very poor inhibitor of matrix crystallization, irrespective of the drug loading.

### 4.5.4   Impact of HPMCAS on Crystal Growth Rate

It is interesting that the supersaturation that was generated by the rapid, albeit partial release of CEX was maintained for 16 h and was not reduced by the presence of the crystals produced by matrix crystallization. Typically, the presence of crystal seeds would be expected to lead to rapid desupersaturation as the crystals grow at the expense of the solution concentration, until the equilibrium crystal solubility is reached[39]. The lack of desupersaturation suggests that that HPMCAS is able to inhibit crystal growth, at least at the supersaturation achieved by dissolution of the ASD. Crystal growth inhibition can be evaluated by adding crystal seeds to a solution of known supersaturation. If this is done in the presence and absence of a polymer, then the effectiveness of a polymer can be assessed[36, 39, 40].

Figure 4-9 shows results from independent seeded crystallization experiments in the presence and absence of HPMCAS at two supersaturations. In the absence of polymer, desupersaturation is rapid, and immediate, without the short lag time seen for the induction

time experiments. It is clear that HPMCAS is indeed an effective inhibitor of CEX crystal growth at both high and lower supersaturations. At an initial concentration of 11 µg/mL, very little desupersaturation was seen for the duration of the experiment. This explains why any crystals formed during the dissolution of the PAA ASDs did not lead to desupersaturation when HPMCAS was present; at the supersaturation generated, HPMCAS is able to effectively block crystal growth. HPMCAS is a less effective inhibitor of growth at a higher supersaturation, in agreement with theoretical models[41] and previous studies[40], although the rate of desupersaturation at the highest supersaturation tested (22 µg/mL CEX) is still fairly slow for the two polymer concentrations studied. By measuring the slopes of the desuperaturation profiles, the relative crystal growth rates can be quantified as[36]:

$$R_0/R_p \tag{5}$$

Where $R_0$ is the mass growth rate in the absence of the polymer and $R_p$ is the mass growth rate in the presence of the polymer. The slope of the linear region in the seeded desupersaturation curves in the absence of HPMCAS over the initial 5 minutes was used as $R_0$. For simplicity, the slope of the seeded desupersaturation curves over the entire 16h in the presence of HPMCAS was used to approximate $R_p$. From this analysis, we found the relative growth rates were approximately 130 CEX 11µg/mL, HPMCAS 11µg/mL), 70 (CEX 22 µg/mL, HPMCAS 5µg/mL) and 158 (CEX 22µg/mL, 22 µg/mL) based on the data shown in Figure 4-9.

It has also been suggested that the relative growth rate data can be used in combination with induction time data to estimate the relative impact of the polymer on the nucleation rate by application of the following equation[39, 42]:

$$\frac{J_0}{J_p} = \left(\frac{R_p}{R_0}\right)^3 \left(\frac{t_{u,p}}{t_{u,0}}\right)^4 \qquad (6)$$

Where $J_0$ and $J_p$ are the nucleation rates in the absence and presence of a polymer, respectively, and $t_{u,0}$ and $t_{u,p}$ are the induction time in the absence and presence of a polymer, respectively. For induction time measurements at 22 µg/mL initial CEX concentration with 5 µg/mL predissolved HMCAS, we failed to observe a sharp change in the slope of desupersaturation profile over the experimental timeframe. Therefore, 960 minutes was used as the value for $t_{u,p}$. In this case, using an $R_0/R_p$ ratio of 70, the calculated relative impact of the polymer on the nucleation rate was ~4000.

From this analysis, it can be surmised that, although the presence of 5µg/mL HPMCAS resulted in substantial inhibition of both nucleation and crystal growth of CEX in SPB, the relative impact of HPMCAS on nucleation was still far more pronounced than its impact on crystal growth, despite the fact that the nucleation induction time in the presence of HPMCAS was underestimated.

### 4.5.5   Characterization of Ternary CEX:PAA:HPMCAS Dispersions

The next logical step was to add HPMCAS to the CEX: PAA ASD, with the aim of inhibiting the matrix crystallization of CEX that occurs when the drug is formulated with PAA, while still maintaining a rapid release rate. Shown in Figure 4-10 are the dissolution profiles of CEX: PAA: HPMCAS ternary ASDs which vary with respect to drug loading as well as the amount of each polymer. At 4:5:1 and 5:4:1 ratios, where HPMCAS was a minor component, it can be seen that there was an initial burst release of CEX leading to a solution with a concentration between 12-14 µg/mL, whereby the concentration was

sustained for 16 h. While this is a slight improvement over the systems shown in Figure 4-7, where HPMCAS was present only in the dissolution medium, it is apparent that some matrix crystallization was still occurring since complete release was not achieved at either ratio. In an attempt to reduce the matrix crystallization, ASDs where a larger fraction of PAA was replaced by HPMCAS were investigated. This approach appeared to be reasonably successful in inhibiting matrix crystallization for a 5:3:2 CEX:PAA:HPMCAS dispersion, since the highest drug concentration reached was approximately 19 µg/mL and was still increasing by the end of 16h. This is close to the nominal concentration that would be achieved by complete release (22µg/mL). However, the improved matrix stability was achieved at the cost of the release rate, whereby a much smaller extent of initial burst release was observed (rapid release to 6 µg/mL within 5 min), which was followed by a sustained period of much slower release. The origin of this apparent biphasic drug release will be discussed in more detail subsequently, but immediately raises the suspicion of (partial) phase separation between PAA and HPMCAS. Further replacement of PAA by HPMCAS (5:2:3) resulted in even smaller extent of burst release, again followed by a period of sustained slow release. A compromise between drug loading and release rate could be seen at a CEX drug loading of 30% (3:6:1), where full and rapid release was achieved, and the supersaturation was maintained over the experimental time frame. The release profile was similar for the 1:8:1 CEX: PAA: HPMCAS ASD.

Polarized light microscopy studies were interesting. When the CEX: PAA: HPMCAS 3:6:1 ASD was exposed to buffer (Figure 4-11), rapid initial dissolution was observed and the solid matrix collapsed with the generation of fine particles. In agreement with the dissolution results, where complete release was observed, no crystals could be detected for

this system based on the absence of birefringence under cross polarized light. At 2:1:1 ratio (Figure 4-12), the initial dissolution of the ASD was still very fast. It was followed by generation of more particles of various sizes which then dissolved slowly. Again, no crystallization was observed in this case.

### 4.5.6 Characterization of Dispersions Containing CEX, PAA and HPMC

While the ternary dispersions of CEX with PAA and HPMCAS showed improvement in terms of both release rate and crystallization inhibition over the respective binary dispersions, it was not possible to achieve both rapid and complete release at a drug loading of 50%. In addition, the biphasic dissolution profiles observed, while interesting, suggest that a formulation strategy combining PAA and HPMCAS would lead to very complex systems. HPMC is also a very effective nucleation inhibitor for CEX (Figure 4-3), hence binary and ternary dispersions were evaluated with this polymer.

Similar to the binary CEX: HPMCAS ASDs, the dissolution rate of binary CEX: HPMC ASDs decreased with an increase in drug loading, as shown in Figure 4-13, and were even slower than the corresponding HPMCAS ASDs, whereby release was incomplete at the end of 16 h from the higher drug loading dispersions. The ternary ASDs showed a much faster release rate, benefiting from the presence of the fast releasing PAA. At a 30% drug loading, the ternary ASD containing 60% PAA and 10% HPMC dissolved much more rapidly than the corresponding binary HPMC ASD, and essentially complete CEX release was achieved by 2hrs, with the supersaturation being sustained for an additional 14 h. At a 50% drug loading, the ternary ASD containing 10% HPMC exhibited fast dissolution and yielded about 85% release. Again the supersaturation generated was substantially

maintained. This dispersion achieved a greater extent of release than the corresponding ternary dispersion with PAA and HPMCAS, with only a slightly slower release rate.

The 2:1:1 CEX: PAA: HPMC ASD did not exhibit the biphasic dissolution behavior seen with the high drug loading CEX: PAA: HPMCAS ASDs (which showed a burst release followed by much slower dissolution at the 5:2:3 or 5:3:2 ratios, Figure 4-10). Dissolution experiments of CEX: PAA: HPMC ASDs at 5:2:3 and 5:3:2 ratios were not carried out because their profiles were expected to be similar to that at 2:1:1 ratio. Figure 4-14 shows that a different pattern of dissolution was observed for the CEX: PAA: HPMC ASD (3:6:1 ratio) ASD when viewed under the microscope. In this case, the initial particles remained intact, gradually decreasing in size as dissolution proceeded, with the particles eroding from the particle edges. They showed no evidence of disintegration into smaller particles as seen for the ternary systems formulated with HPMCAS.

The different pattern of dissolution, whereby the particles undergo a slower erosion process rather than an initial burst release as seen for some of the CEX:PAA:HPMCAS systems appears to be beneficial to the initiation and maintenance of supersaturation. To prevent matrix crystallization and/or subsequent desupersaturation, it is important that the inhibitory polymer remains in close contact with the drug during hydration, and is released simultaneously. Since the HPMC-containing dispersions appear to undergo erosion, then drug and HPMC should remain in contact during hydration and release should occur concurrently.

### 4.5.7 Miscibility Characterization

Despite some practical limitations, DSC analysis remains the most common technique to determine the mixing state of a drug with a polymer[43]. The measured Tg of each pure component and the ASDs at 1:1 ratio are listed in Table 4-3. Each binary ASDs at a 1:1 ratio had a Tg value in between that of the two pure components, which indicates that the drug has some miscibility with each polymer.

IR spectroscopy can be used to interrogate the miscibility in polymer blends[44] and was used to better understand the PAA-HPMCAS and PAA-HPMC systems. Unfortunately, it was not possible to use DSC analysis for this purpose due to the similarity in the glass transition temperature values for the polymers used as shown in Table 4-3. The IR spectra (wavenumber range from $1600cm^{-1}$ to $1800 \ cm^{-1}$) of spin coated films of pure PAA, HPMCAS, HPMC or binary mixtures of PAA and the cellulose polymers are shown in Figure 4-15 and Figure 4-16. Pure PAA has a peak at $1710cm^{-1}$, which may be assigned to C=O stretching of dimerized carboxylic acid[22, 45]. Pure HPMCAS has a C=O stretching peak at $1743cm^{-1}$. The spectra of PAA and HPMCAS mixtures show both of these peaks with little change in the wavenumber. In other words, the spectra of the mixtures are additive, suggesting a lack of specific intermolecular interactions between PAA and HPMCAS.

Hence the IR data suggest that PAA and HPMCAS are immiscible. This is not necessarily very surprising. Because of the low entropy of mixing for two large molecules[46], polymers are typically only miscible when they can form specific interactions and hence have a favorable enthalpic contribution to the free energy of mixing[47]. PAA forms carboxylic acid dimers[22] in the pure polymer, which would only be disrupted if a more favorable

intermolecular interaction can be formed. It thus appears that HPMCAS lacks the ability to form favorable intermolecular interactions with PAA and that these two polymer consequently do not mix. Examples of poor miscibility with other components have been reported for both polymers. For example, PAA has been reported to be immiscible with the small molecule, felodipine, due to the lack of favorable drug-polymer interactions[48]. HPMCAS has been reported to be only partially miscible with one cellulose derivative, carboxymethyl cellulose acetate butyrate, but miscible with another cellulose derivative, HPMC, illustrating the challenges with predicting polymer miscibility *a priori*[49]. Furthermore, when CEX (which has no signal in the carbonyl region) was mixed with the polymer blend polymer, the polymer carbonyl peaks still showed very little change in wavenumber relative to in the pure polymer spectra (Figure 4-15), suggesting that adding CEX does not result in improved miscibility of the two polymers.

If PAA and HPMCAS do not mix in the ternary dispersion, but CEX exhibits some degree of miscibility with each polymer, as suggested by the DSC data shown above, a situation can be envisaged where CEX exists in two domains; dispersed in a PAA-rich domain, and dispersed in a HPMCAS-rich domain. Such phase separation would explain the observed biphasic dissolution profiles and sequence of events seen from the microscope images. Thus, during the dissolution of the ternary ASDs, a fraction of CEX is rapidly released into solution due to the very fast dissolution of the PAA-rich domains, whereas the release from the HPMCAS-rich domains is much slower, as seen for the binary CEX-HPMCAS dispersions. This would also provide an explanation about why it is was hard to inhibit matrix crystallization by adding HPMCAS; presumably the inhibitory polymer needs to be in reasonably close contact with the drug to inhibit crystallization, and this may not occur

for all drug molecules if substantial phase separation occurs because the polymers are not miscible.

In blends of HPMC and PAA, a shoulder at 1735cm$^{-1}$ emerged and increased at the expense of the peak at 1710cm$^{-1}$ as the ratio of PAA:HPMC decreased (Figure 4-16). Pure HPMC does not have any absorption peaks in this spectral region. This observation indicates that the presence of HPMC may disrupt the PAA carboxylic acid dimers. This might occur through either the formation of hydrogen bonding between the OH group of HPMC and the C=O group of PAA or due to hydrogen bond interactions between the OH group of PAA with acceptor groups on HPMC. The change in the hydrogen bonding of PAA in the presence of HPMC suggests that these two polymers exhibit some degree of miscibility. In the ternary blend of CEX:PAA:HPMC, that same spectroscopic pattern is seen in the carbonyl region, indicating that the addition of CEX does not lead to demixing of PAA and HPMC. Again, this observation is consistent with the dissolution results obtained for ternary dispersions formulated with combinations of HPMC and PAA where it was observed that the release rate was intermediate to that of the binary dispersions with each polymer, while the extent of release was improved due to the matrix crystallization inhibitory properties of HPMC.

## 4.6    Conclusions

HPMCAS and HPMC were effective inhibitors of CEX solution nucleation. These polymers were also very effective at inhibiting crystallization from the matrix of an ASD during the hydration stage of dissolution. However, the drug release rates from ASDs formulated with either polymer at moderate to high drug loadings (30-50% drug) were slow,

and could only be improved at the expense of drug loading. Conversely, PAA was a poor inhibitor of solution crystallization but led to extremely fast drug release (albeit incomplete due to crystallization), even at high drug loadings. The expected advantages of combining a fast release polymer, PAA, with a good matrix and solution crystallization inhibitor, HPMC or HPMCAS were realized at a drug loading of 30% and partially realized at higher drug loadings.  Combining two polymers to optimize both drug release and supersaturation thus appears to be a viable formulation strategy, although attention needs to be paid to the miscibility of the ternary systems.

Table 4-1 List of the ASDs evaluated and their total mass used for dissolution studies

| System | Drug:Polymer Weight Ratio. The value in parentheses indicates the total mass of ASD used in dissolution study to give a theoretical CEX concentration of 22 µg/mL |
|---|---|
| CEX: PAA | 5:5 (17.6mg), 3:7 (29.3mg), 1:9 (88mg) |
| CEX: HPMCAS | 6:4 (14.7mg), 5:5 (17.6mg), 3:7 (29.3mg)and 1:9 (88mg) |
| CEX: HPMC | 5:5 (17.6mg) and 3:7 (29.3mg) |
| CEX: PAA: HPMCAS | 5:2:3 (17.6mg) , 5:3:2 (17.6mg), 5:4:1 (17.6mg), 4:5:1 (22mg), 3:6:1 (29.3mg), and 1:8:1 (88mg) |
| CEX: PAA: HPMC | 2:1:1 (17.6mg), 5:4:1 (17.6mg), and 3:6:1 (29.3mg) |

Table 4-2 Crystalline CEX solubility in the absence and presence of pre-dissolved polymers

|  | No Polymer | PAA | HPMCAS | HPMC |
|---|---|---|---|---|
| CEX solubility ( µg/mL) | 1.5±0.1 | 1.72±0.06 | 1.89±0.02 | 2.05±0.03 |

Table 4-3 Tg of the pure drug, pure polymers, and the ASDs

| Material | Tg |
|---|---|
| CEX | 56±1 |
| HPMCAS | 117±1 |
| HPMC | 140±5 |
| PAA | 128±1 |
| CEX: HPMCAS 1:1 | 67±1 |
| CEX: HPMC 1:1 | 71±6 |
| CEX: PAA 1:1 | 83±2 |
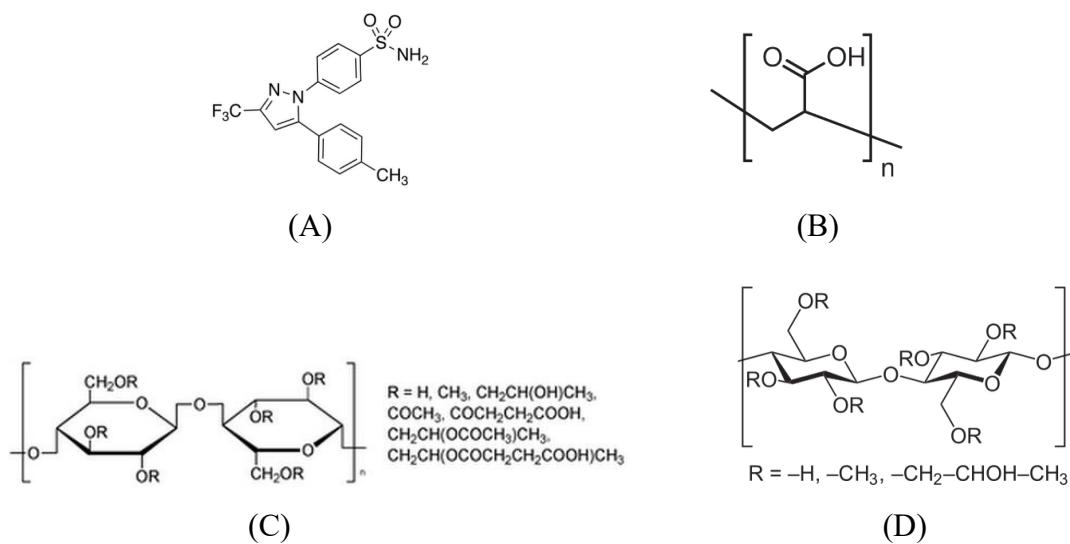
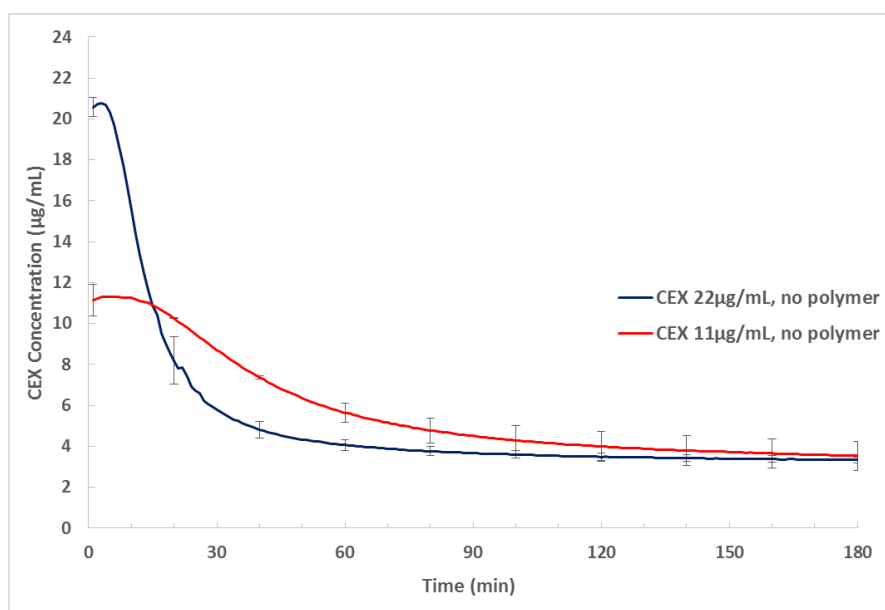Figure 4-1 Chemical structures of CEX (A), PAA (B), HPMCAS (C), and HPMC (D).



Figure 4-2 Induction time measurements of CEX in the absence of polymers
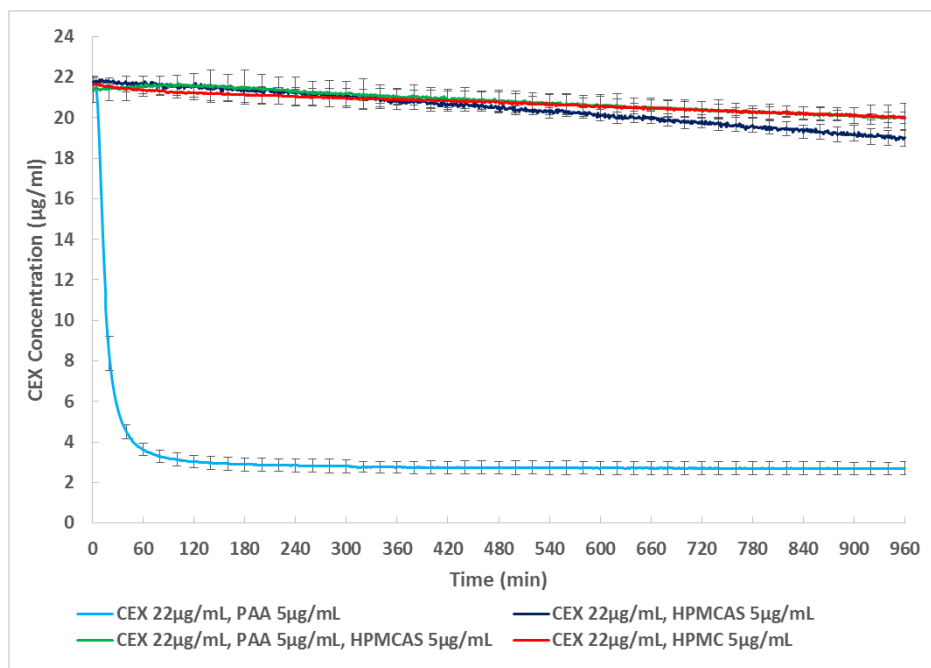
Figure 4-3 Induction time measurements of CEX in the presence of different polymers
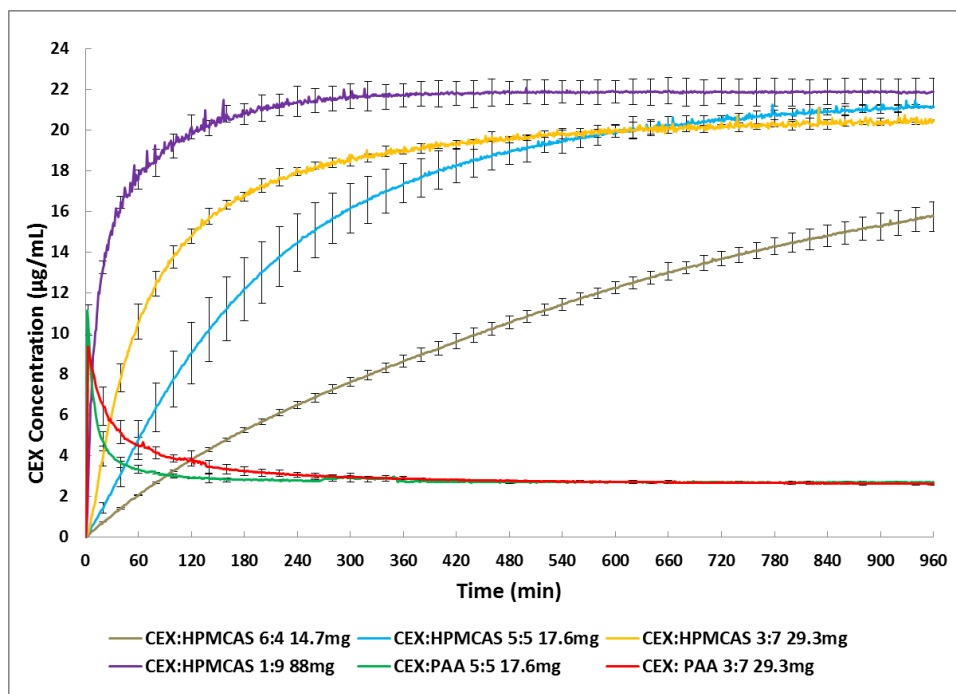


Figure 4-4 Dissolution Profiles of CEX: PAA and CEX: HPMCAS ASDs. The total mass of dispersion added to the medium to achieve a theoretical CEX concentration of 22μg/mL is indicated.
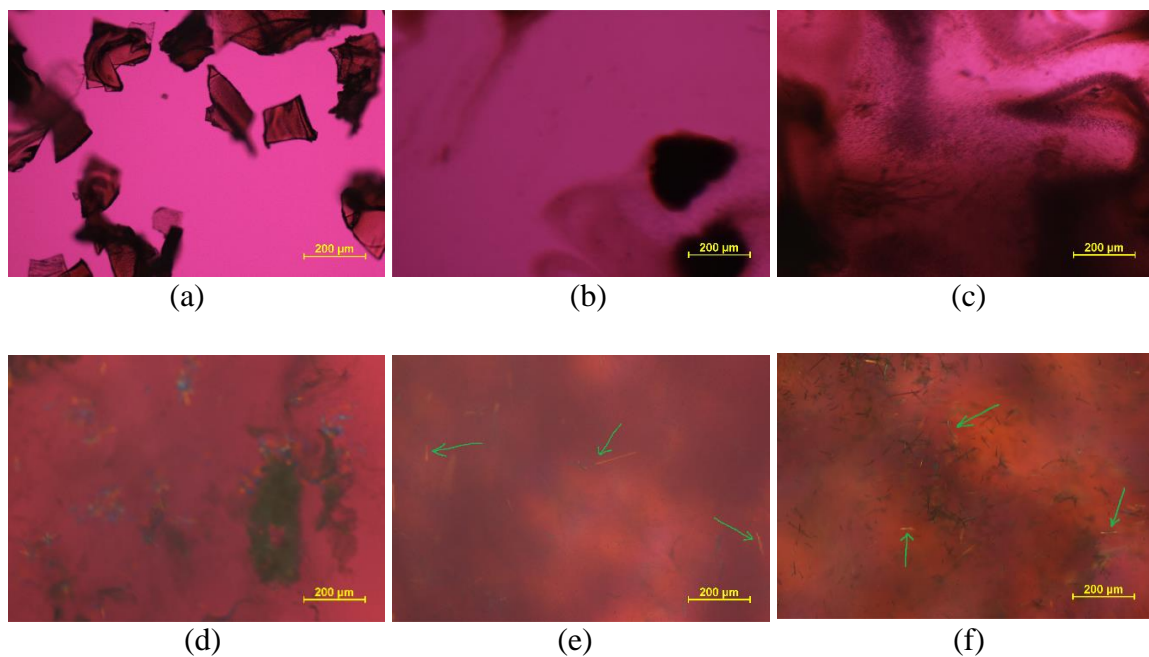
Figure 4-5 CEX:PAA 5:5 ASD in air (a) and after 20sec(b), 1min(c), 3mins(d), 5mins(e), and 10mins(f) following addition of SPB. The arrows indicated obvious needle-shaped crystals.
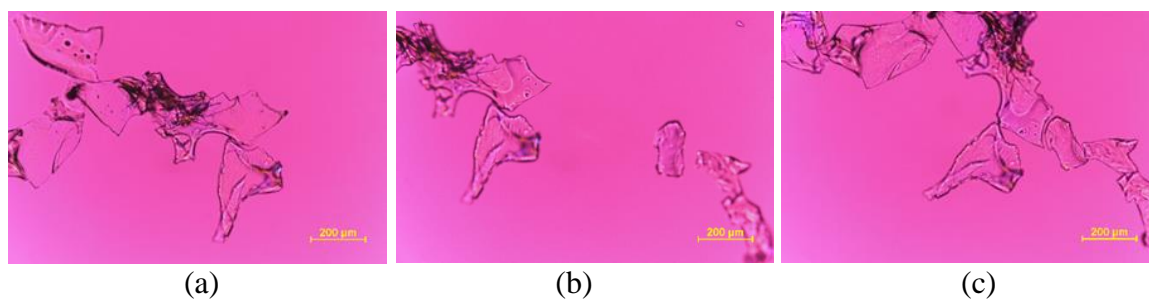


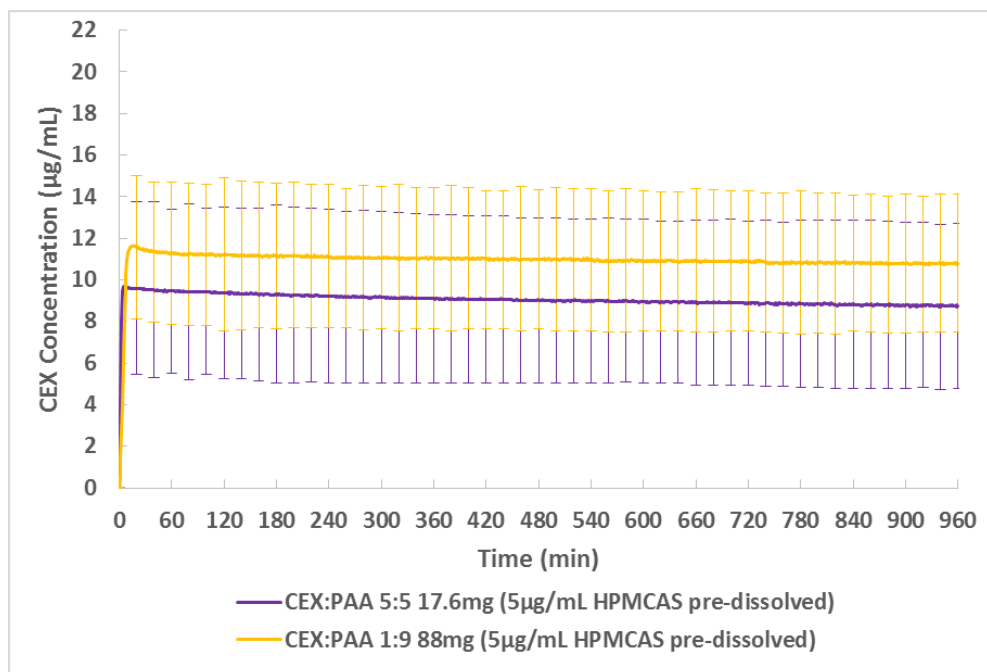Figure 4-6 CEX:HPMCAS 3:7 ASD after 5mins (a), 15mins (b), and 30mins (c) following addition of SPB.

Figure 4-7 Dissolution profiles of CEX: PAA ASDs in the presence of pre-dissolved HPMCAS. The total mass of dispersion added to the medium to achieve a theoretical CEX concentration of 22μg/mL is indicated.
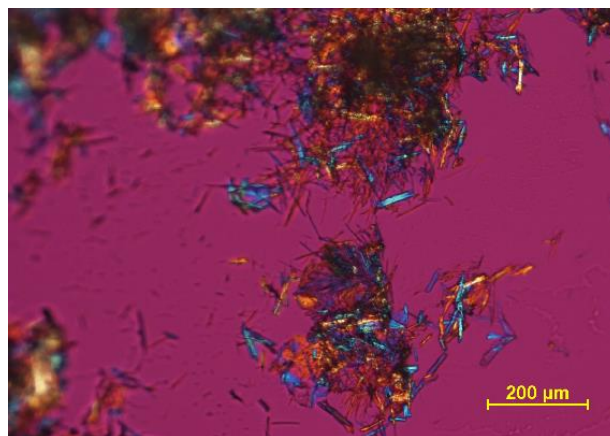


Figure 4-8 Solids retrieved soon after the peak concentration was reached during dissolution of a 5:5 CEX: PAA ASD in SPB with pre-dissolved HPMCAS
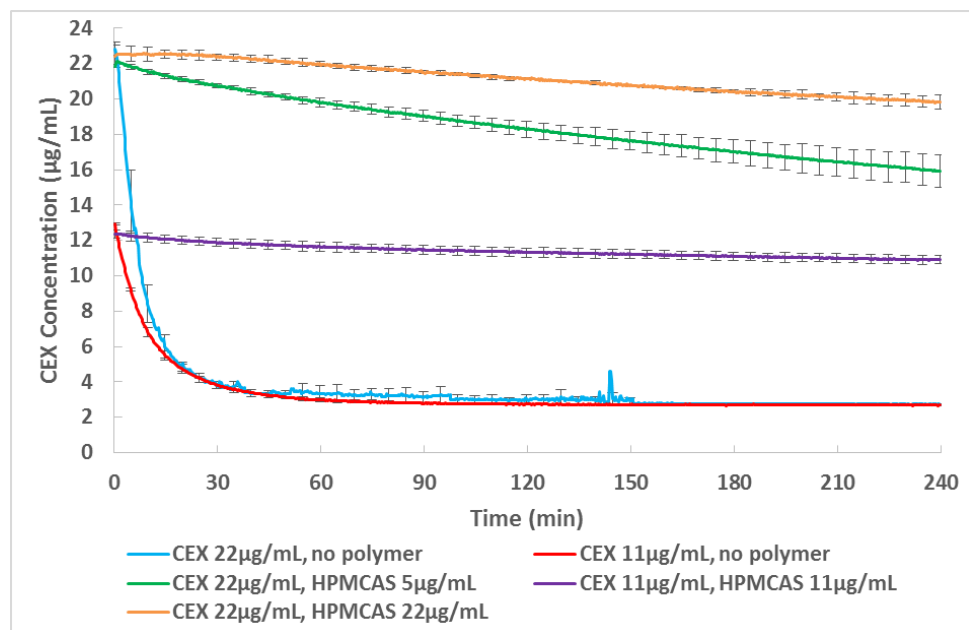
Figure 4-9 Seeded Desupersaturation of CEX in the presence and absence of pre-dissolved HPMCAS
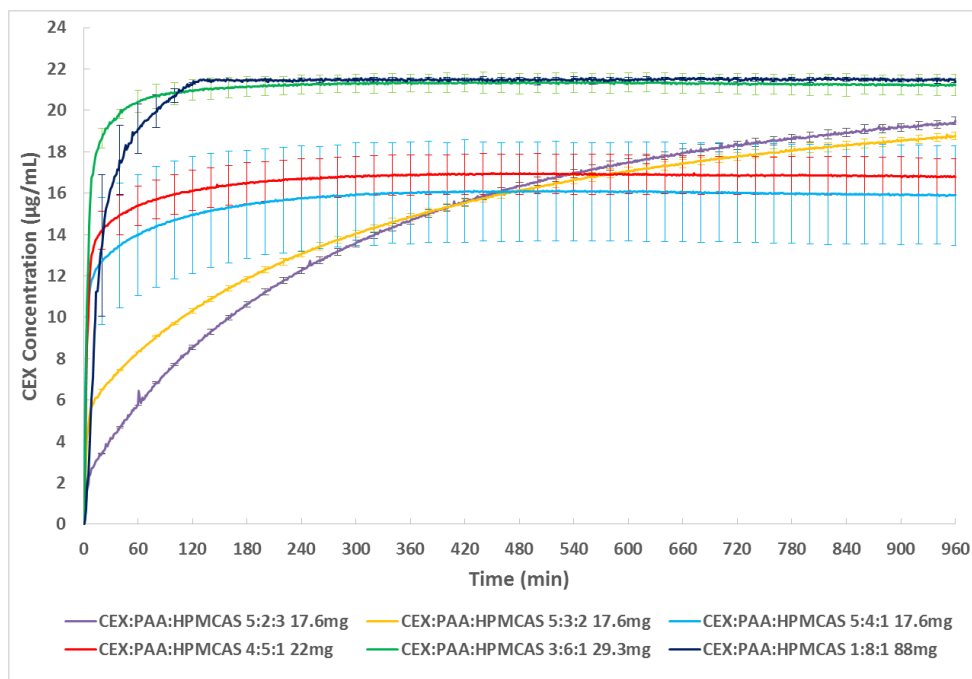


Figure 4-10 Dissolution Profiles of CEX: PAA: HPMCAS ternary ASDs. The total mass of dispersion added to the medium to achieve a theoretical CEX concentration of 22µg/mL is indicated.
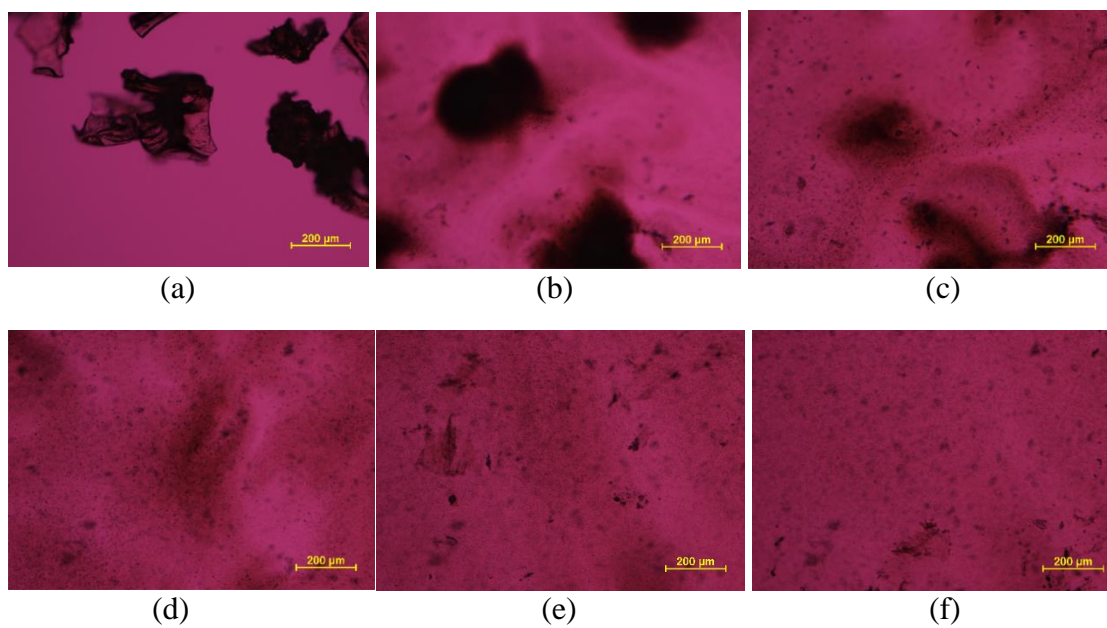
Figure 4-11 CEX: PAA: HPMCAS 3:6:1 ASD: Unexposed (a), 20sec (b), 1min (c), 2mins (d), 5mins (e), and 10mins (f).
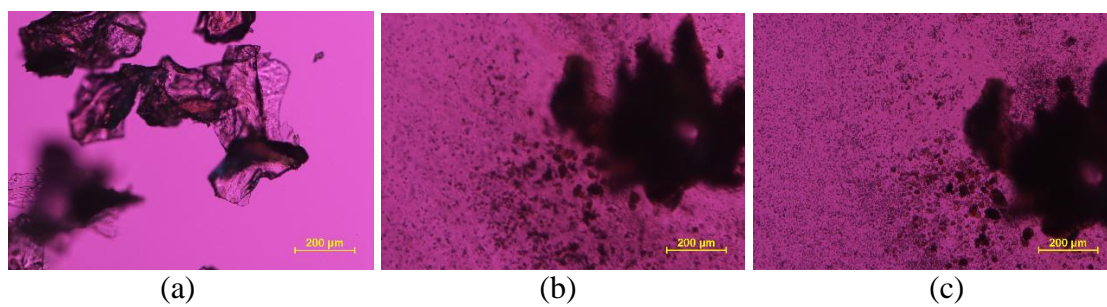


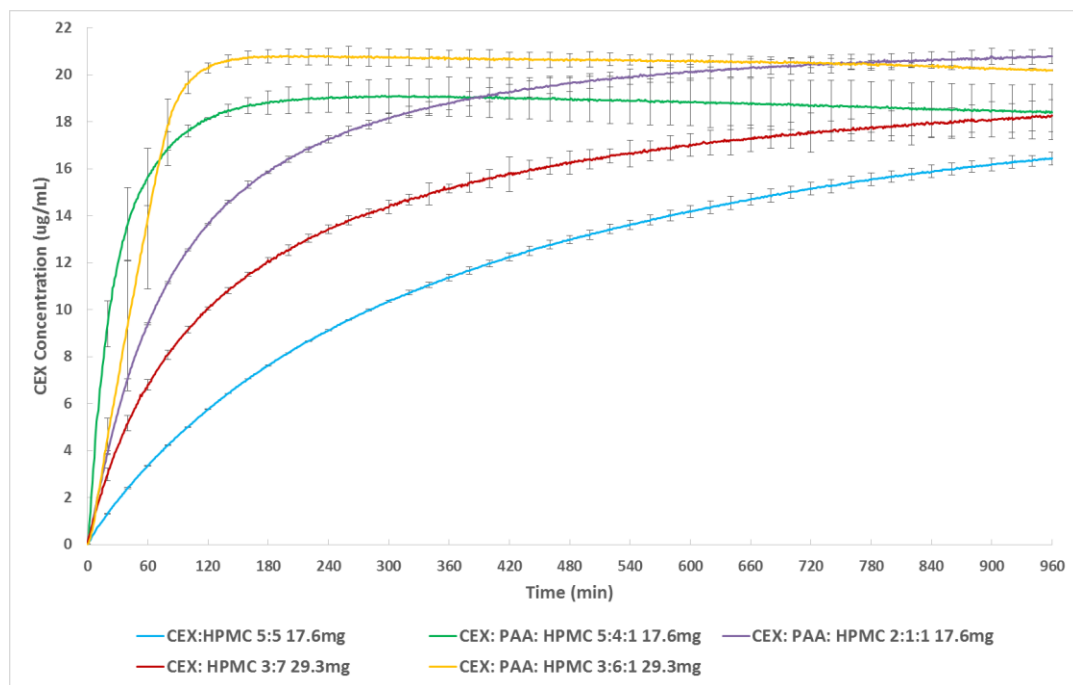Figure 4-12 CEX: PAA: HPMCAS 2:1:1 ASD: Unexposed (a), 5min (b), and 30min (c)

Figure 4-13 Dissolution profiles of CEX: HPMC and CEX: PAA: HPMC ASDs. The total mass of dispersion added to the medium to achieve a theoretical CEX concentration of 22μg/mL is indicated.
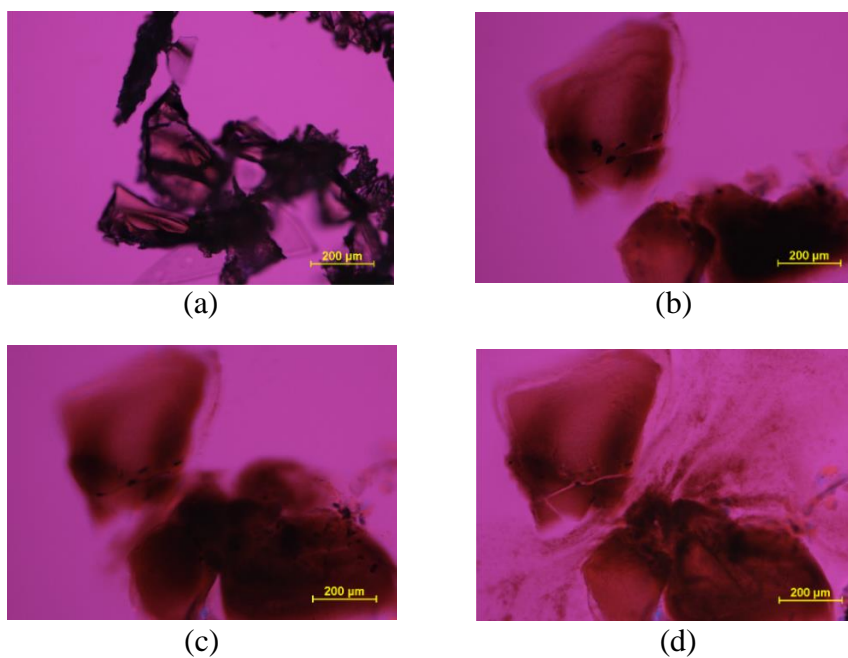


Figure 4-14 CEX: PAA: HPMC 3:6:1 ASD: Unexposed (a), 1min (b), 3mins(c), and 20mins (d)

Figure 4-15 Infrared spectra of spin coated polymeric films showing wavenumber range from 1600cm$^{-1}$ to 1800cm$^{-1}$: pure PAA (yellow), pure HPMCAS (red),  PAA: HPMCAS 7:3 (pink), 5:5 (blue), 3:7 (green) and CEX: PAA: HPMCAS 2:1:1 (black)
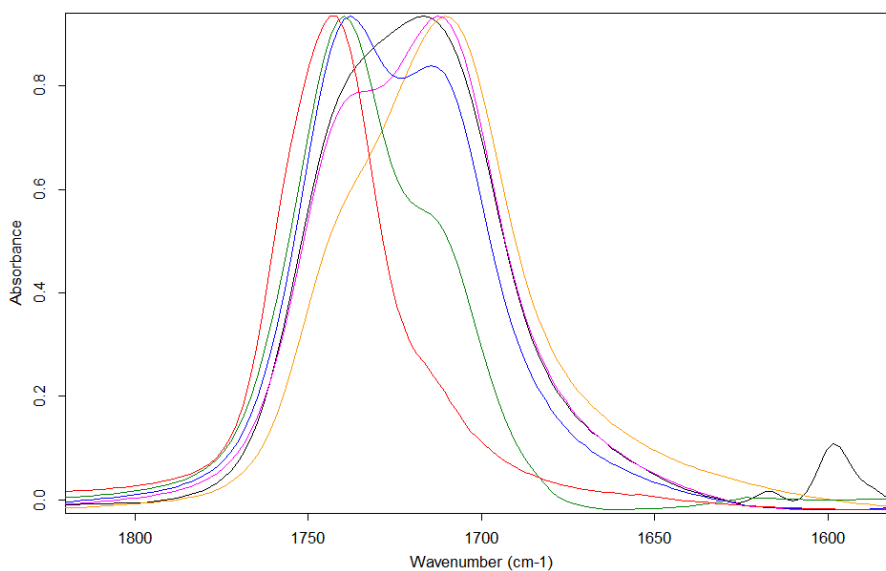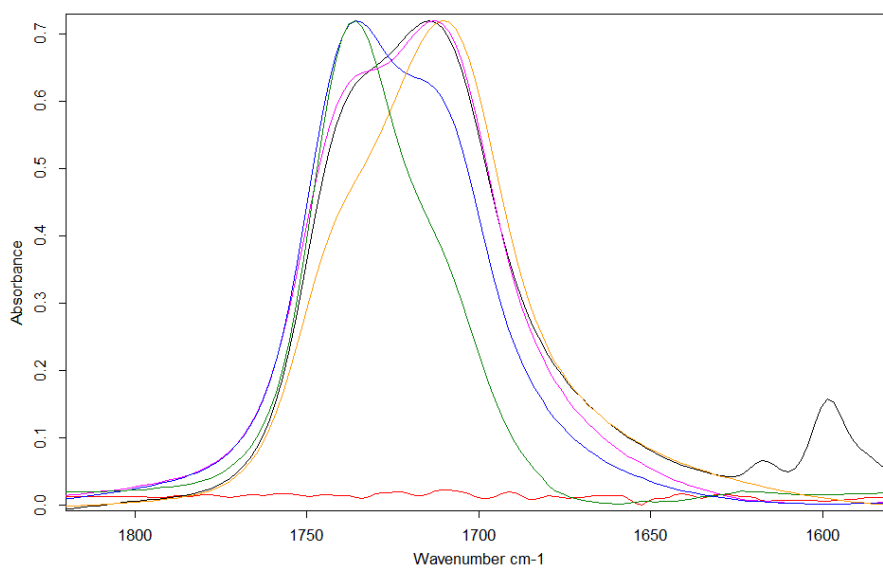


Figure 4-16 Infrared spectra of spin coated polymeric films showing wavenumber range from 1600cm$^{-1}$ to 1800cm$^{-1}$: pure PAA (yellow), pure HPMC (red),  PAA: HPMC 7:3 (pink), 5:5 (blue), 3:7 (green) and CEX: PAA: HPMC 2:1:1 (black).

## 4.7    Reference

1.      Babu, N. J.; Nangia, A.   Solubility Advantage of Amorphous Drugs and Pharmaceutical Cocrystals. *Cryst Growth Des* **2011,** *11*, (7), 2662-2679.
2.      Williams, H. D.; Trevaskis, N. L.; Charman, S. A.; Shanker, R. M.; Charman, W. N.; Pouton, C. W.; Porter, C. J. H.  Strategies to Address Low Drug Solubility in Discovery and Development. *Pharmacological Reviews* **2013,** *65*, (1), 315-499.
3.      Brouwers, J.; Brewster, M. E.; Augustijns, P.  Supersaturating drug delivery systems: the answer to solubility-limited oral bioavailability? *J Pharm Sci* **2009,** *98*, (8), 2549-72.
4.      Raina, S. A.; Zhang, G. G. Z.; Alonzo, D. E.; Wu, J.; Zhu, D.; Catron, N. D.; Gao, Y.; Taylor, L. S.  Enhancements and Limits in Drug Membrane Transport Using Supersaturated Solutions of Poorly Water Soluble Drugs. *J Pharm Sci-Us* **2014,** *103*, (9), 2736-2748.
5.      Dahan, A.; Miller, J. M.  The Solubility–Permeability Interplay and Its Implications in Formulation Design and Development for Poorly Soluble Drugs. *The AAPS Journal* **2012,** *14*, (2), 244-251.
6.      Morgen, M.; Bloom, C.; Beyerinck, R.; Bello, A.; Song, W.; Wilkinson, K.; Steenwyk, R.; Shamblin, S.  Polymeric Nanoparticles for Increased Oral Bioavailability and Rapid Absorption Using Celecoxib as a Model of a Low-Solubility, High-Permeability Drug. *Pharm Res-Dordr* **2012,** *29*, (2), 427-440.
7.      Vasconcelos, T.; Sarmento, B.; Costa, P.  Solid dispersions as strategy to improve oral bioavailability of poor water soluble drugs. *Drug Discovery Today* **2007,** *12*, (23–24), 1068-1075.
8.      Corrigan, O. I.  Mechanisms of Dissolution of Fast Release Solid Dispersions. *Drug Development and Industrial Pharmacy* **1985,** *11*, (2-3), 697-724.
9.      Chiou, W. L.; Riegelman, S.  Pharmaceutical applications of solid dispersion systems. *J Pharm Sci-Us* **1971,** *60*, (9), 1281-1302.
10.     Alonzo, D. E.; Zhang, G. G. Z.; Zhou, D. L.; Gao, Y.; Taylor, L. S.  Understanding the Behavior of Amorphous Pharmaceutical Systems during Dissolution. *Pharm Res-Dordr* **2010,** *27*, (4), 608-618.
11.     Suzuki, H.; Sunada, H.  Influence of Water-Soluble Polymers on the Dissolution of Nifedipine Solid Dispersions with Combined Carriers. *CHEMICAL & PHARMACEUTICAL BULLETIN* **1998,** *46*, (3), 482-487.
12.     Alonzo, D. E.; Gao, Y.; Zhou, D.; Mo, H.; Zhang, G. G. Z.; Taylor, L. S.  Dissolution and precipitation behavior of amorphous solid dispersions. *J Pharm Sci-Us* **2011,** *100*, (8), 3316-3331.
13.     Simonell.Ap; Mehta, S. C.; Higuchi, W. I.  DISSOLUTION RATES OF HIGH ENERGY POLYVINYLPYRROLIDONE (PVP)-SULFATHIAZOLE COPRECIPITATES. *J Pharm Sci-Us* **1969,** *58*, (5), 538-&.
14.     Simonelli, A. P.; Mehta, S. C.; Higuchi, W. I.  Dissolution Rates of High Energy Polyvinylpyrrolidone (PVP)-Sulfathiazole Coprecipitates. *J Pharm Sci-Us* **1969,** *58*, (5), 538-549.

15.      Paulson, S. K.; Vaughn, M. B.; Jessen, S. M.; Lawal, Y.; Gresk, C. J.; Yan, B.; Maziasz, T. J.; Cook, C. S.; Karim, A.  Pharmacokinetics of Celecoxib after Oral Administration in Dogs and Humans: Effect of Food and Site of Absorption. *Journal of Pharmacology and Experimental Therapeutics* **2001,** *297*, (2), 638-645.

16.      Gupta, P.; Kakumanu, V. K.; Bansal, A. K.  Stability and solubility of celecoxib-PVP amorphous dispersions: a molecular perspective. *Pharm Res* **2004,** *21*, (10), 1762-9.

17.      Abu-Diak, O. A.; Jones, D. S.; Andrews, G. P.  An Investigation into the Dissolution Properties of Celecoxib Melt Extrudates: Understanding the Role of Polymer Type and Concentration in Stabilizing Supersaturated Drug Concentrations. *Mol Pharmaceut* **2011,** *8*, (4), 1362-1371.

18.      Albers, J.; Alles, R.; Matthée, K.; Knop, K.; Nahrup, J. S.; Kleinebudde, P.  Mechanism of drug release from polymethacrylate-based extrudates and milled strands prepared by hot-melt extrusion. *Eur J Pharm Biopharm* **2009,** *71*, (2), 387-394.

19.      Dong, J.; Ozaki, Y.; Nakashima, K.  Infrared, Raman, and Near-Infrared Spectroscopic Evidence for the Coexistence of Various Hydrogen-Bond Forms in Poly(acrylic acid). *Macromolecules* **1997,** *30*, (4), 1111-1117.

20.      Janssens, S.; Van den Mooter, G.  Review: physical chemistry of solid dispersions. *Journal of Pharmacy and Pharmacology* **2009,** *61*, (12), 1571-1586.

21.      Curatolo, W.; Nightingale, J.; Herbig, S.  Utility of Hydroxypropylmethylcellulose Acetate Succinate (HPMCAS) for Initiation and Maintenance of Drug Supersaturation in the GI Milieu. *Pharm Res-Dordr* **2009,** *26*, (6), 1419-1431.

22.      Ilevbare, G. A.; Liu, H. Y.; Edgar, K. J.; Taylor, L. S.  Maintaining Supersaturation in Aqueous Drug Solutions: Impact of Different Polymers on Induction Times. *Cryst Growth Des* **2013,** *13*, (2), 740-751.

23.      Mullin, J. W., *Crystallization*. Butterworth-Heinemann: 2001.

24.      Murdande, S. B.; Pikal, M. J.; Shanker, R. M.; Bogner, R. H.  Solubility advantage of amorphous pharmaceuticals: I. A thermodynamic analysis. *J Pharm Sci-Us* **2010,** *99*, (3), 1254-1264.

25.      Almeida e Sousa, L.; Reutzel-Edens, S. M.; Stephenson, G. A.; Taylor, L. S.  Assessment of the Amorphous "Solubility" of a Group of Diverse Drugs Using New Experimental and Theoretical Approaches. *Mol Pharmaceut* **2014,** *12*, (2), 484-495.

26.      Chen, J.; Ormes, J. D.; Higgins, J. D.; Taylor, L. S.  Impact of Surfactants on the Crystallization of Aqueous Suspensions of Celecoxib Amorphous Solid Dispersion Spray Dried Particles. *Mol Pharmaceut* **2015,** *12*, (2), 533-541.

27.      Van Eerdenbrugh, B.; Raina, S.; Hsieh, Y.-L.; Augustijns, P.; Taylor, L.  Classification of the Crystallization Behavior of Amorphous Active Pharmaceutical Ingredients in Aqueous Environments. *Pharm Res-Dordr* **2014,** *31*, (4), 969-982.

28.      Sohnel, O.; Mullin, J. W.  Interpretation of Crystallization Induction Periods. *J Colloid Interf Sci* **1988,** *123*, (1), 43-50.

29.      Schram, C. J.; Taylor, L. S.; Beaudoin, S. P.  Influence of Polymers on the Crystal Growth Rate of Felodipine: Correlating Adsorbed Polymer Surface Coverage to Solution Crystal Growth Inhibition. *Langmuir* **2015**.

30.      Warren, D. B.; Benameur, H.; Porter, C. J.; Pouton, C. W.  Using polymeric precipitation inhibitors to improve the absorption of poorly water-soluble drugs: A mechanistic basis for utility. *Journal of drug targeting* **2010,** *18*, (10), 704-731.

31.	Curatolo, W.; Nightingale, J. A.; Herbig, S. M.  Utility of hydroxypropylmethylcellulose acetate succinate (HPMCAS) for initiation and maintenance of drug supersaturation in the GI milieu. *Pharm Res-Dordr* **2009,** *26*, (6), 1419-1431.

32.	Kurkuri, M. D.; Aminabhavi, T. M.  Poly(vinyl alcohol) and poly(acrylic acid) sequential interpenetrating network pH-sensitive microspheres for the delivery of diclofenac sodium to the intestine. *Journal of Controlled Release* **2004,** *96*, (1), 9-20.

33.	Chawla, G.; Gupta, P.; Thilagavathi, R.; Chakraborti, A. K.; Bansal, A. K.  Characterization of solid-state forms of celecoxib. *Eur J Pharm Sci* **2003,** *20*, (3), 305-317.

34.	Alonzo, D. E.; Raina, S.; Zhou, D.; Gao, Y.; Zhang, G. G. Z.; Taylor, L. S.  Characterizing the Impact of Hydroxypropylmethyl Cellulose on the Growth and Nucleation Kinetics of Felodipine from Supersaturated Solutions. *Cryst Growth Des* **2012,** *12*, (3), 1538-1547.

35.	Ilevbare, G. A.; Liu, H.; Edgar, K. J.; Taylor, L. S.  Inhibition of solution crystal growth of ritonavir by cellulose polymers - factors influencing polymer effectiveness. *Crystengcomm* **2012,** *14*, (20), 6503-6514.

36.	Kubota, N.; Mullin, J. W.  A kinetic model for crystal growth from aqueous solution in the presence of impurity. *Journal of Crystal Growth* **1995,** *152*, (3), 203-208.

37.	Verdoes, D.; Kashchiev, D.; van Rosmalen, G. M.  Determination of nucleation and growth rates from induction times in seeded and unseeded precipitation of calcium carbonate. *Journal of Crystal Growth* **1992,** *118*, (3–4), 401-413.

38.	Qian, F.; Huang, J.; Hussain, M. A.  Drug–polymer solubility and miscibility: Stability consideration and practical challenges in amorphous solid dispersion development. *J Pharm Sci-Us* **2010,** *99*, (7), 2941-2947.

39.	Kuo, S.-W.; Shih, C.-C.; Shieh, J.-S.; Chang, F.-C.  Specific interactions in miscible polymer blends of poly(2-hydroxypropyl methacrylate) with polyvinylpyrrolidone. *Polymer International* **2004,** *53*, (2), 218-224.

40.	Silverstein, R. M.; Webster, F. X.; Kiemle, D.; Bryce, D. L., *Spectrometric identification of organic compounds*. John Wiley & Sons: 2014.

41.	Coleman, M. M.; Painter, P. C.; Graf, J. F., *Specific interactions and the miscibility of polymer blends*. CRC Press: 1995.

42.	Marsac, P.; Shamblin, S.; Taylor, L.  Theoretical and Practical Approaches for Prediction of Drug–Polymer Miscibility and Solubility. *Pharm Res-Dordr* **2006,** *23*, (10), 2417-2426.

43.	Rumondor, A. F.; Ivanisevic, I.; Bates, S.; Alonzo, D.; Taylor, L.  Evaluation of Drug-Polymer Miscibility in Amorphous Solid Dispersion Systems. *Pharm Res-Dordr* **2009,** *26*, (11), 2523-2534.

44.	Marks, J. A.; Wegiel, L. A.; Taylor, L. S.; Edgar, K. J.  Pairwise Polymer Blends for Oral Drug Delivery. *J Pharm Sci-Us* **2014,** *103*, (9), 2871-2883.

VITA

VITA

Tian Xie received his Bachelor of Science degree in Pharmaceutics from East China University of Science and Technology in 2006 and Master of Engineering degree in Pharmaceutical Engineering from Univerisity of Michigan in 2008. He joined the Ph.D. program in the department of Industrial and Physical Pharmacy at Purdue University in August 2009. His research focused on utilizing polymer combinations to optimize the performance characteristics of amorphous solid dispersions.